Characterization of hydrothermal vent faunal assemblages in the Mariana Back-Arc Spreading Centre

by

Thomas Normand Giguère
B.Sc., University of Guelph, 2017

A Thesis Submitted in Partial Fulfillment
of the Requirements for the Degree of

MASTER OF SCIENCE

in the School of Earth and Ocean Sciences

Supervisory Committee

Characterization of hydrothermal vent faunal assemblages in the Mariana Back-Arc Spreading Centre

by

Thomas Normand Giguère
B.Sc. University of Guelph, 2017

Supervisory Committee

Dr. Verena Tunnicliffe, School of Earth and Ocean Sciences
Supervisor

Dr. John Dower, School of Earth and Ocean Sciences
Departmental Member

Dr. Brian Starzomski, School of Environmental Studies
Outside Member

Abstract

Researchers have learned much about the biological assemblages that form around hydrothermal vents. However, identities of species in these assemblages and their basic ecological features are often lacking. In 2015, the first leg of the Hydrothermal Hunt expedition identified likely new vent sites in the Mariana Back-arc Spreading Center (BASC). In 2016, the second leg of the expedition used a remotely operated vehicle (ROV) to confirm and sample two new sites and two previously known sites. My first objective is to identify the animals collected from these four vent sites. In these samples, I identify 42 animal taxa, including the discovery of four new vent-associated species, five potentially new species and six taxa not previously reported in the Mariana BASC vents. My second objective is to combine these new data with previous studies and examine the species distributions among all known vent sites in the Mariana BASC using the α-, β-, and γ-diversity framework. I present updated species absence-presence lists for all eight Mariana BASC vent sites, which begin to resolve some of the issues with species identification. In this thesis, my approach to assessing β-diversity is novel in the field of hydrothermal vent ecology. My work also provides the first intra-regional scale assessments of β-diversity that include all sites known in a vent system. My third objective is to explore environmental factors driving these species distribution patterns. The α-diversity of BASC vent sites gradually increases with latitude, and the β-diversity calculated using the Raup-Crick index correlates with distance to nearby vent sites. Stochastic assembly processes likely shape the diversity patterns throughout the Mariana BASC as few environmental variables are known to correlate with these patterns. My fourth objective is to compare the β-diversity patterns between the Mariana BASC vent sites and those in two other vent systems: the Mariana Arc and the Juan de Fuca Ridge. The γ- and average α-diversity values for the BASC vents are relatively low compared to the other two systems. The Jaccard index revealed that the average number of

shared species among the Arc vent sites is much lower than those of the BASC and the Juan de Fuca Ridge. The Raup-Crick index indicates that stochastic processes explain the average β-diversity of the Mariana BASC vents better than those of the Mariana Arc and Juan de Fuca Ridge.

Table of Contents

List of Tables

List of Figures

Acknowledgements

First, I would like to thank Dr. Verena Tunnicliffe for being the best advisor anyone could ask for. With the perfect combination of patience and hardness, Verena's guidance has given me an invaluable learning experience, which has greatly improved my abilities as a biologist. I am tremendously grateful for all the opportunities Verena has given me and it has been an absolute privilege to learn from such an extraordinary person.

The content in this thesis would not be possible without the contributions of many people. Thank you to my committee members, Dr. John Dower and Dr. Brian Starzomski, for assisting with my progression throughout this thesis. Thank you to the Captain Heiko Volz, his crew on the *R/V Falkor*, and the ROV *SuBastian* team. Thank you to the chief scientists Joseph Resing, William Chadwick and Dave Butterfield, and the other participants in the science party during the 2015 and 2016 expeditions; the work of everyone on these expeditions was absolutely crucial for acquiring the samples analyzed in this thesis. Thank you to National Geographic Society, NSERC Canada and NOAA Earth-Ocean Interactions Programs, University of Southampton for financial support. Thank you to all the staff and graduate students in the School of Earth and Ocean Sciences, and many of Verena's previous graduate students for inspiring and supporting me throughout this endeavour. I want to thank Nick Brown, Dr. John Nelson, Malloy Van Wyndgaarden, and Amy Liu in particular; thank you to Nick for preliminarily sorting the biological samples prior to my arrival, and thank you to John, Mallory and Amy for their assistance with genetic sequencing. A special thank you to all the taxonomic experts who identified difficult taxa that I could not identify myself: Dr. Tomoyuki Komai, Dr. Hiromi Watanabe, Dr. Yasunori Kano, Dr. Nicholas Puillandre, Dr. Greg Rouse, Dr. James Reimer, Dr. Tammy Horton, Dr. Claudia Arango and Dr. Lothar Beck. Thank you to Dr. Stace Beaulieu for providing some species occurrence data from settling plates placed in the Snail vent site. Thank you to Dr. Melissa Anderson for improving my understanding of the geology in the Mariana region.

Finally, I would like to express my deep gratitude for my parents, Norm and Renée. Thank you for providing me with your love and support throughout my entire life. As my first teachers, you are reason I find myself with a wonderful life. I am truly lucky to have such fantastic parents. A special thanks to my partner, Izzy, as well. Despite the challenges of a distant relationship, she was a great source of support through my most stressful times.

Dedication

To Mom

Without our great fortune this past year, my life would be very different right now.
I am forever grateful that you are happy, healthy and here to witness this accomplishment.
I love you.

Chapter 1: General Introduction:

Species Diversity and Distributions:

The entire concept of a species is rooted in the need to recognize the diversity of organisms that inhabit the Earth and differentiate the populations that comprise an ecosystem. In the field of ecology, the biodiversity component is one of the most important sets of data needed for this type of study. As a way to better understand the mechanisms that shape diversity patterns, Whittaker (1960) introduced the terms α-diversity, β-diversity and γ-diversity. The term α-diversity refers to the number of species, or the species richness, present in a given sample, site or any other unit of biological grouping. Similarly, the term γ-diversity refers to the number of species present in the group of biological groupings. For example, if one was to measure the diversity of plants in an archipelago, the α-diversity would be the species richness of each island and the γ-diversity would be the species richness of the entire archipelago. The term β-diversity refers to how biologically distinct one biological group is to another. Using the same archipelago example, β-diversity would be a measure of how the plant community of one island compositionally differs from that of another; this term is particularly important for understanding the environmental drivers that shape the diversity patterns across all ecosystems.

Species distribution information is also foundational to many ecological studies and researchers use these data to tackle a wide variety of questions. For example, some studies seek to understand the changes in distribution ranges of a particular species or groups of species (e.g. Mainali et al. 2015), while others seek to understand the spatial patterns of species richness as a whole (e.g. MacArthur and Wilson, 1967). Many disciplines have developed around different research questions regarding species distributions, though researchers do not entirely agree upon the definitions of the terms that have emerged. For instance, Fisher (2002) considers the field of

macroecology to be a subset of biogeography. However, Blackburn and Gaston (2002) consider biogeography to be the study of biodiversity distribution patterns and macroecology as the study of ecological interactions between species and the environment that influence the distribution patterns. Regardless of the labels, these disciplines either examine and document these patterns (descriptive studies) or attempt to explain the mechanisms driving these patterns (interpretive studies) (Posadas et al. 2006).

While these objectives may seem relatively straight forward, in practice, they are often difficult to pursue, especially in habitats that are difficult to access, like those in the deep-sea (Macpherson, 2003). The interactions between organism characteristics and environmental properties shape the distributions of the species (Itescu, 2019). Therefore, these mechanisms may vary across different habitats and ecosystems; an environmental property shaping species distributions in one habitat may have a negligible influence on distribution patterns in another. However, general patterns appear to transcend many different types of habitats and organisms (e.g. range size-body size relationship, Gaston and Blackburn, 1996).

One of the critical ecological factors shaping modern species distributions is their dispersal potential. However, dispersal potential does not always positively correlate with species range size (e.g. Lester et al. 2007). Dispersal strategies of species are highly variable and depend on both their physical abilities and the characteristics of their environment (Burgess et al. 2016). Some species actively disperse in their adult forms, such as many fish species (e.g. Guzman et al. 2018; Domeier and Speare, 2012), whereas others passively disperse by wind, ocean currents, or animal transport (e.g. Leis, 1984; Cowen and Sponaugle, 2009; Terui and Miyazaki, 2015). Some species have great dispersal potential, capable of travelling hundreds of kilometres, whereas others are more limited in their dispersal abilities. Environmental barriers,

such as the deep ocean for shallow species (Macpherson, 2003), play a significant role in the dispersal potential of organisms and often affect species disproportionately. Environmental corridors also play an essential role when barriers are present. For instance, when dry land acts as a barrier for many freshwater species, rivers and streams connecting lakes and wetlands act as corridors, facilitating dispersal throughout entire watersheds (e.g. Mandrak and Crossman, 1992).

Species are unevenly scattered throughout their ranges because ecosystems contain a mosaic of different habitats. Essential resources required for survival are spread heterogeneously across space on both large and small scales (Boer, 1968), so populations typically gather around these resource patches. As a result, metapopulations emerge, especially among species with large distribution ranges (Hanski and Gilpin, 1991). The emergence of metapopulations is another important dynamic that shapes species distributions because they bolster the resilience of species through extinction-colonization dynamics. Species that only consist of a single population are at high risk of extinction if faced with a substantial disturbance event or a reduction of essential resources. However, metapopulation dynamics provide resilience because while some populations may experience a decline or extinction, others may grow or remain the same size. Therefore, as long as populations can exchange individuals across habitat patches, a strong population can help sustain a weaker population via immigration; ecologists generally refer to this as connectivity (Taylor et al. 1993; Calabrese and Fagan, 2004).

Dispersal is essential to maintain connectivity between populations because it is the foundational mechanism that allows organisms to move through space; barriers and corridors between habitat patches have a major influence on this. Recruitment is the ability for individuals to survive in the area where they settle (Pineda et al. 2010; Cowen and Sponaugle, 2009), which

depends on the suitability of the habitat relative to the ecological niche that the organism occupies. The potential for recruitment depends on the life-history traits of the species; habitat generalists can establish themselves in a wide variety of habitats, while specialists require a narrow range of ecological conditions (Büchi and Vuilleumier, 2014).

While mainland populations do not have strict boundaries between them, even if they are spatially structured (Hanski and Gilpin, 1991), islands are habitat patches with conspicuous boundaries, so they are ideal habitats to study biogeography (MacArthur and Wilson, 1967). For example, the study of island biogeography seeks to understand the mechanisms that influence the potential for species from the mainland to distribute to and successfully establish themselves on islands (MacArthur and Wilson, 1967). Similarly, it also seeks to understand the mechanisms that control the overall species richness on islands. One general trend is that larger islands typically support greater species richness than smaller ones, known as the species-area relationship (Rosenzweig, 1995). Species are more likely to disperse to larger islands because they have higher potential for immigrating organisms to arrive than smaller islands. Larger islands also tend to have greater habitat diversity, thus can support more species than smaller islands. Another general trend MacArthur and Wilson (1967) identified is that islands closer to the mainland tend to be more species-rich than those that are more isolated, known as the species-isolation relationship. Species are less likely to disperse to more isolated islands because the likelihood of arriving at them by chance is lower than islands closer to the mainland. Isolated islands are also more difficult to reach because it is more challenging for organisms to cross a wider, semi-permeable barrier than one that is shorter. However, it is pertinent to note that the equilibrium theory of biogeography only accounts for the distance of the island to the mainland; it does not account for the ‘stepping stone’ effect of nearby islands (Hanski and Gilpin, 1991).

Many researchers have also applied the theory of island biogeography to other insular systems, but the general species-area and species-isolation relationships are only sometimes present in these habitats (Itescu, 2019).

Phenomena that occur on geologic time-scales, but are not operative on short time-scales, such as plate tectonics and evolution, are also important factors that structure modern-day species range sizes (Gaston, 1996); phylogeography is the discipline that investigates questions regarding the historical changes in organism distributions throughout speciation and extinction events (Kumar and Kumar, 2018). Species range sizes expand, contract and fragment over time depending on their interactions with the biotic and abiotic environment (Kumar and Kumar, 2018). For example, as tectonic plates move, they create and destroy both barriers and corridors in both terrestrial and marine ecosystems over evolutionary time. Therefore, the connectivity between populations changes over large time-scales. Populations that separate due to distance or barriers, and are exposed to different environmental pressures for long enough, speciate by allopatry, which typically reduces the range size of the original metapopulation. Thus, broad regionalized patterns emerge across the planet, known as biogeographic provinces (Oliver and Irwin 2008).

Hydrothermal Vents and Their Biotic Assemblages:

Hydrothermal circulation is the process in which water percolates through fractures in the Earth's crust and approaches a magma source where it superheats and leeches minerals and compounds from the surrounding rock (e.g. Butterfield et al. 1997). Newly formed hydrothermal fluids rise through the crust and emerge as "vents." They are typically present along tectonic margins, such as mid-ocean ridges (MORs), submarine volcanoes and back-arc spreading centers

(BASCs) (Beaulieu et al. 2013). The abiotic conditions of hydrothermal vents are highly variable among different locations. Their properties depend on the characteristics of their fluids and their geologic settings. For example, some vents are low-temperature, releasing hydrothermal effluent that exceeds ambient deep-sea temperatures by only a few degrees (e.g. Kelley et al. 2001). Others are high-temperature, releasing effluent approaching or exceeding 400˚C at the crust-ocean interface (e.g. Koschinsky et al. 2008).

Substratum porosity and the thermal activity within the crust influence how the effluent escapes into the ocean. Porous substrata allow hydrothermal fluids to escape diffusely across a relatively large area, typically at a slow rate (Anderson et al. 2019). In contrast, dense lithologies tend to focus the hydrothermal flow, causing them to escape from a confined area and at a higher rate. The formation of chimney structures is a common feature of vents. As high-temperature effluent emerges and quickly cools, the dissolved compounds, such as metal sulphides, precipitate to create the chimneys and the "smoke" usually associated with them (e.g. Hekinian et al. 1983). Chimneys vary in size and composition, with the tallest chimney known to date being a carbonate structure at 60 m tall, located in the Lost City vent site on the Mid-Atlantic Ridge (Ludwig et al. 2006). Hydrothermal effluent is also usually acidic (e.g. Gamo et al. 2013), but depending on the geochemistry of the system, hydrothermal fluids can (rarely) be very alkaline, generating chimneys composed of carbonate minerals rather than sulphides (e.g. Kelley et al. 2001; Goffredi et al. 2017). Due to the anoxia within the crust, many chemicals within hydrothermal effluent are also in a reduced state. As they mix with deep ocean waters, they quickly oxidize; therefore, vent fluids act as oxygen sinks (Johnson et al. 1988).

The combination of steep temperature gradients, toxic chemicals, extreme pH conditions, low oxygen, and, sometimes, frequent disturbances (e.g. volcanic eruptions) makes hydrothermal

vents a challenging habitat for organisms. Nevertheless, despite these challenges, hydrothermal vents usually support substantially higher biomass than the surrounding deep sea. The reduced chemicals in the hydrothermal fluids (e.g. H_2S) act as an energy source for chemosynthetic microbes (Hügler and Sievert, 2011). Therefore, since vents support relatively high primary production, they are one of the few habitats in the deep sea that generate an abundant food source and do not rely on photosynthetic-derived food from the ocean surface. However, without numerous, substantial adaptations, animals cannot penetrate these habitats to access this food source (McMullin et al. 2007). As a result, animals that live in vent habitats usually possess highly specialized adaptations; the high proportion of vent-endemic species present in vent assemblages reflects this condition (Tunnicliffe et al. 1998).

Although most vent species do not share a common, vent-endemic ancestor, some adaptations to vent conditions convergently evolved across many taxa. For example, many species have evolved the capacity to harbour chemoautotrophic bacteria within their tissues or on their body surfaces to benefit directly from the primary production. Some examples include snails (e.g. Suzuki et al. 2006; Johnson et al. 2015), mussels (e.g. Nelson et al. 1995), and shrimp (e.g. Petersen et al. 2010); tubeworms are the most iconic taxon for this adaptation because they have entirely opted out of eating as adults and instead derive all their nutrition from this symbiotic relationship (Hilario et al. 2011). Another convergently evolved adaptation among many vent-endemic species relates to their mitochondria and the associated enzymes. Generally, with increasing temperature, metabolic activity increases to a maximum, then rapidly declines (Schulte, 2015), and the temperature of maximum activity differs between species. Vent-endemic species reach maximum activity at much higher temperatures compared to their respective, closely-related, non-vent counterparts (Dahlhoff et al. 1991). Furthermore, despite the high

thermal tolerance, many vent species have also adopted the behaviour to seek temperatures cooler than their maximum tolerance compared to their non-vent counterparts (Bates et al. 2010).

Most vent-endemic species are invertebrates that passively disperse as larvae (but see France et al. 1992), which means that ocean currents play a substantial role in their dispersal potential. These currents can act as either corridors or barriers, especially as they interact with the topography of the seafloor. For example, Mitarai et al. (2016) demonstrate that back-arc basins may help to retain vent larvae and maintain relatively high connectivity between the vent sites within their respective regions. Similarly, since vents tend to occur along tectonic boundaries, rift valleys can act as corridors that facilitate larval dispersal between nearby vent sites (e.g. McGillicuddy Jr et al. 2010). In contrast, transform faults separating ridge segments can also act as barriers (e.g. Johnson et al. 2008). However, bottom currents do not entirely dictate the dispersal potential of vent larvae because some species use vertical migration to disperse at different depths (e.g. Adams et al. 2012; Yahagi et al. 2017). Some species migrate to surface waters; although warmer ocean temperatures increase their metabolism and reduce their time to settle on suitable habitat, they are also able to take advantage of photosynthetic-derived food sources before they settle in vent sites (e.g. Stevens et al. 2008). In contrast, some species tend to disperse in the cold, bottom waters (e.g. Mullineaux et al. 2005); each strategy has its risks and advantages.

Vent Diversity:

Since the first discovery of hydrothermal vents (Corliss et al. 1979), taxonomists have identified hundreds of species living in these habitats over the last 43 years, and there is still much to learn about them. Chapman et al. (2019) provide a list with 646 species present in vents,

but only include those that were described before 2017 and have data available about their functional traits; researchers have identified many more species from vents, but very little is known about their traits (Tunnicliffe, pers. comm.). These species typically belong to one of three phyla: Arthropoda, Mollusca and Annelida (Tunnicliffe et al. 1998). However, some cnidarians (e.g. Lutz et al. 1998; Rodríguez and Daly, 2010), echinoderms (e.g. Stohr and Segonzac, 2006), chordates (e.g. Weber et al. 2003), nematodes (e.g. Vanreusel et al. 1997) and nemerteans (e.g. Shields and Segonzac, 2007) are sometimes also present in vent habitats. Given that many species and higher taxonomic groups (i.e. genera, families and superfamilies) are endemic to hydrothermal habitats (McArthur and Tunnicliffe, 1998), undescribed species are often collected from newly discovered vent sites (e.g. Hessler and Lonsdale, 1991; Hashimoto et al. 2001; Rogers et al. 2012); many taxa also remain undescribed. Therefore, taxonomic studies of vent fauna are crucial, especially because the collection rate of undescribed species can be higher than the rate at which they are formally described.

Morphological analysis is a non-trivial task that requires a substantial amount of time to complete, and it has worked well to describe many vent species. The relatively recent addition of molecular tools increases the amount of time required to describe some species. However, by revealing their underlying genetic complexity, these tools have improved the accuracy of their identities and delineate the degree of relatedness between different species. For example, some molecular studies have exposed the presence of multiple morphologically cryptic species once believed to be the same species; others have synonymized different species names under the same identity of a single, phenotypically plastic species (Vrijenhoek, 2009). Furthermore, molecular studies have provided clues to both the evolutionary history of vent-endemic species and their phylogenetic relationships to non-vent species.

For one, taxonomists initially classified tubeworms under their own Phylum (Vestimentifera) due to their unusual morphologic features (Jones, 1985), but more recent analyses using molecular tools have revealed that they actually form a family - the Siboglinidae of polychaete worms (McHugh, 1997). Secondly, molecular studies have shown that vent species from different oceans are more closely related to each other than they are to their respective, local, non-vent counterparts (e.g. Martin and Haney, 2005), further illustrating the long history and isolated nature of vent communities. Thirdly, diversity studies have provided some clues into the evolutionary connections between vent communities and those found in other chemosynthetic-based habitats, like cold seeps, wood falls and whale falls. Although species present in vent assemblages are mostly endemic to vents, some species are found in both vents and other chemosynthetic habitats (e.g. Hashimoto and Okutani, 1994; Smith et al. 2002); many higher taxonomic groups also contain species present only in chemosynthetic habitats (e.g. Goffredi et al. 2003; Martin and Haney, 2005; Krylova and Sahling, 2010). These studies have even provided clues into the non-vent origins of some vent-endemics (e.g. Distel et al. 2000; Samadi et al. 2007).

Although diversity studies are a substantial component in hydrothermal vent research, the difficulty in accessing these deep-sea habitats limits the number of samples that researchers can collect during each expedition. Nevertheless, they still utilize these data to assess the species richness of vent sites; as exploration and sample collection continues, the diversity estimates become incrementally more accurate. Many vent studies report both the α-diversity and γ-diversity values for their given spatial scopes, and although these studies are mostly descriptive, some researchers have applied statistical tests to either provide more accurate estimates of α- or γ-diversity (e.g. Tsurumi and Tunnicliffe, 2001; Gauthier et al. 2010) or assess spatial

distribution patterns (e.g. Marcus, 2003). Some studies have also used common β-diversity indices to calculate the faunal (dis)similarities between different vent locations. For example, on a small spatial scale, Tsurumi (2003) assessed the α-diversity of individual vent fields within a few sites on the Juan de Fuca Ridge and calculated the β-diversity between them to determine if there was a notable difference between 'patchy' and 'continuous' vent sites. Similarly, Sen et al. (2014) also calculated the β-diversity within vent sites in the Eastern Lau BASC and Valu Fa Ridge, but instead calculated it over time to measure the faunal (dis)similarity across different phases in vent community succession. In contrast, some studies have applied β-diversity indices to identify the faunal (dis)similarities between different vent regions on an inter-regional scale (e.g. Zhou et al. 2018). In general, the use of β-diversity indices is a valuable tool for diversity studies in vent habitats. Like molecular tools, quantifying faunal dissimilarity patterns on large spatial scales can reveal some aspects of the evolutionary history of vent communities (e.g. Tunnicliffe and Fowler, 1996). On small spatial scales, the use of β-diversity can identify both zonation patterns across space and community succession patterns across time. Vent studies have not yet used β-diversity on an intra-regional scale, but doing so would be useful for understanding how vent communities are structured over a relatively large area, but across a short time-scale.

The spatial extents that delineate both local and regional diversity, which are essential parameters to calculate β-diversity, differ among studies depending on their geographic scope. For my study, habitat terms are used as follows. A 'vent' is a small area on the seafloor where hydrothermal effluent emerges (Figure 1a). Vents can release fluids diffusely or in focussed flow, but they typically consist of a single outflow feeding an area less than about 10 m^2. I consider a chimney-structure with multiple outflow sites along its trunk as a single vent. A 'vent

field' is an area with multiple vents spread across the seafloor, typically on a scale of 10s to 100s of meters squared (Figure 1b). 'Vent sites' are often synonymized with vent fields, and they are similar, but if multiple, discrete vent fields lie within 1.5 km of each other, I consider them to be part of the same vent site (Figure 1c). However, vent sites sometimes only consist of a single vent field. A 'vent system' is a much larger area that supports multiple vent sites, and is typically defined by the geologic structure that facilitates the hydrothermal processes, such as a volcanic arc, or a series of seafloor spreading segments (Figure 1d). Vent regions often only include a single vent system, but some regions contain multiple systems. I consider a volcanic arc and its adjacent BASC as a single vent region because the same geologic structure supports them both – a subducting plate boundary. However, I consider arcs and BASCs to be two separate systems because both their magma sources and vent communities are notably different, despite their close geographic proximity. In the context of global biogeography, a 'vent province' is a large area, sometimes covering millions of km^2 and supporting taxonomically similar communities (e.g. Rogers et al. 2012). However, biological characteristics define provinces rather than their geologic features or spatial proximity.

Study System - The Mariana Back-Arc Spreading Centre:

In this study, I investigate the fauna living at the vent sites of the Mariana BASC (Figure 2) in the Northwestern Pacific (Anderson et al. 2017). The Mariana BASC is a part of the larger Izu-Bonin-Mariana (IBM) subduction factory, which is the geologic expression of the subducting plate boundary between the Pacific and Philippine plates (Stern et al. 2003). Directly along this plate boundary lays the well-known Mariana Trench in the south and the Izu-Bonin Trench in the North; cumulatively, these two trenches stretch 2800 km (Stern et al. 2003). To the west, the Mariana and Izu-Bonin arcs run parallel with the trenches. The Mariana BASC is

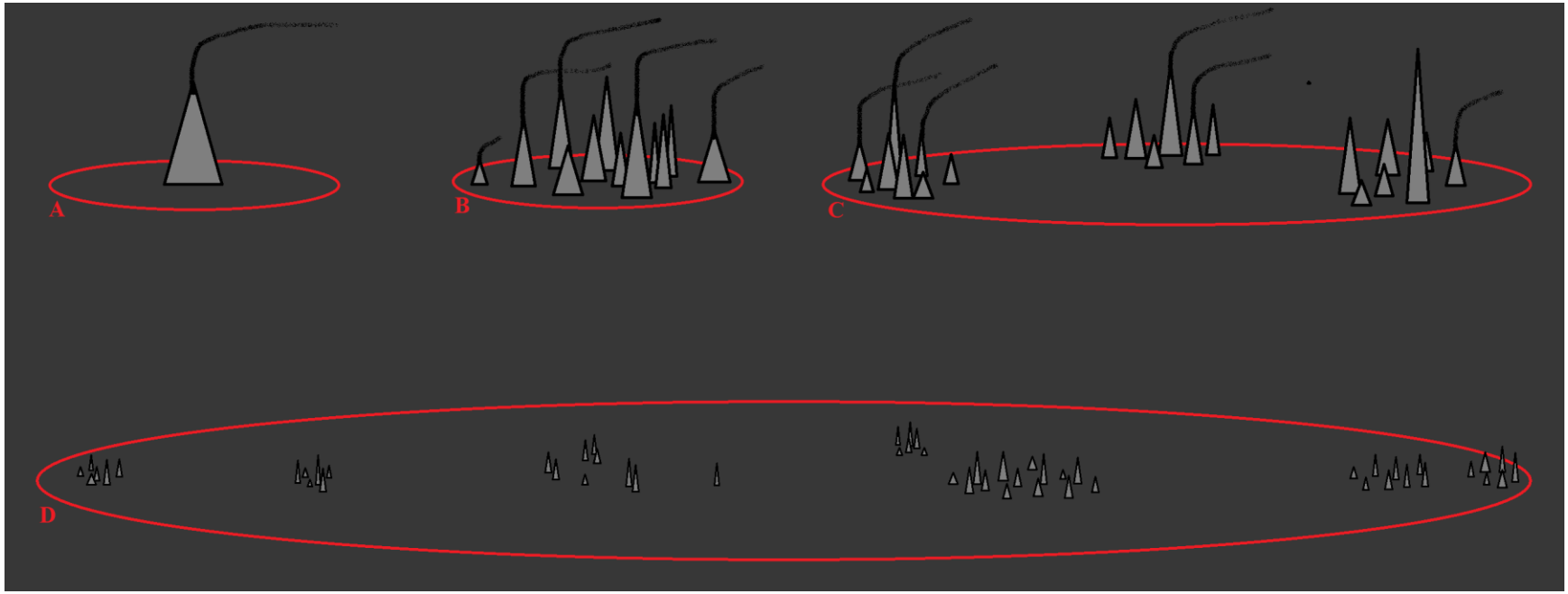

Figure 1. A visual representation of the habitat terms used in this study – scales relevant to Mariana BASC.

A. Single vent, circle diameter 10 to 30 m.
B. Vent field, circle diameter 30 to 300 m.
C. Vent site with three fields, circle diameter ~ 1 km.
D. Vent system with five sites, circle diameter ~ 500 km.

unique in the IBM system because, unlike the trenches and arcs, the BASC is only present on the Mariana portion of the IBM system in the south. The processes that sustain the magma beneath the BASC are different from those that sustain the magma beneath the arc. As the Pacific plate subducts beneath the Mariana arc and dehydrates, it hydrates the overlying mantle. This hydrated mantle then rises due to its buoyancy, providing the magma for the arc volcanoes (Stern et al. 2013). In contrast, the subduction of the Pacific plate stretches the Philippine plate, causing it to thin and fracture, creating the BASC. As the plate fractures, the reduced pressure on the underlying mantle causes it to rise and melt, which provides the magma for the BASC (Allaby, 2013).

The Mariana back-arc basin reaches a maximum depth of ~ 5km (Anderson et al. 2017), flanked by the West Mariana Ridge and the Mariana arc (Stern et al. 2003). A series of seafloor-spreading segments separated by strike-slip faults are present in the basin, roughly running parallel with the volcanic arc (Anderson et al. 2017). The northern-most and southern-most ends of this spreading axis lie closest to the arc, whereas the center is furthest from the arc. The spreading rates of the segments closer to the arc are faster than those of the segments further from the arc (Baker et al. 2017). Therefore, in the southern half of the BASC, the spreading rates of the segments decrease in a northward direction, ranging from an intermediate to slow spreading-rate (Mullineaux et al. 2018). Although the northern-most segment exhibits the geomorphology of an intermediate spreading rate, this area does not undergo seafloor spreading, but instead, is in the early, rifting stage of back-arc formation (Martínez et al. 1995; Yamazaki et al. 2003). Anderson et al. (2017) and Baker et al. (2017) outline four distinct types of spreading segment geomorphologies in the southern half of the BASC. These relate to the magmatic and

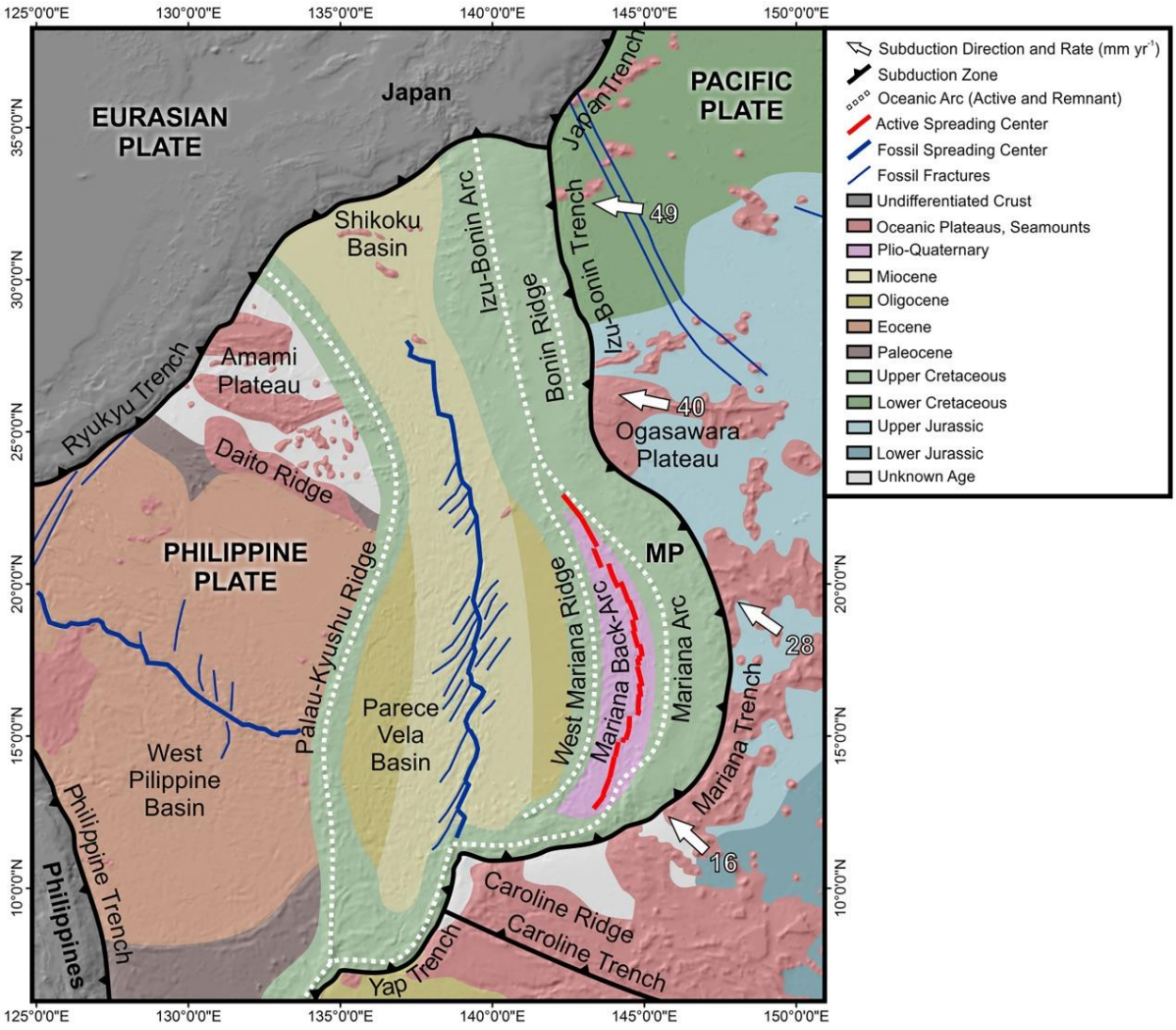

Figure 2. Geologic map of the Izu-Bonin Subduction Factory (Stern, Fouch, and Klemperer 2003) and the surrounding seafloor features, as presented by Anderson et al. (2017). The red lines illustrate the Mariana Back-Arc Spreading Centre where new seafloor is formed, flanked by the active Mariana Arc and the inactive West Mariana Ridge.

tectonic activity occurring within each of the segments, primarily expressed as the axial rises and valleys shaping their cross-sectional profiles (Anderson et al. 2017; Baker et al. 2017). Magmatic activity most strongly influences the southern-most segments; the proximity between the BASC and the arc causes the magma derived from hydration melting to mix with and enhance the magma derived from decompression melting (Stern et al. 2013; Pearce et al. 2005; Masuda and Fryer 2015), which has created a geomorphology with axial rises, but without valleys (Type 1;

Anderson et al. 2017). A similar phenomenon also occurs in other arc-BASC systems (e.g. Martinez and Taylor, 2002). Although the northern-most segments are not actively spreading, arc-derived magma still heavily influences these segments, as indicated by the notable similarity between arc-derived and BASC-derived lavas (Martínez et al. 1995). The arc-derived magma influences all BASC segments in the Mariana region, but its influence on segment geomorphology decreases with the distance between these two systems. Tectonic activity more strongly influences the central segments, which is reflected by their axial valleys of varying depths (Types 2-4; Anderson et al. 2017). As a result, the segments south of 13.7˚N are ~1 km shallower than those further to the north (Baker et al. 2017).

In regards to hydrothermal activity, vents are present along both the Mariana arc and BASC, and they represent distinctly separate systems within the Mariana Region; this is because their different magma sources cause the chemistry of their respective vents to differ substantially (Butterfield et al. in prep.). At the start of 2009, the U.S. Government established National Wildlife Refuges around all the vent sites known along the arc and BASC (Menini & Van Dover, 2019); these designated, circular areas center on each vent site and have a radius of one nautical mile. These protected vent sites are also a part of the larger Marianas Trench Marine National Monument. In the BASC, half of the known vent sites consist of multiple vent fields (Table 1). More vents are present along the southern spreading segments closest to the arc than those that are further away, suggesting that density of vents along the BASC relates to distance between the arc and the BASC as well (Baker et al. 2017); it is unclear if hydrothermal vents are present in the northern half of the Mariana BASC. Similar to the spreading rates, the arc-derived magma influencing the southern-most segments is likely driving the higher density of vents. The relatively high temperatures cause the crust in Type 1 segments near the arc to be too malleable

for deep faults to form (Anderson et al. 2017). Therefore, hydrothermal circulation can only occur at relatively shallow depths in the crust, which supports the conditions suitable for smaller vents to emerge in a relatively high density. In contrast, the crust of segments lying further from the arc is lower in temperature, allowing deep faults and hydrothermal circulation to occur, providing the conditions for larger vents to form, albeit, at a lower density (Anderson et al. 2017).

Tunnicliffe (1988) investigated the biogeography of vents, and many studies have since proposed several models to delineate the biogeographic provinces of the world's vents. Tunnicliffe and Fowler (1996) were the first to propose a model of global biogeographic provinces for vent habitats. They grouped all vent regions known in the West Pacific at the time as a single province, and Tunnicliffe (1997) revised this model to distinguish the Mariana and Okinawa regions as a distinct province separate from the other West Pacific regions. However, Van Dover et al. (2002) later regrouped all the West Pacific vent regions as a single province. As researchers continued to discover new vent sites, Bachraty et al. (2009) proposed an updated biogeographic model for vents using more rigorous statistical methods absent from the previous studies. Like the model outlined by Tunnicliffe (1997), they generated a model that separated the West Pacific vent regions into northern and southern provinces. However, they separated the Okinawa and Mariana BASC regions. The Northwest Pacific province included the Okinawa region with newly discovered vent sites along the Izu-Ogasawara Arc (part of the IBM system). The Southwest Pacific province is the largest in this model, and it groups the Mariana region with all the other western Pacific vent regions, plus the Loihi vent site off the Hawaiian coast and those in the Indian Ocean. Rogers et al. (2012) later revised this model; they removed the Indian Ocean and the Kermadec Arc from the large, Southwestern Pacific province. However, Moalic et

Table 1. The vent sites and characteristics examined in the Mariana BASC.

	Illium-Alice Springs	**Burke**	**Hafa Adai**	**Perseverance**	**Forecast**	**Snail**	**Archaean**	**Urashima-Pika**
Location	18˚12.71'N 144 ˚42.45'E	18˚10.95'N 144˚43.19'E	16˚57.68'N 144˚52.15'E	15˚28.80'N 144˚30.46'E	13˚23' N 143˚56'E	12˚57.20'N 143˚37.20'E	12˚56'N 143˚38'E	12˚55.10'N 143˚38.90'E
Depth (m)	3597	3630	3279	3910	1470	2850	2990	2846
Distance from the Arc (km)	109	108	101	97	23	11	8	6
Distance to Next Site South (km)	3.5	136.7	169.2	241.2	58.6	2.7	2.3	NA
Number of Fields Within Site	2 (Illium; Alice Springs)	1	2	1	1	2 (Snail; Yamanaka)	1	2 (Urashima; Pika)
Highest Temperature (˚C)	165 287 – end-member calculation (Ishibashi et al. 2015)	50	345	264	280 (Fujikura et al. 1997)	248 (Wheat et al. 2003)	345 (Yoshikawa et al. 2012)	330 (Urabe et al. 2004)
Active Smoker Structures	Absent	Absent	Present	Present	Present	Present	Present	Present
Description: Fluid delivery, substratum, community dominants	Clear, diffuse flow through basalt rubble and sulphides. Hairy snails dominate areas surrounding effluent. White anemones dominate the periphery.	Clear, diffuse flow through basalt rubble and sulphides. Barnacles dominate areas surrounding effluent. White anemones dominate the periphery.	Black, direct flow through sulphide structures. Clear, diffuse flow through sulphides. Shrimp and bythograeid crabs dominate areas surrounding effluent. Galatheids crabs dominate the periphery. Largest vent site in the Mariana BASC.	Clear, diffuse flow through sulphides and basalt cracks Shrimp dominate areas surrounding effluent and the periphery.	Clear, diffuse flow through basalt rubble and sulphides. Hairy snails dominate areas surrounding effluent. Galatheid crabs on periphery. Geologic setting in transition between Arc and BASC (Stern et al. 2013).	Clear, direct flow through sulphides. Clear, diffuse flow through basalt cracks. Hairy snails dominate areas surrounding effluent. Filamentous microbes.	Black and clear, direct flow through sulphides. Shrimp and bythograeid crabs dominate areas surrounding effluent. Galatheid crabs on periphery.	Black and clear, direct flow through sulphides. Sparse fauna and thick iron deposits. A lot of iron deposits and sparse macrofauna. White microbial mat.

al. (2011) created a biogeographic model using network theory that combined all the West Pacific vent regions into a single province once again. Despite the discrepancy between these various studies, it is clear that the faunal communities in the Mariana region are most similar to those in other West Pacific regions, which is consistent with the tectonic history (Tunnicliffe and Fowler 1996) and dispersal capabilities of vent larvae (Mitarai et al. 2016). However, every study proposing these biogeographic provinces do not include biological data from Mariana Arc vent sites; instead, these studies only include the vents in the Mariana BASC.

Hydrothermal Hunt Cruises:

In the winter of 2015, the *Research Vessel* (*R/V*) *Falkor* embarked on the first of the two-leg "Hydrothermal Hunt" mission to explore the Mariana region, and systematically searched the southern half of the BASC system for evidence of new vent sites using hydrothermal CTD casts and an autonomous underwater vehicle. The only sites previously discovered in the system are those in the southern BASC between 12.9˚N and 13.4˚N and in the central BASC on segment 18.2˚N (Anderson et al. 2017) (Figure 3). However, during this first leg, the research team identified potential new vent sites in the BASC between 12.8 and 18.2˚N. The purpose of the second leg of this mission was to confirm and explore the new sites using a remotely operated vehicle (ROV) and assess the biological, chemical and geological features. During the following winter, the *R/V Falkor* returned to the Mariana BASC with *ROV SuBastian* and documented the new vent sites named Hafa Adai (segment 17.0˚N) and Perseverance (segment 15.5˚N) (Anderson et al. 2017). The research team also explored the previously discovered sites in the central BASC (segment 18.2˚N); other researchers had visited the southern sites more recently (e.g. Yoshikawa et al. 2012) than those in the central BASC (e.g. Fujikura et al. 1997). During the second leg of this two-leg expedition, the ROV collected biological samples from all four

vent sites. My research goals focus on identifying the animals collected during the 2016 (second leg) Hydrothermal Hunt cruise and updating the Mariana BASC species list. These data then allow me to describe species distribution patterns among the sites. Chapter Two gives further detail on the objectives. In the process of identifying the collected animals, I highlight the discovery of a newly discovered shrimp species, *Rimicaris falkorae*. These specimens allow me to pursue the incidental goal of learning the process of species description. My morphological and genetic analyses contributed to the co-authored publication of this new species (Komai & Giguère, 2019) (Appendix 1).

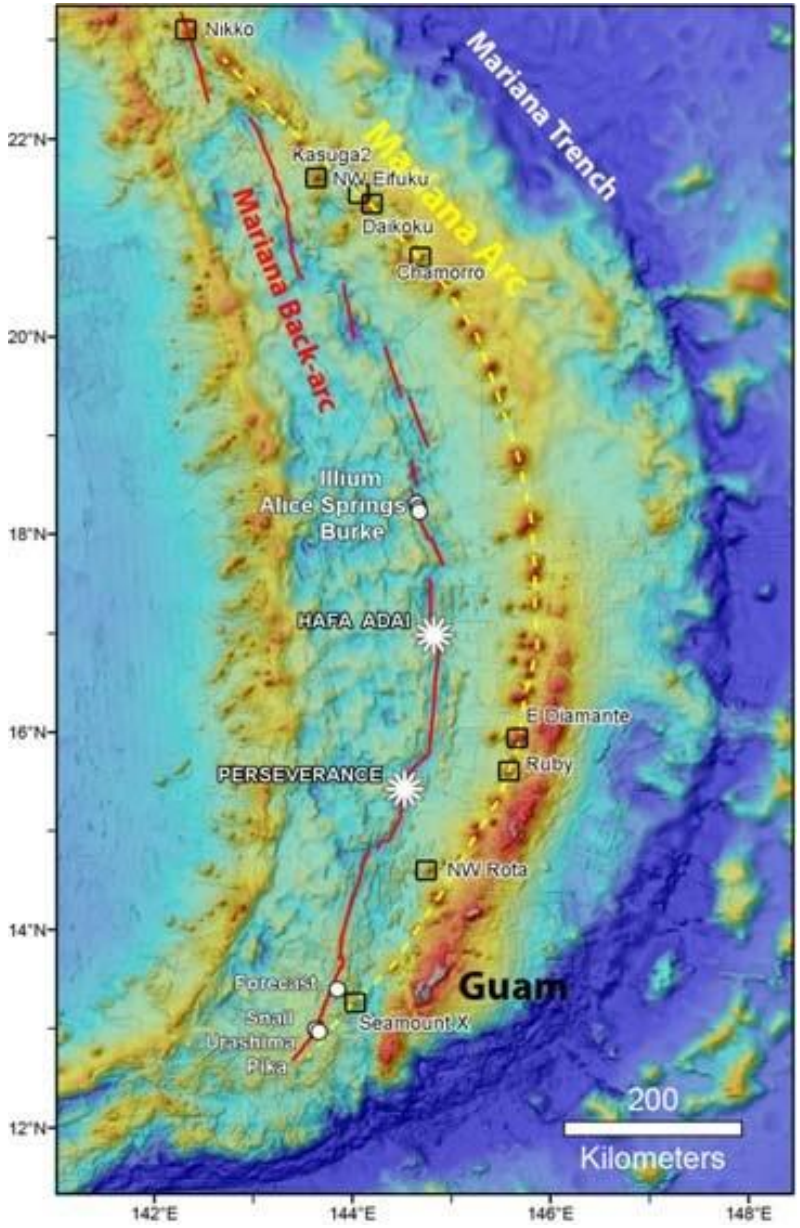

Figure 3. A bathymetric map of the Mariana region, indicating the locations of the vent sites present in the Mariana back-arc spreading centre (BASC) with circles and those on the Mariana volcanic arc with squares. The locations of the two newly discovered sites, Hafa Adai and Perseverance, are indicated by the star-shaped symbols. The red lines indicate the spreading axis of the BASC. The dashed yellow line indicates the volcanic arc. Courtesy Dr. W. Chadwick (Univ. Oregon/NOAA).

References:

Adams, D. K., Arellano, S. M., & Govenar, B. (2012). Larval dispersal: Vent life in the water column. *Oceanography, 25*(1), 256-268.

Allaby, M. (Ed.). (2013). *A dictionary of geology and earth sciences*: Oxford University Press.

Anderson, M. O., Chadwick Jr, W. W., Hannington, M. D., Merle, S. G., Resing, J. A., Baker, E. T., . . . Augustin, N. (2017). Geological interpretation of volcanism and segmentation of the Mariana back-arc spreading center between 12.7° N and 18.3° N. *Geochemistry, Geophysics, Geosystems, 18*(6), 2240-2274.

Anderson, M. O., Hannington, M. D., McConachy, T. F., Jamieson, J. W., Anders, M., Wienkenjohann, H., . . . Petersen, S. (2019). Mineralization and alteration of a modern seafloor massive sulfide deposit hosted in mafic volcaniclastic rocks. *Economic Geology, 114*(5), 857-896.

Bachraty, C., Legendre, P., & Desbruyères, D. (2009). Biogeographic relationships among deep-sea hydrothermal vent faunas at global scale. *Deep Sea Research Part I: Oceanographic Research Papers, 56*(8), 1371-1378.

Baker, E. T., Walker, S. L., Resing, J. A., Chadwick Jr, W. W., Merle, S. G., Anderson, M. O., . . . Michael, S. (2017). The effect of arc proximity on hydrothermal activity along spreading centers: New evidence from the Mariana Back Arc (12.7 N–18.3 N). *Geochemistry, Geophysics, Geosystems, 18*(11), 4211-4228.

Bates, A. E., Lee, R. W., Tunnicliffe, V., & Lamare, M. D. (2010). Deep-sea hydrothermal vent animals seek cool fluids in a highly variable thermal environment. *Nature Communications, 1*, 14.

Beaulieu, S. E., Baker, E. T., German, C. R., & Maffei, A. (2013). An authoritative global database for active submarine hydrothermal vent fields. *Geochemistry, Geophysics, Geosystems, 14*(11), 4892-4905.

Blackburn, T. M., & Gaston, K. J. (2002). Macroecology is distinct from biogeography. *Nature, 418*(6899), 723.

Büchi, L., & Vuilleumier, S. (2014). Coexistence of specialist and generalist species is shaped by dispersal and environmental factors. *The American Naturalist, 183*(5), 612-624.

Burgess, S. C., Baskett, M. L., Grosberg, R. K., Morgan, S. G., & Strathmann, R. R. (2016). When is dispersal for dispersal? Unifying marine and terrestrial perspectives. *Biological Reviews, 91*(3), 867-882.

Butterfield, D., Jonasson, I., Massoth, G., Feely, R., Roe, K., Embley, R., . . . Delaney, J. (1997). Seafloor eruptions and evolution of hydrothermal fluid chemistry. *Philosophical Transactions of the Royal Society of London. Series A: Mathematical, Physical and Engineering Sciences, 355*(1723), 369-386.

Calabrese, J. M., & Fagan, W. F. (2004). A comparison-shopper's guide to connectivity metrics. *Frontiers in Ecology and the Environment, 2*(10), 529-536.

Chapman, A. S., Beaulieu, S. E., Colaço, A., Gebruk, A. V., Hilario, A., Kihara, T. C., . . . Bates, A. E. (2019). sFDvent: A global trait database for deep-sea hydrothermal-vent fauna. *Global Ecology and Biogeography, 28*(11), 1538-1551.

Corliss, J. B., Dymond, J., Gordon, L. I., Edmond, J. M., von Herzen, R. P., Ballard, R. D., . . . van Andel, T. H. (1979). Submarine thermal springs on the Galapagos Rift. *Science, 203*(4385), 1073-1083.

Cowen, R. K., & Sponaugle, S. (2009). Larval dispersal and marine population connectivity. *Annual Review of Marine Science, 1*, 443-466.

Dahlhoff, E., O'Brien, J., Somero, G. N., & Vetter, R. D. (1991). Temperature effects on mitochondria from hydrothermal vent invertebrates: Evidence for adaptation to elevated and variable habitat temperatures. *Physiological Zoology, 64*(6), 1490-1508.

den Boer, P. (1968). Spreading of risk and stabilization of animal numbers. *Acta Biotheoretica, 18*(1), 165-194.

Distel, D. L., Baco, A. R., Chuang, E., Morrill, W., Cavanaugh, C., & Smith, C. R. (2000). Do mussels take wooden steps to deep-sea vents? *Nature, 403*(6771), 725.

Domeier, M. L., & Speare, P. (2012). Dispersal of adult black marlin (*Istiompax indica*) from a Great Barrier Reef spawning aggregation. *PLoS One, 7*(2), e31629.

Fisher, H. J. (2002). Macroecology: New, or biogeography revisited? *Nature, 417*(6891), 787-787.

France, S. C., Hessler, R. R., & Vrijenhoek, R. C. (1992). Genetic differentiation between spatially-disjunct populations of the deep-sea, hydrothermal vent-endemic amphipod *Ventiella sulfuris*. *Marine Biology, 114*(4), 551-559.

Fujikura, K., Yamazaki, T., Hasegawa, K., Tsunogai, U., Stern, R. J., Ueno, H., . . . Okutani, T. (1997). Biology and earth scientific investigation by the submersible "Shinkai 6500" system of deep-sea hydrothermal and lithosphere in the Mariana back-arc basin. *JAMSTEC Journal of Deep Sea Research, 13*, 1-20.

Gamo, T., Ishibashi, J., Tsunogai, U., Okamura, K., & Chiba, H. (2013). Unique geochemistry of submarine hydrothermal fluids from arc-back-arc settings of the western Pacific. In *Back-Arc Spreading Systems: Geological, Biological, Chemical, and Physical Interactions* (pp. 147-161): Wiley.

Gaston, K. J. (1996). Species-range-size distributions: Patterns, mechanisms and implications. *Trends in Ecology & Evolution, 11*(5), 197-201.

Gaston, K. J., & Blackburn, T. M. (1996). Range size-body size relationships: Evidence of scale dependence. *Oikos 75*(3), 479-485.

Gauthier, O., Sarrazin, J., & Desbruyères, D. (2010). Measure and mis-measure of species diversity in deep-sea chemosynthetic communities. *Marine Ecology Progress Series, 402*, 285-302.

Goffredi, S., Hurtado, L., Hallam, S., & Vrijenhoek, R. (2003). Evolutionary relationships of deep-sea vent and cold seep clams (Mollusca: Vesicomyidae) of the "*pacifica/lepta*" species complex. *Marine Biology, 142*(2), 311-320.

Goffredi, S. K., Johnson, S., Tunnicliffe, V., Caress, D., Clague, D., Escobar, E., . . . Vrijenhoek, R. (2017). Hydrothermal vent fields discovered in the southern Gulf of California clarify role of habitat in augmenting regional diversity. *Proceedings of the Royal Society B: Biological Sciences, 284*(1859), 20170817.

Guzman, H. M., Gomez, C. G., Hearn, A., & Eckert, S. A. (2018). Longest recorded trans-Pacific migration of a whale shark (*Rhincodon typus*). *Marine Biodiversity Records, 11*(1), 8.

Hanski, I., & Gilpin, M. (1991). Metapopulation dynamics: Brief history and conceptual domain. *Biological Journal of the Linnean Society, 42*(1-2), 3-16.

Hashimoto, J., Ohta, S., Gamo, T., Chiba, H., Yamaguchi, T., Tsuchida, S., . . . Kitazawa, M. (2001). First hydrothermal vent communities from the Indian Ocean discovered. *Zoological Science, 18*(5), 717-722.

Hashimoto, J., & Okutani, T. (1994). Four new mytilid mussels associated with deepsea chemosynthetic communities around Japan. *Venus (Japanese Journal of Malacology), 53*(2), 61-83.

Hekinian, R., Francheteau, J., Renard, V., Ballard, R., Choukroune, P., Cheminee, J., . . . Boulegue, J. (1983). Intense hydrothermal activity at the axis of the east pacific rise near 13˚N: Submersible witnesses the growth of sulfide chimney. *Marine Geophysical Researches, 6*(1), 1-14.

Hessler, R. R., & Lonsdale, P. F. (1991). Biogeography of Mariana Trough hydrothermal vent communities. *Deep Sea Research Part A. Oceanographic Research Papers, 38*(2), 185-199.

Hilario, A., Capa, M., Dahlgren, T. G., Halanych, K. M., Little, C. T., Thornhill, D. J., . . . Glover, A. G. (2011). New perspectives on the ecology and evolution of siboglinid tubeworms. *PLoS One, 6*(2), e16309.

Hügler, M., & Sievert, S. M. (2011). Beyond the Calvin cycle: Autotrophic carbon fixation in the ocean. *Annual Review of Marine Science, 3*, 261-289.

Itescu, Y. (2019). Are island-like systems biologically similar to islands? A review of the evidence. *Ecography, 42*(7), 1298-1314.

Johnson, K. S., Childress, J. J., Hessler, R. R., Sakamoto-Arnold, C. M., & Beehler, C. L. (1988). Chemical and biological interactions in the Rose Garden hydrothermal vent field, Galapagos

spreading center. *Deep Sea Research Part A. Oceanographic Research Papers, 35*(10-11), 1723-1744.

Johnson, S. B., Warén, A., Tunnicliffe, V., Dover, C. V., Wheat, C. G., Schultz, T. F., & Vrijenhoek, R. C. (2015). Molecular taxonomy and naming of five cryptic species of *Alviniconcha* snails (Gastropoda: Abyssochrysoidea) from hydrothermal vents. *Systematics and Biodiversity, 13*(3), 278-295.

Johnson, S. B., Warén, A., & Vrijenhoek, R. C. (2008). DNA barcoding of *Lepetodrilus* limpets reveals cryptic species. *Journal of Shellfish Research, 27*(1), 43-52.

Jones, M. L. (1985). On the Vestimentifera, new phylum: Six new species, and other taxa, from hydrothermal vents and elsewhere. *Bulletin of the Biological Society of Washington, 6*, 117-158.

Kelley, D. S., Karson, J. A., Blackman, D. K., FruÈh-Green, G. L., Butterfield, D. A., Lilley, M. D., . . . the AT3-60 Shipboard Party (2001). An off-axis hydrothermal vent field near the Mid-Atlantic Ridge at 30˚N. *Nature, 412*(6843), 145-149.

Koschinsky, A., Garbe-Schönberg, D., Sander, S., Schmidt, K., Gennerich, H.-H., & Strauss, H. (2008). Hydrothermal venting at pressure-temperature conditions above the critical point of seawater, 5˚S on the Mid-Atlantic Ridge. *Geology, 36*(8), 615-618.

Krylova, E. M., & Sahling, H. (2010). Vesicomyidae (Bivalvia): Current taxonomy and distribution. *PLoS One, 5*(4), e9957.

Kumar, R., & Kumar, V. (2018). A review of phylogeography: Biotic and abiotic factors. *Geology, Ecology, and Landscapes, 2*(4), 268-274.

Leis, J. (1984). Larval fish dispersal and the East Pacific Barrier. *Océanographie Tropicale, 19*(2), 181-192.

Lester, S. E., Ruttenberg, B. I., Gaines, S. D., & Kinlan, B. P. (2007). The relationship between dispersal ability and geographic range size. *Ecology Letters, 10*(8), 745-758.

Ludwig, K. A., Kelley, D. S., Butterfield, D. A., Nelson, B. K., & Früh-Green, G. (2006). Formation and evolution of carbonate chimneys at the Lost City Hydrothermal Field. *Geochimica et Cosmochimica Acta, 70*(14), 3625-3645.

Lutz, R. A., Desbruyères, D., Shank, T. M., & Vrijenhoek, R. C. (1998). A deep-sea hydrothermal vent community dominated by Stauromedusae. *Deep Sea Research Part II: Topical Studies in Oceanography, 45*(1-3), 329-334.

MacArthur, R., & Wilson, E. (1967). The theory of island biogeography. *Monograph Population Biology, 1*.

Macpherson, E. (2003). Species range size distributions for some marine taxa in the Atlantic Ocean. Effect of latitude and depth. *Biological Journal of the Linnean Society, 80*(3), 437-455.

Mainali, K. P., Warren, D. L., Dhileepan, K., McConnachie, A., Strathie, L., Hassan, G., . . . Parmesan, C. (2015). Projecting future expansion of invasive species: Comparing and improving methodologies for species distribution modeling. *Global Change Biology, 21*(12), 4464-4480.

Mandrak, N. E., & Crossman, E. (1992). Postglacial dispersal of freshwater fishes into Ontario. *Canadian Journal of Zoology, 70*(11), 2247-2259.

Marcus, J. (2003). *Community ecology of hydrothermal vents at Axial Volcano, Juan de Fuca Ridge, northeast Pacific* (Doctoral dissertation).

Martin, J. W., & Haney, T. A. (2005). Decapod crustaceans from hydrothermal vents and cold seeps: A review through 2005. *Zoological Journal of the Linnean Society, 145*(4), 445-522.

Martínez, F., Fryer, P., Baker, N. A., & Yamazaki, T. (1995). Evolution of backarc rifting: Mariana Trough, 20–24 N. *Journal of Geophysical Research: Solid Earth, 100*(B3), 3807-3827.

Martinez, F., & Taylor, B. (2002). Mantle wedge control on back-arc crustal accretion. *Nature, 416*(6879), 417.

Masuda, H., & Fryer, P. (2015). Geochemical characteristics of active backarc basin volcanism at the southern end of the Mariana Trough. In *Subseafloor Biosphere Linked to Hydrothermal Systems* (pp. 261-273): Springer, Tokyo.

McArthur, A., & Tunnicliffe, V. (1998). Relics and antiquity revisited in the modern vent fauna. *Geological Society, London, Special Publications, 148*(1), 271-291.

McGillicuddy Jr, D., Lavelle, J. W., Thurnherr, A. M., Kosnyrev, V., & Mullineaux, L. S. (2010). Larval dispersion along an axially symmetric mid-ocean ridge. *Deep Sea Research Part I: Oceanographic Research Papers, 57*(7), 880-892.

McHugh, D. (1997). Molecular evidence that echiurans and pogonophorans are derived annelids. *Proceedings of the National Academy of Sciences, 94*(15), 8006-8009.

McMullin, E. R., Bergquist, D. C., & Fisher, C. R. (2007). Metazoans in extreme environments: Adaptations of hydrothermal vent and hydrocarbon seep fauna. *Gravitational and Space Research, 13*(2), 13-24.

Menini, E. & Van Dover, C. L. (2019). An atlas of protected hydrothermal vents. *Marine Policy, 108*, 103654.

Mitarai, S., Watanabe, H., Nakajima, Y., Shchepetkin, A. F., & McWilliams, J. C. (2016). Quantifying dispersal from hydrothermal vent fields in the western Pacific Ocean. *Proceedings of the National Academy of Sciences, 113*(11), 2976-2981.

Moalic, Y., Desbruyères, D., Duarte, C. M., Rozenfeld, A. F., Bachraty, C., & Arnaud-Haond, S. (2011). Biogeography revisited with network theory: Retracing the history of hydrothermal vent communities. *Systematic Biology, 61*(1), 127-137.

Mullineaux, L. S., Metaxas, A., Beaulieu, S. E., Bright, M., Gollner, S., Grupe, B. M., . . . Won, Y. -J. (2018). Exploring the ecology of deep-sea hydrothermal vents in a metacommunity framework. *Frontiers in Marine Science, 5*(49).

Mullineaux, L. S., Mills, S. W., Sweetman, A. K., Beaudreau, A. H., Metaxas, A., & Hunt, H. L. (2005). Vertical, lateral and temporal structure in larval distributions at hydrothermal vents. *Marine Ecology Progress Series, 293*, 1-16.

Nelson, D., Hagen, K., & Edwards, D. (1995). The gill symbiont of the hydrothermal vent mussel *Bathymodiolus thermophilus* is a psychrophilic, chemoautotrophic, sulfur bacterium. *Marine Biology, 121*(3), 487-495.

Oliver, M. J., & Irwin, A. J. (2008). Objective global ocean biogeographic provinces. *Geophysical Research Letters, 35*(15), L15601.

Pearce, J. A., Stern, R. J., Bloomer, S. H., & Fryer, P. (2005). Geochemical mapping of the Mariana arc-basin system: Implications for the nature and distribution of subduction components. *Geochemistry, Geophysics, Geosystems, 6*(7).

Petersen, J. M., Ramette, A., Lott, C., Cambon-Bonavita, M. A., Zbinden, M., & Dubilier, N. (2010). Dual symbiosis of the vent shrimp *Rimicaris exoculata* with filamentous gamma-and epsilonproteobacteria at four Mid-Atlantic Ridge hydrothermal vent fields. *Environmental Microbiology, 12*(8), 2204-2218.

Pineda, J., Porri, F., Starczak, V., & Blythe, J. (2010). Causes of decoupling between larval supply and settlement and consequences for understanding recruitment and population connectivity. *Journal of Experimental Marine Biology and Ecology, 392*(1-2), 9-21.

Posadas, P., Crisci, J. V., & Katinas, L. (2006). Historical biogeography: A review of its basic concepts and critical issues. *Journal of Arid Environments, 66*(3), 389-403.

Rodríguez, E., & Daly, M. (2010). Phylogenetic relationships among deep-sea and chemosynthetic sea anemones: Actinoscyphiidae and Actinostolidae (Actiniaria: Mesomyaria). *PLoS One, 5*(6), e10958.

Rogers, A. D., Tyler, P. A., Connelly, D. P., Copley, J. T., James, R., Larter, R. D., . . . Zwirglmaier, K. (2012). The discovery of new deep-sea hydrothermal vent communities in the Southern Ocean and implications for biogeography. *PLoS Biology, 10*(1), e1001234.

Rosenzweig, M. L. (1995). *Species diversity in space and time*: Cambridge University Press.

Samadi, S., Quéméré, E., Lorion, J., Tillier, A., von Cosel, R., Lopez, P., . . . Boisselier-Dubayle, M.-C. (2007). Molecular phylogeny in mytilids supports the wooden steps to deep-sea vents hypothesis. *Comptes Rendus Biologies, 330*(5), 446-456.

Schulte, P. M. (2015). The effects of temperature on aerobic metabolism: Towards a mechanistic understanding of the responses of ectotherms to a changing environment. *Journal of Experimental Biology, 218*(12), 1856-1866.

Sen, A., Podowski, E. L., Becker, E. L., Shearer, E. A., Gartman, A., Yücel, M., . . . Fisher, C. R. (2014). Community succession in hydrothermal vent habitats of the eastern Lau Spreading Center and Valu Fa Ridge, Tonga. *Limnology and Oceanography, 59*(5), 1510-1528.

Shields, J. D., & Segonzac, M. (2007). New nemertean worms (Carcinonemertidae) on bythograeid crabs (Decapoda: Brachyura) from Pacific hydrothermal vent sites. *Journal of Crustacean Biology, 27*(4), 681-692.

Smith, C. R., Baco, A. R., & Glover, A. G. (2002). Faunal succession on replicate deep-sea whale falls: Time scales and vent-seep affinities. *Cahiers de Biologie Marine, 43*(3/4), 293-298.

Stern, R. J., Fouch, M. J., & Klemperer, S. L. (2003). An overview of the Izu-Bonin-Mariana subduction factory. *Inside the subduction factory, 138*, 175-222.

Stern, R. J., Tamura, Y., Masuda, H., Fryer, P., Martinez, F., Ishizuka, O., & Bloomer, S. H. (2013). How the Mariana Volcanic Arc ends in the south. *Island Arc, 22*(1), 133-148.

Stevens, C. J., Limén, H., Pond, D. W., Gélinas, Y., & Juniper, S. K. (2008). Ontogenetic shifts in the trophic ecology of two alvinocaridid shrimp species at hydrothermal vents on the Mariana Arc, western Pacific Ocean. *Marine Ecology Progress Series, 356*, 225-237.

Stohr, S., & Segonzac, M. (2006). Two new genera and species of ophiuroid (Echinodermata) from hydrothermal vents in the East Pacific. *Species Diversity, 11*(1), 7-32.

Suzuki, Y., Kojima, S., Watanabe, H., Suzuki, M., Tsuchida, S., Nunoura, T., . . . Horikoshi, K. (2006). Single host and symbiont lineages of hydrothermal-vent gastropods *Ifremeria nautilei* (Provannidae): Biogeography and evolution. *Marine Ecology Progress Series, 315*, 167-175.

Taylor, P. D., Fahrig, L., Henein, K., & Merriam, G. (1993). Connectivity is a vital element of landscape structure. *Oikos*, 571-573.

Terui, A., & Miyazaki, Y. (2015). A "parasite-tag" approach reveals long-distance dispersal of the riverine mussel *Margaritifera laevis* by its host fish. *Hydrobiologia, 760*(1), 189-196.

Tsurumi, M. (2003). Diversity at hydrothermal vents. *Global Ecology and Biogeography, 12*(3), 181-190.

Tsurumi, M., & Tunnicliffe, V. (2001). Characteristics of a hydrothermal vent assemblage on a volcanically active segment of Juan de Fuca Ridge, northeast Pacific. *Canadian Journal of Fisheries and Aquatic Sciences, 58*(3), 530-542.

Tunnicliffe, V. (1988). Biogeography and evolution of hydrothermal-vent fauna in the eastern Pacific Ocean. *Proceedings of the Royal Society of London. Series B. Biological Sciences, 233*(1272), 347-366.

Tunnicliffe, V. (1997). Hydrothermal vents: A global ecosystem. *JAMSTEC Journal of Deep Sea Research*, 105-110.

Tunnicliffe, V., & Fowler, C. M. R. (1996). Influence of sea-floor spreading on the global hydrothermal vent fauna. *Nature, 379*(6565), 531-533.

Tunnicliffe, V., McArthur, A. G., & McHugh, D. (1998). A biogeographical perspective of the deep-sea hydrothermal vent fauna. In *Advances in Marine Biology* (Vol. 34, pp. 353-442): Academic Press.

Van Dover, C. L., German, C., Speer, K. G., Parson, L., & Vrijenhoek, R. (2002). Evolution and biogeography of deep-sea vent and seep invertebrates. *Science, 295*(5558), 1253-1257.

Vanreusel, A., Van den Bossche, I., & Thiermann, F. (1997). Free-living marine nematodes from hydrothermal sediments: similarities with communities from diverse reduced habitats. *Marine Ecology Progress Series, 157*, 207-219.

Vrijenhoek, R. C. (2009). Cryptic species, phenotypic plasticity, and complex life histories: Assessing deep-sea faunal diversity with molecular markers. *Deep Sea Research Part II: Topical Studies in Oceanography, 56*(19-20), 1713-1723.

Weber, R. E., Hourdez, S., Knowles, F., & Lallier, F. (2003). Hemoglobin function in deep-sea and hydrothermal-vent endemic fish: *Symenchelis parasitica* (Anguillidae) and *Thermarces cerberus* (Zoarcidae). *Journal of Experimental Biology, 206*(15), 2693-2702.

Whittaker, R. H. (1960). Vegetation of the Siskiyou Mountains, Oregon and California. *Ecological Monographs, 30*(3), 279-338.

Yahagi, T., Kayama Watanabe, H., Kojima, S., & Kano, Y. (2017). Do larvae from deep-sea hydrothermal vents disperse in surface waters? *Ecology, 98*(6), 1524-1534.

Yamazaki, T., Seama, N., Okino, K., Kitada, K., Joshima, M., Oda, H., & Naka, J. (2003). Spreading process of the northern Mariana Trough: Rifting-spreading transition at 22°N. *Geochemistry, Geophysics, Geosystems, 4*(9).

Yoshikawa, S., Okino, K., & Asada, M. (2012). Geomorphological variations at hydrothermal sites in the southern Mariana Trough: Relationship between hydrothermal activity and topographic characteristics. *Marine Geology, 303*, 172-182.

Zhou, Y., Zhang, D., Zhang, R., Liu, Z., Tao, C., Lu, B., . . . Wang, C. (2018). Characterization of vent fauna at three hydrothermal vent fields on the Southwest Indian Ridge: Implications for biogeography and interannual dynamics on ultraslow-spreading ridges. *Deep Sea Research Part I: Oceanographic Research Papers, 137*, 1-12.

Chapter 2: Diversity Distribution of Hydrothermal Vent Fauna

Introduction:

Beta Diversity:

Ecologists use a variety of β-diversity indices to measure pairwise dissimilarity between biotic assemblages; the results then provide a way to identify species richness and distribution patterns across space or time. Although no single β-diversity measure is universally applicable and there is still debate on the β-diversity measures that are most appropriate for different research questions and datasets, many existing indices are sufficient for identifying the broad differences between sites or samples (Tuomisto, 2010). Several of the first β-diversity measures developed for ecological studies, like the Jaccard index and the simple matching coefficient, are relatively simple in their mathematical formulas (Anderson et al. 2011). They provide direct proportions of shared species between pairs of sites or samples, and ecologists still use many of these measures in modern studies, especially the Jaccard index. However, these simple β-diversity measures have some limitations.

Biotic assemblages can vary in their number of species (α-diversity) and they can vary because they contain different species (Baselga 2010); often, both species richness and composition differences are responsible for the dissimilarity between assemblages. However, as simple measures of β-diversity cannot separate the relative contributions of richness and composition, more complex measures are able to partition these components, called ‘turnover’ and ‘nestedness’ (e.g. Baselga, 2010; Legendre, 2014; Soininen et al. 2018). Turnover only measures compositional differences and nestedness only measures richness differences; by partitioning these two components, researchers can gain insight into the mechanisms that drive the disparity between sites or samples.

Null model-based measures of β-diversity are an alternative to those that partition the turnover and nestedness components. The Raup-Crick index is one example, and, like turnover, it only measures compositional differences between pairs of assemblages (Chase et al. 2011). Using this index with a simple β-diversity measure, such as the Jaccard index, can reveal the relative influence that the species richness (α-diversity) component has on the overall dissimilarity. For example, Anderson et al. (2011) use both the Jaccard (β_J) and Raup-Crick (β_{RC}) indices to measure the temporal change in β-diversity of coral reef transects before and after an El Niño event. After this disturbance event occured, they found that the α-diversity of the transects greatly decreased, the β_J-diversity of the reef significantly increased and the β_{RC}-diversity did not significantly change. Given that species richness only influences the β_J-diversity, these results indicate that the El Niño event created a disturbance that non-selectively reduced the α-diversity of the transects, rather than selecting for disturbance-tolerant coral species.

Furthermore, the Raup-Crick index helps to infer the relative influences that stochastic and deterministic community assembly processes have in shaping the dissimilarity between sites (Chase et al. 2011). Unlike most β-diversity indices, the Raup-Crick index does not directly measure the proportion of shared species between a pair of sites. Instead, using a null model, it calculates the estimated probability that the observed number of shared species, or fewer, would occur randomly. As outlined by Chase et al. (2011), the null expectation is that stochastic assembly processes shape the diversity dissimilarity patterns, so the β_{RC} values that fall beyond the 95% confidence intervals of the null model indicate significant deviation from the null expectation, which suggests that deterministic factors are likely responsible for the observed disparity in species instead.

The factors that shape β-diversity patterns differ in their proportional influence at different spatial scales; for example, historical connectivity largely drives global-scale, biogeographic patterns, but has little to do with smaller-scale patterns. In benthic habitats, habitat variability positively correlates with β-diversity on spatial scales ranging from 10s of meters (e.g. Hewitt et al. 2005) to 10s of kilometers (e.g. Ellingsen, 2002; Bergquist et al. 2003); in hydrothermal vent habitats, abiotic conditions can be highy variable at these spatial scales. On the smallest spatial scale (i.e. individual vents), faunal zonation patterns reflect thermal and chemical gradients associated with hydrothermal fluids, thus driving intra-vent scale species differences (e.g. Gebruk et al. 1997; Sen et al. 2013). With increasing spatial scales, vent habitats can become increasingly more variable. For example, chimney structures in vent sites along the Mid-Atlantic Ridge (MAR) are mostly composed of sulfides and release hot and highly acidic fluids (e.g. Douville et al. 2002). However, one vent site in the MAR hosts carbonate chimneys releasing relatively cool and highly alkaline fluids (Kelley et al. 2001). This degree of habitat variability among vent sites drives high β-diversity; this is also clear in the Gulf of California where both sulfide and carbonate chimneys are also present (Goffredi et al. 2017). However, researchers have not yet investigated β-diversity patterns of vent habitats on a system-wide spatial scale that include all known vent sites.

Tectonic features also impose broad environmental differences in vent sites on an intra-oceanic scale. Given that hydrothermal activity requires a magma source, vent sites are located on mid-ocean ridges (MORs), volcanoes and BASCs (Baker et al. 2016; Levin et al. 2016). However, the magma sources and their associated hydrothermal habitats broadly differ among these three tectonic features (Keith et al. 2017). For example, hydration melting driven by subducted oceanic crust provides the magma that induces hydrothermal circulation on a volcanic

arc, whereas decompression melting driven by seafloor spreading provides the magma that supports BASC-hosted vent systems (Sleep 1975; Stern et al. 2003). The chemical composition of the magma differs between these two different sources, which influence their associated hydrothermal activity; arc-hosted vents exhibit greater variability in fluid chemistry than those located in BASCs (Keith et al. 2017). The magma from arcs can also influence their associated BASCs, depending on proximity (Baker et al. 2017), whereas MORs are not influenced by arc volcanoes. The depth variability of arc-hosted vents is also much greater than that of BASC or MOR-hosted vents. Overall, it is possible that the β-diversity of vent sites along any discrete tectonic structure will reflect the behaviour of their underlying heat source.

*Mariana BASC Hydrothermal Vents***:**

Researchers have only explored the southern half (~600km) of the Mariana BASC in search of active hydrothermal vents. The first vent site discoveries in this system occurred in 1987; they included the Illium-Alice Springs and Burke sites (Figures 3 & 4), plus an additional unnamed site 20 km south of Burke (Hessler and Lonsdale, 1991). They are all located on the 18.2˚N segment (Anderson et al. 2017). In 1992, the Forecast vent site, located ~80km west of Guam, was the next site discovered. Its off-axis location on a seamount led researchers to initially classify Forecast as an Arc-hosted vent site (Embley et al. 2007). However, Stern et al. (2013) demonstrate that its geologic setting is in transition between the Mariana Arc and BASC with a mixed magma supply. Despite this transitional state, Kojima and Watanabe (2015) indicate that the Forecast fauna more closely resemble those of the BASC-hosted vents than the arc-hosted vents.

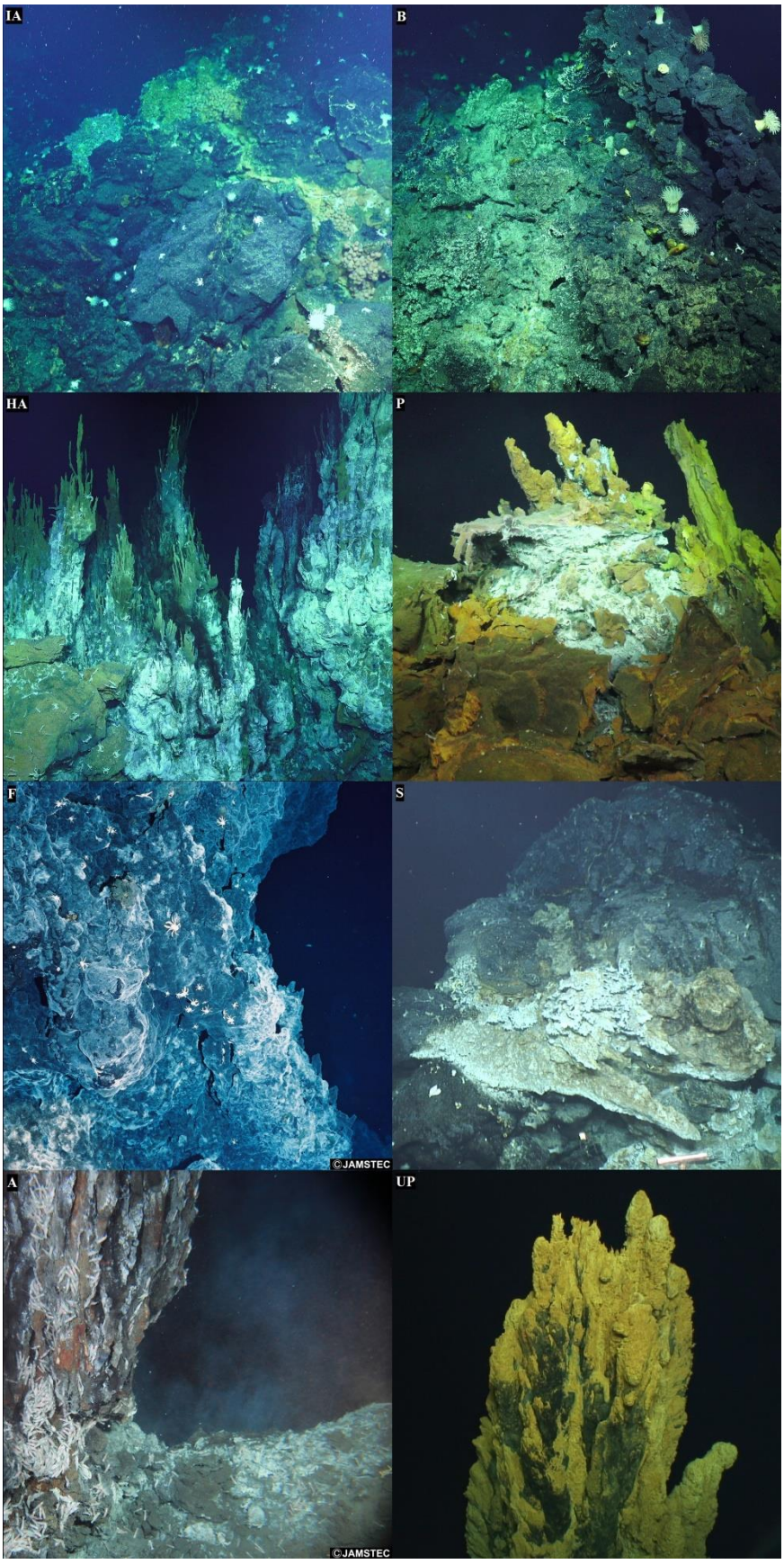

Figure 4. Photo plate of each vent site explored in the Mariana BASC. The letters in the top-left corner of each image indicates the vent site identities. The vent sites are ordered from northern-most to southern-most. (IA) Illium-Alice Springs: The image is from the Illium vent field on Dec 5, 2016. (B) Burke: The image is from Dec 7, 2016. (HA) Hafa Adai (new site): The image is from the Alba vent field on Dec 8, 2016. (P) Perseverance (new site): The image is from the Leaning Tower vent field on Dec 16, 2016. (F) Forecast: The image is from Oct 17, 1993, and was captured by the Japan Agency for Marine-Earth Science and Technology (JAMSTEC). (S) Snail: The image is from Dec 1, 2014, and was captured during the Submarine Ring of Fire – Iron Man cruise. (A) Archaean: The image is from Oct 4, 2010, and was captured by the JAMSTEC. (UP) Urashima-Pika: The image is from the Urashima vent field on Dec 18, 2014, and was captured during the Submarine Ring of Fire – Iron Man cruise.

Researchers discovered many more vent sites in the southern Mariana BASC between 1999 and 2010, both on and off the axis of the spreading center. Among these southern vent sites, biologists surveyed the faunal assemblages in Snail, Archaean and Urashima-Pika (Figures 3 & 4). In 2015, the first leg of the Hydrothermal Hunt expedition surveyed the water column above the southern and central Mariana BASC in search of more hydrothermal vent sites. These surveys lead to the discovery of two new vent sites: Hafa Adai and Perseverance (Baker et al. 2017; Trembath-Reichert et al. 2019). In total, researchers have conducted biological surveys in eight Mariana BASC vent sites, spanning the full southern-most 600km of the Mariana BASC (Figures 3 & 4).

*Mariana BASC Vent Fauna***:**

Hessler and Lonsdale (1991) provide the first vent-obligate taxon list for the Mariana BASC system. They collected a total of 28 taxa from the Illium-Alice Springs and Burke sites; 23 (82%) of them represented new species discoveries at the time. They photographed another two taxa, indicating the presence of at least 30 vent-obligate species. After the discovery of the Forecast vent site, Fujikura et al. (1997) expanded the list to a total of 36 taxa. However, there are only two species-level identities for these six new taxa, and they are both designated *con forma* (cf.) to indicate the uncertainty of their identities (Bengtson, 1988); therefore, they did not confirm any new species discoveries. They also report that 17 (47%) of the taxa are present in both the Forecast and Illium-Alice Springs sites.

Subsequent studies contributed to the identification of a few Mariana BASC species (e.g. Johnson et al. 2008; Fujita et al. 2009), suggesting that 93% of the taxa originally collected by Hessler and Lonsdale (1991) represent new species discoveries. The discovery and biological

surveys of the Snail, Archaean and Urashima-Pika vent sites in the south contributed to the growing taxon list, bringing it to 51 taxa (Kojima & Watanabe, 2015). However, the 15 additional taxa collected during these surveys do not yet have species-level identities, thus novelty is not known. It also seems likely that some novel taxa that Kojima & Watanabe (2015) report represent previously identified taxa, resulting in alternative reports of the same species. Nonetheless, Kojima & Watanabe (2015) document all reported locations and provide the first list of vent species in the Snail, Archaean and Urashima-Pika vent sites.

*Objectives***:**

With the discovery of the Hafa Adai and Perseverance vent sites, the biological samples presented in this study provide an opportunity to expand diversity discoveries within this hydrothermal vent system initiated by Hessler and Lonsdale (1991), Fujikura et al. (1997) and Kojima and Watanabe (2015). The central position of these two new vent sites also provides an excellent opportunity to explore the distribution patterns of the vent fauna along the continuous spreading ridge of the central and southern Mariana BASC.

My first objective is to identify the species present at the Illium-Alice Springs, Burke, Hafa Adai and Perseverance vent sites, with a focus on the two newly discovered locations. My second objective is to examine the distribution of species among all known vent sites in this system. The null hypothesis is that species composition is the same along the BASC; alternatively, both species richness and composition may differ. My third objective is to explore some abiotic variables that could be driving the α- and β-diversity patterns in the Mariana BASC using the available environmental data. My fourth objective is to compare the β-diversity structure of the Mariana BASC to those of the Juan de Fuca Ridge (Northeast Pacific) and the

adjacent Mariana Arc. Given that Arc-hosted vents exhibit greater variability in fluid chemistry and depth than those hosted by MORs or BASCs, I hypothesize that the vent habitat heterogeneity is greater in arc systems. Based on the positive relationship between β-diversity and habitat heterogeneity generally observed in benthic habitats (e.g. Astorga et al. 2014), I predict that β-diversity is higher in the Mariana Arc system on average compared to the Mariana BASC and Juan de Fuca Ridge systems.

Methods:

*Sampling Locations***:**

R/V Falkor visited the Mariana BASC in winter, 2016 (Dec. 1 – 18), to conduct the FK161129 (Hydrothermal Hunt – Part 2) cruise. Using the remotely operated vehicle (ROV) *SuBastian*, the researchers sought to characterize the biology, geochemistry and geology of the hydrothermal vent habitats in the central Mariana BASC. They explored and collected biological samples from three previously known vent fields - Illium, Alice Springs and Burke - and the two newly discovered sites (Table 1). ROV *SuBastian* explored these locations across ten dives, each lasting approximately seven to eight hours. However, some dives lasted for only four hours and one dive was abandoned after an hour and a half due to technical issues.

*Sample Collection***:**

At the direction of the onboard biologists, the ROV *SuBastian* pilots used two techniques to collect the biological samples. “Grabs” included retrieval of sessile and sedentary animals attached to loose substratum using either the manipulator claw or a scoop held in the claw; the samples were placed into closable “bioboxes”. “Slurps” included retrieval of mobile animals using the suction sampler; the samples were stored in a series of swivelling jars mounted on the

ROV. Due to time limitations and other objectives, it was not possible for the ROV pilots to retrieve the fauna in a quantitative manner, and instead, they retrieved them opportunistically and haphazardly. Most biological samples came from within and directly adjacent to focused and diffuse hydrothermal fluid flowing through basalt and sulphide. Some samples also came from the periphery of these vent habitats. In total, they collected 31 biological samples from eight of the ten dives. Using the HD Multi SeaCam 6150 and the SULIS 4K cameras mounted on the ROV, all the dives were also video recorded in both HD and 4K resolution.

*Sample Processing and Identification***:**

Once the biological samples reached the ship deck, the onboard biologists roughly sorted and preserved them in either 80% ethanol or 7% buffered formalin. Back at the University of Victoria, a lab technician initially separated the macrofauna from the meiofauna using a 1 mm sieve. I then sorted them into apparent "same-species" groups. To determine the taxonomic identities of the specimens, I first compared their morphologies to the published descriptions of species reported from the Mariana BASC vent sites. Once I identified those species in the collection, I compared the remaining specimens to the published descriptions of morphologically similar species documented in the literature from other oceanic regions. Using this method, I assigned each specimen to the lowest taxonomic classification possible. However, I could not identify every specimen to the species-level using this method alone.

I extracted tissue samples from 12 taxa and sent them to the Barcode of Life Database (BoLD) facility at the University of Guelph to have a portion of their cytochrome *c* oxidase subunit I (COI) gene sequenced (Ratnasingham and Hebert, 2007). The BoLD facility used a variety of primers to extract these sequences (Appendix 2). As an additional identification tool, I

compared the sequences provided by the BoLD facility to those of closely related species available in the GenBank database (Clark et al. 2016). BoLD had success with 92% of the taxa sent and 72% of the specimens sent. However, even with the sequencing success, matches to known sequences were uncommon. In some cases, when neither morphological nor molecular analyses could identify specimens to the species level, I sent specimens to taxonomic experts to assist with the identification. Using the taxa identified in the collection, I created a preliminary taxon occurrence table (Appendix 3).

*Determination of a New Shrimp Species***:**

As there is some confusion in the literature on shrimp identities in the western Pacific vents, I sent tissue samples (abdominal muscle) from 119 *Rimicaris* shrimp collected from the Illium-Alice Springs, Burke, Hafa Adai and Perseverance vent sites, and 25 *Rimicaris* shrimp collected from the Forecast vent site during a previous cruise to the BoLD facility. Using the BoLD software, I aligned the available sequences and generated a similarity tree using the neighbour-joining method and the Kimura-2-Parameter (K2P) distance model for the pairwise estimates of genetic divergence (Kimura, 1980; Ratnasingham and Hebert, 2007).

I acquired COI sequences of other Alvinocaridid shrimp species from the GenBank database to compare with those provided by BoLD. Using the MEGA-X software, I generated nucleotide distance trees comparing these sequences using both the neighbour joining and maximum likelihood methods (Kumar et al. 2018). I used the K2P distance model with 1000 replicate bootstrap values for both trees (Kimura, 1980) (Appendix 4). Using the ‘ape’ package in R, I performed a nucleotide dissimilarity analysis to identify the average percent dissimilarity of the COI sequences between each species (Paradis and Schliep, 2018; R Core Team 2019). I

subsequently compared the morphology of the shrimp to identify the features that distinguish the clades. I then sent samples to the taxonomic expert, Dr. T. Komai, to confirm my results.

*Distributions of Species***:**

I reviewed the FK161129 video footage from eight of the nine ROV dives that collected specimens to supplement the preliminary taxon occurrence data derived from the samples; due to technical issues, the footage from one dive was unavailable for viewing. I also reviewed video footage available from previous cruises that explored some of the southern vent sites: MGLN02MV (Ring of Fire) cruise in 2006 ("Forecast" – Segment 13.3˚N) and RR1413 (Ironman) cruise in 2014 ("Snail" and "Urashima" – Segment 12.8˚N). It is clear from the video that the onboard researchers did not collect every species present during the dives. Therefore, I conservatively added the species I could confidently identify in the video to the taxon occurrence data (Appendix 3).

To supplement these data, I reviewed all the available literature that report the taxa present in all the known hydrothermal vent sites in the Mariana BASC. These papers include initial species descriptions from the system (e.g. Okutani and Ohta, 1988; Martin, 1990) and papers reporting taxon occurrence lists (e.g. Fujikura et al. 1997; Kojima and Watanabe, 2015). Literature review is especially important for occurrence data from the southern vent sites since the FK161129 cruise did not contribute information for those locations. Communication with other researchers also provided minor additions to the occurrence data for the Mariana BASC vent fauna. Using all the data from the samples, video, literature and personal communication, I compiled a full taxon occurrence list (Appendix 5).

*Data Processing***:**

Once I had assigned identities to all the taxa, I made a scatter plot illustrating the taxa to species ratio for each grab and slurp sample collected on the 2016 cruise in R. Using the 'vegan' package, I generated rarefaction curves for each of the central Mariana BASC vent sites and the combined data using the 'rarecurve' function (Hurlbert, 1971; Oksanen et al. 2013). I excluded all the taxa collected from the Snail Graveyard because they likely include taxa that are not endemic to vent habitats. This tool compensates for differences in the number of specimens collected when comparing the taxon richness of the vent sites (Raup, 1975). Curve shapes indicate the likelihood that the samples represent all the taxa present in the vent sites; curves reaching an asymptote indicate that the samples likely represent all the taxa present in the vent sites, and those that do not reach the asymptote indicate that the samples likely do not represent all the taxa present in the sites.

For the diversity indices and data analyses, I reduced the data in Appendix 5 to create a presence-absence table that includes only macrofauna that I have confirmed to be a single species. I excluded taxa that may represent multiple species in the analysis as they could cause the faunal assemblages of the vent sites to seem more similar than they are. I confirmed that some taxa without species-level identities do represent a single species, and thus, they are also included in the presence-absence table. As sampling and sorting effort of meiofauna is inconsistent across the vent sites, I also exclude this group from the analysis. Meiofauna are present in the samples collected from the central BASC vent sites, but previous studies of the vent fauna in this system have largely ignored the meiofauna (but see Humes, 1990). Since the presence-absence data are binary, I also exclude species represented by singletons and doubletons to avoid over-emphasis of their ecological relevance.

*Data Analysis***:**

I determined the local (α-diversity) and regional (γ-diversity) species richness by enumerating species on the presence-absence table. Researchers often define local and regional diversity using different spatial scales depending on the context of the study (e.g. Tsurumi, 2003; Zhou et al. 2018). In this study, α-diversity represents the number of species present in each vent site. A 'vent site' is a collection of hydrothermally active locations that lie within 1.5 km of each other. Thus, the Alice Springs and Illium vent fields, only ~350 m apart, are combined, as are the Pika and Urashima fields in the south. In this study, I define the Mariana BASC as a single 'system' given the distinct geological nature of this hydrothermal setting (Stern et al. 2003).

The pairwise dissimilarities in species composition among the vent sites in the Mariana BASC system represent β-diversity. Using the 'vegan' package in R, I calculated two types of β-diversity indices: the Jaccard (β_J) index (Jaccard, 1912) and the Raup-Crick (β_{RC}) index (Raup and Crick, 1979). Here, I calculated the β_{RC}-diversity using the modified Raup-Crick index based on the methods outlined by Chase et al. (2011) (Oksanen et al. 2013; R Core Team, 2019).

The Jaccard index is one of the most widely used dissimilarity indices in ecological studies that use presence-absence data. It measures β-diversity (β_J) as the direct pairwise proportion of species shared between sites and excludes joint absences. Exclusion of joint-absences is typically preferred, unless their inclusion is informative to the objective of the study, such as those that investigate changes in communities over time (Anderson et al. 2011). For this study, it is not informative to include joint-absences because I cannot be sure that the species absences are real, due to the haphazard sampling. The Jaccard index simply divides the number of species shared between a pair of sites (sites A and B) by the total number of species present in both sites (1). This gives a measure of similarity on a scale from 0 to 1; to get a measure of dissimilarity, I subtracted the similarity value from one. One of the major limitations of the

Jaccard index is that it does not account for differences in α-diversity between sites or samples relative to the γ-diversity. Larger pairwise differences in α-diversity automatically result in larger β_J values, which can imply that the pair of sampling locations are more dissimilar in species composition than they are (Anderson et al. 2011; Chase et al. 2011).

$$Jaccard\ (A, B) = 1 - \frac{|A \cap B|}{|A \cup B|} \quad (1)$$

The Raup-Crick index is an increasingly common index that emphasizes the species composition component of β-diversity (β_{RC}) by controlling for pairwise differences in α-diversity. The β_{RC}-diversity uses a null model approach based on the hypothesis that random assembly is solely responsible for the differences in species composition between a pair of sites. To calculate a β_{RC} value, the α-diversity of the given pair of sites, their observed β_J value, the regional species pool and the relative frequency of all the species among all the sites in the region are all required. Using the 'raupcrick()' function of the 'vegan' package, species are randomly drawn from the regional species pool for both sites to create a pair of hypothetical species assemblages (Chase et al. 2011); once a species is drawn, it is removed from the pool for the following draws so that it is not drawn again (Raup and Crick, 1979), which is repeated until the hypothetical α-diversity matches the observed α-diversity for each site. The likelihood of drawing each species is also proportional to their relative frequency in the region. The 'raupcrick()' function then calculates a hypothetical β_J value using the two hypothetical assemblages; I programmed the 'raupcrick()' function to repeat these steps and create 9999 hypothetical β_J values for each β_{RC} value. By comparing the observed β_J-diversity to the distribution of these hypothetical β_J values randomly generated from the regional species pool,

the β_{RC}-diversity indicates the probability that the observed β_J values falls outside a designated confidence interval on the curve.

As discussed by Chase et al. (2011), converting the β_{RC} values to a scale between negative one and positive one is useful for interpreting the results. The proximity of the β_{RC} values to zero expresses the likelihood that the observed β_J-diversity would occur randomly; values close to zero indicate that the dissimilarities between sites are likely to occur randomly and those close to negative or positive one signify that the dissimilarities are unlikely to occur randomly. Values that fall beyond the 95% confidence intervals (CIs) of the null model demonstrate significant deviation from the null expectation. The β_{RC} values also express faunal dissimilarities between sites relative to the null model; negative values indicate greater similarity than expected by random chance and positive values signify greater dissimilarity than expected by random chance. Although ecologists broadly define β-diversity as a measure of biotic variability between sites or samples, it is important to emphasize that β_J- and β_{RC}-diversity have different definitions and researchers should not compare them as if they represent the same information.

To explore the relationships between the diversity indices (α-, β_J- and β_{RC}-diversity) and some environmental characteristics of the vent sites (Table 1), I generated linear regression models using R (R Core Team, 2019). The explanatory variables I used are isolation, depth, and distance from the volcanic arc. Given the isolated nature of vents, they are a suitable habitat to test the species-isolation relationship proposed for islands by MacArthur and Wilson (1967). Therefore, in the models I generated for the α-diversity data, I defined isolation as the distance of each vent site from the next closest site; I derived these distances from their geographic coordinates presented in the cruise reports. Given that β-diversity values are assigned to pairs of

sites or samples, here, I defined isolation as the distance between each pair of vent sites in the regression models generated for the β-diversity data. Depth is a significant environmental gradient that drives strong vertical patterns in oceanic communities (Somero 1992), and thus, may also exist in vents (e.g. Desbruyères et al. 2000). The depth values I used for the α-diversity models are those present in the cruise reports and subsequent studies (e.g. Kojima and Watanabe, 2015). For the β-diversity models, I calculated the differences in depth between each pair of vent sites.

The distance of the BASC from the volcanic arc is, at least in part, responsible for the topographic settings of the vent sites. The spreading ridges closer to the arc at the southern Mariana BASC form distinct axial rises (Type 1 in Anderson et al. 2017), whereas further from the arc, spreading ridges are characterized by deep axial valleys (Types 2-4 in Anderson et al. 2017; Stern et al. 2013; Yoshikawa et al. 2012). This broad difference in topography could influence the number of larval immigrants settling in these sites. Similar to the dynamics presented by Thomson et al. (2003) on the Juan de Fuca Ridge, vent sites within valleys may experience a greater settlement rate of immigrant larvae because the valley walls constrain ocean currents; in contrast, vent sites on axial highs would not benefit from constrained flow. Therefore, based on the same principle proposed in the species-area relationship (MacArthur and Wilson, 1967), that higher immigration rates support greater species richness, I would expect that vent sites within valleys tend to support more species than those on axial highs. I calculated the distance from the volcanic arc using the geographic coordinates of each vent site and the volcanic arc axis (Anderson et al. 2017) for the α-diversity models. For the β-diversity models, I defined distance from the arc as the difference in this distance between each pair of vent sites.

For the α-diversity models, I generated both simple and multiple regression models using every combination of dependent and independent variables to determine the strength of the correlations. For the β-diversity models, I only generated simple regression models using each independent variable, as suggested by Anderson et al. (2011). Using the adjusted R^2 values, I chose a subset of models that best explained the variability in the dependent variables. I checked to confirm that these models do not violate the assumptions of simple and multiple linear regressions. I selected the best models based on their conformation to these assumptions, their adjusted R^2 values and a small sample Akaike Information Criterion (AICc) (Hu, 2007). Details for assumption tests and model selection are outlined in Appendix 6.

Using the species presence-absence data available in Butterfield et al. (in prep.) and Chapman et al. (2019), I also calculated the β_J- and β_{RC}-diversity among vent sites of the Mariana Volcanic Arc and Juan de Fuca Ridge to compare with the Mariana BASC system. Using the 'average' method in the 'hclust' function of the 'vegan' package in R, I generated dendrograms using the β_J-diversity matrices for each system to visualize the dissimilarity in species composition among their vent sites (Oksanen et al. 2013; R Core Team, 2019). To specifically compare the β_J- and β_{RC}-diversity between the Mariana BASC and Arc vent systems, I combined the species presence-absence data of the vent sites from both systems and calculated their combined β_J- and β_{RC}-diversity values. To illustrate these β_J- and β_{RC}-diversity values, I also generated non-metric multi-dimensional scaling (NMDS) plots using the 'metaMDS' function from the 'vegan' package (Appendix 6). To determine if there is a significant difference in β-diversity between the Mariana systems, I performed a permutation dispersion analysis. I calculated the distance-to-centroid values using the 'betadisper', 'anova' and 'permutest' functions from the 'vegan' package in R to ultimately obtain *F* ratios and *P* values for each β-

diversity index (Oksanen et al. 2013; R Core Team, 2019). The Juan de Fuca Ridge region is not included in the permutation dispersion analysis.

Results:

*Taxa Identified from the Sample Collection***:**

*Features of the Biological Collection***:**

Forty three distinct taxa are present among the collected samples; I have assigned species-level identities to twenty four (53%) of these taxa (Tables 2 & 3). They are all benthic invertebrates and arthropods compose the majority (47%). Molluscs and annelids comprise 44% collectively, whereas the remaining 9% consists of cnidarians, nematodes and ciliophorans. In total, 1,951 specimens are present in the samples; five species represent 45% of the collection. The barnacle *Neoverruca bachylepadoformis* is the most abundant species (14%), but the gastropods *Alviniconcha hessleri*, *Provanna nassariaeformis*, *Desbruyeresia marianaensis* and *Lepetodrilus* aff. *schrolli* MT collectively comprise another 31%. Singletons and doubletons represent eight of the taxa in the collection, but it is clear in the video footage that two of these taxa are common in some vent sites: *Phymorhynchus wareni* and *Marianactis bythios*. Macrofauna (size 1 – 200 mm) dominate the samples; the meiofauna (size 64 – 1000 μm) constitute only 20% of the identified taxa and 9% of the collection.

Reliance on Taxonomic Identification Methods:

Morphological comparison was sufficient to confidently identify the majority of the taxa to the levels assigned (Tables 2 & 3). Molecular comparison of the partial COI sequences also proved useful in some cases. The taxonomic experts provided the most reliable identities for

Table 2. Taxonomic and identification information for the taxa collected during the FK161129 (Hydrothermal Hunt) cruise (2016). Size class: 1 = meiofauna; 2 = macrofauna. Identification Methods: 1 = identified using morphological features; 2 = identified using partial COI gene sequences; 3 = identified by taxonomic experts using morphological features and/or genetic sequencing. New species are presented in bold in the "Species" column. The taxonomic names prefixed with 'cf.' (con forma) are the most likely identities based on the evidence, but they are not certain. Those prefixed with 'aff.' is similar to 'cf.', but represents greater certainty.

Phylum	Class	Upper Taxon	Family	Species	Authority	Size Class	Identification Methods	Certainty
Arthropoda	Malacostraca	Decapoda	Alvinocarididae	*Rimicaris vandoverae*	Martin & Hessler (1990)	2	1, 2	High
Arthropoda	Malacostraca	Decapoda	Alvinocarididae	*Rimicaris* cf. *variabilis*	Komai & Tsuchida (2015)	2	1, 2, 3	High
Arthropoda	Malacostraca	Decapoda	Alvinocarididae	***Rimicaris falkorae***	Komai & Giguère (2019)	2	1, 2, 3	High
Arthropoda	Malacostraca	Decapoda	Bythograeidae	*Austinograea williamsi*	Hessler & Martin (1989)	2	1	High
Arthropoda	Hexanauplia	Cirripedia	Neoverrucidae	*Neoverruca brachylepadoformis*	Newman (1989)	2	1, 2	High
Arthropoda	Hexanauplia	Cirripedia	Eolepadidae	***Vulcanolepas* nov sp.**	Watanabe (in prep.)	2	1, 3	High
Arthropoda	Hexanauplia	Copepoda: Siphonostomatoida	Dirivultidae	*Chasmatopontius thescalus*	Humes (1990)	1	1	High
Arthropoda	Hexanauplia	Copepoda: Siphonostomatoida	Dirivultidae	Unknown sp.		1	1	High
Arthropoda	Hexanauplia	Copepoda: Harpacticoida	Miraciidae	Unknown sp.		1	1	Medium/High
Arthropoda	Hexanauplia	Copepoda: Harpacticoida	Laophontidae	Unknown sp.		1	1	Medium/High
Arthropoda	Hexanauplia	Copepoda: Harpacticoida	Unknown	Unknown sp.		1	1	High
Arthropoda	Hexanauplia	Copepoda: Cyclopoida	Cyclopinidae	Unknown sp.		1	1	Medium/High
Arthropoda	Hexanauplia	Copepoda: Unknown	Unknown	Unknown sp.		1	1	High
Arthropoda	Arachnida	Acari	Halacaridae	*Copidognathus*	Dr. Gerald	1	1, 3	High

				papillatus	Krantz (pers. comm.)			
Arthropoda	Pycnogonida	Pantapoda	Ammotheidae	*Sericosura cochleifovea*	Child (1989)	2	1, 3	High
Mollusca	Bivalvia	Mytilida	Mytilidae	*Bathymodiolus septemdierum*	Hashimoto & Okutani (1994)	2	1	High
Mollusca	Gastropoda	Caenogastropoda	Provannidae	*Alviniconcha hessleri*	Okutani & Ohta (1988)	2	1, 3	High
Mollusca	Gastropoda	Caenogastropoda	Provannidae	*Provanna nassariaeformis*	Okutani (1990)	2	1	Medium
Mollusca	Gastropoda	Caenogastropoda	Provannidae	*Desbruyeresia marianaensis*	Okutani (1990)	2	1, 2	Medium/High
Mollusca	Gastropoda	Caenogastropoda	Raphitomidae	*Phymorhynchus wareni*	Dr. Nicholas Puillandre (pers. comm.)	2	1, 3	High
Mollusca	Gastropoda	Vetigastropoda	Lepetodrilidae	*Lepetodrilus* aff. *schrolli* MT	Johnson et al. (2008)	2	1, 2	High
Mollusca	Gastropoda	Vetigastropoda	Lepetodrilidae	*Pseudorimula marianae*	McLean (1989)	2	1	High
Mollusca	Gastropoda	Patellogastropoda	Pectinodontidae	*Bathyacmaea* sp.	Dr. Lothar Beck (pers. comm.)	2	1, 3	High
Mollusca	Gastropoda	Neritimorpha	Phenacolepadidae	***Shinkailepas* nov. sp.**	Dr. Yasunori Kano (pers. comm.)	2	1, 3	High
Mollusca	Gastropoda	Neomphaliones	Neomphalidae	*Symmetromphalus regularis*	McLean (1990)	2	1	High
Mollusca	Aplacophora	Unknown	Unknown	Unknown sp.	Dr. Verena Tunnicliffe (pers. comm.)	1	1, 3	High
Annelida	Polychaeta	Errantia	Polynoidae	*Levensteiniella raisae*	Pettibone (1989)	2	1	High
Annelida	Polychaeta	Errantia	Polynoidae	*Lepidonotopodium minutum*	Pettibone (1989)	2	1	High
Annelida	Polychaeta	Errantia	Polynoidae	*Branchinotogluma marianus*	Pettibone (1989)	2	1	High

Annelida	Polychaeta	Errantia	Hesionidae	*Sirsoe hessleri*	Blake (1991)	2	1	Medium/High
Annelida	Polychaeta	Sedentaria	Spionidae	cf. *Prionospio* sp.		2	1	Medium/High
Annelida	Polychaeta	Sedentaria	Alvinellidae	*Paralvinella hessleri*	Desbruyeres & Laubier (1982)	2	1	High
Annelida	Polychaeta	Sedentaria	Ampharetidae	***Amphisamytha* nov. sp.**	Dr. Greg Rouse (pers. comm.)	2	1, 3	High
Cnidaria	Anthozoa	Actinaria	Kadosactinidae	*Marianactis bythios*	Fautin & Hessler (1989)	2	1	Medium
Cnidaria	Anthozoa	Zoantharia	Epizoanthidae	*Epizoanthus* cf. nov. sp.	Dr. James Reimer (pers. comm.)	2	1, 3	High
Nematoda	Unknown	Unknown	Unknown	Unknown sp.		1	1	High
Ciliophora	Heterotrichea	Heterotrichida	Folliculinidae	cf. *Folliculinopsis* sp.	Dr. Verena Tunnicliffe (pers. comm.)	1	1, 3	High

Table 3. Taxonomic and identification information for the taxa collected from the Snail Graveyard location (16˚57.70'N, 144˚52.15'E) at the Hafa Adai vent site during the FK161129 (Hydrothermal Hunt) cruise (2016). Size class: 1 = meiofauna; 2 = macrofauna. Identification Methods: 1 = identified using morphological features; 2 = identified using partial COI gene sequences; 3 = identified by taxonomic experts using morphological features and/or genetic sequencing.

Phylum	Class	Upper Taxon	Family	Species	Authority	Size Class	Identification Methods	Certainty
Arthropoda	Malacostraca	Decapoda	Munidopsidae	*Munidopsis* cf. nov. sp.		2	1	High
Arthropoda	Malacostraca	Amphipoda	Synopiidae	Unknown sp.	Dr. Tammy Horton (pers. comm.)	1	1, 3	High
Arthropoda	Malacostraca	Amphipoda	Pardaliscidae	*Princaxelia* sp.	Dr. Tammy Horton (pers. comm.)	1	1, 3	High
Arthropoda	Malacostraca	Isopoda	Munnopsidae	*Ilyarachna* sp.	Dr. Tammy Horton (pers. comm.)	1	1, 3	High
Arthropoda	Hexanauplia	Copepoda: Siphonostomatoida	Dirivultidae	Unknown sp.		1	1	High
Arthropoda	Hexanauplia	Copepoda: Harpacticoida	Miraciidae	Unknown sp.		1	1	Medium/High
Arthropoda	Hexanauplia	Copepoda: Harpacticoida	Laophontidae	Unknown sp.		1	1	Medium/High
Arthropoda	Hexanauplia	Copepoda: Harpacticoida	Unknown	Unknown sp.		1	1	High
Arthropoda	Hexanauplia	Copepoda: Cyclopoida	Cyclopinidae	Unknown sp.		1	1	Medium/High
Arthropoda	Hexanauplia	Copepoda: Unknown	Unknown	Unknown sp.		1	1	High
Arthropoda	Pycnogonida	Pantapoda	Ammotheidae	*Sericosura* sp.	Dr. Claudia Arango (pers. comm.)	2	1, 3	High
Annelida	Polychaeta	Sedentaria	Maldanidae	*Nicomache* sp.		2	1	High
Nematoda	Unknown	Unknown	Unknown	Unknown sp.		1	1	High

difficult taxa, which include one family-level, five genus-level and eight species-level identities. However, I am less confident in some assigned identities, such as the various copepod taxa.

*Undescribed Species***:**

New discoveries have emerged from the samples. The molecular comparison of the partial COI sequences from the *Rimicaris* shrimp revealed three distinct species in the Mariana BASC (Figure 5). The most common is *R. vandoverae*, originally described from the vents on Segment 18.2˚N (Martin, 1990; Anderson et al. 2017). A single sequence from the Forecast vent site differed from the *R. vandoverae* specimens by ~6%, but matched very closely (~2% dissimilar) to those of *R. variabilis* (GenBank Accession Numbers KT948642 – KT948644), a species described from the southwest Pacific. However, morphological differences are present between *R. variabilis* and this unknown species, so it is unclear if they are the same species (Komai, pers. comm.); for now, I have labelled this species *R.* cf. *variabilis*. Morphological comparison of all the collected shrimp revealed that this species is present among every known vent site in the central Mariana BASC (Appendix 3). Others have also collected this species from the Snail and Urashima-Pika vent sites in the southern BASC (Watanabe, pers. comm.).

GenBank contains COI sequences from seven of the eight known *Rimicaris* species, and none matched closely with those of the third shrimp species in the Mariana BASC (Table 4; Appendix 5), suggesting it is an undescribed species. After morphological inspection, I discovered many features that differentiate this species from the rest (Table 5). After consultation with Dr. T. Komai, he confirmed and expanded my diagnosis. The new species, *Rimicaris falkorae*, is illustrated in Figure 6 (Komai and Giguère, 2019); see Appendix 1. *R. falkorae* is morphologically most similar to other *Rimicaris* species, but the COI sequences match most closely with those of *Shinkaicaris leurokolos* (Table 4).

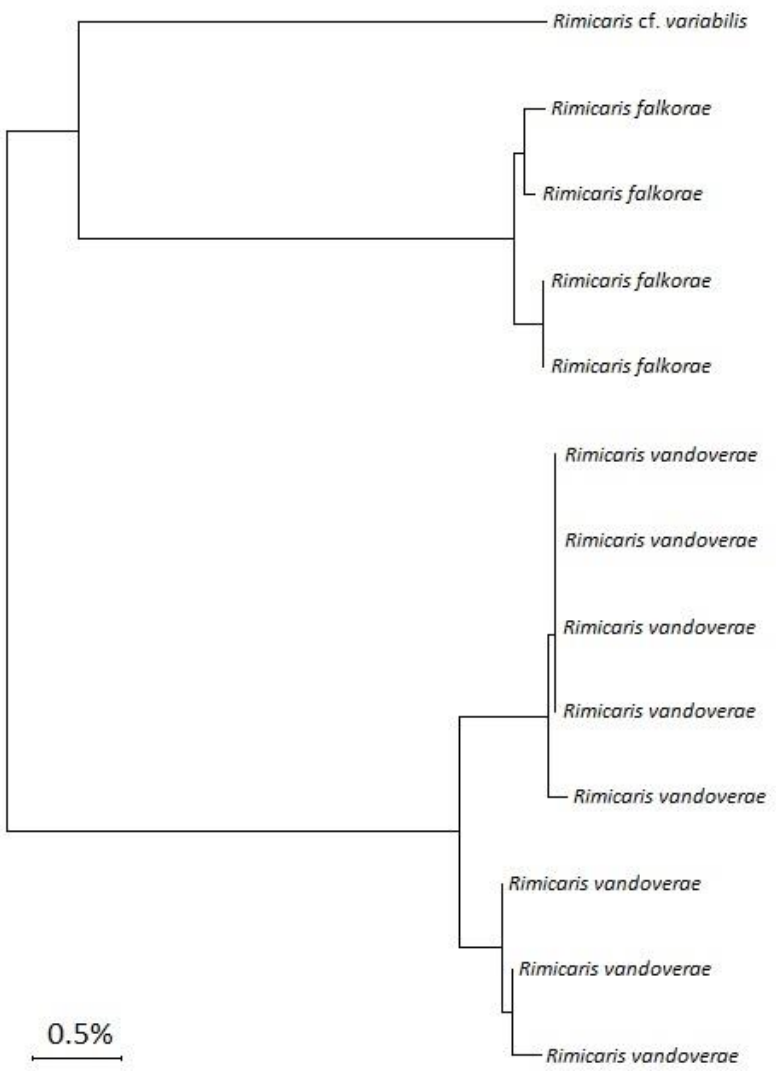

Figure 5. COI dissimilarity tree between the three species of *Rimicaris* collected from the central Mariana BASC vent sites on the FK161129 cruise.

Taxonomic experts have recognized three more new species from this collection: a *Vulcanolepas* barnacle (Watanabe, in prep.), a *Shinkailepas* limpet (Kano, pers. comm.) (Figure 7) and an *Amphisamytha* polychaete (Rouse, pers. comm.) (Table 2). Other potentially new species are also present, but confirmations from taxonomic experts are required. The taxa I assigned with the "cf." nomenclature indicate that their assigned identities may be correct, but are uncertain (Bengtson, 1988). For example, I have assigned "cf. nov. sp." to the *Epizoanthus*

Table 4. Percent differences in COI nucleotide sequences between Alvinocarididae shrimp species.

	R. falkorae	*R. vandoverae*	*R. hybisae*	*R. chacei*	*Opaepele loihi*	*R. kairei*	*R. exoculata*	*R. parva*	*R. variabilis*	*S. leurokolos*
R. vandoverae	7.48%									
R. hybisae	8.20%	11.9%								
R. chacei	8.08%	12.0%	0.10%							
O. loihi	8.50%	12.3%	4.49%	4.38%						
R. kairei	7.96%	9.50%	8.64%	8.52%	10.1%					
R. exoculata	7.59%	8.36%	8.76%	8.88%	10.1%	1.35%				
R. parva	7.01%	7.64%	10.5%	10.4%	11.7%	9.59%	9.21%			
R. variabilis	7.23%	7.96%	11.1%	11.0%	10.9%	10.3%	9.90%	7.56%		
S. leurokolos	5.70%	6.71%	10.8%	10.6%	10.6%	7.67%	7.16%	6.55%	5.74%	
Mirocaris fortunata	20.6%	20.4%	20.0%	20.0%	20.8%	19.7%	18.8%	19.8%	19.3%	20.3%

Table 5. Morphological differences between the three *Rimicaris* species present among the hydrothermal vent sites of the Mariana BASC (Komai & Giguère, 2019).

Characteristics	***R. vandoverae***	***R.* cf. *variabilis***	***R. falkorae* n. sp.**
Dorsal carapace	Sparse setae	Very sparse setae	Numerous scattered setae, sometimes with faint, saddle-like depression.
Rostrum	Wide and blunt	Wide, and varies from blunt to acute	Wide, short and blunt
Pterygostomial angle of carapace	Produced or non-produced, subactute, with numerous setae	Strongly produced, acute or subacute, with sparse setae	Very strongly produced, acute or subacute, with sparse setae
Stylocerite of antennular peduncle	Reaching half the length of the second antennular segment.	Falling slightly short of distal margin of the second antennular segment.	Reaching to or slightly beyond the distal margin of the second antennular segment.
Dorsolateral spines on telson	Armed with 7 – 9 pairs of spines in sinuous rows	Armed with 6 – 8 pairs of spines in sinuous rows	Armed with 5 – 6 pairs of spines in rows curved towards the midline.
Fifth abdominal somite	Bears no denticles	Bears 0 – 4 denticles	Bears 0 – 2 denticles

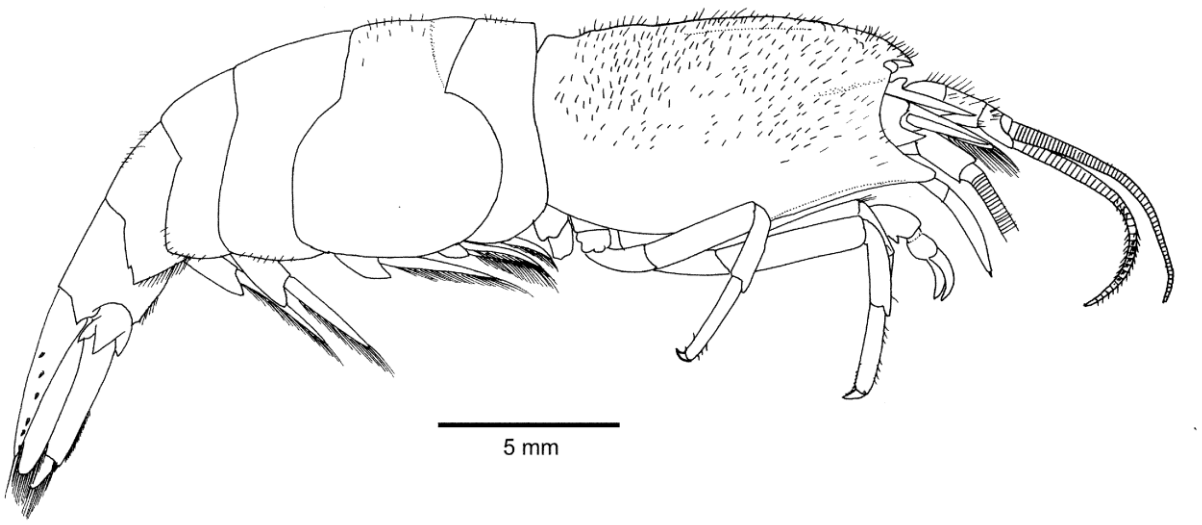

Figure 6. A lateral view of the new species, *Rimicaris falkorae* (Komai & Giguère, 2019).

species. Very little is known about deep-sea zoanthids (Reimer, pers. comm.), so it is likely that this is an undescribed species, but it is not yet confirmed (Figure 7).

The taxa given "sp." instead of a species-level (or genus-level) identity are those that do not have a close species-level match in the literature. In Table 3, the only taxa given the "sp." nomenclature are those sent to taxonomic experts; the *Princaxelia* sp. and *Ilyarachna* sp. specimens are too damaged to identify to the species-level (Horton, pers. comm.), and the *Sericosura* sp. singleton is too young to identify to the species level (Arango pers. comm.). "Unknown sp." do not have a genus-level identity (Tables 2 & 3), such as most of the copepods that I identified; although it is likely that many, if not all, of these copepods are new species, they require expert assessment.

Figure 7. Plate of photos of some new/potentially new species collected from the central Mariana BASC vent sites in 2016. The top-left image shows a specimen of *Vulcanolepas* nov. sp. collected from the newly discovered Hafa Adai vent site; the total length of specimen is ~4.5 cm. The top-right photo shows the *Epizoanthus* cf. nov. sp. *in situ* in the Alice Springs vent field; the image is about 8 cm across. The bottom photo shows a specimen of *Shinkailepas* nov. sp. collected from a vent site in the central Mariana BASC in 2016 at three different angles: dorsal, ventral and lateral. The shell length is ~10 mm.

Johnson et al. (2008) designated the identity of the *Lepetodrilus* limpets in the Mariana BASC as "*L.* aff. *schrolli* MT" because they fall in a larger species complex of *L. schrolli*. The "aff." nomenclature represents a higher level of certainty than "cf.", and indicates that the specimens are an undescribed species or subspecies, but are not formally described (Bengtson

1988). The “MT” differentiates the “Mariana Trough” specimens from others in the species complex with a COI genetic separation of 5 – 15%.

*The Snail Graveyard***:**

During the first exploration of the Hafa Adai vent site, the researchers discovered a small pile of empty *A. hessleri* shells in a hollow 18 m downslope from an active hydrothermal vent: the Snail Graveyard (Figure 8). There were no living *A.hessleri* snails here, but other species associated with the pile included *P. wareni* snails, *Austinograea williamsi* crabs, and *Munidopsis* crabs. This location provided a good opportunity to sample the peripheral habitat of this new vent site, and three suction samples provided new discoveries as well (Table 3). Morphological analysis of two small *Munidopsis* crabs revealed that they are neither of the two *Munidopsis* species described from the Mariana BASC: *M. marianica* and *M. gracilis*. A further comparison with the published descriptions of most other known *Munidopsis* species revealed that these specimens may represent another undescribed species. Unknown species of copepods, isopods, amphipods and nematodes are also present among the Snail Graveyard samples.

*Mariana BASC Species Richness & Distribution Patterns***:**

Due to the haphazard method of sampling the fauna, the number and size of the samples varied greatly in the four central Mariana BASC vent sites (Figure 9). However, rarefaction curves account for these differences when assessing their taxon richness (Figure 10). These curves indicate that the Perseverance vent site exhibits the lowest richness of these four vent sites. The Illium-Alice Springs and Burke curves are very similar and intersect in two locations between 100 and 200 specimens. Although it is typically impossible to conduct diversity

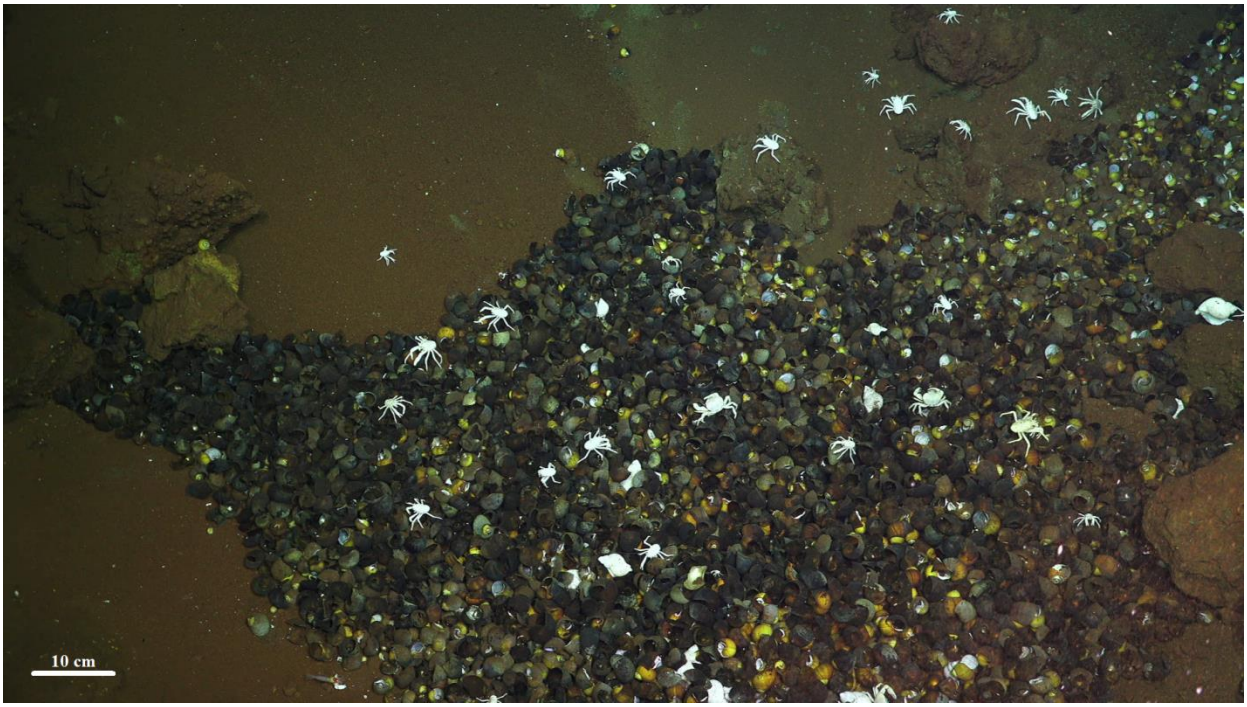

Figure 8. Video frame grab of Snail Graveyard in the Hafa Adai vent site. White squat lobsters (*Munidopsis* sp.) are most abundant on and around this pile of *Alviniconcha hessleri* shells. However, white snails (*Phymorhynchus wareni*) and white crabs (*Austinograea williamsi*) are also visible on the snail pile.

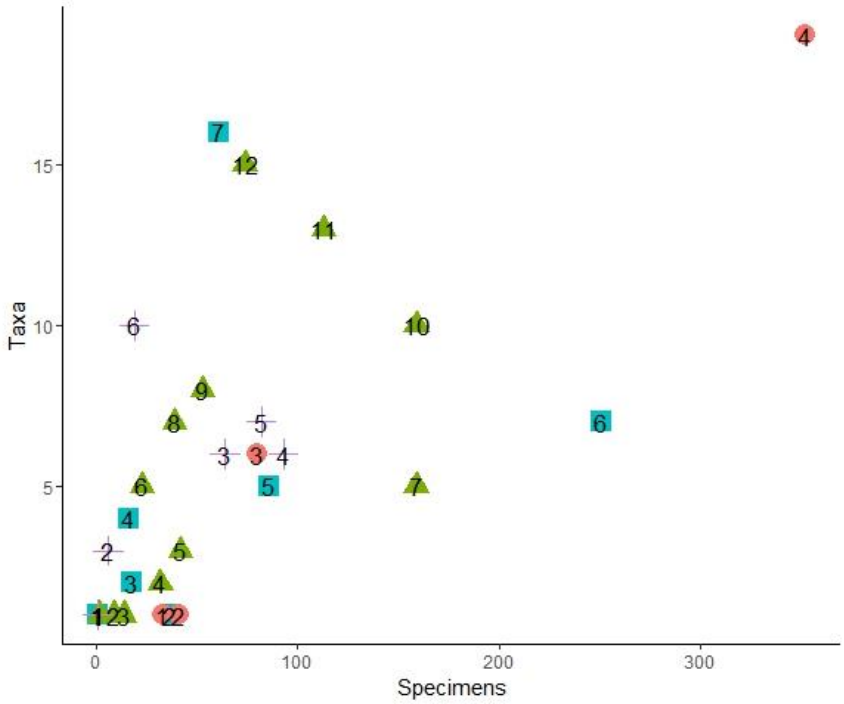

Figure 9. Ratios between the number of specimens and taxa present in the samples collected from the central Mariana BASC vent sites during the FK161129 cruise. Red circle = Burke vent site. Green triangle = Hafa Adai vent site. Blue square = Illium-Alice Springs vent site, Purple cross = Perseverance vent site. Numbers in each shape represent the number of samples collected from each vent site; the numbers ascend with the number of taxa identified in each sample (y-axis).

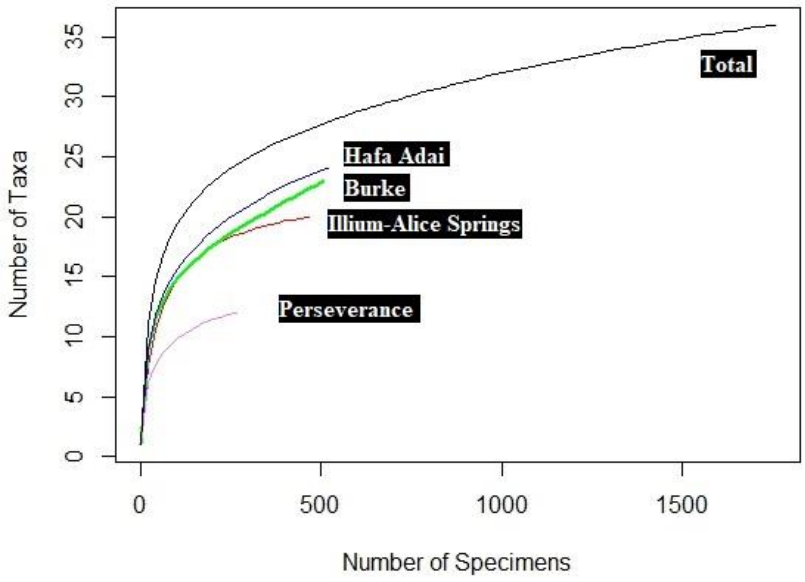

Figure 10. Rarefaction curves for each vent site sampled during the 2016 Hydrothermal Hunt cruise. The rarefaction curve labeled "Total" represents the combined results from all four vent sites.

assessments with rarefaction curves that intersect (Raup, 1975), the Burke vent site seems to be slightly richer in taxa than the Illium-Alice Springs vent site; the Illium-Alice Springs curve is closer to reaching its asymptote than the Burke curve. The Hafa Adai curve does not intersect with other curves and exhibits the highest taxon richness. None of the rarefaction curves reach an asymptote, indicating that undiscovered taxa are likely still present in all the central Mariana BASC vent sites

Based on the reduced occurrence list of taxa with confirmed species-identities (Table 6), the macrofaunal γ-diversity of the Mariana BASC system used for the analyses is 30 species, and the average α-diversity is 16.88 ± 2.49 species (Table 7). The α-diversity ranges from 9 (Snail) to 26 (Illium-Alice Springs) species. The newly discovered vent sites, Hafa Adai and Perseverance, have α-diversities of 25 and 15 species respectively. The α-diversity is generally higher in the central BASC than in the southern BASC (Table 7). Four species are present at every vent site in the system: *R. vandoverae*, *A. williamsi*, *N. brachylepadoformis* and *A. hessleri*. Two species are

present in only one vent site: *S. cochleifovea* and *Pachydermia* cf. *sculpta* (Fujikura et al. 1997). The vent-obligate species in this system most commonly inhabit four of the eight known vent sites (Figure 11). The samples and video collected during the FK161129 cruise provide data that expand the known distribution range for many species (Appendices S2 & S4).

The average β_J-diversity of the Mariana BASC vent system is 0.52 (Table 8), indicating that these vent sites share ~48% of their species on average. The Hafa Adai and Illium-Alice Springs vent sites are the most similar in the system, sharing ~96% of their species (Figure 12A); the Snail and Illium-Alice Springs vent sites are the least similar in the system, sharing only ~30% of their species. On a scale of negative one to positive one, the average β_{RC}-diversity of the Mariana BASC vent system is very close to zero (-0.11). This indicates that the average β_J-diversity of the system deviates very little from the null expectation of random assembly (Table 8). However, six pairs of vent sites exhibit β_{RC} values that fall beyond the negative CI of the null model (Table 8), indicating that these pairs differ significantly from the null expectation.

There are three linear regression models that best fit the α-diversity data ($p < 0.01$), but it is unclear which of these three is best. The first model uses distance from the arc as the explanatory variable, the second model uses the log-transformed values for distance from the arc, and the third model uses both depth and distance from the arc. The third model displays the highest adjusted R^2 value, indiciating that it explains ~85% of the variability in the species richness data; distance from the arc has a greater influence on this variability than depth (Table 9). However, the values for depth and distance from the arc are nearly collinear ($p = 0.06$), which suggests this model may not be the most appropriate to use. Furthermore, one data point in this model is a significant outlier; this is typically not an issue with large data sets, but in a small data

Table 6. Species presence-absence data for the vent-endemic macrofauna present among the Mariana BASC hydrothermal vent region. The vent sites present in this region are listed in the top row. Reduced data from Appendix 5.

	Illium-Alice Springs	**Burke**	**Hafa Adai**	**Perseverance**	**Forecast**	**Snail**	**Archaean**	**Urashima-Pika**
Rimicaris vandoverae	1	1	1	1	1	1	1	1
Rimicaris cf. *variabilis*	1	1	1	1	1	1	0	1
Rimicaris falkorae	0	1	0	1	0	0	0	0
Austinograea williamsi	1	1	1	1	1	1	1	1
Munidopsis marianica	1	1	1	1	1	1	0	1
Neoverruca brachylepadoformis	1	1	1	1	1	1	1	1
Vulcanolepas nov. sp.	1	0	1	0	0	0	0	0
Sericosura cochleifovea	0	1	0	0	0	0	0	0
Bathymodiolus septemdierum	1	1	1	0	1	0	0	0
Alviniconcha hessleri	1	1	1	1	1	1	1	1
Provanna nassariaeformis	1	1	1	1	0	0	0	0
Desbruyeresia marianaensis	1	1	1	1	1	0	1	1
Lepetodrilus aff. *schrolli* MT	1	1	1	1	1	0	1	0
Pseudorimula marianae	1	1	1	0	1	0	0	0
Ventsia cf. *tricarinata*	1	0	0	0	1	0	0	0
Pachydermia cf. *sculpta*	0	0	0	0	1	0	0	0
Bathyacmaea sp.	1	1	1	1	1	0	1	0
Shinkailepas nov. sp. 1	1	1	1	1	0	0	1	0
Shinkailepas nov. sp. 2	0	0	0	0	1	1	1	1
Symmetromphalus regularis	1	1	1	0	1	0	0	0
Phymorhynchus wareni	1	1	1	0	1	1	1	1
Branchinotogluma burkensis	1	1	1	0	1	0	0	0
Branchinotogluma marianus	1	0	1	0	1	0	0	0
Lepidonotopodium minutum	1	1	1	0	0	0	0	0
Levensteiniella raisae	1	0	1	1	0	0	0	0
Sirsoe hessleri	1	0	1	0	0	0	0	0
Paralvinella hessleri	1	1	1	1	0	0	0	1
Amphisamytha nov. sp.	1	1	1	0	0	1	0	0
Marianactis bythios	1	1	1	0	1	0	0	0
Epizoanthus cf. nov. sp.	1	1	1	0	0	0	0	0

Table 7. The γ-diversity for the Mariana BASC hydrothermal vent region and the α-diversity of each vent site within the region.The average α-diversity is 16.9 ± 2.5 species, and the median α-diversity is 16 species.

	Illium-Alice Springs	**Burke**	**Hafa Adai**	**Perseverance**	**Forecast**	**Snail**	**Archaean**	**Urashima-Pika**
Location	Central BASC				Southern BASC			
α-diversity	26	23	25	15	17	9	10	10
γ-diversity	30							

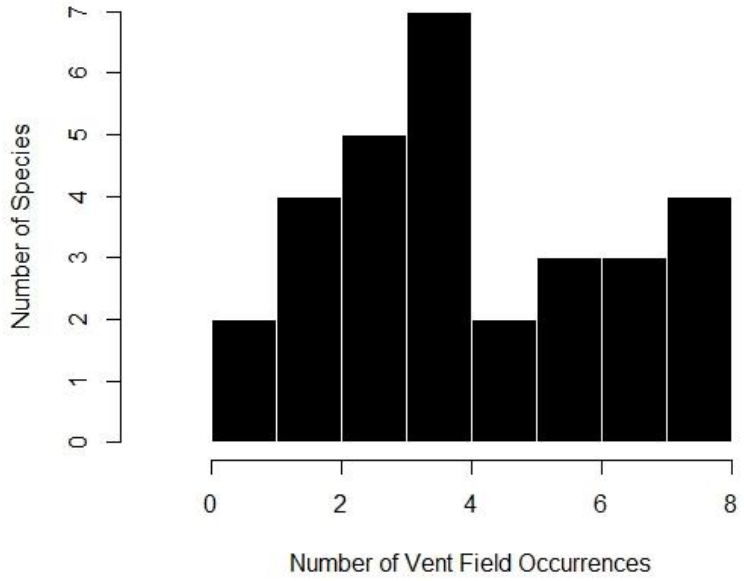

Figure 11. Derived from the data on Table 5. The x-axis represents the number of vent sites where a species is present. The y-axis represents the number of taxa that occur in each group on the x-axis.

Table 8. The pairwise β-diversity values of the Mariana BASC vent sites. The β_J-diversity values are above the diagonal line. The β_{RC}-diversity values are below the diagonal line and they are presented on a scale between 1 and -1. The average β_J = 0.5161 and the median β_J = 0.5443. The average β_{RC} = -0.1078 and the median β_{RC} = -0.0539. β_{RC}-diversity values that fall outside the 95% confidence intervals are presented in bold. The vent sites are presented as follows: IA = Illium-Alice Springs, B = Burke, HA = Hafa Adai, P = Perseverance, F = Forecast, S = Snail, A = Archaean, UP = Urashima-Pika.

	IA	**B**	**HA**	**P**	**F**	**S**	**A**	**UP**
IA	-	0.2500	0.0385	0.5185	0.3928	0.7037	0.6667	0.6667
B	0.1676	-	0.2222	0.4583	0.4444	0.6667	0.6250	0.6250
HA	**-0.9932**	-0.4068	-	0.5000	0.4286	0.6923	0.6538	0.6538
P	0.3254	-0.5790	-0.0272	-	0.6250	0.6471	0.5000	0.5000
F	0.5742	0.6324	0.7660	0.6842	-	0.6000	0.5500	0.5500
S	0.6864	0.0604	0.5058	-0.4218	-0.6696	-	0.5385	0.2727
A	0.6378	-0.0806	0.4166	**-0.9116**	-0.7776	**-0.9044**	-	0.4615
UP	0.6366	-0.0820	0.3992	**-0.9144**	-0.7736	**-0.9994**	**-0.9702**	-

Table 9. Partial correlations (PC) of the explanatory variables for the multiple linear regression applied to the α-diversity data of the Mariana BASC vent sites. These values were calculated in R and the procedures are outlined in Appendix 6.

Best Linear Model (BLM)	**(PC) Distance From the Arc**	**(PC) Depth**	**Adjusted R^2**	**p-value**
BLM 3 (α-diversity)	0.9372	0.7462	0.8472	0.004

set such as this (n = 8), this outlier is also a concern (Bissonette, 1999). The first model displays a relatively high adjusted R^2 value as well, indicating that it explains ~71% of the richness variability. Colinearity is not an issue in simple linear regressions and there are no significant outliers like in the third model (Appendix 6). Therefore, the first model may be more appropriate than the third. Given the small size of the data set, it is unclear if this model violates the assumption of linearity; to rectify this potential error of non-linearity, I generated the second model. However, it is unclear if the second model is violating the assumption of positive variability in its explanatory variable values (Appendix 6), which creates a potential issue that is absent in both the first or third models. The AICc indicates that the third model is slightly better than the first and second, but all three AICc values are nearly identical.

The best model that fit the β_J-diversity data used the log-transformed distance from the arc values as the only explanatory variable. Although this regression model showed a significant relationship ($p < 0.01$), it only explains about 34% of the variability. The model that best fits the β_{RC}-diversity data ($p < 0.01$) uses isolation as the explanatory variable. This model explains ~46% of the variability in the β_{RC} data.

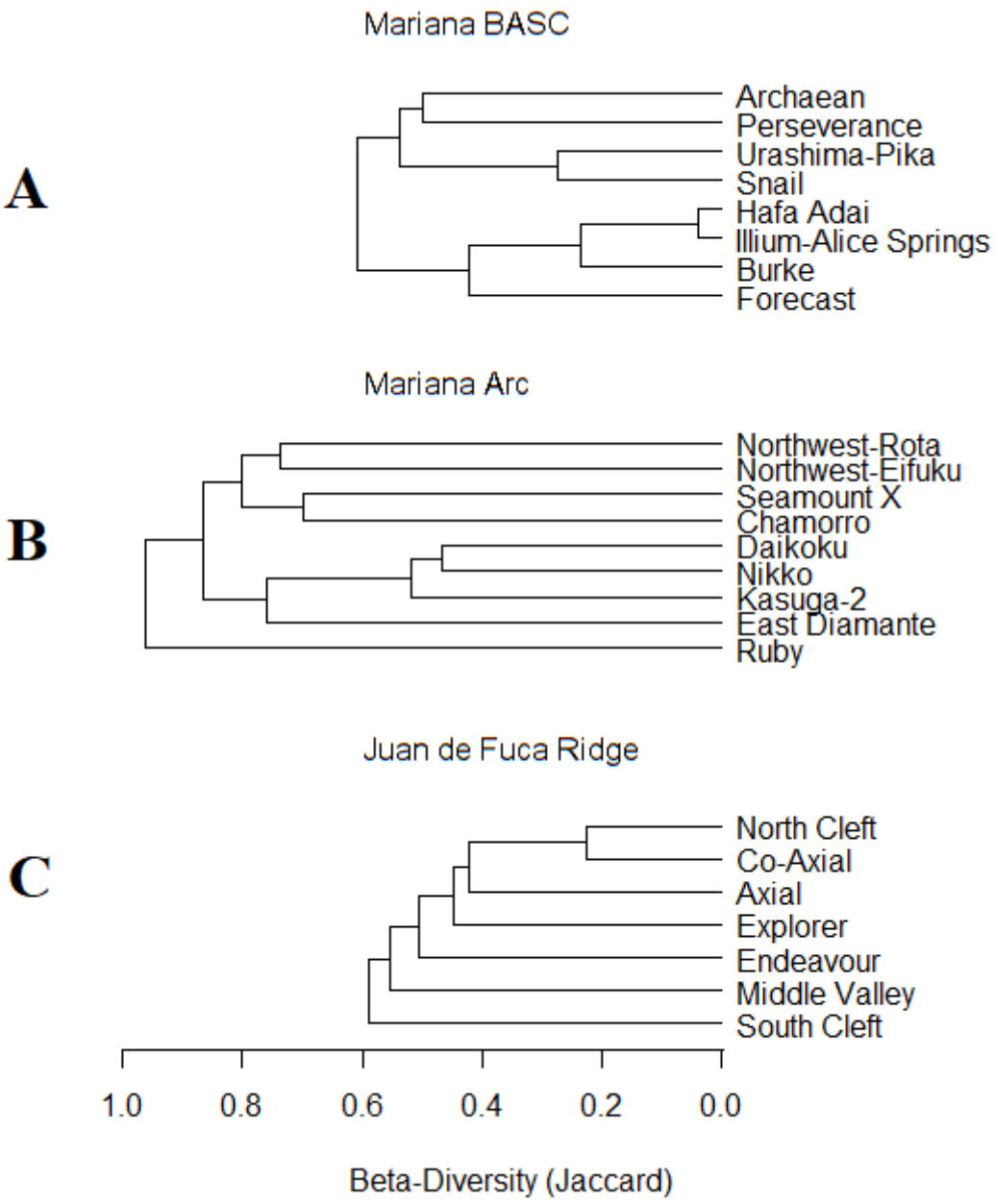

Figure 12. Dendrograms illustrating the β_J-diversity of the Mariana BASC (A), Mariana Arc (B) and Juan de Fuca Ridge (C) systems; the names of each vent site are given on the right of each dendrogram. The dendrograms are generated from the β_J values on Tables 8, 10 & 11 and are constructed using the unweighted pair group method with arithmetic mean (UPGMA).

*Other Regional Species Richness and Distribution Patterns***:**

Based on Butterfield et al. (in prep.), the macrofaunal γ-diversity of the Mariana Arc system is at least 37 species and the average α-diversity is 9.78 ± 1.52 species. The α-diversity ranges from 3 (Ruby) to 17 (Northwest Eifuku) species. The average β_J-diversity is 0.83 (Table 10), indicating that these vent sites share only ~17% of their species on average. The Nikko and Daikoku vent sites are the most similar in this system, sharing ~53% of their species (Figure 12B); the Ruby vent site shares no species with the NW Eifuku, Chamarro, NW Rota and Seamount X sites (100% dissimilar). On a scale of negative one to positive one, the average β_{RC}-diversity for this system is not close to zero (0.42). This indicates that the average β_J-diversity of the system deviates from the null expectation more than that of the Mariana BASC. Ten pairs of vent sites in the Arc exhibit β_{RC} values that exceed the 95% CIs on the positive end of the null models; three additional pairs exhibit β_{RC} values that fall beyond the negative end of the null models (Table 10).

Based on Chapman et al. (2019), the macrofauna γ-diversity of the Juan de Fuca Ridge region is 71 species and the average α-diversity is 31.71 ± 3.80 species. The α-diversity ranges from 16 (South Cleft) to 45 (Middle Valley) (Tunnicliffe, pers. comm.). The average β_J-diversity is 0.51 (Table 11), indicating that these vent sites share ~49% of their species on average. The CoAxial and North Cleft vent sites are the most similar in this region, sharing ~77% of their species (Figure 12C); the Middle Valley and South Cleft vent sites are the least similar in the region, sharing only ~30% of their species. Like the Mariana Arc, the average β_{RC}-diversity is not close to zero on a scale of negative one to positive one (Table 11). However, unlike the Mariana Arc, the average β_{RC}-diversity of the Juan de Fuca Ridge is much closer to negative one (-0.51). Twelve pairs of vent sites in this region exceed the 95% CI on the negative end of the

null models; one additional pair exhibits a β_{RC} value that exceeds the positive end of the null model.

Table 10. The pairwise β-diversity values of the Mariana Arc vent sites. The β_J-diversity values are above the diagonal line. The β_{RC}-diversity values are below the diagonal line and they are presented on a scale between 1 and -1. The average $\beta_J = 0.8322$ and the median $\beta_J = 0.8667$. The average $\beta_{RC} = 0.4156$ and the median $\beta_{RC} = 0.6701$. β_{RC}-diversity values that fall outside the 95% confidence intervals are presented in bold. The vent sites are presented as follows: N = Nikko, K2 = Kasuga-2, NW-E = Northwest Eifuku, D = Daikoku, C = Chamorro, ED = East Diamante, R = Ruby, NW-R = Northwest Rota, SX = Seamount X.

	N	**K2**	**NW-E**	**D**	**C**	**ED**	**R**	**NW-R**	**SX**
N	-	0.5333	0.84	0.4667	0.8667	0.8261	0.9286	0.8125	0.8889
K2	**-0.936**	-	0.875	0.5	0.9286	0.75	0.9167	0.8667	0.8
NW-E	**0.9746**	**0.9792**	-	0.88	0.9	0.8148	1	0.7368	0.75
D	**-0.9802**	**-0.9712**	**0.9932**	-	0.9333	0.7	0.9231	0.875	0.8824
C	0.425	0.8052	0.8122	0.8606	-	0.8235	1	0.8	0.7
ED	**0.9242**	0.2978	**0.9896**	-0.0302	0.0418	-	0.9412	0.9	0.85
R	0.651	0.4916	**1.0000**	0.5714	**1.0000**	0.7824	-	1	1
NW-R	0.2544	0.6022	-0.342	0.6892	-0.275	**0.9216**	**1.0000**	-	0.75
SX	0.8632	0.1628	0.0008	0.7948	-0.7638	0.7854	**1.0000**	-0.4144	-

Table 11. The pairwise β-diversity values of the Juan de Fuca Ridge vent sites. The β_J-diversity values are above the diagonal line. The β_{RC}-diversity values are below the diagonal line and they are presented on a scale between 1 and -1. The average $\beta_J = 0.5114$ and the median $\beta_J = 0.5094$. The average $\beta_{RC} = -0.5147$ and the median $\beta_{RC} = -0.912$. β_{RC}-diversity values that fall outside the 95% confidence intervals are presented in bold. The vent sites are presented as follows: Ex = Explorer, MV = Middle Valley, En = Endeavor, CA = Co-Axial, A = Axial, NC = North Cleft, SC = South Cleft.

	Ex	**MV**	**En**	**CA**	**A**	**NC**	**SC**
Ex	-	0.5306	0.4889	0.4571	0.4524	0.4286	0.5667
MV	-0.5724	-	0.5424	0.6154	0.4909	0.5962	0.7021
En	-0.8788	**0.9616**	-	0.5532	0.5094	0.4667	0.6429
CA	**-0.985**	0.6172	-0.3352	-	0.4524	0.2258	0.5667
A	**-0.9668**	0.4648	0.4524	**-0.9628**	-	0.3902	0.5789
NC	**-0.9948**	0.5356	**-0.9098**	**-0.9998**	**-0.9942**	-	0.4828
SC	**-0.9826**	-0.366	**-0.912**	**-0.9834**	**-0.9974**	**-0.9996**	-

*Vent System Comparisons***:**

The Mariana BASC exhibits the lowest γ-diversity of these three systems, but it has a higher average α-diversity than the Mariana Arc. The median β_J-diversity of the Mariana BASC is very similar to that of the Juan de Fuca region, but the median β_J-diversity of the Mariana Arc

is much higher (Figure 13). The animal assemblages in the Mariana Arc vent sites are significantly more dissimilar than those of Mariana BASC vent sites (β_J permutation dispersion: *F* ratio = 19.366, P < 0.01). The median β_{RC}-diversity of the Mariana BASC is closest to zero, whereas that of the Juan de Fuca Ridge is closest to negative one and that of the Mariana Arc is closest to positive one (Figure 14). The distribution patterns of vent fauna of the Arc deviate from the null expectation of stochastic assembly significantly more than those of the Mariana BASC (β_{RC} permutation dispersion: *F* ratio = 19.366, *P* < 0.01; Figure 15).

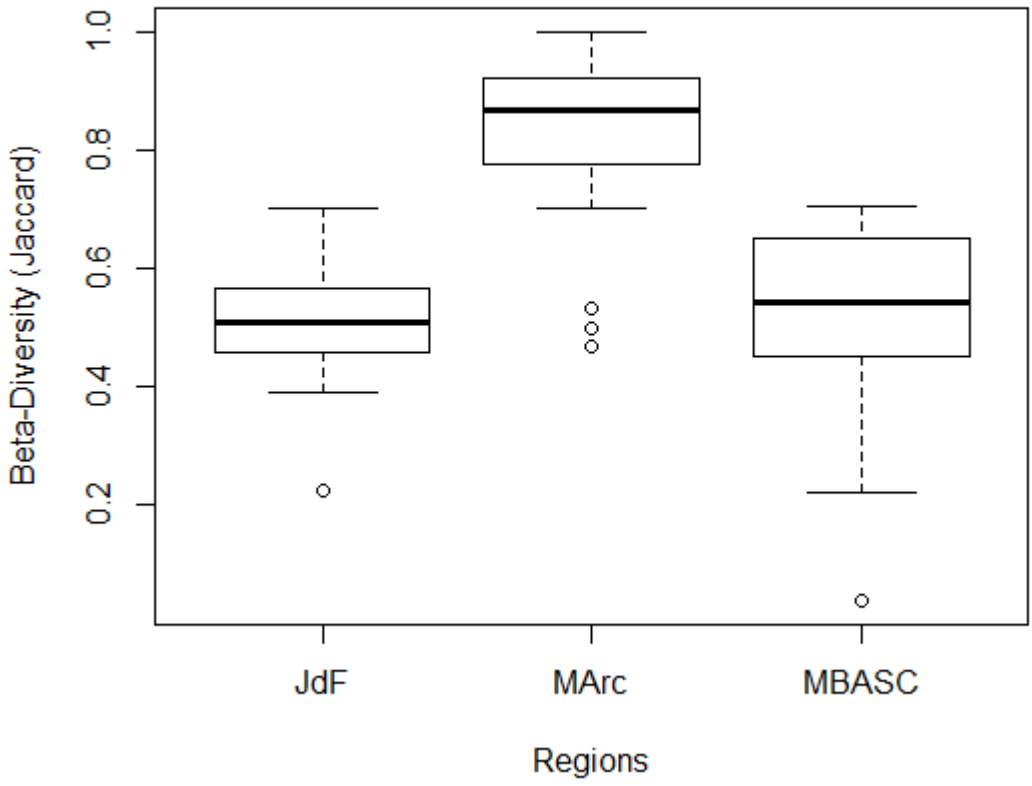

Figure 13. Boxplots representing the regional β_J-diversity for the Juan de Fuca Ridge (JdF), the Mariana Arc (MArc) and the Mariana BASC (MBASC) vent sites. The β-diversity axis represents dissimilarity values; lower values indicate that the vent assemblages are more similar than higher values.

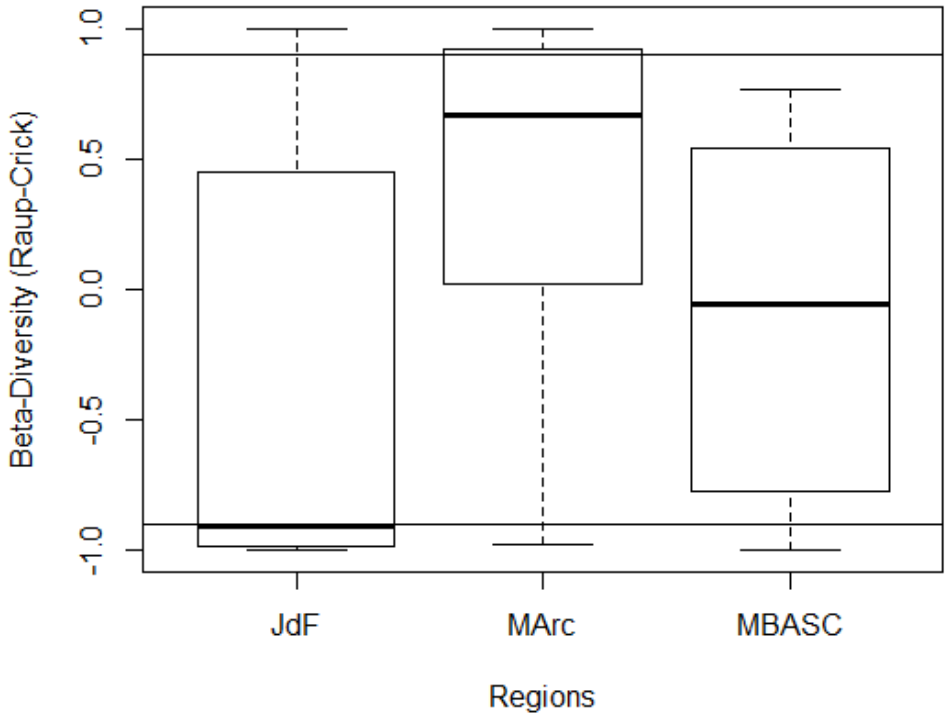

Figure 14. Boxplots representing the regional β_{RC}-diversity for the Juan de Fuca Ridge (JdF), the Mariana Arc (MArc) and the Mariana BASC (MBASC) vent sites, calculated using the Raup-Crick Index. On the β-diversity axis, values below zero indicate that the vent assemblages are more similar to each other than expected by random chance and values above zero indicate that assemblages are more dissimilar than expected by random chance. The horizontal lines on the 0.9 and -0.9 β-diversity values indicate significant deviation from the null expectation of random assembly used in the Raup-Crick index.

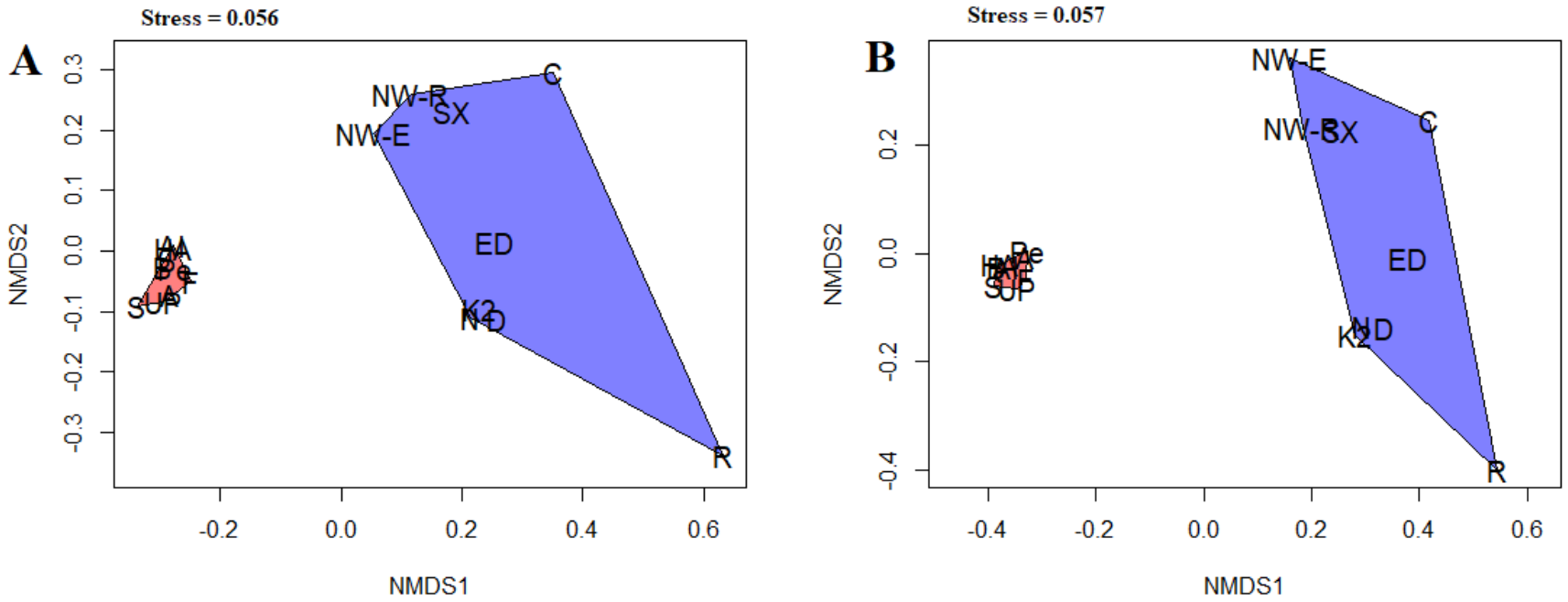

Figure 15. A non-metric multidimensional scaling (nMDS) plot illustrating the (dis)similarity in species composition between the animal assemblages present among the vent sites of the Mariana BASC and Arc using the β_J values (image A) and the β_{RC} values (image B). F = Forecast, HA = Hafa Adai, AI = Illium-Alice Springs, B = Burke, S = Snail, UP = Urashima-Pika, Pe = Perseverance, A = Archaean, R = Ruby, C = Chamorro, SX = Seamount X, NW-E = Northwest Eifuku, NR-R = Northwest Rota, ED = East Diamante, K2 = Kasuga-2, N = Nikko, D = Daikoku.

Discussion:

*The Challenges of Hydrothermal Vent Diversity Studies***:**

There are many challenges associated with community ecology research in hydrothermal vent habitats (Tunnicliffe et al. 1998) and comparing results among independent vent studies can compound these challenges. It is difficult and expensive to access the deep-sea, and both time constraints and harsh weather conditions on the open ocean can further complicate the process of exploration and sample collection. For studies in vent biodiversity, the relatively high frequency of unknown species collected from newly discovered habitats also introduces another complexity; researchers often cannot access the specimens reported in prior studies, so without published species descriptions, different research groups may assign distinct species to the same taxon. For example, many researchers have reported one worm species (*Amphisamytha galapagensis*) from different vent regions around the world, but Stiller et al. (2013) later revealed by morphological and genetic analyses that this species is restricted to only the Galapagos Rift and the East Pacific Rise regions, whereas other regions host related, but distinct, new species; the Mariana BASC species is similarly new (Stiller, pers. comm.). Conversely, the same species could be assigned different names (e.g. *Bathymodilous septemdierum* – Breusing et al. 2015).

In community ecology, a consistent sampling method is an essential tool for acquiring and comparing relative abundance data, but researchers have not yet developed a method to sample vent sites in the same manner across all habitat types. The structural complexity of vent sites vary greatly and it is necessary to use several tools to collect samples from these different habitats because specific methods work better for different substrata (Gauthier, Sarrazin, and Desbruyères 2010). Therefore, the quantitative community studies of vent sites are usually limited to a single habitat type (e.g. Van Dover et al. 2002; Tsurumi and Tunnicliffe, 2003;

Bergquist et al. 2007). Those that rely on video footage can analyze several vent habitats but are limited to the animals visible in the imagery (e.g. Du Preez and Fisher, 2018). Diverse sampling methods are also ideal for collecting animals of different size ranges. For example, scoops are better for collecting larger animals, whereas suction samples are better for collecting smaller animals (Gauthier et al. 2010).

My study addresses animal diversity in all the accessible habitats of the Mariana BASC hydrothermal vent sites. Given the exploratory nature of the most recent cruise to this system, the main field objective was to collect as many species as possible from every visited site, especially the two newly discovered vent sites, Hafa Adai and Perseverance. Thus, the pilots used a variety of sampling tools. However, these tools ("scoops," grabs and "slurps") are not quantitative (Gauthier et al. 2010), thus, comparative assessments of relative species abundance are not possible. Instead, these methods provided the best samples to represent the species diversity in each vent site. Therefore, samples, video footage and previous studies provide the best presence-absence data available for qualitative analyses of the species richness and composition patterns in this system.

Sample coverage issues also constrain the present study; the rarefaction curves indicate undiscovered species likely remain in these four central BASC vent sites (Figure 10). It is certain that some of the species unaccounted for in the rarefaction curves include some abundant species observed in the video footage that were rarely collected or not collected at all (e.g. *Marianactis bythios* and *Munidopsis marianus*). Therefore, it is likely that the undiscovered species include those too small to observe in the imagery and those that are rare. Although sampling targeted the meiofauna, the diversity was low. Given that the four vent sites in the southern Mariana BASC (Forecast, Snail, Archaean and Urashima-Pika) were not sampled during the Hydrothermal Hunt

cruise, the presence-absence data are informed solely by the literature and available imagery; thus, I could not generate rarefaction curves for these vent sites. Previous studies do not document sampling effort in these southern vent sites, so it is difficult to estimate the potential for additional undiscovered species in these sites.

Some unconfirmed taxa reported by this study and previous work are not included in the estimates of species richness because I take a conservative approach to calculate the diversity indices using a reduced presence-absence dataset. Although this reduced dataset limits the richness estimates, it does not overestimate the richness of these vents; neither my study nor prior studies give species-level identities to all taxa reported from the Mariana BASC vents, so multiple reporting of some species has likely occurred. An estimate of "taxonomic richness" would also be possible given the available data, but it is less tractable for comparisons between studies than reduced lists of species with confirmed identities (Gauthier et al. 2010). It is essential to be aware of these limitations while interpreting the data. However, these data represent the best estimate of the minimum species diversity in the central and southern Mariana BASC vent sites given the intrinsic limitations of deep-sea vent research. Further sampling of all eight vent sites will help improve the species diversity data in the system.

*Faunal Diversity of the Central Mariana BASC Vent Sites***:**

My study examines specimens from the first two and the two most recently discovered vent sites in the Mariana BASC (Illium-Alice Springs and Burke, and Hafa Adai and Perseverance respectively). Of the 31 taxa initially reported from the former sites (Hessler and Lonsdale, 1991; Fujikura et al. 1997), 20 (65%) were present in my samples from the two new vent sites and 25 (81%) were present in my samples from all four vent sites; including the

observations in the imagery, 28 (90%) were observed or collected during this most recent cruise. The copepods *Stygiopontius pectinatus* and *S. stabilitus*, (Humes, 1990) and the gastropod *Ventsia* cf. *tricarinata* (Fujikura et al. 1997) were the only absent species. Both this study and previous literature have since changed the taxonomic identities of many taxa initially reported by Hessler and Lonsdale (1991) (Table 12). I report an additional 12 taxa previously unknown in the Mariana BASC vents (Appendix 5), nine of which occur in multiple vent sites. Nine (75%) of these taxa are meiofauna, a group poorly represented in previous reports. Thus, despite the relatively low meiofaunal diversity in the system, the effort allocated to collecting these meiofauna has more than doubled the number observed in these vents. Many of the most abundant vent species in the central BASC sites are also present among those in the southern BASC. Although the vent species diversity is higher in the central sites, a few additional species are present only in the southern sites (Appendix 5).

Table 12. Previous taxonomic identities of vent fauna previously reported from the Mariana BASC given updated identities based on the results from present study and more recent publications.

Previous Identities	Identity Updates
"Buccinidae indet." (Hessler & Lonsdale, 1991) "*Phymorhynchus* cf. *starmeri*" (Fujikura et al. 1997)	"*Phymorhynchus wareni*" (Puillandre, pers. comm.)
"Acmaeidae n. gen. n. sp." (Hessler & Lonsdale, 1991)	"*Bathyacmaea* sp."
"*Shinkailepas* cf. *kaikatensis*" (Hessler & Lonsdale, 1991)	"*Shinkailepas* nov. sp." (Kano, pers. comm.)
"*Amphisamytha galapagensis*" (Hessler & Lonsdale, 1991)	"*Amphisamytha* nov. sp." (Rouse, pers. comm.)
"Small anemones" – photograph only (Hessler & Lonsdale, 1991)	*"Epizoanthus* cf. nov. sp." (Reimer, pers. comm.)
"Scalpellomorpha" – photograph only (Hessler & Lonsdale, 1991)	*"Vulcanolepas* nov. sp." (Watanabe, pers. comm.)
"*Opisthotrochopodus marianus*" (Hessler & Lonsdale, 1991)	*"Branchinotogluma marianus"*
"*Hesiocaeca* n. sp." (Hessler & Lonsdale, 1991)	*"Sirsoe hessleri*" (Böggemann, 2009)
"*Nicomache arwidssoni*" (Hessler & Lonsdale, 1991) "*Nicomache* cf. *ohtai* (Desbruyeres et al. 2006)	*"Nicomache* sp." (Kojima & Watanabe, 2015)
"Bathymodiolus n sp." (Hessler & Lonsdale, 1991)	*"Bathymodiolus septemdierum*" (Fujita et al. 2009)
"Provanna marianaensis" (Hessler & Lonsdale, 1991)	*"Desbruyeresia marianaensis"* (Waren & Bouchet, 1993)
"Chorocaris vandoverae" (Hessler & Lonsdale, 1991)	*"Rimicaris vandoverae*" (Vereshchaka et al. 2015)

Located 137 km south of Burke, Hafa Adai is the largest vent site in the Mariana BASC. It exhibits both diffuse hydrothermal flow through basalt rubble and direct flow through sulfide chimneys and talus, supporting a wide variety of vent habitats. Although chimneys are present in the southern sites (Yoshikawa et al. 2012), the current observations indicate that Hafa Adai hosts the largest structure in the system - a 30m tall chimney named 'Sequoia.' Although the conservative estimate of α-diversity indicates that Illium-Alice Springs is the most species rich vent site in the system (Table 7), the samples from Hafa Adai contain the most taxa (Figure 10). Of the 37 taxa in all active vent samples (Table 2), 25 (68%) occur in Hafa Adai samples and one taxon occurs in Hafa Adai exclusively; only 21 (57%) occur in the Illium-Alice Springs samples and every taxon in this vent site is present in at least one other (Appendix 3). Furthermore, it is important to note that the sampling effort used to generate the diversity measures in Table 6 is much greater for Illium-Alice Springs (three separate cruises) than Hafa Adai (one cruise). Comparatively, diversity in the Perseverance vent site, ~169 km south of Hafa Adai, is much more limited. The vent habitats in this site are markedly smaller than those in Hafa Adai and although many dead chimneys are present in Perseverance, the team could not locate active black smokers. Animal assemblages here appeared noticeably less diverse and less abundant than the three other central Mariana BASC vent sites, and every taxon in Perseverance occurs elsewhere in the Mariana BASC.

Both Anderson et al. (2017) and Baker et al. (2017) report other locations in the central Mariana BASC where they detected vent plumes on the 2015 leg of the Hydrothermal Hunt cruise. High-temperature plumes centered over all previously known vent sites; three others were also present. The most intense plume centered over Hafa Adai and another centered over Perseverance. The following cruise explored a third, high-temperature plume, but no active

venting was discovered; instead, new lava was present, suggesting a recent eruption. Low temperature plumes are likely either transitory from high-temperature plumes, or they originated from vents with activity lower than all known sites; such locations would have very low vent-endemic species diversity and future exploration may not reveal new species (Baker et al. 2016). However, ~600km of the northern Mariana BASC remains unexplored, so it is possible that large, highly active vent sites and undiscovered species lie north of Illium-Alice Springs.

Overall, diffuse hydrothermal flow through basalt pillows or sulfide talus mostly characterizes the vent sites in the central Mariana BASC and broad zonation patterns center around the areas of outflow. Similar to the vent sites in the Lau Basin (Henry et al. 2008), *Alviniconcha* snails have a high thermal tolerance and dominate the areas closest to hydrothermal discharge along with the less abundant *Paralvinella* polychaetes. *Neoverruca* barnacles dominate the areas of intermediate hydrothermal flow around the *Alviniconcha*. These intermediate areas seem to be the most diverse habitats in the vent sites, as *Bathymodiolus* mussels and many gastropod and polychaete species are interspersed here as well. The relative dominance of the *Alviniconcha* and *Neoverruca* in a vent field depends on the vigour of the hydrothermal fluid; assemblages surrounding less vigorous effluent tend to be *Neoverruca* dominated, as at Burke. These macrofaunal diversity patterns are similar to those in the Galapagos Rift (Hessler and Smithey, 1983) and East Pacific Rise (Gollner et al. 2015); although the species differ between these regions, the same genera and families are spatially structured the same way.

Like most vent-associated anemones (e.g. López-González et al. 2003; Bennett et al. 2015; Sen et al. 2016; Zhou et al. 2018), *Marianactis* anemones typically dominate and are only present in the low temperature periphery, sometimes alongside dense mats of *Epizoanthus*. Endosymbiotic sulfur-oxidizing bacteria do not occur in *Marianactis* (Fautin and Hessler, 1989)

or vent-associated anemones in general (e.g. Bennett et al. 2015; Van Audenhaege et al. 2019), so it is plausible that they do not require close proximity to hydrothermal outflow to benefit from the associated productivity, unlike *Alviniconcha*. Like the anemones in the Mid-Atlantic Ridge (e.g. Gebruk et al. 1997), those in the Mariana BASC may acquire nutrition from both chemosynthesis and photosynthesis. Their complete absence from higher temperature zones also suggests that these anemones simply cannot tolerate these temperatures or their associated chemical concentrations as observed in other vent ecosystems (e.g. Marsh et al. 2012; Sen et al. 2016; Zhou et al. 2018).

Rimicaris shrimp, *Austinograea* crabs and *Munidopsis* crabs are the dominant mobile fauna in this system. *Rimicaris* and *Austinograea* are most abundant in the warmer waters surrounding the snails and barnacles, which is consistent with other vent regions (e.g. Desbruyères et al. 2000; Podowski et al. 2009; Sen et al. 2016; Zhou et al. 2018); *Munidopsis* crabs are present only on the periphery. The shrimp occupy the warmer waters because they primarily graze on the sulphide-oxidizing bacteria growing on the substratum close to the hydrothermal fluids (Van Dover and Fry, 1989). Both *Austinograea* and *Munidopsis* crabs are scavengers (Van Dover and Fry, 1989), but *Austinograea* are also the top predators in these vent sites (Van Dover and Fry, 1989), so they may outcompete *Munidopsis* for resources in the warmer fluids. Alternatively, the *Munidopsis* may be unable to tolerate the conditions of the warmer waters. *Austinograea* belongs to a superfamily of vent-endemic brachyuran crabs (Bythograeidae), in which at least one species shows notable physiological adaptations to sulphide and thermal stresses (Arp and Childress, 1981). *Munidopsis*, prevalent throughout a variety of deep sea habitats beyond vents (Van Dover et al. 1985; Schnabel et al. 2011), has less

extreme modifications for vent conditions. Therefore, the *Austinograea* appears better adapted to hydrothermal conditions than *Munidopsis*.

In basalt hosted vents, such as those in Illium-Alice Springs and Burke, the sessile and sedentary fauna dominate the assemblages, whereas mobile animals are more abundant in sulfide-hosted vents, such as those in Hafa Adai and Perseverance. This difference may be due to higher variability in temperature and chemical concentrations surrounding sulfide substrata than basalt, which is more difficult for sessile and sedentary fauna to tolerate. For example, Desbruyères et al. (2000) found that aggregations of *Rimicaris* were associated with high levels of heavy metals and chlorine, whereas aggregations of *Bathymodiolus* were associated with low levels. Alternatively, basalt is a stronger substrate and may be more suitable for the recruitment of sessile and sedentary species than sulfides.

My work presents estimates of the total regional (γ) diversity of the Mariana BASC. Based on the reduced data in Table 6, the γ-diversity is 30 species, but based on all the taxonomic occurrence data in Appendix 5, the actual regional diversity of this system is likely much higher. Kojima and Watanabe (2015) provide the most recent survey of these vent species by combining the results of previous studies with their findings. My study augments these data with other relevant studies to a total of 70 possible taxa (Appendix 5). However, since some reports originate from dispersed collections that are difficult to compare, multiple reports of the same species has likely occurred. For example, both Hessler and Lonsdale (1991) and Kojima and Watanabe (2015) report a taxon of Acmaeidae limpet. However, since the latter authors could not compare the two collections, they treat them as separate taxa; I suspect they treated all the taxa with this level of caution. Dr. Hessler's original collection appears to be lost (C. Seid,

UCSD, pers. comm), so I also cannot determine if these two taxa represent the same species. Taking possible multiple reporting into account reduces the estimate to 56 species (Appendix 5).

The species composition of the Mariana BASC defines a distinct biogeographic region, both globally (Bachraty et al. 2009; Moalic et al. 2011) and in the Western Pacific (Desbruyères et al. 2006; Kojima and Watanabe, 2015). Its composition most closely resembles those of the vent assemblages in the Manus, Fiji and Lau BASCs, although several species are shared with the Okinawa Trough. All four BASC systems contain the symbiont-hosting *Alviniconcha* (Johnson et al. 2015), *Lepetodrilus* limpets (Johnson, Warén, and Vrijenhoek 2008), *Austinograea* (Guinot and Segonzac, 2018), *Munidopsis* (Desbruyères et al. 1994; Thaler et al. 2014), *Bathymodiolus* (Breusing et al. 2015) and alvinocaridid shrimp (Komai and Segonzac, 2005; Komai and Tsuchida, 2015). However, the most notable distinctive feature of the Mariana BASC is the relatively low diversity.

Vent sites generally host a variety of foundation species – those that positively alter the habitat for the rest of the community (Govenar, 2010); siboglinid tubeworms, mytilid mussels, vesicomyid clams and large provannid snails are common foundation species in vents (e.g. Govenar 2010; Luther III et al. 2012). Foundation species in the Lau BASC include the mussel *B. septemdierum*, several species of *Alviniconcha* and the *Ifremeria nautilei* provannid snail (Sen et al. 2013; Johnson et al. 2015). However, *A. hessleri* is virtually the only foundation species in the Mariana BASC; vesicomyid clams and siboglinid tubeworms are completely absent and, although *Bathymodiolus* are present, they are too uncommon to form 'beds'. As with *Alviniconcha*, diversity within other taxonomic groups in the Mariana BASC vents is also low. Several species of *Austinograea* inhabit the North Fiji and Lau BASC vent sites, but only one is present in the Mariana BASC (Guinot and Segonzac, 2018). Several genera of alvinocaridid

shrimp occur at Manus, Fiji and Lau BASC vents (Komai and Tsuchida, 2015), whereas only one occurs in the Mariana BASC.

New Species of Rimicaris *Shrimp***:**

After the first exploration of Illium-Alice Springs and Burke in 1987, Hessler and Lonsdale (1991) reported one shrimp species, *R. vandoverae*. Comparison of the partial COI sequences between our specimens and alvinocaridid shrimp species available on GenBank provides evidence that the distribution of *R. vandoverae* is restricted to the Mariana BASC; reports from other Western Pacific vent regions (e.g. Galkin, 1997; Sen et al. 2013) are now recognized as *R. variabilis* (Komai & Tsuchida, 2015). Subsequently, Kojima and Watanabe (2015) reported an additional, unknown species of *Rimicaris* from the Snail and Urashima-Pika vent sites that we now know to be *R.* cf. *variabilis* (Watanabe, pers. comm.); the current taxonomic status is unclear. Although the partial COI gene sequences between *R. variabilis* from Lau (Komai et al. 2016) and *R.* cf. *variabilis* from Mariana are very similar, morphological differences have emerged (Komai, pers. comm.). Work on another gene is underway in Japan. In the course of my study, I discovered a third species, now published as *Rimicaris falkorae* (Komai and Giguère, 2019).

There is little information on the biology or ecology of the three *Rimicaris* species in the Mariana BASC vent sites. Komai and Giguère (2019) report grazing and scavenging behaviour in shrimp at the Burke vent site. However, as the species are indistinguishable in video imagery, it is impossible to detect behavioural differences. Van Dover and Fry (1989) performed stable isotope analyses on the shrimp collected from the Illium-Alice Springs and Burke vent sites and found that their $\delta^{15}N$ values were consistent with the primary consumer trophic position of a

grazer. However, as two and three shrimp species are present at the Illium-Alice Springs and Burke sites respectively, their analyses may have combined more than one species.

These species likely partition their habitat, as do five alvinocaridid species (in two genera) on the Mid-Atlantic Ridge (Gebruk et al. 2000), where differences in both feeding strategies and microdistribution patterns are evident. Based on stable isotope analyses of Manus Basin shrimp, Van Audenhaege et al. (2019) propose the possibility that *R. variabilis* are symbiotrophs like *R. exoculata* in the Mid-Atlantic Ridge (Gebruk et al. 2000). My *R.* cf. *variabilis* specimens may have a similar habit. Future studies investigating the ecological differences of the three Mariana BASC species will provide an excellent opportunity to test both the competitive exclusion principle and the hypothesis of functional redundancy (Rodríguez et al. 2015).

*The Snail Graveyard***:**

The Snail Graveyard of Hafa Adai is an accumulation of dead *Alviniconcha* shells about 18m downhill from an active vent. Here, both peripheral vent species and deep-sea animals take advantage of the detritus where thermal and chemical conditions of vents are absent. *Munidopsis* crabs dominate the assemblage with *Phymorhynchus* snails and *Austinograea* present in lower numbers; *Marianactis* anemones are absent. It is unclear if the unknown species of *Munidopsis* and *Sericosura* sea spider are vent-endemic species. Meiofauna were more abundant than in venting habitats with some taxa occurring only here; isopods and amphipods were present only in Snail Graveyard samples. There are no previous reports of isopods from the Mariana BASC vent sites and only Fujikura et al. (1997) report an unidentified amphipod taxon from the Forecast vent site. Therefore, the Graveyard isopods and amphipods are probably non-vent

species intermingling with peripheral vent species. This intermingling of vent and non-vent species is common in peripheral vent habitats (Hashimoto et al. 1995; Tsurumi and Tunnicliffe, 2003; Levin et al. 2016). Overall, the Snail Graveyard provides a good snapshot of chemosynthetic-derived primary production transferring into the unproductive deep-sea (Levin et al. 2016).

The status of the copepods is less clear. To date, dirivultids are known only as associates of chemosynthetic communities (Humes 1988; Gollner, Ivanenko, et al. 2010). Three other copepod families (known from the deep sea) occurred both at vents and the Graveyard, but I cannot determine if the species are the same in the two habitats. Only further investigation of these and future specimens will reveal if these taxa are associated with vent habitats. The thermal and chemical conditions of vents may be responsible for lower meiofaunal diversity compared to peripheral habitats, as at East Pacific Rise sites (Gollner et al. 2010). Gollner et al. (2015) also suggest that the physiological characteristics related to a small body size, such as their small thermal mass and limited methods of tolerating these environmental stresses, contribute to this pattern.

*Alpha Diversity in the Mariana BASC***:**

The vent sites in the central Mariana BASC appear more species-rich than those in the south (Table 7). The three best linear models for the α-diversity data indicate that species richness most strongly correlates with distance from the arc compared to all other explanatory variables. Therefore, it seems that the geographic locations of the sites play a role in shaping the richness patterns in the BASC in some way. While seafloor topography of the central sites may facilitate larval exchange better than among southern sites, other potential factors related to the

distance from the arc may affect diversity. For example, since the spreading rate of the southern BASC is faster than the central portion (Baker et al. 2017) and spreading rate correlates with disturbance events in hydrothermal habitats (Juniper & Tunnicliffe, 1997), it's possible that lower habitat stability in the southern sites drive their lower diversity. Low habitat stability could prevent the southern sites from reaching a state of equilibrium, keeping the assemblages in lower diversity, early successional stages. Alternatively, higher disturbance frequencies in the southern sites may also select for disturbance-tolerant subset of species from the regional species pool. Distance from the arc may also affect the size of vents sites or the chemistry of their fluid characteristics, which could influence the habitat suitability for the vent-endemics. Given that this model does not indicate that isolation significantly correlates with species richness, it appears that a species-isolation relationship is not present in the hydrothermal vents of the Mariana BASC. Although I would expect the species-area relationship to apply in this vent system, I do not have the data to test it. Explanatory variables I could not analyze, but expect could explain the species richness patterns in the BASC, include: habitat area, habitat heterogeneity and fluid chemistry.

*Beta Diversity in the Mariana BASC***:**

Numerous methods are available to calculate β-diversity (Tuomisto 2010) and, although they each have their inherent benefits and limitations, using multiple β-diversity indices in tandem reduces these limitations while retaining their benefits (Anderson et al. 2011; Chase et al. 2011). As demonstrated by many recent studies (e.g. Anderson et al. 2013; Vanschoenwinkel et al. 2013; Ellingsen et al. 2015; Catano et al. 2017; Petsch et al. 2017), the Jaccard and Raup-Crick indices are a practical pair of β-diversity measures to use for species presence-absence data. The β_J-diversity provides the direct pairwise proportion of shared species between sites,

and the β_{RC}-diversity provides the probability that the observed β_J-diversity would occur by random chance, which can implicate deterministic processes as influences on biotic differences between sites (Chase et al. 2011).

Kojima and Watanabe (2015) provide strong evidence to reject the null hypothesis that all the vent species in the Mariana BASC are present in every vent site; my findings are similar. The β_J-diversity results in this study generally support the dissimilarity patterns reported in Kojima and Watanabe (2015). Firstly, the Snail, Archaean and Urashima-Pika vent sites share a larger proportion of species with each other than they do with Forecast and Illium-Alice Springs. Secondly, Figure 12A and the cladogram in Kojima and Watanabe (2015) both indicate that Forecast shares a larger proportion of species with Illium-Alice Springs than Snail, Archaean and Urashima-Pika. My findings are similar, but Kojima and Watanabe (2015) do not present their β_J values, so a comparison is not possible.

Although the three southern sites share only 46-73% of their species, their pairwise β_{RC} values fall beyond the negative CI of the null model, indicating that they share significantly more species than expected by random chance alone (Table 8). Low α-diversity values inflate the measures of β-diversity for indices that exclude joint absences, like the Jaccard index (Clarke et al. 2006; Vellend et al. 2007), thereby causing species-poor sites to seem more biologically distinct from diverse sites. Snail, Archaean and Urashima-Pika exhibit the lowest α-diversity values in the system (Table 7), which suggests that the richness component inflated their β_J values in both this study and Kojima and Watanabe (2015). Given that the Raup-Crick index controls for α-diversity, their significantly low β_{RC} values provide insights into the dissimilarity among these sites that the relatively high β_J values cannot reveal. Admittedly, the measures provided by the Raup-Crick index are also limited for species-poor sites because it is more

difficult for this index to detect significant deviations from the null model when sites have low α-diversity values (Chase et al. 2011). Nonetheless, despite this limitation, the Raup-Crick index still detected the significant deviation from the null model for these three vent sites. Thus, deterministic factors are probably operative here. Given that these three vent sites lie within 5 km of each other, proximity may be a factor driving these similarities, as in other insular habitats (e.g. Simberloff, 1974; Kadmon and Pulliam, 1993). The linear regression model also indicates that distance between vent sites (ie. isolation) has a significant, positive correlation with the β_{RC}-diversity values; with increasing distance, vent sites are increasingly different from each other with respect to the null model. Alternatively, if the southern sites are exposed to a greater disturbance frequency, the significant β_{RC}-diversity values between the three southern-most sites provide evidence for the selection of disturbance-tolerant species in these sites.

Overall, only 21% of the β_{RC} values exceed the negative CI of the null models, which suggests that stochastic assembly processes are mainly responsible for the observed differences among vent sites. If stochastic processes are mainly responsible, then I hypothesize that vent sites would resemble closer sites more than those that are further away because, given random chance, there should be a higher likelihood of larval exchange between closer pairs of vent sites; this is similar to the mechanism behind the species-isolation relationship in island biogeography. Unknown deterministic factors may also have a secondary influence on the vent assemblages that are responsible for the significant similarities between certain pairs of vent sites. The relevant linear model only explains 46% of the variability in the β_{RC} data, so it is possible that one or several unknown environmental variables are partially responsible for the β_{RC} patterns.

Regional Comparisons:

The β_J values of both the Mariana BASC and the Juan de Fuca Ridge indicate that, within each system, vent sites share about the same proportion of species (~ 47% and ~49% respectively). However, ~62% of the β_{RC} values for the Juan de Fuca vent sites exceed the CIs of the null model and the average β_{RC} value is much lower than that of the Mariana BASC (Tables 8 and 10).These β_{RC} values suggest that deterministic factors present a much larger influence on the Juan de Fuca vent diversity distribution patterns, driving the sites to be significantly more similar than expected by random chance alone on average. However, one β_{RC} value exceeds the positive CI, indicating that the Endeavour and Middle Valley sites are significantly more different than expected by random chance. Middle Valley exhibits the highest α-diversity and is the most distinct vent site in the region (Table 11). It is the only sedimented vent site in the Juan de Fuca Ridge, and this habitat dissimilarity is an important deterministic factor driving its distinct species composition (Juniper et al. 1992). The distinctness of Middle Valley is likely also an important factor behind the significant similarities between many of the other vent sites relative to the null model. Both γ- and average α-diversity values of the Juan de Fuca Ridge region are much higher than those of the Mariana BASC, but the average α- to γ-diversity ratio (β-diversity originally defined by Whitaker as a measure of similarity) of the Mariana BASC vent sites is higher than that of the Juan de Fuca Ridge (56 and 45 respectively). The greater similarity between the BASC vent assemblages suggests that vent sites of Juan de Fuca Ridge may support greater habitat variability than those in the Mariana BASC.

Despite the uncertainty of the true γ-diversity in the Mariana BASC system, the best minimum estimate of 37 species is low relative to other vent systems around the world (Table 11). For example, Hashimoto et al. (1995) collected 48 taxa from the Minami-Ensei Knoll site in the Okinawa Trough region on the first expedition compared to the 35 taxa identified from Hafa

Adai, including those collected from the Snail Graveyard. Thus, the relatively low diversity of the Mariana BASC is likely not an artifact of differences in sampling effort. Higher habitat variability could be driving the higher regional species richness in vent systems. For example, only hard substratum habitats are present in the Mariana BASC vents, whereas both sedimented and hard substratum habitats are both prevalent at the Okinawa Trough vents (Nakamura, 1990; Kimura, 1996). Like Middle Valley on the Juan de Fuca Ridge, the presence of both substratum types may explain why the Okinawa Trough vents are more species rich. The ages of the spreading systems may affect species richness as well. The Juan de Fuca Ridge is older than the Mariana BASC (Tunnicliffe and Fowler, 1996; Stern et al. 2003), which may foster greater species accumulation in the former. The back-arcs in the western Pacific are also both smaller in extent than MORs and are poorly connected (Mitarai et al. 2016).

*The Mariana Region***:**

The close proximity between the Mariana BASC and the Mariana Arc suggests they should share many features. However, the vent faunae of the BASC and the Arc differ in many ways. The regional (γ-) diversity is higher and the average local (α-) diversity is lower for Arc vents compared to the BASC. Based on the distance-to-centroid analyses, β_J values indicate that the BASC sites share significantly higher proportions of species than the Arc sites (Figure 15a). It also indicates that Arc β_{RC} values are significantly higher than those of the BASC (Figure 15b), which implies that BASC sites are significantly more similar to each other relative to the null expectation than are Arc sites. Given that both indices indicate that β-diversity is higher among the Arc vents, it appears the species composition component is driving these differences. These results also support the hypothesis that Arc-hosted vent systems exhibit higher β-diversity

than BASC-hosted systems. In total, 62 identified macrofaunal, vent-obligate taxa are present in these two Mariana systems, but only five (8%) of the species are shared between them.

A greater proportion of Arc β_{RC} values exceed the CIs of the null model (~36%) than those of the BASC. Thus, while random assembly processes are the dominant influence on Arc vent assemblages, as in the BASC, deterministic influences have a greater impact on them. Most of the significant β_{RC} values for the Arc indicate major divergence in species compositions between the respective pairs of vent sites from the null expectation. However, three sites in the northern Arc are significantly more similar to each other than expected by random chance as well.

A difference in dispersal or colonization ability of BASC versus Arc vent larvae could be one plausible cause for the differing β-diversity patterns. Catano et al. (2017) found that greater dispersal abilities of herbaceous plants significantly correlated with both a higher α-diversity and a lower β_J-diversity in their communities. Such enhanced connectivity reduces ecological drift within a system. This homogenizes and increases the α- to γ-diversity ratios of the assemblages by allowing a greater proportion of the regional species pool to spread throughout the system (e.g. Wandrag et al. 2017; Gilbert and Levine, 2017). Given that the BASC vents exhibit both higher average α-diversity and lower β_J-diversity relative to the Arc vents, differences in connectivity may be operative. Considering that the vent fauna disperse nearly exclusively by ocean currents, with some vertical migration, the differing topographies of the BASC and the Arc seafloor may influence connectivity within these two systems. The BASC vents lie within a basin, whereas the Arc vents lie on the relatively shallow peaks of seamounts (Embley et al. 2007). It is possible that larvae released from within the basin are better retained than those released from the seamount peaks, which would support better connectivity among BASC sites.

Differences in habitat heterogeneity may also support greater assemblage similarity in the BASC sites compared to those of the Arc. Studies show a general positive relationship between habitat heterogeneity and all the common diversity indices (α-, β- & γ-diversity), although there are some exceptions to these general trends (e.g. Tews et al. 2004; Heino et al. 2015). Resing et al. (2009) report wide variability in both hydrothermal activity and fluid chemistry among Arc sites. This hydrothermal variability reflects magmatic variability beneath the seamounts. For example, the distance between volcano summit and the underlying magma chamber influences the chemistry of the hydrothermal fluids (Resing et al. 2009). The magma driving hydrothermal activity on the Arc originates from hydration-induced melting of down-thrust crust with considerable variability in behaviour and composition of the rising magma. This wide range of rock composition directly drives high fluid variability in arc-hosted vents (e.g. de Ronde et al. 2001). The magma in the BASC originates from decompression melting of dry rock, likely due to upwelling of underlying mantle (Stern et al. 2003; Stern et al. 2013). Unlike hydration-induced melting, decompression melting does not generate magma chambers with variable depths. Rock composition originating from back-arc spreading is also much less variable than that formed on arc volcanoes, and instead, basalts formed in MOR and BASC settings are quite similar (Stern et al. 2003). Although variability in magmatic conditions is also present below the BASC vent sites (Baker et al. 2017), especially Forecast (Stern et al. 2013), the greater variability in magmatic conditions below the Arc-hosted vents causes the associated vents to have much greater variability in fluid chemistry than the BASC vents (Butterfield et al. in prep.). Given that underlying magmatic and geologic conditions influence vent habitat size, habitat heterogeneity (Anderson et al. 2017) and fluid chemistry (e.g. Lilley et al. 2003) that likely

influences microbial composition and net productivity, the higher hydrothermal variability along the Arc may explain the greater β-diversity.

References:

Anderson, M. J., Crist, T. O., Chase, J. M., Vellend, M., Inouye, B. D., Freestone, A. L., . . . Swenson, N. G. (2011). Navigating the multiple meanings of β diversity: A roadmap for the practicing ecologist. *Ecology Letters, 14*(1), 19-28.

Anderson, M. J., Tolimieri, N., & Millar, R. B. (2013). Beta diversity of demersal fish assemblages in the North-Eastern Pacific: Interactions of latitude and depth. *PLoS One, 8*(3), e57918.

Anderson, M. O., Chadwick Jr, W. W., Hannington, M. D., Merle, S. G., Resing, J. A., Baker, E. T., . . . Augustin, N. (2017). Geological interpretation of volcanism and segmentation of the Mariana back-arc spreading center between 12.7° N and 18.3° N. *Geochemistry, Geophysics, Geosystems, 18*(6), 2240-2274.

Arp, A. J., & Childress, J. J. (1981). Functional characteristics of the blood of the deep-sea hydrothermal vent brachyuran crab. *Science, 214*(4520), 559-561.

Astorga, A., Death, R., Death, F., Paavola, R., Chakraborty, M., & Muotka, T. (2014). Habitat heterogeneity drives the geographical distribution of beta diversity: The case of New Zealand stream invertebrates. *Ecology and Evolution, 4*(13), 2693-2702.

Bachraty, C., Legendre, P., & Desbruyères, D. (2009). Biogeographic relationships among deep-sea hydrothermal vent faunas at global scale. *Deep Sea Research Part I: Oceanographic Research Papers, 56*(8), 1371-1378.

Baker, E. T., Resing, J. A., Haymon, R. M., Tunnicliffe, V., Lavelle, J. W., Martinez, F., . . . Nakamura, K. (2016). How many vent fields? New estimates of vent field populations on ocean ridges from precise mapping of hydrothermal discharge locations. *Earth and Planetary Science Letters, 449*, 186-196.

Baker, E. T., Walker, S. L., Resing, J. A., Chadwick Jr, W. W., Merle, S. G., Anderson, M. O., . . . Michael, S. (2017). The effect of arc proximity on hydrothermal activity along spreading centers: New evidence from the Mariana Back Arc (12.7˚N–18.3˚N). *Geochemistry, Geophysics, Geosystems, 18*(11), 4211-4228.

Baselga, A. (2010). Partitioning the turnover and nestedness components of beta diversity. *Global Ecology and Biogeography, 19*(1), 134-143.

Bengtson, P. (1988). Open nomenclature. *Palaeontology, 31*(1), 223-227.

Bennett, S. A., Van Dover, C., Breier, J. A., & Coleman, M. (2015). Effect of depth and vent fluid composition on the carbon sources at two neighboring deep-sea hydrothermal vent fields (Mid-Cayman Rise). *Deep Sea Research Part I: Oceanographic Research Papers, 104*, 122-133.

Bergquist, D. C., Ward, T., Cordes, E. E., McNelis, T., Howlett, S., Kosoff, R., . . . Fisher, C. R. (2003). Community structure of vestimentiferan-generated habitat islands from Gulf of Mexico cold seeps. *Journal of Experimental Marine Biology and Ecology, 289*(2), 197-222.

Breusing, C., Johnson, S. B., Tunnicliffe, V., & Vrijenhoek, R. C. (2015). Population structure and connectivity in Indo-Pacific deep-sea mussels of the *Bathymodiolus septemdierum* complex. *Conservation Genetics, 16*(6), 1415-1430.

Catano, C. P., Dickson, T. L., & Myers, J. A. (2017). Dispersal and neutral sampling mediate contingent effects of disturbance on plant beta-diversity: A meta-analysis. *Ecology Letters, 20*(3), 347-356.

Chapman, A. S., Beaulieu, S. E., Colaço, A., Gebruk, A. V., Hilario, A., Kihara, T. C., . . . Bates, A. E. (2019). sFDvent: A global trait database for deep-sea hydrothermal-vent fauna. *Global Ecology and Biogeography, 28*(11), 1538-1551.

Chase, J. M., Kraft, N. J., Smith, K. G., Vellend, M., & Inouye, B. D. (2011). Using null models to disentangle variation in community dissimilarity from variation in α-diversity. *Ecosphere, 2*(2), 1-11.

Clark, K., Karsch-Mizrachi, I., Lipman, D. J., Ostell, J., & Sayers, E. W. (2016). GenBank. *Nucleic Acids Research 44*, D67–D72.

Clarke, K. R., Somerfield, P. J., & Chapman, M. G. (2006). On resemblance measures for ecological studies, including taxonomic dissimilarities and a zero-adjusted Bray–Curtis coefficient for denuded assemblages. *Journal of Experimental Marine Biology and Ecology, 330*(1), 55-80.

de Ronde, C. E., Baker, E. T., Massoth, G. J., Lupton, J. E., Wright, I. C., Feely, R. A., & Greene, R. R. (2001). Intra-oceanic subduction-related hydrothermal venting, Kermadec volcanic arc, New Zealand. *Earth and Planetary Science Letters, 193*(3-4), 359-369.

Desbruyères, D., Alayse-Danet, A.-M., & Ohta, S. (1994). Deep-sea hydrothermal communities in Southwestern Pacific back-arc basins (the North Fiji and Lau Basins): Composition, microdistribution and food web. *Marine Geology, 116*(1-2), 227-242.

Desbruyères, D., Almeida, A., Biscoito, M., Comtet, T., Khripounoff, A., Le Bris, N., . . . Segonzac, M. (2000). A review of the distribution of hydrothermal vent communities along the northern Mid-Atlantic Ridge: Dispersal vs. environmental controls. In *Island, Ocean and Deep-Sea Biology* (pp. 201-216): Springer, Dordrecht.

Desbruyères, D., Hashimoto, J., & Fabri, M.-C. (2006). Composition and biogeography of hydrothermal vent communities in western Pacific back-Arc basins. *Geophysical Monograph Series, 166*, 215-234.

Douville, E., Charlou, J., Oelkers, E., Bienvenu, P., Colon, C. J., Donval, J., . . . Appriou, P. (2002). The rainbow vent fluids (36˚14′N, MAR): The influence of ultramafic rocks and phase separation on trace metal content in Mid-Atlantic Ridge hydrothermal fluids. *Chemical Geology, 184*(1-2), 37-48.

Du Preez, C., & Fisher, C. R. (2018). Long-term stability of back-arc basin hydrothermal vents. *Frontiers in Marine Science, 5*(54).

Ellingsen, K. E. (2002). Soft-sediment benthic biodiversity on the continental shelf in relation to environmental variability. *Marine Ecology Progress Series, 232*, 15-27.

Ellingsen, K. E., Anderson, M. J., Shackell, N. L., Tveraa, T., Yoccoz, N. G., & Frank, K. T. (2015). The role of a dominant predator in shaping biodiversity over space and time in a marine ecosystem. *Journal of Animal Ecology, 84*(5), 1242-1252.

Embley, R. W., Baker, E. T., Butterfield, D. A., Chadwick, W. W., Lupton, J. E., Resing, J. A., . . . Merle, S. G. (2007). Exploring the submarine ring of fire: Mariana Arc-Western Pacific. *Oceanography, 20*(4), 68-79.

Fautin, D., & Hessler, R. (1989). *Marianactis bythios*, a new genus and species of actinostolid sea anemone (Coelenterata: Actiniaria) from the Mariana vents. *Proceedings of the Biological Society of Washington, 102*(4), 815-825.

Fujikura, K., Yamazaki, T., Hasegawa, K., Tsunogai, U., Stern, R. J., Ueno, H., . . . Okutani, T. (1997). Biology and earth scientific investigation by the submersible "Shinkai 6500" system of deep-sea hydrothermal and lithosphere in the Mariana back-arc basin. *JAMSTEC Journal of Deep Sea Research, 13*, 1-20.

Fujita, Y., Matsumoto, H., Fujiwara, Y., Hashimoto, J., Galkin, S., Ueshima, R., & Miyazaki, J. (2009). Phylogenetic relationships of deep-sea *Bathymodiolus* mussels to their mytilid relatives from sunken whale carcasses and wood. *Venus, 67*(3-4), 123-134.

Galkin, S. (1997). Megafauna associated with hydrothermal vents in the Manus back-arc basin (Bismarck Sea). *Marine Geology, 142*(1-4), 197-206.

Gauthier, O., Sarrazin, J., & Desbruyères, D. (2010). Measure and mis-measure of species diversity in deep-sea chemosynthetic communities. *Marine Ecology Progress Series, 402*, 285-302.

Gebruk, A., Southward, E., Kennedy, H., & Southward, A. (2000). Food sources, behaviour, and distribution of hydrothermal vent shrimps at the Mid-Atlantic Ridge. *Journal of the Marine Biological Association of the United Kingdom, 80*(3), 485-499.

Gebruk, A. V., Galkin, S., Vereshchaka, A., Moskalev, L., & Southward, A. (1997). Ecology and biogeography of the hydrothermal vent fauna of the Mid-Atlantic Ridge. In *Advances in Marine Biology* (Vol. 32, pp. 93-144): Elsevier.

Gilbert, B., & Levine, J. M. (2017). Ecological drift and the distribution of species diversity. *Proceedings of the Royal Society B: Biological Sciences, 284*(1855), 20170507.

Goffredi, S. K., Johnson, S., Tunnicliffe, V., Caress, D., Clague, D., Escobar, E., . . . Vrijenhoek, R. (2017). Hydrothermal vent fields discovered in the southern Gulf of California clarify role of habitat in augmenting regional diversity. *Proceedings of the Royal Society B: Biological Sciences, 284*(1859), 20170817.

Gollner, S., Govenar, B., Fisher, C. R., & Bright, M. (2015). Size matters at deep-sea hydrothermal vents: Different diversity and habitat fidelity patterns of meio-and macrofauna. *Marine Ecology Progress Series, 520*, 57-66.

Gollner, S., Ivanenko, V. N., Arbizu, P. M., & Bright, M. (2010). Advances in taxonomy, ecology, and biogeography of Dirivultidae (Copepoda) associated with chemosynthetic environments in the deep sea. *PLoS One, 5*(8), e9801.

Gollner, S., Riemer, B., Arbizu, P. M., Le Bris, N., & Bright, M. (2010). Diversity of meiofauna from the 9˚50′ N East Pacific Rise across a gradient of hydrothermal fluid emissions. *PLoS One, 5*(8), e12321.

Govenar, B. (2010). Shaping vent and seep communities: habitat provision and modification by foundation species. In *The vent and seep biota* (pp. 403-432): Springer, Dordrecht.

Guinot, D., & Segonzac, M. (2018). A review of the brachyuran deep-sea vent community of the western Pacific, with two new species of *Austinograea* Hessler & Martin, 1989 (Crustacea, Decapoda, Brachyura, Bythograeidae) from the Lau and North Fiji Back-Arc Basins. *Zoosystema, 40*(1), 1-37.

Harrison, R. G. (2012). The language of speciation. *Evolution: International Journal of Organic Evolution, 66*(12), 3643-3657.

Hashimoto, J., Ohta, S., Fujikura, K., & Miura, T. (1995). Microdistribution pattern and biogeography of the hydrothermal vent communities of the Minami-Ensei Knoll in the Mid-Okinawa Trough, Western Pacific. *Deep Sea Research Part I: Oceanographic Research Papers, 42*(4), 577-598.

Heino, J., Melo, A. S., & Bini, L. M. (2015). Reconceptualising the beta diversity-environmental heterogeneity relationship in running water systems. *Freshwater Biology, 60*(2), 223-235.

Henry, M. S., Childress, J. J., & Figueroa, D. (2008). Metabolic rates and thermal tolerances of chemoautotrophic symbioses from Lau Basin hydrothermal vents and their implications for species distributions. *Deep Sea Research Part I: Oceanographic Research Papers, 55*(5), 679-695.

Hessler, R. R., & Lonsdale, P. F. (1991). Biogeography of Mariana Trough hydrothermal vent communities. *Deep Sea Research Part A. Oceanographic Research Papers, 38*(2), 185-199.

Hessler, R. R., & Smithey, W. M. (1983). The distribution and community structure of megafauna at the Galapagos Rift hydrothermal vents. In *Hydrothermal Processes at Seafloor Spreading Centers* (pp. 735-770): Springer, Boston, MA.

Hewitt, J. E., Thrush, S. F., Halliday, J., & Duffy, C. (2005). The importance of small-scale habitat structure for maintaining beta diversity. *Ecology, 86*(6), 1619-1626.

Hu, S. (2007). Akaike information criterion. *Center for Research in Scientific Computation, 93*.

Humes, A. G. (1988). Copepoda from deep-sea hydrothermal vents and cold seeps. *Hydrobiologia, 167*(1), 549-554.

Humes, A. G. (1990). Copepods (Siphonostomatoida) from a deep-sea hydrothermal vent at the Mariana Back-Arc Basin in the Pacific, including a new genus and species. *Journal of Natural History, 24*(2), 289-304.

Hurlbert, S. H. (1971). The nonconcept of species diversity: A critique and alternative parameters. *Ecology, 52*(4), 577-586.

Jaccard, P. (1912). The distribution of the flora in the alpine zone. *New Phytologist, 11*(2), 37-50.

Johnson, S. B., Warén, A., Tunnicliffe, V., Dover, C. V., Wheat, C. G., Schultz, T. F., & Vrijenhoek, R. C. (2015). Molecular taxonomy and naming of five cryptic species of *Alviniconcha* snails

(Gastropoda: Abyssochrysoidea) from hydrothermal vents. *Systematics and Biodiversity, 13*(3), 278-295.

Johnson, S. B., Warén, A., & Vrijenhoek, R. C. (2008). DNA barcoding of *Lepetodrilus* limpets reveals cryptic species. *Journal of Shellfish Research, 27*(1), 43-52.

Juniper, S. K. & Tunnicliffe, V. (1997). Crustal accretion and the hot vent ecosystem. *Philosophical Transactions of the Royal Society of London. Series A: Mathematical, Physical and Engineering Sciences, 355*(1723), 459-474.

Juniper, S. K., Tunnicliffe, V., & Southward, E. C. (1992). Hydrothermal vents in turbidite sediments on a Northeast Pacific spreading centre: Organisms and substratum at an ocean drilling site. *Canadian Journal of Zoology, 70*(9), 1792-1809.

Kadmon, R., & Pulliam, H. R. (1993). Island biogeography: Effect of geographical isolation on species composition. *Ecology, 74*(4), 977-981.

Keith, M., Haase, K. M., Klemd, R., Schwarz-Schampera, U., & Franke, H. (2017). Systematic variations in magmatic sulphide chemistry from mid-ocean ridges, back-arc basins and island arcs. *Chemical Geology, 451*, 67-77.

Kelley, D. S., Karson, J. A., Blackman, D. K., FruÈh-Green, G. L., Butterfield, D. A., Lilley, M. D., . . . the AT3-60 Shipboard Party (2001). An off-axis hydrothermal vent field near the Mid-Atlantic Ridge at 30˚N. *Nature, 412*(6843), 145-149.

Kimura, M. (1980). A simple method for estimating evolutionary rates of base substitutions through comparative studies of nucleotide sequences. *Journal of Molecular Evolution, 16*(2), 111-120.

Kimura, M. (1996). Active rift system in the Okinawa Trough and its northeastern continuation. *Bulletin of the Disaster Prevention Research Institute, Kyoto University, 45*, 27-38.

Kojima, S., & Watanabe, H. (2015). Vent fauna in the Mariana Trough. In *Subseafloor Biosphere Linked to Hydrothermal Systems* (pp. 313-323): Springer, Tokyo.

Komai, T., & Giguère, T. (2019). A new species of alvinocaridid shrimp *Rimicaris* Williams & Rona, 1986 (Decapoda: Caridea) from hydrothermal vents on the Mariana Back Arc Spreading Center, northwestern Pacific. *Journal of Crustacean Biology, 39*(5), 640-650.

Komai, T., Menot, L., & Segonzac, M. (2016). New records of caridean shrimp (Crustacea: Decapoda) from hydrothermally influenced fields off Futuna Island, Southwest Pacific, with description of a new species assigned to the genus *Alvinocaridinides* Komai & Chan, 2010 (Alvinocarididae). *Zootaxa, 4098*(2), 298-310.

Komai, T., & Segonzac, M. (2005). A revision of the genus *Alvinocaris* Williams and Chace (Crustacea: Decapoda: Caridea: Alvinocarididae), with descriptions of a new genus and a new species of *Alvinocaris*. *Journal of Natural History, 39*(15), 1111-1175.

Komai, T., & Tsuchida, S. (2015). New records of Alvinocarididae (Crustacea: Decapoda: Caridea) from the southwestern Pacific hydrothermal vents, with descriptions of one new genus and three new species. *Journal of Natural History, 49*(29-30), 1789-1824.

Kumar, S., Stecher, G., Li, M., Knyaz, C., & Tamura, K. (2018). MEGA X: molecular evolutionary genetics analysis across computing platforms. *Molecular Biology and Evolution, 35*(6), 1547-1549.

Legendre, P. (2014). Interpreting the replacement and richness difference components of beta diversity. *Global Ecology and Biogeography, 23*(11), 1324-1334.

Levin, L. A., Baco, A. R., Bowden, D. A., Colaco, A., Cordes, E. E., Cunha, M. R., . . . Watling, L. (2016). Hydrothermal vents and methane seeps: Rethinking the sphere of influence. *Frontiers in Marine Science, 3*(72).

Lilley, M. D., Butterfield, D. A., Lupton, J. E., & Olson, E. J. (2003). Magmatic events can produce rapid changes in hydrothermal vent chemistry. *Nature, 422*(6934), 878-881.

López-González, P., Rodríguez, E., Gili, J., & Segonzac, M. (2003). New records on sea anemones (Anthozoa: Actiniaria) from hydrothermal vents and cold seeps. *Zoologische Verhandelingen*, 215-244.

Luther III, G. W., Gartman, A., Yücel, M., Madison, A. S., Moore, T. S., Nees, H. A., . . . Shank, T. M. (2012). Chemistry, temperature, and faunal distributions at diffuse-flow hydrothermal vents: Comparison of two geologically distinct ridge systems. *Oceanography, 25*(1), 234-245.

MacArthur, R., & Wilson, E. (1967). The theory of island biogeography. *Monograph Population Biology, 1*.

Marsh, L., Copley, J. T., Huvenne, V. A., Linse, K., Reid, W. D., Rogers, A. D., . . . Tyler, P. A. (2012). Microdistribution of faunal assemblages at deep-sea hydrothermal vents in the Southern Ocean. *PLoS One, 7*(10), e48348.

Martin, J. W. (1990). *Chorocaris vandoverae*, a new genus and species of hydrothermal vent shrimp (Crustacea, Decapoda, Bresiliidae). *Contributions in Science, 417*, 1-11.

Mironov, A. N., Gebruk, A. V., & Moskalev, L. I. (1998). Biogeographical patterns of the hydrothermal vent fauna: A comparison with 'nonvent biogeography'. *Cahiers de Biologie Marine, 39*, 367-368.

Mitarai, S., Watanabe, H., Nakajima, Y., Shchepetkin, A. F., & McWilliams, J. C. (2016). Quantifying dispersal from hydrothermal vent fields in the western Pacific Ocean. *Proceedings of the National Academy of Sciences, 113*(11), 2976-2981.

Moalic, Y., Desbruyères, D., Duarte, C. M., Rozenfeld, A. F., Bachraty, C., & Arnaud-Haond, S. (2011). Biogeography revisited with network theory: Retracing the history of hydrothermal vent communities. *Systematic Biology, 61*(1), 127.

Nakamura, K. (1990). Discovery of a black smoker vent and a pockmark emitting CO_2-rich fluid on the sea-floor hydrothermal mineralization field at the Izena Cauldron in the Okinawa Trough. *Kaiyoukagakugijutusenta Houkoku (Jamstectr Deepsea Research), 6*, 33-50.

Oksanen, J., Blanchet, F. G., Kindt, R., Legendre, P., Minchin, P. R., O'hara, R., . . . Wagner, H. (2013). Package 'vegan'. *Community ecology package, version, 2*(9), 1-295.

Okutani, T., & Ohta, S. (1988). A new gastropod mollusk associated with hydrothermal vents in the Mariana Back-Arc Basin, Western Pacific. *Venus (Japanese Journal of Malacology), 47*(1), 1-9.

Paradis, E., & Schliep, K. (2018). ape 5.0: an environment for modern phylogenetics and evolutionary analyses in R. *Bioinformatics, 35*(3), 526-528.

Petsch, D. K., Schneck, F., & Melo, A. S. (2017). Substratum simplification reduces beta diversity of stream algal communities. *Freshwater Biology, 62*(1), 205-213.

Podowski, E. L., Moore, T. S., Zelnio, K. A., Luther III, G. W., & Fisher, C. R. (2009). Distribution of diffuse flow megafauna in two sites on the Eastern Lau Spreading Center, Tonga. *Deep Sea Research Part I: Oceanographic Research Papers, 56*(11), 2041-2056.

Ramirez-Llodra, E., Shank, T. M., & German, C. R. (2007). Biodiversity and biogeography of hydrothermal vent species: Thirty years of discovery and investigations. *Oceanography, 20*(1), 30-41.

Ratnasingham, S., & Hebert, P. D. (2007). BOLD: The Barcode of Life Data System (http://www. barcodinglife. org). *Molecular Ecology Notes, 7*(3), 355-364.

Raup, D. M. (1975). Taxonomic diversity estimation using rarefaction. *Paleobiology, 1*(4), 333-342.

Raup, D. M., & Crick, R. E. (1979). Measurement of faunal similarity in paleontology. *Journal of Paleontology*, 1213-1227.

Resing, J. A., Baker, E. T., Lupton, J. E., Walker, S. L., Butterfield, D. A., Massoth, G. J., & Nakamura, K. -i. (2009). Chemistry of hydrothermal plumes above submarine volcanoes of the Mariana Arc. *Geochemistry, Geophysics, Geosystems, 10*(2).

Rodríguez, R. A., Herrera, A. M., Santander, J., Miranda, J. V., Fernández-Rodríguez, M. J., Quirós, Á., . . . Delgado, J. D. (2015). Uncertainty principle in niche assessment: A solution to the dilemma redundancy vs. competitive exclusion, and some analytical consequences. *Ecological Modelling, 316*, 87-110.

Rogers, A. D., Tyler, P. A., Connelly, D. P., Copley, J. T., James, R., Larter, R. D., . . . Zwirglmaier, K. (2012). The discovery of new deep-sea hydrothermal vent communities in the Southern Ocean and implications for biogeography. *PLoS Biology, 10*(1), e1001234.

Schnabel, K. E., Cabezas, P., McCallum, A., Macpherson, E., Ahyong, S. T., & Baba, K. (2011). Worldwide distribution patterns of squat lobsters. *The Biology of Squat Lobsters*, (pp. 149-182): CSIRO.

Sen, A., Becker, E. L., Podowski, E. L., Wickes, L. N., Ma, S., Mullaugh, K. M., . . . Fisher, C. R. (2013). Distribution of mega fauna on sulfide edifices on the Eastern Lau Spreading Center and Valu Fa Ridge. *Deep Sea Research Part I: Oceanographic Research Papers, 72*, 48-60.

Sen, A., Kim, S., Miller, A. J., Hovey, K. J., Hourdez, S., Luther III, G. W., & Fisher, C. R. (2016). Peripheral communities of the Eastern Lau Spreading Center and Valu Fa Ridge: Community composition, temporal change and comparison to near-vent communities. *Marine Ecology, 37*(3), 599-617.

Simberloff, D. S. (1974). Equilibrium theory of island biogeography and ecology. *Annual Review of Ecology and Systematics, 5*(1), 161-182.

Sleep, N. H. (1975). Formation of oceanic crust: Some thermal constraints. *Journal of Geophysical Research, 80*(29), 4037-4042.

Soininen, J., Heino, J., & Wang, J. (2018). A meta-analysis of nestedness and turnover components of beta diversity across organisms and ecosystems. *Global Ecology and Biogeography, 27*(1), 96-109.

Somero, G. (1992). Biochemical ecology of deep-sea animals. *Experientia, 48*(6), 537-543.

Stern, R. J., Fouch, M. J., & Klemperer, S. L. (2003). An overview of the Izu-Bonin-Mariana subduction factory. *Inside the subduction factory, 138*, 175-222.

Stern, R. J., Tamura, Y., Masuda, H., Fryer, P., Martinez, F., Ishizuka, O., & Bloomer, S. H. (2013). How the Mariana Volcanic Arc ends in the south. *Island Arc, 22*(1), 133-148.

Stiller, J., Rousset, V., Pleijel, F., Chevaldonné, P., Vrijenhoek, R. C., & Rouse, G. W. (2013). Phylogeny, biogeography and systematics of hydrothermal vent and methane seep *Amphisamytha* (Ampharetidae, Annelida), with descriptions of three new species. *Systematics and Biodiversity, 11*(1), 35-65.

R Core Team (2019). A language and environment for statistical computing. Vienna, Austria: R Foundation for Statistical Computing; 2012. *URL https://www. R-project. org*.

Tews, J., Brose, U., Grimm, V., Tielbörger, K., Wichmann, M., Schwager, M., & Jeltsch, F. (2004). Animal species diversity driven by habitat heterogeneity/diversity: The importance of keystone structures. *Journal of Biogeography, 31*(1), 79-92.

Thaler, A. D., Plouviez, S., Saleu, W., Alei, F., Jacobson, A., Boyle, E. A., . . . Van Dover, C. L. (2014). Comparative population structure of two deep-sea hydrothermal-vent-associated decapods (*Chorocaris* sp. 2 and *Munidopsis lauensis*) from southwestern Pacific back-arc basins. *PLoS One, 9*(7), e101345.

Thomson, R. E., Mihály, S. F., Rabinovich, A. B., McDuff, R. E., Veirs, S. R., & Stahr, F. R. (2003). Constrained circulation at Endeavour ridge facilitates colonization by vent larvae. *Nature, 424*(6948), 545-549.

Thurnherr, A., Reverdin, G., Bouruet-Aubertot, P., St Laurent, L., Vangriesheim, A., & Ballu, V. (2008). Hydrography and flow in the Lucky Strike segment of the Mid-Atlantic Ridge. *Journal of Marine Research, 66*(3), 347-372.

Trembath-Reichert, E., Butterfield, D. A., & Huber, J. A. (2019). Active subseafloor microbial communities from Mariana back-arc venting fluids share metabolic strategies across different thermal niches and taxa. *The ISME Journal, 13*(9), 2264-2279.

Tsurumi, M. (2003). Diversity at hydrothermal vents. *Global Ecology and Biogeography, 12*(3), 181-190.

Tsurumi, M., & Tunnicliffe, V. (2003). Tubeworm-associated communities at hydrothermal vents on the Juan de Fuca Ridge, northeast Pacific. *Deep Sea Research Part I: Oceanographic Research Papers, 50*(5), 611-629.

Tunnicliffe, V. (1988). Biogeography and evolution of hydrothermal-vent fauna in the eastern Pacific Ocean. *Proceedings of the Royal society of London. Series B. Biological Sciences, 233*(1272), 347-366.

Tunnicliffe, V. (1997). Hydrothermal vents: a global ecosystem. *JAMSTEC Journal of Deep Sea Research,* 105-110.

Tunnicliffe, V., & Fowler, C. M. R. (1996). Influence of sea-floor spreading on the global hydrothermal vent fauna. *Nature, 379*(6565), 531-533.

Tunnicliffe, V., McArthur, A. G., & McHugh, D. (1998). A biogeographical perspective of the deep-sea hydrothermal vent fauna. In *Advances in Marine Biology* (Vol. 34, pp. 353-442): Academic Press.

Tuomisto, H. (2010). A diversity of beta diversities: Straightening up a concept gone awry. Part 2. Quantifying beta diversity and related phenomena. *Ecography, 33*(1), 23-45.

Tyler, P. A., & Young, C. (1999). Reproduction and dispersal at vents and cold seeps. *Journal of the Marine Biological Association of the United Kingdom, 79*(2), 193-208.

Van Audenhaege, L., Fariñas-Bermejo, A., Schultz, T., & Van Dover, C. L. (2019). An environmental baseline for food webs at deep-sea hydrothermal vents in Manus Basin (Papua New Guinea). *Deep Sea Research Part I: Oceanographic Research Papers*, *148*, 88-99.

Van Dover, C., & Fry, B. (1989). Stable isotopic compositions of hydrothermal vent organisms. *Marine Biology, 102*(2), 257-263.

Van Dover, C. L., Factor, J. R., Williams, A. B., & Berg Jr, C. J. (1985). Reproductive patterns of decapod crustaceans from hydrothermal vents. *Bulletin of the Biological Society of Washington, 6*, 223-227.

Van Dover, C. L., German, C., Speer, K. G., Parson, L., & Vrijenhoek, R. (2002). Evolution and biogeography of deep-sea vent and seep invertebrates. *Science, 295*(5558), 1253-1257.

Vanschoenwinkel, B., Buschke, F., & Brendonck, L. (2013). Disturbance regime alters the impact of dispersal on alpha and beta diversity in a natural metacommunity. *Ecology, 94*(11), 2547-2557.

Vellend, M., Verheyen, K., Flinn, K. M., Jacquemyn, H., Kolb, A., Van Calster, H., . . . Hermy, M. (2007). Homogenization of forest plant communities and weakening of species–environment relationships via agricultural land use. *Journal of Ecology, 95*(3), 565-573.

Wandrag, E. M., Dunham, A. E., Duncan, R. P., & Rogers, H. S. (2017). Seed dispersal increases local species richness and reduces spatial turnover of tropical tree seedlings. *Proceedings of the National Academy of Sciences, 114*(40), 10689-10694.

Wilson, G. D., & Hessler, R. R. (1987). Speciation in the deep sea. *Annual Review of Ecology and Systematics, 18*(1), 185-207.

Yoshikawa, S., Okino, K., & Asada, M. (2012). Geomorphological variations at hydrothermal sites in the southern Mariana Trough: Relationship between hydrothermal activity and topographic characteristics. *Marine Geology, 303*, 172-182.

Zhou, Y., Zhang, D., Zhang, R., Liu, Z., Tao, C., Lu, B., . . . Wang, C. (2018). Characterization of vent fauna at three hydrothermal vent fields on the Southwest Indian Ridge: Implications for biogeography and interannual dynamics on ultraslow-spreading ridges. *Deep Sea Research Part I: Oceanographic Research Papers, 137*, 1-12.

Chapter 3: Conclusions and Future Directions

Major Outcomes:

*Collected Taxa***:**

My work presents the results of 31 biological samples collected across ten dives from the four vent sites explored during the 2016 Hydrothermal Hunt expedition. I identify the taxa in these samples, update the Mariana BASC vent species list and describe their overall spatial distribution patterns. I also explore some abiotic variables possibly driving these patterns and I compare the diversity results to those of two other vent systems – the Mariana Arc and the Juan de Fuca Ridge. A total of 43 taxa are present in my biological samples, and of these taxa, I have assigned 24 species-level identities. The samples collected from the newly discovered Perseverance site contained the least taxa compared to the other three explored sites; the newly discovered Hafa Adai site provided the most. However, virtually all the taxa present in these two new vent sites are also present in at least one other vent site in the Mariana BASC system. The samples also include four newly identified species – a shrimp, a limpet, a polychaete worm, and a barnacle. My work included the description of the new shrimp species, *Rimicaris falkorae* (Komai & Giguère, 2019) (Appendix 1).

I combine the results from these biological samples with the species occurrence data from the Mariana BASC vents present in the literature. Previous studies report many taxa present in this system. However, in addition to the new species discoveries, I have also identified taxa not previously reported, some of which may be undescribed species and require further analysis. Although relatively few meiofauna are present in this collection, many potentially new copepod taxa are present. This collection also contained a single mite, *Copidognathus papillatus* (Krantz, pers. comm.); this specimen is the first confirmation that this species, originally described from

the Galapagos Rift (Krantz 1982), is also present in this system. The cf. *Prionospio* sp. is also a taxon not previously reported from the Mariana BASC and represents the first record of a polychaete species in the family Spionidae in this vent system. Furthermore, two *Munidopsis* specimens are present in a sample from the Snail Graveyard, and, although previous studies describe two *Munidopsis* species from the Mariana BASC (Williams and Baba, 1990; Cubelio et al. 2007), after reviewing most descriptions of the species in the Munidopsidae family, these specimens seem to represent an undescribed species. However, since they are from the Snail Graveyard, it is unclear if these specimens represent a vent-endemic species. My work has also updated some of the identities of taxa previously observed or collected from the BASC (Table 12).

*Diversity Distributions in the Mariana BASC***:**

The various research groups studying the Mariana BASC have likely reported some of the same taxa multiple times, but with different identities (Appendix 5). After combining my data with those of previous studies and taking all possible multiple reports into account, my best estimate for the regional diversity in the Mariana BASC vents is within the range of 37 to 55 vent species. However, to calculate the diversity indices, I synthesized these data to include only the vent-endemic macrofaunal taxa representing a single species that were identified using more than two specimens; I used this conservative approach to ensure that my diversity calculations are as accurate as possible. Based on this conservative approach, the γ-diversity is 30 species. The α-diversity values range from 9 to 26 species and the average is ~17 species. Generally, the central BASC sites are more species rich than those in the south. The β_J-diversity values range from 0.04 to 0. 70, and, on average, the vent sites share ~48% of species. The β_{RC}-diversity values range from -0.999 to 0.766, and the average is ~ -0.11. Only 21% of β_{RC} values indicate

significant deviation from the null expectation of stochastic assembly mechanisms indicating such processes are the primary factors shaping species distribution patterns within the Mariana BASC. My results reject the null hypothesis that states the species composition of each vent site in the Mariana BASC is the same across the system.

*Environmental Drivers***:**

Data exploration provided good, preliminary results for future question and hypothesis generation, as suggested by Bissonette (1999). Linear regression models indicate that the distance of a vent site from the volcanic arc correlates best with α-diversity, although the reason for this is unclear. It may be the case that the topographic setting, which correlates with distance from the arc (Anderson et al. 2017), might be the mechanism shaping the richness pattern among the vent sites, possibly because the topography may influence larval recruitment at the sites (e.g. Thomson et al. 2003). The geologic setting of the BASC segments close to the arc also provides ideal conditions for generating many small, closely spaced vent sites. In contrast, segments further from the arc support the conditions for creating larger and more widely spaced vent sites (Anderson et al. 2017). If vent sites farther from the arc are bigger than those that are closer, the species-area relationship may explain the higher species richness in the central BASC. Although I did not find any abiotic variable that describes the β_J-diversity patterns well, I did find that isolation significantly correlates with the β_{RC}-diversity patterns. This correlation with β_{RC}-diversity indicates that the species compositions of the vent sites more closely resemble nearby vent sites than those farther away.

*Regional Comparisons***:**

The comparison between the Juan de Fuca Ridge, Mariana Arc and BASC systems revealed some interesting differences. The γ-diversity of the Mariana Arc is higher than that of

the BASC, but the average α-diversity of the BASC is notably higher than that of the arc. In contrast, both the γ- and average α-diversity of the Juan de Fuca Ridge are considerably higher than those of both Mariana systems. The β_J-diversity values of the Mariana BASC and the Juan de Fuca Ridge are notably similar to each other, but those of the arc are significantly higher than those of the BASC. In contrast, the β_{RC}-diversity values of these three systems are all substantially different from each other (Figure 14). The Mariana BASC is distinct from the other two systems in a couple of ways. For one, the average β_{RC} is very close to zero, indicating that stochastic processes generally dominate the species assembly mechanisms in the BASC vents. Second, although some β_{RC} values are significantly lower than the null expectation, not a single β_{RC} value is significantly higher than the null expectation. In contrast, the median β_{RC} of the Juan de Fuca Ridge is significantly lower than the null expectation, yet, contains a value that is significantly higher than this expectation. Additionally, both the average and median β_{RC} of the Mariana Arc is quite high – though not significantly – and there are β_{RC} values that are both significantly higher and lower than the null expectation. These results suggest that deterministic assembly mechanisms play a more substantial role in shaping the β-diversity patterns in both the Mariana Arc and the Juan de Fuca Ridge than the BASC system.

Big Picture:

*A Novel Approach to β-diversity Research in Hydrothermal Vents***:**

The general use of β-diversity techniques is uncommon in vent studies, and of those that do include these tools, the majority of them seem to focus on microbial communities (e.g. Xu et al. 2018; Flores et al. 2011; Campbell et al. 2013) rather than macrofaunal assemblages. Among the studies focusing on the vent-obligate animals, few studies investigate β-diversity as a main objective; β-diversity is often either briefly mentioned without specific calculations (e.g. Chown

2012; Goffredi et al. 2017), or it is simply calculated to generally describe dissimilarity patterns (e.g. Rogers et al. 2012). Many of these vent studies also typically use one β-diversity index (e.g. Zhou et al. 2018), despite the wide variety that are available (Anderson et al. 2011), and those that use more than one index often do not provide justification for their choices (e.g. Tsurumi 2003; Sen et al. 2014).

Although my methods for assessing β-diversity are not novel in the field of ecology, their novelty is in their application to hydrothermal vents, especially in the Mariana BASC. Only Kojima & Watanabe (2015) have applied β-diversity techniques to the vent-obligate animals in the Mariana BASC, but the authors only used one index (β_J-diversity). The limitations of using the Jaccard index alone are well documented (Clarke et al. 2006; Anderson et al. 2011). By providing insight into how the observed β_J-diversity compared to what would be expected by random chance, my inclusion of the Raup-Crick index (β_{RC}-diversity) proved useful in reducing the inherent limitations of the Jaccard index. While some previous vent studies have utilized multiple β-diversity indices, to my knowledge, my thesis is the only study that purposefully used a pair of indices that are known to reduce each-others inherent limitations (Anderson et al. 2011; Chase et al. 2011). Although Rogers et al. (2012) seem to be the only other vent study that utilizes the Raup-Crick index, the authors only used it to generate a dendrogram comparing community compositions between vent sites of various regions; they also used this index alone. Part of the novelty in my approach is utilizing the β_{RC}-diversity to gain insight into the relative influences that stochastic and deterministic assembly mechanisms have on the species distribution patterns. To my knowledge, Marcus (2003) is the only other study that has implemented a null model to determine if random processes are responsible for diversity differences among different vent animal assemblages.

The spatial scale I focus on in my thesis is also novel among β-diversity studies in hydrothermal vents; previous studies addressing β-diversity in vents focus either on relatively small or very large spatial-scales. For instance, small-scale studies addressing vent animals tend to examine β-diversity on individual vents (Sen et al. 2014), among discrete biological assemblages, like tubeworm bushes (e.g. Marcus, 2003), or among multiple, but not all, vent fields within the same system (e.g. Tsurumi, 2003). In contrast, large-scale studies addressing faunal β-diversity tend to focus on inter-regional scales, comparing vent sites across different geologic settings or ocean basins (e.g. Rogers et al. 2012; Kojima & Watanabe, 2015; Zhou et al. 2018). My thesis presents the results of the first intra-regional assessments of β-diversity that incorporates every site known in a single vent system.

*Contributions to the Global Context***:**

The discovery of the two new vent sites, Hafa Adai and Perseverance, contributes to the growing database of known vent sites currently recognized around the world (Beaulieu et al. 2013). Recognition of these two sites by the U.S. Government is particularly important because currently, they are not protected as National Wildlife Refuges like the other vent sites in this system. The new species identified in this animal collection also contribute to the growing database of global vent biodiversity. Furthermore, some discoveries from my research also contributed to the expansion of known range sizes for some vent species. Although most expansions to the species ranges are minor, the most notable update to species range data is that of *Phymorhynchus wareni*. Previous records of this species only came from the Manus basin (Zhang and Zhang, 2017), but my thesis provides the first record of this species in the Mariana BASC (Puillandre, pers. comm.). Despite the diversity differences among the Mariana BASC's vent sites, its relatively low γ-, average β_J-, and average β_{RC}-diversity values indicate that this is

an example of a vent system with relatively simple and homogenous biological assemblages in the context of all global vent systems.

The comparison between the Mariana Arc and BASC systems reveals an important insight into the context of global vent biogeography – specifically the delineation of hydrothermal biogeographic provinces. For one, all previous biogeographic models for the world's vent systems exclude the Mariana Arc vents (e.g. Bachraty et al. 2009; Moalic et al. 2011; Rogers et al. 2012). Therefore, the "Mariana" region in these models only represents the BASC vents. The two Mariana systems only share 8% of their species, they significantly differ in their β-diversity values (Figure 15) and they exhibit notably different fluid chemistries (Butterfield et al. in prep.). Incorporating all vent settings in the Mariana region is important for a complete biogeographic analysis. Therefore, researchers should consider both the Mariana systems for future studies that seek to further refine the global vent biogeographic province models.

Although the results in my thesis only provide hints for the environmental factors that possibly shape the diversity distribution patterns in the Mariana BASC, they are still important contributions because this type of data is generally sparse throughout the vent literature. It is clear that the species richness of the vent sites in the Mariana BASC broadly correlates to their distances from the arc, but the reason for this is unclear. Given that arc-derived magma influences the southern-most vents more strongly than those in the central BASC, and that the magma influences the chemistry of hydrothermal fluids, fluid characteristics may be a factor shaping the distribution patterns throughout this system. It is apparent that fluid exposure influences the small-scale distribution patterns of vent-fauna (e.g. Podowski et al. 2009; Podowski et al. 2010; Sen et al. 2013; Marsh et al. 2012; Du Preez and Fisher, 2018), and some

studies have also highlighted a correlation between fluid chemistry and vent fauna assemblage characteristics on larger spatial scales (e.g. Desbruyères et al. 2000). Furthermore, Butterfield et al. (in prep.) have demonstrated that variability in fluid conditions correlates with β-diversity between the Mariana Arc and BASC, so there is a possibility that fluid chemistry differences among the BASC sites influence the diversity distribution patterns in some way.

Given that the β_{RC}-diversity values for the BASC suggest that stochastic factors are the main mechanisms driving the vent species distribution patterns within this system, the influence of fluid chemistry, or any other environmental variable, is likely minor. In contrast, the β_{RC}-diversity values of the Mariana Arc indicate that deterministic factors play a greater role in shaping these vent assemblages. Therefore, fluid conditions likely influence the diversity distribution patterns among the arc vents more heavily than those among the BASC. Furthermore, there are major differences in fluid conditions between the Mariana Arc and BASC vents (Butterfield et al. in prep.), and this is likely the reason only 8% of vent-obligate species are present in both the arc and BASC vent sites.

Overall, this novel approach to β-diversity has proven useful for gaining insight into the relative influence that deterministic factors have had in shaping the system-wide vent species distribution patterns in the Juan de Fuca Ridge, Mariana BASC and Arc. Future researchers should continue to apply this β-diversity approach to the other vent systems around the world. It is a great source for developing future questions and hypotheses regarding the environmental drivers shaping diversity patterns across whole vent systems; this is especially important for vent studies, given the time and money required to sample such remote habitats. This approach is also relatively straightforward and it only requires species presence-absence data, which are much easier to collect from vent sites than abundance data.

Future Studies in the Mariana Region:

The Mariana BASC stretches from 12.4˚N to 24.0˚N (Yamazaki et al. 2003; Baker et al. 2017), a distance of ~1200 km. To date, surveys have only explored between 12.4˚N to 18.2˚N. Therefore, the entire northern half of the Mariana BASC still requires thorough exploration to determine if other vent sites exist. Additional data from the northern half of the Mariana BASC will help to clarify the details of the general, northward increase in vent α-diversity presented in my thesis. If α-diversity continues increasing in a northward direction and the northern-most sites are the most species rich, this would indicate that there is no significant relationship between distance from the arc and α-diversity. Alternatively, if α-diversity gradually decreases from Illium-Alice Springs in a northward direction, then this would further support the correlation with distance from the arc. Yamazaki et al. (2003) demonstrate that the geomorphology of the northern-most spreading segment is very similar to that of the two southern-most segments (Type 1 in Anderson et al. 2017); they all occupy shallower depths than the other spreading segments, and they all exhibit axial highs without rift valleys. The similar geomorphology suggests that the magma sources are relatively similar between the northern-most and southern-most segments. Therefore, I predict that the species richness of possible northern vent sites would be low, similar to the southern-most vent sites. However, based on significant correlation between isolation and β_{RC}-diversity, I also predict that the species composition of such northern vent sites would more closely resemble each other than the sites that are further south. Therefore, I predict that the most considerable compositional difference would occur between the northern-most and southern-most vents, even if their α-diversity values are very similar.

Although it seems that new vent discoveries are more likely to occur along the spreading axis in the northern half of the Mariana BASC, there is another set of geologic features worth searching for hydrothermal activity. Due to the curved nature of the Mariana region, crustal extension in the Mariana microplate has occurred; this has created several cross-chain volcanos aligned perpendicularly to the trench, arc and BASC at various latitudes (Anderson et al. 2017). As suggested by Anderson (pers. comm.), these volcanos are also worth investigating, as they should contain sufficient heat sources for hydrothermal circulation to emerge. Given that off-axis vent sites are present in this system, like Archaean, Urashima-Pika and Forecast, it seems likely that some of the large, cross-chain volcanoes could support vents as well. Similar to the Forecast vent site (Stern et al. 2013), vents present on the cross-chain volcanoes would likely have magma sources in transition from hydration melting to decompression melting. Therefore, they would provide an excellent opportunity to investigate many questions related to the vent biology of the Mariana region, if present. For one, if vent sites are present on these volcanos, it would be essential to determine if they are arc-hosted or BASC-hosted vents. Secondly, multiple vent sites on cross-chain volcanos would also provide an ideal alternative approach to further test the relationship between α-diversity and distance from the arc.

Overall, further exploration of all vent sites in the Mariana BASC is required to move forward with many future research topics. In regards to the individual biological assemblages, a lot of work is still required for identifying all the vent-associated taxa to the species level. The discovery of three *Rimicaris* species in this study also provides an excellent opportunity to investigate how they partition their ecological niches, since they are, presumably, very similar. Relative abundance measures of these three species require further collection and habitat characterization from all the vent sites in the Mariana BASC. Given the discovery of another

potentially new species of *Munidopsis* associated with vents in the Mariana BASC, researchers could also use the *Munidopsis* species to investigate how they partition their niches.

Continued research into the species distributions of Mariana BASC vent fauna would greatly benefit from thorough habitat characterization of each vent site with detailed descriptions of environmental factors. Researchers should continue sampling the hydrothermal fluids, as this information can sometimes be sparse, depending on the vent site. Future expeditions should also specifically attempt to measure vent habitat area, as this would be crucial to test the species-area relationship in this system. Furthermore, continued investigation into the ecophysiology of the vent fauna would be highly beneficial. With a better understanding of the environmental factors relevant to the absence/presence or relative abundance of vent species, future researchers studying this vent system would have a better idea of the abiotic vent characteristics that should be thoroughly measured among these vent sites to better understand the environmental drivers shaping species distribution patterns.

References:

Anderson, M. J., Crist, T. O., Chase, J. M., Vellend, M., Inouye, B. D., Freestone, A. L., . . . Swenson, N. G. (2011). Navigating the multiple meanings of β diversity: A roadmap for the practicing ecologist. *Ecology Letters, 14*(1), 19-28.

Anderson, M. O., Chadwick Jr, W. W., Hannington, M. D., Merle, S. G., Resing, J. A., Baker, E. T., . . . Augustin, N. (2017). Geological interpretation of volcanism and segmentation of the Mariana back-arc spreading center between 12.7° N and 18.3° N. *Geochemistry, Geophysics, Geosystems, 18*(6), 2240-2274.

Bachraty, C., Legendre, P., & Desbruyères, D. (2009). Biogeographic relationships among deep-sea hydrothermal vent faunas at global scale. *Deep Sea Research Part I: Oceanographic Research Papers, 56*(8), 1371-1378.

Baker, E. T., Walker, S. L., Resing, J. A., Chadwick Jr, W. W., Merle, S. G., Anderson, M. O., . . . Michael, S. (2017). The effect of arc proximity on hydrothermal activity along spreading centers: New evidence from the Mariana Back Arc (12.7˚N–18.3˚N). *Geochemistry, Geophysics, Geosystems, 18*(11), 4211-4228.

Beaulieu, S. E., Baker, E. T., German, C. R., & Maffei, A. (2013). An authoritative global database for active submarine hydrothermal vent fields. *Geochemistry, Geophysics, Geosystems, 14*(11), 4892-4905.

Bissonette, J. A. (1999). Small sample size problems in wildlife ecology: A contingent analytical approach. *Wildlife Biology, 5*(1), 65-72.

Campbell, B.J., Polson, S.W., Allen, L.Z., Williamson, S.J., Lee, C.K., Wommack, K.E. & Cary, S.C. (2013). Diffuse flow environments within basalt- and sediment-based hydrothermal vent ecosystems harbor specialized microbial communities. *Frontiers in Micobiology 4*: 182.

Chown, S.L. (2012). Antarctic marine biodiversity and deep-sea hydrothermal vents. *PLoS Biology, 10*(1): e1001232

Clarke, K. R., Somerfield, P. J., & Chapman, M. G. (2006). On resemblance measures for ecological studies, including taxonomic dissimilarities and a zero-adjusted Bray–Curtis coefficient for denuded assemblages. *Journal of Experimental Marine Biology and Ecology, 330*(1), 55-80.

Cubelio, S. S., Tsuchida, S., & Watanabe, S. (2007). New species of Munidopsis (Decapoda: Anomura: Galatheidae) from hydrothermal vent areas of Indian and Pacific Oceans. *Journal of the Marine Biological Association of the United Kingdom, 88*(1), 111-117.

Desbruyères, D., Almeida, A., Biscoito, M., Comtet, T., Khripounoff, A., Le Bris, N., . . . Segonzac, M. (2000). A review of the distribution of hydrothermal vent communities along the northern Mid-Atlantic Ridge: Dispersal vs. environmental controls. In *Island, Ocean and Deep-Sea Biology* (pp. 201-216): Springer, Dordrecht.

Desbruyères, D., Hashimoto, J., & Fabri, M.-C. (2006). Composition and biogeography of hydrothermal vent communities in western Pacific back-Arc basins. *Geophysical Monograph Series, 166*, 215-234.

Du Preez, C., & Fisher, C. R. (2018). Long-term stability of back-arc basin hydrothermal vents. *Frontiers in Marine Science, 5*(54). doi: 10.3389/fmars.2018.00054

Flores, G.E., Campbell, J.H., Kirshtein, J.D., Meneghin, J., Podar, M., Steinberg, J.I., ... Reysenbach, A. -L. (2011). Microbial community structure of hydrothermal deposits from geochemically different vent fields along the Mid-Atlantic Ridge. *Environmental Microbiology 13*(8): 2158-2171.

Fujikura, K., Yamazaki, T., Hasegawa, K., Tsunogai, U., Stern, R. J., Ueno, H., . . . Okutani, T. (1997). Biology and earth scientific investigation by the submersible "Shinkai 6500" system of deep-sea hydrothermal and lithosphere in the Mariana back-arc basin. *JAMSTEC Journal of Deep Sea Research, 13*, 1-20.

Goffredi, S. K., Johnson, S., Tunnicliffe, V., Caress, D., Clague, D., Escobar, E., . . . Vrijenhoek, R. (2017). Hydrothermal vent fields discovered in the southern Gulf of California clarify role of

habitat in augmenting regional diversity. *Proceedings of the Royal Society B: Biological Sciences, 284*(1859), 20170817.

Kojima, S., & Watanabe, H. (2015). Vent fauna in the Mariana Trough. In *Subseafloor Biosphere Linked to Hydrothermal Systems* (pp. 313-323): Springer, Tokyo.

Krantz, G. (1982). A new species of *Copidognathus* Trouessart (Acari: Actinedida: Halacaridae) from the Galapagos Rift. *Canadian Journal of Zoology, 60*(7), 1728-1731.

Ludwig, K. A., Kelley, D. S., Butterfield, D. A., Nelson, B. K., & Früh-Green, G. (2006). Formation and evolution of carbonate chimneys at the Lost City Hydrothermal Field. *Geochimica et Cosmochimica Acta, 70*(14), 3625-3645.

Marcus, J. (2003). *Community ecology of hydrothermal vents at Axial Volcano, Juan de Fuca Ridge, northeast Pacific* (Doctoral dissertation).

Marsh, L., Copley, J. T., Huvenne, V. A., Linse, K., Reid, W. D., Rogers, A. D., . . . Tyler, P. A. (2012). Microdistribution of faunal assemblages at deep-sea hydrothermal vents in the Southern Ocean. *PLoS One, 7*(10), e48348.

Moalic, Y., Desbruyères, D., Duarte, C. M., Rozenfeld, A. F., Bachraty, C., & Arnaud-Haond, S. (2011). Biogeography revisited with network theory: Retracing the history of hydrothermal vent communities. *Systematic Biology, 61*(1), 127.

Podowski, E. L., Ma, S., Luther III, G. W., Wardrop, D., & Fisher, C. R. (2010). Biotic and abiotic factors affecting distributions of megafauna in diffuse flow on andesite and basalt along the Eastern Lau Spreading Center, Tonga. *Marine Ecology Progress Series, 418*, 25-45.

Podowski, E. L., Moore, T. S., Zelnio, K. A., Luther III, G. W., & Fisher, C. R. (2009). Distribution of diffuse flow megafauna in two sites on the Eastern Lau Spreading Center, Tonga. *Deep Sea Research Part I: Oceanographic Research Papers, 56*(11), 2041-2056.

Rogers, A. D., Tyler, P. A., Connelly, D. P., Copley, J. T., James, R., Larter, R. D., . . . Zwirglmaier, K. (2012). The discovery of new deep-sea hydrothermal vent communities in the Southern Ocean and implications for biogeography. *PLoS Biology, 10*(1), e1001234.

Sen, A., Becker, E. L., Podowski, E. L., Wickes, L. N., Ma, S., Mullaugh, K. M., . . . Fisher, C. R. (2013). Distribution of mega fauna on sulfide edifices on the Eastern Lau Spreading Center and Valu Fa Ridge. *Deep Sea Research Part I: Oceanographic Research Papers, 72*, 48-60.

Sen, A., Podowski, E. L., Becker, E. L., Shearer, E. A., Gartman, A., Yücel, M., . . . Fisher, C. R. (2014). Community succession in hydrothermal vent habitats of the eastern Lau Spreading Center and Valu Fa Ridge, Tonga. *Limnology and Oceanography, 59*(5), 1510-1528.

Stern, R. J., Tamura, Y., Masuda, H., Fryer, P., Martinez, F., Ishizuka, O., & Bloomer, S. H. (2013). How the Mariana Volcanic Arc ends in the south. *Island Arc, 22*(1), 133-148.

Thomson, R. E., Mihály, S. F., Rabinovich, A. B., McDuff, R. E., Veirs, S. R., & Stahr, F. R. (2003). Constrained circulation at Endeavour ridge facilitates colonization by vent larvae. *Nature, 424*(6948), 545-549.

Tsurumi, M. (2003). Diversity at hydrothermal vents. *Global Ecology and Biogeography, 12*(3), 181-190.

Williams, A. B., & Baba, K. (1990). New squat lobsters (Galatheidae) from the Pacific Ocean: Mariana Back Arc Basin, East Pacific Rise, and Cascadia Basin. *Fishery Bulletin, 87*, 899-910.

Xu, W., Gong, L-f., Pang, K-L. & Luo, Z-H. (2018). Fungal diversity in deep-sea sediments of a hydrothermal vent system in the Southwest Indian Ridge. *Deep Sea Research Part 1: Oceanographic Research Papers 131*: 16-26.

Yamazaki, T., Seama, N., Okino, K., Kitada, K., Joshima, M., Oda, H., & Naka, J. (2003). Spreading process of the northern Mariana Trough: Rifting-spreading transition at 22° N. *Geochemistry, Geophysics, Geosystems, 4*(9).

Zhang, S., & Zhang, S. (2017). A new species of the genus Phymorhynchus (Neogastropoda: Raphitomidae) from a hydrothermal vent in the Manus Back-Arc Basin. *Zootaxa, 4300*(3), 441-444.

Zhou, Y., Zhang, D., Zhang, R., Liu, Z., Tao, C., Lu, B., . . . Wang, C. (2018). Characterization of vent fauna at three hydrothermal vent fields on the Southwest Indian Ridge: Implications for

biogeography and interannual dynamics on ultraslow-spreading ridges. *Deep Sea Research Part I: Oceanographic Research Papers, 137*, 1-12.

Supplementary Information

Appendix 1: Manuscript for the description of the new shrimp, *Rimicaris falkorae*, discovered from the samples collected during the hydrothermal hunt cruise in 2016. Publication citation: "Komai, T. & Giguère, T. 2019. A new species of alvinocaridid shrimp *Rimicaris* Williams & Rona, 1986 (Decapoda: Caridea) from hydrothermal vents on the Mariana Back Arc Spreading Center, northwestern Pacific. *Journal of Crustacean Biology* 1-11. Doi: 10.1093/jcbiol/ruz046."

A new species of alvinocaridid shrimp *Rimicaris* Williams & Rona, 1986 (Decapoda: Caridea) from hydrothermal vents on the Mariana Back Arc Preading Center, northwestern Pacific.

ABSTRACT

A new species of the alvinocaridid shrimp genus *Rimicaris* Williams & Rona, 1986, *R. falkorae* **n. sp**., is described and illustrated based on material from deep-sea hydrothermal vents (3,630–3,912 m deep) on the Mariana Back Arc Spreading Centre, northwestern Pacific, representing the tenth described species of the genus. The new species is morphologically most similar to *R. paulexa* (Martin & Shank, 2005), but the presence of numerous short setae scattered on the carapace surface, the relatively long antennular stylocerite usually reaching the distal margin of article 2 of the antennular peduncle and the spiniform posteromesial projection of the uropodal protopod distinguish the new species from all congeners. Genetic analysis using the barcoding region of the mitochondrial COI gene supports the recognition of the species as new.

Key words: COI, genetic analysis, *Rimicaris falkorae*, taxonomy

INTRODUCTION

The alvinocaridid shrimp genus Rimicaris Williams & Rona, 1986 is currently represented by nine species worldwide (Table 1), all of which are endemic to deep-sea hydrothermal vents (Komai & Segonzac, 2008; Komai & Tsuchida, 2015; Vereshchaka et al., 2015). Vereshchaka et al. (2015) synonymised Chorocaris Martin & Hessler, 1990 under Rimicaris because they demonstrated, on the basis of cladistics analysis, of morphological characters and molecular phylogenetic analysis that species of *Rimicaris* are subordinated within *Chorocaris*, making the latter genus paraphyletic. The species previously assigned to *Chorocaris* were all transferred to *Rimicaris. Rimicaris*, as defined by Vereshchaka et al. (2015) is characterised within Alvinocarididae, by the rostrum being reduced to a dorsoventrally flattened, triangular to rounded projection or obsolescent convexity without any dorsal and ventral armature, the lack of a postrostral ridge on the carapace, the broadly fused eyestalks without trace of corneas, the complete absence of spiniform setae on the ischia and meri of pereopods 3–5, the accessory spiniform setae arranged in two or more longitudinal rows on the dactyli of the pereopods 3–5, and the possession of two spiniform setae on the posterolateral angle of the uropodal exopod (cf. Komai & Segonzac, 2008; Komai & Tsuchida, 2015). The following three species have been recorded from the western Pacific hydrothermal vents: *R. parva* (Komai & Tsuchida, 2015), *R. variabilis* (Komai & Tsuchida, 2015), and *R. vandoverae* (Martin & Hessler, 1990) (Table 1).

During the Hydrothermal Hunt Expedition to the Mariana Back Arc Spreading Center (BASC) in 2016, conducted from the RV *Falkor* of the Schmidt Ocean Institute, Palo Alto, CA, USA, sampling operations of the hydrothermal benthic fauna, using the remotely operated vehicle (ROV) *SuBastian* were conducted at several hydrothermal vent sites, including two sites discovered during the water-column surveys of the spreading ridge (Baker *et al.*, 2017) (the cruise report is available at https://www.pmel.noaa.gov/eoi/marianas/Falkor-2016-FK161129-report-NO-logs.pdf). Many specimens of *Rimicaris* were collected from four sites, which were initially identified as *R. vandoverae*, the only formally described representative of *Rimicaris* previously known from the Mariana BASC area (Komai & Segonzac, 2008). Close morphological examination of specimens combined with a genetic analysis using the barcoding region of the

mitochondrial COI gene has nevertheless revealed that two species, including *R. vandoverae*, were actually represented. We describe herein a new species, *R. falkorae* **n. sp**, on the basis of these specimens.

MATERIALS AND METHODS

The Schmidt Ocean Institute (SOI) conducted the FK161129 (Hydrothermal Hunt) cruise from 1–18 December 2016 on R/V *Falkor* in the Mariana region. The ROV *SuBastian* acquired the studied specimens using a slurp sampler. Specimens of *R. falkorae*

Table S1. Species of *Rimicaris* Williams & Rona, 1986 and their geographical distribution.

Species	Distribution	References
Rimicaris chacei (Williams & Rona, 1986)	Mid-Atlantic Ridge, 1600-3650 m	Komai & Segonzac (2008)
Rimicaris exoculata (Williams & Rona, 1986)	Mid-Atlantic Ridge, 1700-4088 m	Komai *et al.* (2007); Komai & Segonzac (2008)
Rimicaris falkorae **n. sp.**	Mariana Back Arc Spreading Center, NW Pacific, 3630-3912 m	This study
Rimicaris hybisae (Nye, Copley & Plouviez, 2012)	Mid-Cayman Spreading Center, Caribbean, 2300-4960 m	Nye *et al.* (2012)
Rimicaris parva (Komai & Tsuchida, 2015)	Manus Basin, SW Pacific, 1305-1684m	Komai & Tsuchida (2015)
Rimicaris kairei (Watabe & Hashimoto, 2002)	Central Indian Ridge, 2415-3320 m	Watabe & Hashimoto (2002); Komai & Segonzac (2008)
Rimicaris paulexa (Martin & Shank, 2003)	Southern East Pacific Rise, 2573-2832 m	Martin & Shank (2005); Komai & Segonzac (2008)
Rimicris susannae (Komai, Gierre & Segonzac, 2007)	Southern Mid-Atlantic Ridge, 1500-2986 m	Komai *et al.* (2007)
Rimicaris vandoverae (Martin & Hessler, 1990)	Mariana Back Arc Spreading Center, NW Pacific 3274-3909 m	Komai & Segonzac (2008); this study
Rimicaris variabilis (Komai & Tsuchida, 2015)	SW Pacific hydrothermal vents, 1305-1873	Komai & Tsuchida (2015); Komai *et al.* (2016)

Table S2. Average pairwise COI nucleotide percent differences of the species used in the molecular analysis: sequences labeled as "*Rimicaris* sp." were not included in this calculation.

	R. falkorae n. sp.	***R. vandoverae***	***R. hybisae***	***R. chacei***	***O. loihi***	***R. kairei***	***R. exoculata***	***R. parva***	***R. variabilis***	***S. leurokolos***
R. vandoverae	7.48%									
R. hybisae	8.20%	11.88%								
R. chacei	8.08%	12.00%	0.10%							
O. loihi	8.50%	12.26%	4.49%	4.38%						
R. kairei	7.96%	9.50%	8.64%	8.52%	10.10%					
R. exoculata	7.59%	8.36%	8.76%	8.88%	10.10%	1.35%				
R. parva	7.01%	7.64%	10.49%	10.37%	11.70%	9.59%	9.22%			
R. variabilis	7.22%	7.96%	11.11%	10.99%	10.90%	10.315	9.90%	7.56%		
S. leurokolos	5.70%	6.71%	10.75%	10.63%	10.60%	7.67%	7.16%	6.55%	5.74%	
M. fortunata	20.60%	20.41%	20.06%	20.06%	20.80%	19.67%	18.85%	19.77%	19.28%	20.34%

n. sp. were present in samples from two vent fields (Burke and Perseverance), whereas those of *R. vandoverae* were collected from Illium, Burke, Hafa Adai, and Perseverance vent fields. These hydrothermal fields are listed in the Vents Database 3.4 (http://www.interridge.org/IRvents_database). The specimens were preserved on board the ship in 80% ethanol. The MGLN02MV (Submarine Ring of Fire) cruise on R/V *Melville* with ROV *Jason-2* provided comparative specimens of *R. vandoverae* from the Forecast vent field. In total, 82 specimens of the new species were examined, of which 17 specimens were used for taxonomic analysis. Specimens used for taxonomic study are deposited in the Natural History Museum and Institute, Chiba, Japan (CBM), the Canadian Museum of Nature, Ottawa, Canada (CMNO), and the Oxford University Museum of Natural History, U.K. (OUMNH).

Pleonal muscle samples were dissected from 17 specimens of the new species and 25 specimens of *R. vandoverae* and sent to the Barcode of Life Database (BoLD) facility for DNA extraction and sequencing of the barcode region of the mitochondrial cyctochrome c oxidase subunit I (COI) gene (Ratnasingham & Hebert, 2007). The COI gene was amplified using either the ZplankF1_t1 (TGT AAA ACG ACG GCC

AGT TCT ASW AAT CAT AAR GAT ATT GG) and ZplankR1_t1 (CAG GAA ACA GCT ATG ACT TCA GGR TGR CCR AAR AAT CA) forward and reverse primers (Prosser *et al.*, 2013), or the CrustDF1 (GGT CWA CAA AYC ATA AAG AYA TTG G) and CrustDR1 (TAA ACY TCA GGR TGA CCR AAR AAY CA) forward and reverse primers (Steinke *et al.*, 2016). The M13F and M13R sequence primers were used for all specimen (Messing, 1983). GenBank accession numbers of the COI sequences used for genetic analyses are summarised in Supplementary material Table S1.

The phylogenetic tree using the COI gene was generated with MEGA-X software using the maximum likelihood (ML) method with 1,000 replicate bootstrap values to assess the stability of the clades (Kumar *et al.*, 2018). Pairwise estimates for genetic divergence between the new species and the closely related species were calculated using the Kimura-2-parameter (K2P) distance (Kimura, 1980). Additional COI sequences of closely related species were retrieved from the GenBank database (Clark *et al.*, 2016) and included in the tree. Nucleotide percent differences between all the COI sequences used in the tree were calculated using the "dist.dna" function from the "ape" package in R (R Core Team, 2016; Paradis & Schliep, 2019). The average percent difference values between the species used in molecular analyses, except for those labeled as "*Rimicaris* sp.," are summarised on Table 2.

The following specimens were examined for comparison.

Rimicaris vandoverae. ROV *Jason*, dive J185, Forecast, Mariana BASC, 13°26.68′N, 143°53.21′E, 1,447 m, slurp gun, 21 April 2006: CBM-ZC 15279, acc. no. N146-2, 1 female (carapace length (cl) 9.0 mm); CBM-ZC 15280, acc. no. N146-3, 1 female (cl 9.9 mm); CBM-ZC 15281, acc. no. N146-4, 1 male (cl 10.4 mm); CBM-ZC 15282, acc. no. N146-9, 1 female (cl 10.4 mm); OUMNH-ZC 2018-01-119, acc. no. N146-15, 1 female (cl 9.3 mm). ROV *SuBastian*, dive S37, Mkr 138, Ilium site, Mariana Back Arc Basin, 18°12.82′N, 144°42.48′E, 3,582 m deep, slurp gun, 5 December 2016: CBM-ZC 15263, acc. no. N270-6, 1 male (cl 9.2 mm); CBM-ZC 15264, acc. no. N270-7, 1 female (cl 11.0 mm); CBM-ZC 15265, acc. no. N270-9, 1 female (cl 8.8 mm); CBM-ZC 15266, ID No. N270-10, 1 female (cl 8.8 mm); OUMNH-ZC 2018-01-115, ID No. N270-15, 1 male (cl 8.9 mm). Dive S40, Snail Pit, Burke site, Mariana Back Arc Basin, 18°10.95′N, 144°43.19′E, 3,630 m

deep, slurp gun, 7 December 2016: CBM-ZC 15267, acc. no. N269-4, 1 female (cl 10.3 mm); CBM-ZC 15268, acc. no. N269-7, 1 male (cl 10.2 mm); CBM-ZC 15269, acc. no. N269-10, 1 male (cl 9.2 mm); CBM-ZC 15270, acc. no. N269-14, 1 female (cl 8.9 mm); CBM-ZC 15271, acc. no. N269-18, 1 female (cl 13.8 mm); OUMNH-ZC 2018-01-116, acc. no. N269-22, 1 male (cl 9.1 mm). Dive S41, Sequoia Vent, Hafa Adai, Mariana Back Arc Basin, 16°57.67′N, 144°52.01′E, 3,274 m deep, slurp gun, 8 December 2016: CBM-ZC 15272, acc. no. N274-1, 1 male (cl 12.1 mm); CBM-ZC 15273, acc. no. N274-2, 1 male (cl 12.7 mm); CBM-ZC 15274, acc. no. N274-7, 1 female (cl 13.9 mm); CBM-ZC 15275, acc. no. N274-8, 1 male (cl 12.9 mm); OUMNH-ZC 2018-01-117, acc. no. N274-14, 1 ovigerous female (cl 13.1 mm). Dive S47, Stump, Perseverance site, 15°28.80′N, 144°30.46′E, 3,909 m deep, slurp gun, 17 December 2016: CBM-ZC 15276, acc. no. N271-12, 1 ovigerous female (cl 10.7 mm); CBM-ZC 15277, acc. no. N271-13, 1 ovigerous female (cl 10.4 mm); CBM-ZC 15278, acc. no. N271-15, 1 ovigerous female (cl 10.4 mm), Stump, Perseverance site, 15°28.80′N, 144°30.46′E, 3,912 m deep: OUMNH-ZC 2018-01-118, acc. no. N272-14, 1 female (10.7 mm).

Rimicaris paulexa: specimens listed in Komai & Segonzac (2008).

Rimicaris variabilis: specimens listed in Komai & Tsuchida (2015).

SYSTEMATICS

Family Alvinocarididae *Christoffersen, 1986*

***Genus* Rimicaris** *Williams & Rona, 1986*

Rimicaris falkorae *n. sp.*

(Figs. 1–6)

Material examined: Holotype: CBM-ZC 15255, ROV *SuBastian*, dive S47, Stump, Perseverance site, Mariana Back Arc Basin, 15˚28.80′N, 144˚30.46′E, 3,912 m deep, slurp gun, 7 December 2016, ovigerous female (cl 10.1 mm), ID no. N271-14.

Paratypes. ROV *SuBastian*, dive S40, Snail Pit, Burke site, Mariana Back Arc Basin, 18˚10.95’N, 144˚43.19’E, 3,630 m deep, slurp gun, 7 December 2016: CBM-ZC 15251, 1 female (cl 11.5 mm), ID No. N269-1; OMNH-ZC 2018-01-110, 1 female (cl 12.2 mm), ID No. N269-5. ROV *SuBastian*, dive S47, Stump Vent, Perseverance site, Mariana Back Arc Basin,

15˚28.80′N, 144˚30.46’E, 3,909 m deep, slurp gun, 7 December 2016: CBM-ZC 15252, 1 female (cl 12.5 mm), ID No. N271-3; CBM-ZC 15253, 1 female (cl 7.5 mm), ID No. N271-8; CBM-ZC 15254, 1 female (cl 8.1 mm), ID No. N271-9; OUMNH-ZC 2018-01-111, 1 female (cl 5.7 mm), ID No. N271-21. ROV *SuBastian*, dive S47, Stump Vent, Perseverance site, Mariana Back Arc Basin, 15˚28.80′N, 144˚30.46’E, 3,912 m deep, slurp gun, 7 December 2016; CBM-ZC 15256, 1 female (cl 10.9 mm), ID No. N272-5; CBM-ZC 15257, 1 female (cl 10.1 mm), ID No. N272-13; CBM-ZC 15258, 1 male (cl 8.7 mm), ID No. N272-15; CBM-ZC 15259, 1 male (cl 7.9 mm), ID No. N272-16; CBM-ZC 15260, 1 female (cl 7.1 mm), ID No. N272-17; CMNC 2019-0001, 1 female (cl 9.0 mm), ID No. N272-18, 1 female (cl 7.0 mm), ID No. N272-20; CBM-ZC 15261, 1 female (cl 8.5 mm), ID No. N272-21; CBM-ZC 15262, 1 female (cl 6.4 mm), ID No. N272-22; OUMNH-ZC 2018-01-112, 1 female (cl 5.8 mm), ID No. N272-23; OUMNH-ZC 2018-01-113, 1 female (cl 6.7 mm), ID No. N272-24; OUMNH-ZC 2018-01-114, 1 female (cl 6.5 mm), ID No. N272-25.

Diagnosis: Rostrum (Fig. 2A, C, 6A) broadly triangular, distinctly wider than long. Carapace (Figs. 1, 2A, 6A) not particularly inflated laterally, with scattered numerous short setae on dorsal to lateral surfaces; median area forming broad, blunt ridge flanked by shallow longitudinal depressions in fully matured females; faint, saddle-like depression sometimes present on dorsum posterior to midlength; antennal spine blunt to acute; pterygostomial angle very strongly produced into triangular projection with blunt to acute apex, usually exceeding to level of midlength of antennal scaphocerite (Figs. 2B, 6B, C); dorsal organ extension restricted to anterior one-third length of carapace. Pleonal pleuron 4 (Fig. 1) with bluntly pointed posteroventral angle; pleuron 5 (Fig. 1) with 0–2 minute denticles in addition to small posteroventral spine. Telson (Fig. 2D) with 5 or 6 dorsolateral spiniform setae and 2 spiniform setae at posterolateral angle on either side. Fused eyestalks with slight median constriction, median part concealed by rostrum in dorsal view (Fig. 2C). Article 1 of antennular peduncle (Fig. 2B, C) with stylocerite usually reaching distal margin of article 2. Pereopods 3–5 ischia (Fig. 4D–F) always unarmed; dactyli each armed with 10–13 accessory spinules, arranged in 3 longitudinal rows, on flexor

surface. Uropodal protopod with sharply pointed posterolateral angle (Fig. 2F, G); posteromesial process also sharply pointed, spiniform (Fig. 2F, G).

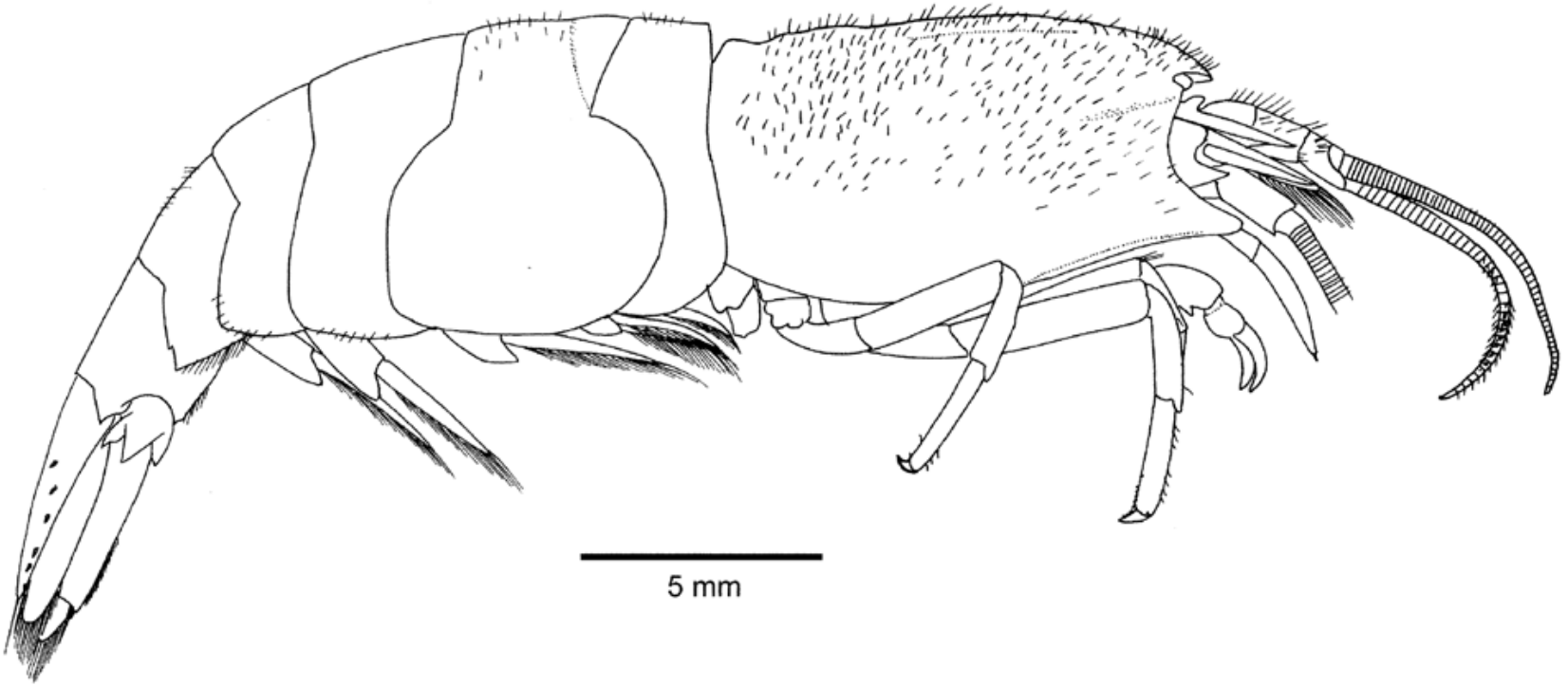

Figure S1. *Rimicaris falkorae* **n. sp.**, holotype, ovigerous female (cl 10.1 mm), CBM-ZC 15255, habitus in right lateral view.

Description: Holotype (*ovigerous female*). Body (Fig. 1) relatively stout; integument fairly thin. Rostrum (Fig. 2A–C) not reaching midlength of article 1 of antennular peduncle, dorsoventrally flattened, broadly triangular with blunt apex in dorsal view; dorsal surface smooth; ventral surface slightly convex. Carapace (Figs. 1, 2A–C) compressed laterally, not particularly inflated on branchial regions; surface with scattered sparse short setae dorsally, laterally; dorsal surface

sloping down anteriorly to rostrum, having faint, saddle-like depression posterior to midlength; anterior half of dorsal midline slightly elevated into low, broad ridge flanked by shallow longitudinal depressions on either side; antennal spine

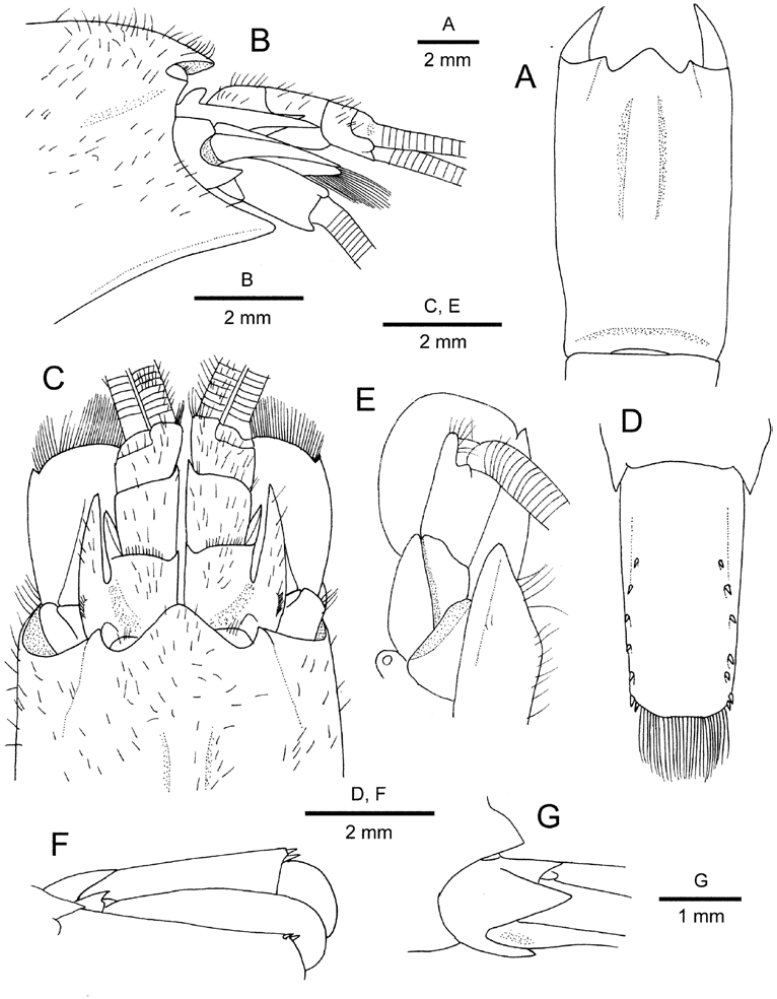

Figure S2. *Rimicaris falkorae* **n. sp.**, holotype, ovigerous female (cl 10.1 mm), CBM-ZC 15255. Carapace, dorsal view (setae omitted) (**A**); anterior part of carapace and cephalic appendages, right lateral view (antennular and antennal flagella partially omitted) (**B**); same, dorsal view (**C**); telson, dorsal view (**D**); left antenna, ventral view (**E**); right uropod, dorsal view (perpendicular against horizontal plane) (**F**); protopod of left uropod, lateral view (**G**).

small, triangular with blunt apex; anterolateral margin strongly concave; pterygostomial angle strongly produced anteriorly into prominent triangular projection with blunt apex, extending to midlength of antennal scaphocerite.

Pleomeres 1–6 (Fig. 1) rounded dorsally; pleura 1–3 broadly rounded, always unarmed; pleuron 4 with bluntly pointed posteroventral angle, otherwise unarmed; pleuron 5 with sharply pointed posteroventral angle and additional minute denticle (right) or unarmed (left) on nearly straight posterolateral margin. Pleomere 6 about 1.2 times as long as pleomere 5, about approximately as long as high, having acute posteroventral angle, posterolateral process terminating in spine. Telson (Fig. 2D) about twice as long as anterior width, falling short of posterior margins of uropods, very slightly narrowed posteriorly, armed with 5 pairs of dorsolateral spiniform setae arranged in sinuous row and 2 pairs at posterolateral angle; posterior margin faintly concave mesially, bearing 27 long plumose setae.

Eyestalks (Fig. 2B, C) broadly fused but shallow median notch still apparent; anterior surface with few short setae; median part concealed by rostrum in dorsal view.

Antennular peduncle (Fig. 2B, C) stout, slightly overreaching distal margin of antennal scaphocerite. Article 1 with strong distolateral and small distomesial spines, former overreaching midlength of article 2; dorsal surface grooved proximal to base of stylocerite, bearing prominent, forwardly directed, bluntly pointed proximolateral tubercle; stylocerite nearly straight, acuminate, narrowly separated from lateral margin of article 1, reaching distal margin of article 2; article 2 approximately as long as wide when measured along lateral margin, with small distomesial spine subequal in size to corresponding spine on article 1; article 3 shorter than article 2; flagella shorter than carapace (Fig. 1).

Antennal peduncle (Fig. 2B, C, E) stout. Basicerite with strong ventrolateral distal spine distinctly overreaching dorsolateral distal projection. Article 5 (= carpocerite) nearly reaching distal margin of scaphocerite. Scaphocerite suboval,

less than 0.3 times as long as carapace, 1.1–1.2 times as long as wide, lateral margin gently convex; dorsal surface with sharply delimited, obliquely longitudinal carina along midline; distolateral spine small, triangular with acute tip, clearly separated from lamella, falling short of broadly rounded distal margin of lamella.

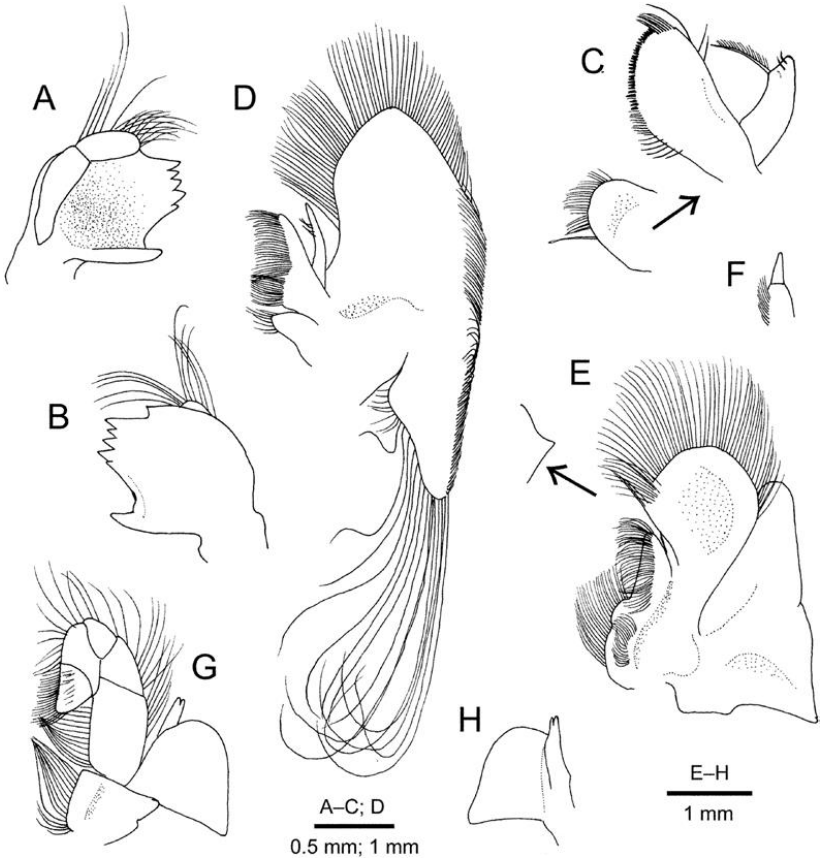

Figure S3. *Rimicaris falkorae* **n. sp.**, holotype, ovigerous female (cl 10.1 mm), CBM-ZC 15255. left mandible, inner view (**A**); same, outer view (**B**); left maxillule (with detached coxal endite), outer view (**C**); left maxilla, outer view (**D**); left maxilliped 1, outer view; inset, rudimentary exopod on mesial margin of caridean lobe, inner view (**E**); endopod of left maxilliped 1, inner view (**F**); left maxilliped 2, outer view (**G**); same, epipod and podobranch, inner view (**H**).

Mandible (Fig. 3A, B) with molar process terminating in blunt tip; incisor process with 6 teeth on mesial margin, anteriormost one clearly separated from other teeth; palp consisting of 2 articles, proximal article narrowing basally, distal article shorter than proximal article, bearing long plumose setae on outer margin. Maxillule (Fig. 3C) with slightly bilobed endopod, inner lobe with long setulose seta apically, outer lobe with 2 submarginal minute setae on outer surface; coxal endite roundly truncate; basial endite with 2 rows of small spiniform setae, obscured by short setae, on mesial margin. Maxilla (Fig. 3D) with broad scaphognathite, no seta-like structure on outer and inner surfaces, posterior lobe produced, narrowed distally, bearing numerous elongated setae on mesial to terminal margin; coxal endite small, rounded distally; basial endite much larger than coxal endite, bilobed; endopod reaching beyond distal margin of basial endite, tapering to subacute tip. Maxilliped 1 (Fig. 3E) with broadly rounded caridean lobe, bearing exopodal flagellum greatly reduced to small triangular lobe on mesial margin (Fig. 3E, inset); no setae-like structure on surfaces of caridean lobe; endopod bi-articulated, distal article small, tapering (Fig. 3F); coxal endite narrow; basial endite larger than coxal endite, slightly bilobed, both endites with thick setation; epipod very broad, faintly bilobed, narrowing anteriorly to rounded terminus, posterolateral margin slightly produced. Maxilliped 2 (Fig. 3G) pediform with stout endopod consisting of 5 articles; epipod large subcircular, with slender, terminally bilobed podobranch (Fig. 3H); no exopod.

Maxilliped 3 (Fig. 4A) overreaching distal margin of antennal scaphocerite by 0.8 length of ultimate article. Coxa with bilobed epipod on lateral face. Antepenultimate article strongly sinuous in dorsal view, with prominent tuft of long setae at proximomesial portion. Distal 2 articles arcuate. Ultimate article 1.4 times as long as penultimate article (= carpus), tapering distally, with minute spiniform setae at apex (Fig. 5A); lateral surface carinate, then cross section trigonal; mesial face with several transverse tracts of stiff setae, forming grooming apparatus.

Pereopod 1 (Fig. 4B) slightly overreaching distal margin of antennal scaphocerite, moderately slender. Articulation between ischium, merus strongly oblique. Carpus broadened distally, cupshaped; flexor margin subdistally with triangular, tooth-like projection; mesial face shallowly depressed, bearing grooming structure consisting of cluster of

stiff setae adjacent to flexor margin and with 3 minute spiniform setae proximal to setal cluster (Fig. 5B). Palm much shorter than fingers, without tuft of short setae on ventral surface; fingers strongly compressed, curved downward, inward; outer surface of both fingers convex, inner surface concave, cutting edges uniformly offset, closing without gap, each armed with fine, microscopic row of closely set teeth, tip of each finger slightly spooned; dactylus 3.5 times longer than palm (Fig. 5C, D).

Pereopod 2 (Fig. 4C) falling slightly short of distal margin of antennal scaphocerite each article with sparse setae. Ischium unarmed. Merus longer than ischium. Carpus slightly widened distally. Chela subequal in length to carpus; tip of each finger terminating in simple chitinous claw; cutting edge of each finger with row of minute chitinous spines; dactylus 1.2 times as long as palm (Fig. 5E).

Pereopods 3–5 (Fig. 4D–F) generally similar, but merus-ischium becoming shorter from third to fifth, whereas carpus-propodus becoming longer from third to fifth. Pereopod 3 (Fig. 4D) overreaching antennal scaphocerite by half length of propodus; ischium and merus unarmed; carpus slightly widened distally, 0.8 times as long as propodus; propodus with 2 rows of minute spiniform setae on flexor surface; dactylus slightly compressed laterally, 0.3 times as long as propodus, terminating in strong, curved unguis clearly demarcated basally, flexor surface with 13 accessory spinules arranged in 3 longitudinal rows (Fig. 5F; mesial row of 4 spiniform setae not visible). Pereopod 4 (Fig. 4E) reaching pterygostomial projection of carapace by 0.2 length of propodus; dactylus with about 12 accessory spinules arranged in 3 rows. Pereopod 5 (Fig. 4F) reaching tip of pterygostomial projection by tip of propodus; flexor spiniform setae on propodus fewer than those on pereopods 3 and 4; dactylus with about 10 accessory spinules arranged in 3 rows.

Pleopod 1 with endopod (Fig. 5G) tapering distally to simple apex. Appendices internae on pleopods 2–4 simple, slender, tapering distally, without terminal cluster of coupling hooks; appendices internae on pleopod 5 normally developed, bearing terminal cluster of coupling hooks. Uropod (Fig. 2F, G) with protopod bearing acute posterolateral process, posteromesial process also acuminate; rami both overreaching posterior margin of telson; exopod slightly longer than endopod, with 2 subequal posterolateral spiniform setae.

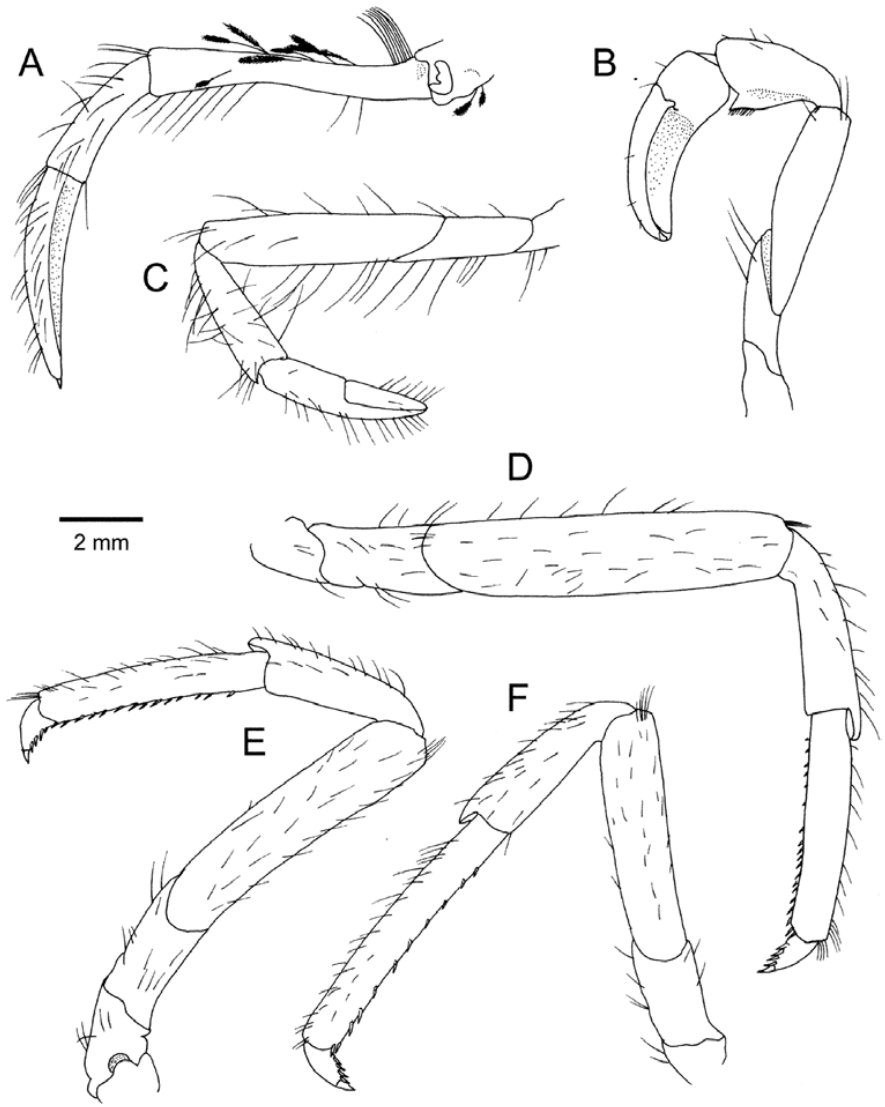

Figure S4. *Rimicaris falkorae* **n. sp.**, holotype, ovigerous female (cl 10.1 mm), CBM-ZC 15255. left maxilliped 3, lateral view (**A**); left pereopod 1, lateral view (**B**); left pereopod 2, lateral view (**C**); right pereopod 3, lateral view (**D**); left pereopod 4, lateral view (**E**); left pereopod 5, lateral view (**F**).

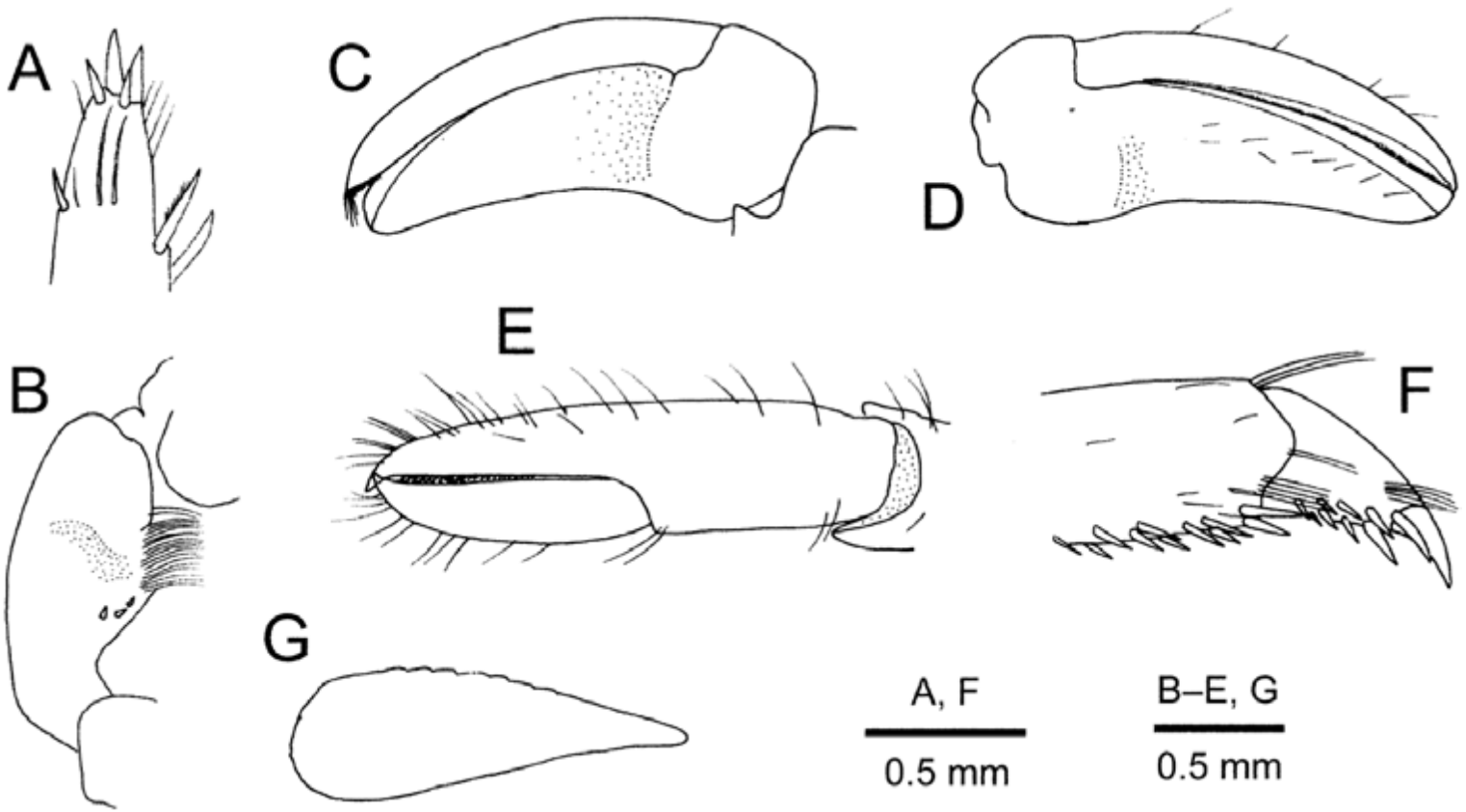

Figure S5. *Rimicaris falkorae* **n. sp.**, holotype, ovigerous female (cl 10.1 mm), CBM-ZC 15255. A, tip of ultimate article of left maxilliped 3 (**A**); carpus of left pereopod 1, mesial view, showing grooming structure (**B**); chela of left pereopod 1, outer view (**C**); same, inner view (**D**); chela of pereopod 2, extensor view (**E**); distal part of propodus and dactylus of right pereopod 3, flexor-lateral view (**F**); endopod of left pleopod 1, anterior view (**G**).

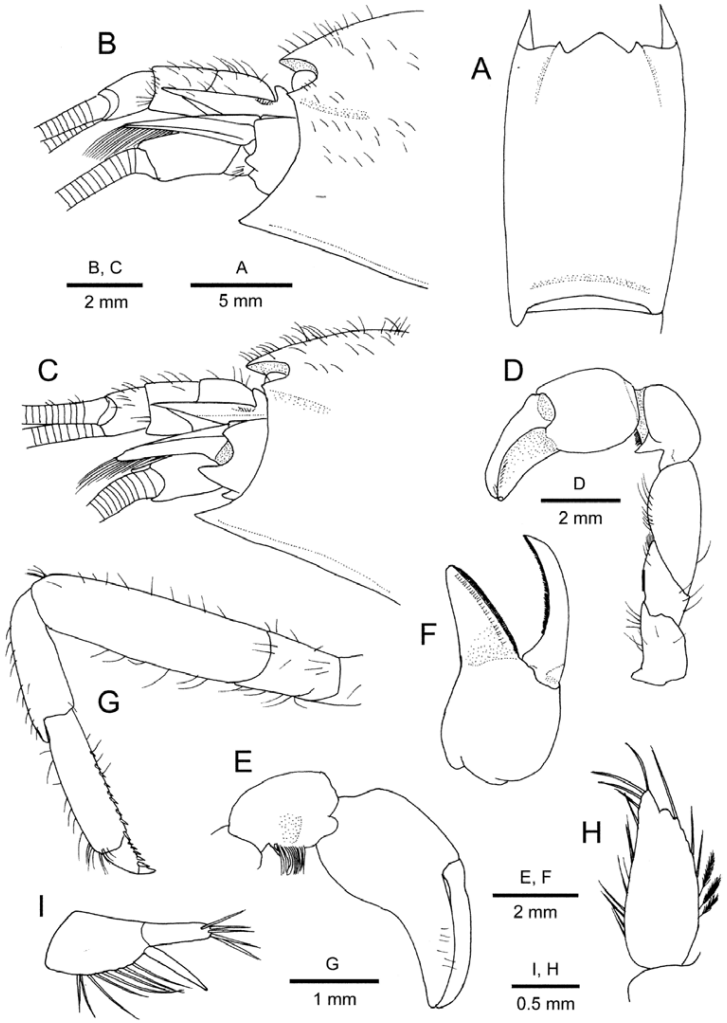

Figure S6. *Rimicaris falkorae* **n. sp.** Paratype female (cl 12.2 mm), OMNH-ZC 2018-01-110 (**A, B, D–F**); paratype male (cl 8.7 mm), CBM-ZC 15258 (**C, G–I**). Carapace, dorsal view (setae omitted) (**A**); anterior part of carapace and cephalic appendages, left lateral view (**B, C**); D, left pereopod 1, lateral view (**D**); same, chela, outer view (**E**); same, carpus and chela, inner (mesial) view (**F**); left pereopod 3, lateral view (**G**); endopod of left pleopod 1, posterior view (**H**); appendices interna and masculina of left pleopod 2, mesial view (**I**).

Paratypes: Ovigerous females very similar to holotype. Nonovigerous females and males having carapace dorsum rounded, without trace of blunt middorsal ridge and shallow longitudinal depressions on either side (Fig. 6A); branchiostegal projection reaching level of midlength to distal margin of article 1 of antennular peduncle (Fig. 6B, C); faint saddle-like depression on dorsum present or absent. No marked sexual dimorphism seen in shape of rostrum and antennal spine of carapace. Pleuron 4 with posteroventral angle bluntly pointed or angular. Pleuron 5 with 0–2 minute denticles on posterolateral margin in addition to posteroventral spine. Pereopod 1 dimorphic: stout (Fig. 6D–F), slender as in holotype; grooming apparatus on mesial face of carpus consisting of setal field and 1–3 spiniform setae proximal to setal field. Stoutness of pereopods 3–5 substantially variable individually (most stout form as illustrated; Fig. 6G). Male pleopod 1 with endopod (Fig. 6H) unequally bilobed distally, mesial lobe prominent, tapering distally, with 5 long bristlelike setae apically, mesially, lateral lobe obsolete; lateral margin with row of setae changing bristle-like to plumose toward proximal; mesial margin with row of simple setae. Pleopod 2 with appendix masculina on endopod (Fig. 6I) slightly longer, much stouter than appendix interna, armed with about 5 spiniform setae distally; appendix interna tapering distally, without coupling hooks terminally.

Variation: As is apparent from the above description, the shape and size of the pterygostomial projection of the carapace, the presence or absence of a shallow saddle-like depression on the carapace dorsum, the armature of the posterolateral margin of the pleuron 5, and the shape of the pereopods 1 and 3 to 5 exhibit substantial intraspecific variation in the new species. The blunt middorsal ridge on the carapace is developed only in females of the ovigerous stage; similar ontogenetic change is known in the five congeners, *Rimicaris parva*, *R. paulexa*, *R. susannae*, *R. vandoverae*, and *R. variabilis*, as well as *Mirocaris fortunata* (Martin & Christiansen, 1995) (cf. Komai & Segonzac, 2003, 2008; Komai & Tsuchida, 2015). Similar variation in the shape of the pereopods 1 and/or 3–5 is also seen in other alvinocaridid species (e.g., Komai & Segonzac, 2003, 2004, 2005, 2008; Komai & Chan, 2010; Komai & Tsuchida, 2015).

Color in life: Body and appendages generally translucent; hepatopancreas visible through integument pale gray; two reflective spots on anterior dorsal surface of cephalothorax, representing dorsal organs. The colouration is identical to that of *R. vandoverae*, and thus these two species cannot be distinguished by colour in video footage.

Distribution and habitat: Presently known from hydrothermal vents on the Marina Back Arc Spreading Center (Burke site, 3,630 m; Perseverance site, 3,912 m).

Rimicaris shrimp are present at all the hydrothermal vent fields in the Mariana BASC (cf. Fig. 7), and they are rarely observed beyond the boundaries of these habitats. Aggregations of these shrimp are mostly observed in areas near focused vent flow, where they are often the dominant biomass. The distinguishing morphological features of *R. falkorae* **n. sp.** are too minor to observe in the video footage (https://www.youtube.com/watch?v=heNU1e1Tvdg&list=PLJGVqQI3okzaRPWwYjL4E9TsmkSa4k4cq&index=7), and there are no obvious behavioural differences that distinguish *R. falkorae* **n. sp.** from the sympatric *R. vandoverae* in these aggregations.

Specimens of *R. falkorae* **n. sp.** were found in three samples from the Burke and Perseverance vent fields. Low numbers of *R. falkorae* occurred together in a sample dominated by *R. vandoverae* (~90%) in the Burke field. The shrimp were clustered around a focused flow venting through basalt, measured at 48 ˚C. Spatial separation of the species is not evident in video footages. Most shrimp were suctioned near the flow among individuals of the mussel *Bathymodiolus septemdierum* Hashimoto & Okutani, 1994 (Bivalvia, Mytilidae), the barnacle *Neoverruca brachylepadoformis* Newman, in Newman & Hessler, 1989 (Hexanauplia, Neoverrucidae), the crab *Austinograea williamsi* Hessler & Martin, 1989 (Brachyura, Bythograeidae), and the limpets *Shinkailepas* Okutani, Saito & Hashimoto, 1989 (Gastropoda, Phenacolepatidae) and *Symmetromphalus* McLean, 1990 (Gastropoda, Neomhalidae). Some shrimp were also suctioned in the flow on an aggregation of the snail *Alviniconcha hessleri* Okutani & Ohta, 1988 (Gastropoda, Provannidae). The shrimp appeared to be grazing on both the snail shells and the basalt substratum. They only swam off the bottom when disturbed by crabs or the ROV. The slurp sampler damaged a mussel during sampling, and within a minute, the

Figure S7. Faunal assemblage and morphology of the habitat where *Rimicaris falkorae* **n. sp.** was collected in the Burke hydrothermal vent field. The snail *Alviniconcha hessleri* are present in the venting fluid, and the mussel *Bathymodiolus septemdierum*, the brachyuran crab *Austinograea williamsi*, the barnacle *Neoverruca brachylepadoformis*, and the sea anemone *Marianactis bythios* are present along the periphery. This figure is available in colour at *Journal of Crustacean Biology* online.

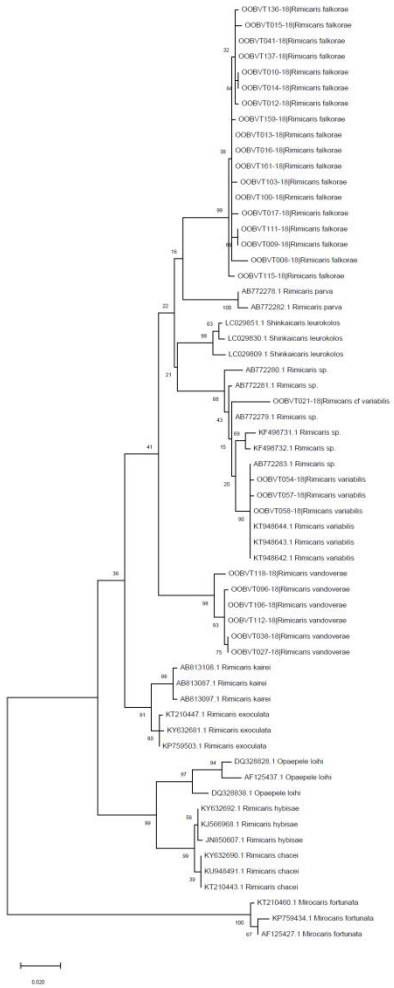

Figure S8. Phylogenetic tree of *Rimicaris falkorae* **n. sp.** and other closely related species based on barcoding regions of cytochrome c oxidase subunit 1 (COI) sequences (443–658 bp), constructed using the maximum likelihood (ML) method with 1000 replicate bootstrap values. *Mirocaris fortunate* (Martin & Christiansen, 1995) is used as the outgroup.

shrimp began to feed on the exposed tissue. It is unclear, however, if *R. falkorae* **n. sp.** was among them.

In the Perseverance field, *R. falkorae* **n. sp.** occurred in two samples where they dominated the collection (*N* = 76; 73%) with *R. vandoverae* comprising the remainder. They were collected from the base of a sulphide chimney, where microbial mat covered the sulphur crusts, and the maximum flow temperature was 16 ˚C. The snail *A. hessleri*, the limpet *Lepetodrilus* sp. (Gastropoda: Lepetodriidae), and the polychaete *Paralvinella hessleri* Desbruyeres & Laubier, 1989 (Polychaeta, Alvinellidae) co-occurred with the shrimp.

Size-frequency and reproductive features: The average carapace length (cl) of the specimens of *R. falkorae* **n. sp.** from Burke is 11.5 ± 1.0 mm, ranging from 8.5 mm to an ovigerous female at 15.0 mm. The average CL of Perseverance specimens is 6.2 ± 0.2 mm with a range from 4.5 mm to an ovigerous female at 13.0 mm. Juveniles dominated, as CL was under 7 mm for 80% of the specimens. Only two males were collected from Perseverance. Of the 80 females examined, only five were brooding eggs. These ovigerous females were mostly the largest specimens collected. The largest ovigerous female (CL

15.0 mm) held the most eggs (> 1,300), whereas the smallest ovigerous female (CL 10.5 mm) held a brood of only 350 eggs.

Nomenclatural statement: A life science identifier (LSID) number was obtained for the new species: urn:lsid:zoobank.org:pub:B4A37E97-01D8-4ACD-954C-7F744ADC94BB.

Remarks: The new species is morphologically similar to the six species previously assigned to *Chorocaris*, but is characterised by the combination of the following features: 1) carapace dorsal to lateral surfaces bearing numerous scattered short setae; 2) rostrum broadly triangular with blunt apex, distinctly wider than long; 3) antennal spine of carapace blunt to subacute; 4) pterygostomial angle of carapace strongly produced, exceeding at most as far as the midlength of the antennal scaphocerite, terminating in acute or subacute apex; 5) stylocerite of article 1 of antennular peduncle reaching distal margin of article 2; 6) ischia of pereopods 3 and 4 always unarmed; 6) uropodal protopod with posterolateral and posteromesial projections both acuminate, spine-like. In particular, the characters 1, 5, and 6 are unique to the new species. The prominence of the pterygostomial angle of the carapace is additionally strongest in the new species when compared with the six congeners, *R. chacei*, *R. parva*, *R. paulexa*, *R. susannae*, *R. vandoverae* and *R. variabilis* (cf. Komai *et al.*, 2007; Komai & Segonzac, 2008; Komai & Tsuchida, 2015).

Among the six allied species, *R. paulexa* is morphologically most similar to *R. falkorae* **n. sp.** in the shape of the rostrum, the general shape of the pterygostomial angle of the carapace and the unarmed ischia of the pereopods 3 and 4. *Rimicarais paulexa* nevertheless has fewer setae on the carapace surfaces; the pterygostomial angle of the carapace is less produced than in *R. falkorae*; the stylocerite reaches slightly beyond the midlength of the article 2 of the antennular peduncle; the posterolateral and posteromesial projections of the uropodal endopod are both bluntly pointed, never spiniform (cf. Martin & Shank, 2005; Komai & Segonzac, 2008). The sympatric *R. vandoverae* is also somewhat similar to *R. falkorae* **n. sp.** particularly in having the distally tapering, prominent pterygostomial angle of the carapace. The former differs from the new species in the above-cited characters for differentiating between *R. paulexa* and the new species.

Furthermore, the rostrum of *R. vandoverae* is rounded in the dorsal view and is more projecting than in *R. falkorae* **n. sp.**

Rimicaris variabilis is similar to *R. falkorae* **n. sp.** in having a prominent, acuminate pterygostomial angle of the carapace and a spiniform posterolateral projection of the uropodal protopod. In *R. variabilis*, however, there are much fewer sparse setae on the carapace surfaces; the rostrum is approximately as long as wide; the stylocerite reaches the midlength of the article 2 of the antennular peduncle; the ischia of the pereopods 3 and 4 are armed with one spiniform setae in males; the posteromesial process of the uropodal protopod is blunt, never spiniform (Komai & Tsuchida, 2015). Males and non-ovigerous stage of females of *R. variablis* are also easily distinguished from the new species in having a sharply pointed rostral apex (Komai & Tsuchida, 2015). The rostral apex of *R. falkorae* is always blunt, not showing an ontogenetic variation.

ML reconstruction using the mitochondrial COI gene (Fig. 8) estimates that *R. falkorae* **n. sp.** is sister to *R. parva*, and the clade comprising of *Shinkaicaris leurokolos* and *R. variabilis* is the next sister group, but the statistical supports are generally low for the major branches. Morphology does not support the position of *S. leurokolos* (see Komai & Segonzac, 2005; Komai & Chan, 2010; Komai & Tsuchida, 2015; Vereshchaka *et al.*, 2015). COI sequences are unfortunately not available for *R. paulexa*, which is morphologically most similar to the present new species. Specimens assigned to a species form well supported clades respectively. The genetic divergence between *R. falkorae* **n. sp.** and the other species of *Rimicaris* available, including the sympatric *R. vandoverae*, is 7.0–8.5% (Table 3). Such large genetic difference is generally considered as species specific in decapod crustaceans (e.g., Shih *et al.*, 2007, Malay & Paulay, 2010, Komai & Tsuchida, 2015). The genetic divergence among the specimens identified as *R. falkorae* **n. sp.** is 0.0–1.9% (average of 0.4%), clearly indicating that they all belong to the same species. Kojima & Watanabe (2015) reported on the occurrence of an unidentified species of *Chorocaris* in the Snail, Pika, and Urashima sites in the Mariana BASC. Dr. Hiromi Watanabe kindly informed us that the specimens he examined are different from our new species (personal communication to TK, 6 February 2019), suggesting the presence of a third species of *Rimicaris* in the area.

Etymology: Named after the SOI's ship R/V *Falkor*, which contributed to collect material of the new species for study.

SUPPLEMENTARY MATERIAL

Table S1. List of species and sequences used in the molecular analysis.

ACKNOWLEDGEMENTS

We deeply thank V. Tunnicliffe, the supervisor of the second author (TG), for collecting the specimens, reviewing the manuscript, and offering support and assistance for the study. We also thank anonymous reviewers and the Associate Editor for reviewing the manuscript and offering valuable suggestions for improvements. The support of the Schmidt Ocean Institute, along with ship and ROV crews, was crucial to the collection of the material studied. NOAA's EOI Program provided logistical support in the field, and we acknowledge the help of D. Butterfield (Chief Scientist), W. Chadwick, and A. Bobbitt. M. van Wyngaarden, and J. Nelson provided assistance for genetic analyses. Additional funding support from the National Geographic Society, NSERC Canada, and the Canada Research Excellence Fund.

REFERENCES

Baker, E.T., Walker, S.L., Resing, J.A., Chadwick, W.W. Jr, Merle, S.G., Anderson, M.O., Butterfield, D.A., Buck, N.J. & Michael, S. 2017. The effect of arc proximity on hydrothermal activity along spreading centers: New evidence from the Mariana back arc (12.7°N–18.3°N). *Geochemistry, Geophysics, Geosystems*, **18**: 4211–4228.

Clark, K., Karsch-Mizrachi, I., Lipman, D.J., Ostell, J. & Sayers, E.W. 2016. GenBank. Nucleic Acids Research, **44**: D67–D72.

Hessler, R.R. & Martin, J.W. 1989. *Austinograea williamsi*, new genus, new species, a hydrothermal vent crab (Decapoda: Bythograeidae) from the Mariana Back-arc Basin, western Pacific. *Journal of Crustacean Biology*, **9**: 645–661.

Kimura, M. 1980. A simple method for estimating evolutionary rates of base substitutions through comparative studies for nucleotide sequences. *Journal of Molecular Evolution*, **16**: 111–120.

Kojima, S. & Watanabe, H. 2015. Vent fauna in the Mariana Trough. In: *Subseafloor biosphere Linked to hydrothermal systems* (J. Ishibashi, K. Okino & M. Sunamura, eds.), pp. 313–323. Springer, Tokyo.

Komai, T. & Chan, T.-Y. 2010. Two new species of alvinocaridid shrimps (Crustacea: Decapoda: Caridea) from hydrothermally influenced field off northeastern Taiwan. *Zootaxa*, **2372**: 15–32.

Komai, T. & Segonzac, M. 2003. A review of the hydrothermal vent shrimp genus *Mirocaris*, redescription of *M. fortunata* (Martin & Christiansen), and reassessment of the taxonomic status of the family Alvinocarididae (Crustacea: Decapoda: Caridea). *Cahiers de Biologie marine*, **44**: 199–215.

Komai, T. & Segonzac, M. 2004. A new genus and species of alvinocaridid shrimp (Crustacea: Decapoda: Caridea) from the North Fiji and Lau Basins, southwestern Pacific. *Journal of the Marine Biological Association of U.K.*, **84**: 1179–1188.

Komai, T. & Segonzac, M. 2005. A revision of the genus *Alvinocaris* Williams and Chace (Crustacea: Decapoda: Caridea: Alvinocarididae), with descriptions of a new genus and a new species of *Alvinocaris. Journal of Natural History*, **39**: 1111–1175.

Komai, T. & Segonzac, M. 2008. Taxonomic review of the hydrothermal vent shrimp genera *Rimicaris* Williams & Rona and *Chorocaris*

Martin & Hessler (Crustacea: Decapoda: Caridea: Alvinocarididae). *Journal of Shellfish Research*, **27**: 21–41.
Komai, T. & Tsuchida, S. 2015. New records of Alvinocarididae (Crustacea: Decapoda: Caridea) from the southwestern Pacific hydrothermal vents, with descriptions of one new genus and three new species. *Journal of Natural History*, **49**(29/30): 1789–1824.
Komai, T., Gierre, O. & Segonzac, M. 2007. New record of alvinocaridid shrimps (Crustacea: Decapoda: Caridea) from hydrothermal vent fields on the southern Mid-Atlantic Ridge, including a new species of the genus *Opaepele*. *Species Diversity*, **12**: 237–253.
Komai, T., Menot, L. & Segonzac, M. 2016. New records of caridean shrimp (Crustacea: Decapoda) from hydrothermally influenced fields off Futuna Island, Southwest Pacific, with description of a new species assigned to the genus *Alvinocaridinides* Komai & Chan, 2010 (Alvinocarididae). *Zootaxa*, **4098**: 298–310.
Kumar, S., Stecher, G., Li, M., Knyaz, C. & Tamura, K. 2018. MEGA-X: Molecular evolutionary genetics analysis across computing platforms. *Molecular Biology and Evolution*, **35**: 1547–1549.
Malay, M.C.D. & Paulay, G. 2010. Peripatric speciation drives diversification and distributional pattern of reef hermit crabs (Decapoda: Diogenidae: *Calcinus*). *Evolution*, **64**: 634–662.
Martin, J.W. & Christiansen, J.C. 1995. A new species of the shrimp genus *Chorocaris* Martin & Hessler, 1990 (Crustacea: Decapoda: Bresiliidae) from hydrothermal vent fields along Mid-Atlantic Ridge. *Proceedings of the Biological Society of Washington*, **108**: 220–227.
Martin, J.W. & Hessler, R.R. 1990. *Chorocaris vandoverae*, a new genus and species of hydrothermal vent shrimp (Crustacea, Decapoda, Bresiliidae) from the Western Pacific. *Contributions to Science*, **417**: 1–11.
Martin, J.W. & Shank, T.M. 2005. A new species of the shrimp genus *Chorocaris* (Decapoda: Caridea: Alvinocarididae) from hydrothermal vents in the eastern Pacific Ocean. *Proceedings of the Biological Society of Washington*, **118**: 183–198.
Messing, J. 1983. New M13 vectors for cloning. *Methods in Enzymology*, **101**: 20–78.
Newman, W.A. & Hessler, R.R. 1989. A new abyssal hydrothermal verrucomorphan (Crustacea: Sessilia): the most primitive living sessile barnacle. *Transactions of the San Diego Society of Natural History*, **21**: 259–273.
Nye, V., Copley, J. & Plouviez, S. 2012. A new species of *Rimicaris* (Crustacea: Decapoda: Caridea: Alvinocarididae) from hydrothermal vent fields on the Mid-Cayman Spreading Centre, Caribbean. *Journal of the Marine Biological Association of the United Kingdom*, **92**: 1057–1072.
Paradis, E. & Schliep, K. 2019. ape 5.0: An environment for modern phylogenetics and evolutionary analyses in R. *Bioinformatics*, **35**: 526–528.
Prosser, S., Martinez-Acre, A. & Elias-Gutierrez, M. 2013. A new set of primers for COI amplification from freshwater microcrustaceans. *Molecular Ecology Resources*, **13**: 1151–1155.
R Core Team. 2016. R: A language and environment for statistical computing. R Foundation for Statistical Computing, Vienna, Australia [https://www.R-project.org/].
Ratnasingham, S. & Hebert, P. D. N. 2007. BOLD: The barcode of life data system (www.barcodinglife.org). *Molecular Ecology Notes*, **7**: 355–364.
Shih, H.-T., Ng, P.K.L., Schubart, C.D., Chang, H.-W. 2007. Phylogeny and phylogeography of the genus *Geothelphusa* (Crustacea: Decapoda, Brachyura, Potamidae) in southwestern Taiwan based on two mitochondrial genes. *Zoological Science*, **24**: 57–66.
Steinke, D., Prosser, S.W.J. & Hebert, P.D.N. 2016. DNA barcoding of marine metazoans. In: *Marine Genomics* (S.J. Bourlat, ed.). Methods in molecular biology, **Vol. 1452**. Springer, New York.
Vereshchaka, A.L., Klagin, D.N. & Lunina, A.A. 2015. Phylogeny and new classification of hydrothermal vent and seep shrimps of the family Alvinocarididae (Decapoda). *PLoS ONE*, **10**(7), e0129975 [doi. org/10.1371/journal.pone.0129975].
Watabe, H. & Hashimoto, J. 2002. A new species of the genus *Rimicaris* (Alvinocarididae: Caridea: Decapoda) from the active hydrothermal vent field, "Kairei Field," on the Central Indian Ridge, the Indian Ocean. *Zoological Science*, **19**: 1167–1174.
Williams, A.B. & Rona, P.A. 1986. Two new caridean shrimps (Bresiliidae) from a hydrothermal field on the Mid-Atlantic Ridge. *Journal of Crustacean Biology*, **6**: 446–462.

Appendix 2: Primers used for COI sequencing.

Primer Name	Primer Type	Taxa Applied To	Gene Sequence	Primer Sequence (5' to 3')	Citation
ZplankF1_t1	Forward Primer	Shrimp	COI	TGT AAA ACG ACG GCC AGT TCT ASW AAT CAT AAR GAT ATT GG	Prosser et al. 2013
ZplankR1_t1	Reverse Primer	Shrimp	COI	CAG GAA ACA GCT ATG ACT TCA GGR TGR CCR AAR AAT CA	
M13F	Sequence Primer	Shrimp & Gastropods	COI	TGTAAAACGACGGCCAGT	Messing, 1983
M13R	Sequence Primer	Shrimp & Gastropods	COI	CAGGAAACAGCTATGAC	
CrustDF1	Forward & Sequence Primer	Shrimp	COI	GGT CWA CAA AYC ATA AAG AYA TTG G	Steinke et al. 2016
Crust DR1	Reverse & Sequence Primer	Shrimp	COI	TAA ACY TCA GGR TGA CCR AAR AAY CA	
18F	Forward & Sequence Primer	Shrimp	18S	GATAACCGTAGTAATTCTAGACTAA	Iwatani et al. 2005
700R	Reverse & Sequence Primer	Shrimp	18S	CGCGGCTGCTGGCACCAGAC	Dreyer & Wägele, 2001
C_GasF1_t1	Forward Primer (cocktail primer)	Gastropods	COI	TGTAAAACGACGGCCAGTTTTCAACAAACCATAARGATATTGG/ TGTAAAACGACGGCCAGTATTCTACAAACCACAAAGACATCGG/ TGTAAAACGACGGCCAGTTTTCWACWAATCATAAAGATATTGG	Prosser (unpublished)
GasR1_t1	Reverse Primer	Gastropods	COI	CAGGAAACAGCTATGACACTTCWGGRTGHCCRAARAATCARAA	
BivF4_t1	Forward Primer	Gastropods	COI	TGTAAAACGACGGCCAGTGKTCWACWAATCATAARGATATTGG	
BivR1_t1	Reverse Primer	Gastropods	COI	CAGGAAACAGCTATGACTAMACCTCWGGRTGVCCRAARAACCA	

Appendix 3: Taxon occurrence list from video footage and the biological samples collected from the Mariana Backarc Spreading Center in 2016. The '*' indicates the taxa were only collected from the Snail Graveyard. "Unk. sp." indicates that the species are unknown, which is assigned to the taxa without genus-level identities.

Species	**Illium – Alice Springs**	**Burke**	**Hafa Adai**	**Perseverance**	**Forecast**	**Urashima-Pika**
Rimicaris vandoverae	X	X	X	X	X	
Rimicaris cf. *variabilis*	X	X	X	X	X	
Rimicaris falkorae		X		X		
Austinograea williamsi	X	X	X		V	
Munidopsis marianica	V	V	V	V		
Munidopsis cf. nov. sp.			X*			
Neoverruca brachylepadoformis	X	X	X	V		
Vulcanolepas nov. sp.			X			
Synopiidae Unk. sp.			X*			
Princaxelia sp.			X*			
Ilyarachna sp.			X*			
Chasmatopontius thescalus			X			
Dirivultidae Unk. sp.	X	X	X	X		
Miraciidae Unk. sp.	X	X	X			
Laophontidae Unk. sp.			X	X		
Cyclopinidae Unk. sp.		X	X			
Harpacticoida Unk.		X	X			

sp.						
Copepoda Unk. sp.			X			
Copidognathus papillatus		X				
Sericosura cochleifovea		X				
Sericosura sp.			X*			
Bathymodiolus septemdierum	X	X	V			
Alviniconcha hessleri	X	X	X	X		
Provanna nassariaeformis	X	X	X	X		
Desbruyeresia marianaensis	X	X	X	V		
Lepetodrilus aff. *schrolli* MT	X	X	X	X		
Pseudorimula marianae	X	X	X			
Bathyacmaea sp.	X	V	X	V		
Shinkailepas nov. sp.	X	X	X	X		
Symmetromphalus regularis		X	V			
Phymorhynchus wareni	V	V	X			
Aplacophora Unk. sp.		X	X			
Levensteiniella raisae	X		X	X		
Lepidonotopodium minutum	X	X	V			
Branchinotogluma marianus			X			
Branchinotogluma burkensis			V			

Sirsoe hessleri	X		X			
cf. *Prionospio* sp.	X		X	X		
Paralvinella hessleri		V	X	X		V
Amphisamytha nov. sp.	X	X	X			
Nicomache sp.			X*			
Marianactis bythios	X	V	V			
Epizoanthus cf. nov. sp.	X	V	V			
Nematoda Unk. sp.	X	X	X			
cf. *Folliculinopsis* sp.			X			

Appendix 4: Reduced COI dissimilarity tree between Alvinocarididae shrimp species (derived from Komai and Giguère, 2019).

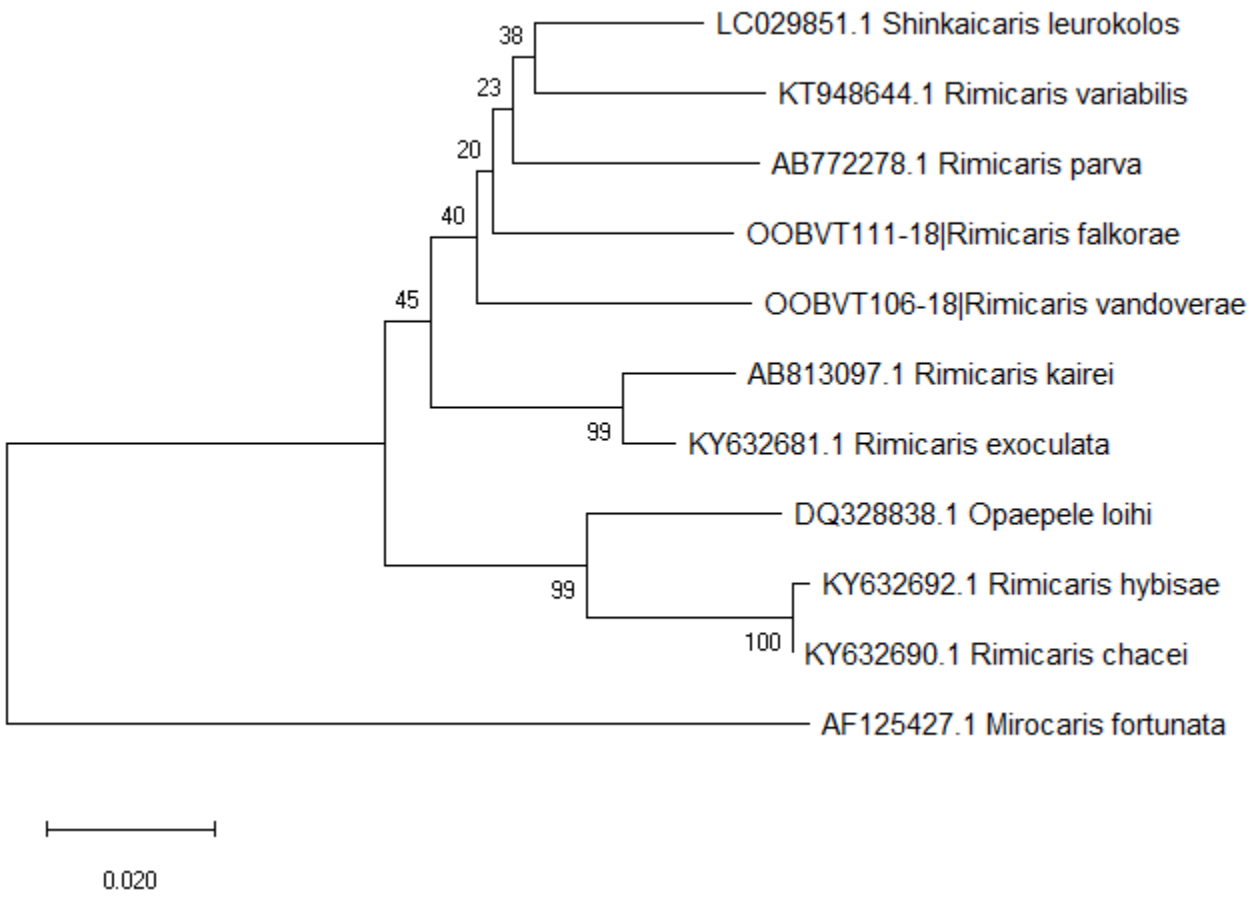

Appendix 5: Full taxon occurrence list from the biological samples, video footage, literature and personal communication. Names of vent fields are abbreviated: IA = Illium-Alice Springs; B = Burke; HA = Hafa Adai; P = Perseverance; F = Forecast; S = Snail, A = Archaean; UP = Urashima-Pika. The following symbols under the vent field columns represent the source of the data: X = sample collection (new and previously reported species); V = video imagery; O = literature report only; C = personal communication from others. Species names in bold indicate the species listed on Table 5. Size class categories include: 1 = meiofauna, and 2 = macrofauna.

#	***Species***	**IA**	**B**	**HA**	**P**	**F**	**S**	**A**	**UP**	***Possible Multiple Reporting***	***Size Class***	***Habitat***	***Literature References***	***Personal Communication***	***Possible Multiple Reporting***
1	***Rimicaris vandoverae***	X	X	X	X	X	O	O	O	No	2	Vent	Kojima & Watanabe (2015)		
2	***Rimicaris* cf. *variabilis***	X	X	X	X	X	C		C	Yes	2	Vent		Dr. Hiromi Watanabe & Dr. Tomo Komai	
3	***Rimicaris falkorae***		X		X					No	2	Vent			
4	*Rimicaris* sp.						O		O	Yes	2	Vent	Kojima & Watanabe (2015)		See #2
5	***Austinograea williamsi***	X	X	X	V	O	O	O	O	No	2	Vent	Kojima & Watanabe (2015)		
6	***Munidopsis marianica***	O	O	V	V	O			V	No	2	Vent	Fujikura et al. (1997)		
7	*Munidopsis gracilis*					O				Yes	2	Vent	Cubelio et al. (2008)		
8	*Munidopsis* cf. nov. sp.			X						Yes	2	Non-Vent			See # 9
9	*Munidopsis* sp.						O		O	Yes	2	Vent	Kojima & Watanabe (2015)		See #s 6, 7, 8
10	***Neoverruca brachylepadoformis***	X	X	X	V	O	O	O	O	No	2	Vent	Kojima & Watanabe (2015)		

11	***Vulcanolepas* nov. sp.**			X						Yes	2	Vent			
12	Scalpellomorpha gen. sp.	O								Yes	2	Vent	Hessler & Lonsdale (1991)		See #11
13	Amphipoda Unk. sp.					O				Yes	?	Vent	Fujikura et al. (1997)		See #s 14 & 15
14	Synopiidae Unk. sp.			X						Yes	1	Non-Vent			See # 13
15	*Princaxelia* sp.			X						Yes	1	Non-Vent			See # 13
16	*Ilyarachna* sp.			X						No	1	Non-Vent			
17	***Sericosura cochleifovea***		X							Yes	2	Vent			
18	*Sericosura* sp.			X						Yes	2	Non-Vent			See #17
19	*Stygiopontius pectinatus*	O								No	1	Vent	Humes (1990)		
20	*Stygiopontius stabilitus*	O								No	1	Vent	Humes (1990)		
21	*Chasmatopontius thescalus*	O		X						No	1	Vent	Humes (1990)		
22	Dirivultidae Unk. sp.	X		X	X		C			Yes	1	Both		Dr. Stace Beaulieu	
23	Miraciidae Unk. sp.	X	X	X			C			Yes	1	Both		Dr. Stace Beaulieu	
24	Laophontidae Unk. sp.			X	X		C			Yes	1	Both		Dr. Stace Beaulieu	
25	Cyclopinidae Unk. sp.		X	X						No	1	Both		Dr. Stace Beaulieu	
26	Harpacticoida Unk. sp.		X	X						No	1	Both		Dr. Stace Beaulieu	
27	Copepoda Unk. sp.			X			C			Yes	1	Both		Dr. Stace Beaulieu	
28	*Copidognthus papillatus*		X				C			No	1	Vent		Dr. Stace Beaulieu	
29	Tanaidacea Unk. sp.						C			No	?	Vent		Dr. Stace	

														Beaulieu	
30	***Bathymodiolus septemdierum***	X	X	V		O				No	2	Vent	Fujikura et al. (1997)		
31	Malletiidae Unk. sp.					O				No	2	Vent	Fujikura et al. (1997)		
32	***Alviniconcha hessleri***	X	X	X	X	O	O	O	O	No	2	Vent	Kojima & Watanabe (2015)		
33	***Provanna nassariaeformis***	O	O							Yes	2	Vent	Okutani (1990); Fujikura et al. (1997)		
34	*Provanna* cf. *nassariaeformis*	X	X	X	X					Yes	2	Vent			See # 33
35	***Desbruyeresia marianaensis***		O			O				Yes	2	Vent	Okutani (1990); Hasegawa et al. (1997)		
36	*Desbruyeresia* cf. *marianaensis*	X	X	X	V	O		O	O	Yes	2	Vent	Kojima & Watanabe (2015)		See #35
37	*Desbruyeresia* cf. *spinosa*	O				O				Yes	2	Vent	Kojima & Watanabe (2015)		See # 35
38	***Lepetodrilus* aff. *schrolli* MT**	X	X	X	X	O				Yes	2	Vent	Fujikura et al. (1997)		
39	*Lepetodrilus* sp.							O		Yes	2	Vent	Kojima & Watanabe (2015)		See # 38
40	***Pseudorimula marianae***	X	X	X		O				No	2	Vent	Fujikura et al. (1997)		
41	***Ventsia* cf. *tricarinata***	O				O				No	2	Vent	Fujikura et al. (1997)		
42	***Bathyacmaea* sp.**	X	V	X	V	V		O		Yes	2	Vent	Kojima & Watanabe		

													(2015)		
43	Acmaeidae Unk. sp. 1	O								Yes	2	Vent	Hessler & Lonsdale (1991)		See # 42
44	Acmaeidae Unk. sp. 2							O	O	Yes	2	Vent	Kojima & Watanabe (2015)		See # 42
45	***Pachydermia* cf. *sculpta***					O				No	2	Vent	Fujikura et al. (1997)		
46	*Lirapex* sp.								O	No	2	Vent	Kojima & Watanabe (2015)		
47	***Shinkailepas* nov. sp. "4"**	X	X	X	X			C		Yes	2	Vent		Dr. Yasunori Kano	
48	*Shinkailepas* nov. sp. "6"								C	Yes	2	Vent		Dr. Yasunori Kano	
49	***Shinkailepas* nov. sp. "7"**					C	C	C	C	Yes	2	Vent		Dr. Yasunori Kano	
50	*Shinkailepas* spp.	O				O	O	O	O	Yes	2	Vent	Kojima & Watanabe (2015)		See #s 48, 49 & 50
51	***Symmetromphalus regularis***	O	X	V		O				No	2	Vent	Fujikura et al. (1997)		
52	*Anatoma* sp.							O		No	2	Vent	Kojima & Watanabe (2015)		
53	*Phymorhynchus* cf. *starmeri*	O				O			O	Yes	2	Vent	Kojima & Watanabe (2015)		See # 56
54	*Phymorhynchus* sp.						O		O	Yes	2	Vent	Kojima & Watanabe (2015)		See # 56
55	***Phymorhynchus Wareni***	V	V	X						Yes	2	Vent			
56	*Thermomya sulcata*						O			No	2	Vent	Chen et al. (2018)		

57	Aplacophora Unk. sp.	O	X	X						Yes	2	Vent	Hessler & Lonsdale (1991)		
58	***Branchinotogluma burkensis***	O	O	V		O				No	2	Vent	Pettibone (1989); Fujikura et al. (1997)		
59	***Branchinotogluma marianus***	O		X		O				No	2	Vent	Fujikura et al. (1997)		
60	***Lepidonotopodium minutum***	O	X	V						No	2	Vent	Fujikura et al. (1997)		
61	***Levensteiniella raisae***	O		X	X					No	2	Vent			
62	***Sirsoe hessleri***	X	O	X						No	2	Vent	Hessler & Lonsdale (1991)		
63	*Nicomache* spp.	O	O	X						No	2	Both	Hessler & Lonsdale (1991)		
64	cf. *Prionospio* sp.	X		X	X					No	2	Vent			
65	***Paralvinella hessleri***	O	V	X	X				V	No	2	Vent	Fujikura et al. (1997)		
66	*Amphisamytha* cf. *galapagensis*	O	O							Yes	2	Vent	Hessler & Lonsdale (1991)		See # 68
67	***Amphisamytha* nov. sp.**	X	X	X			C			Yes	2	Vent		Dr. Greg Rouse	
68	Ampharetidae Unk. sp.	O				O				Yes	2	Vent	Fujikura et al. (1997)		See # 68
69	***Marianactis bythios***	O				O				Yes	2	Vent	Fujikura et al. (1997)		
70	*Marianactis* cf. *bythios*	X	V	V			O		O	Yes	2	Vent	Kojima & Watanabe (2015)		See # 70
71	Actinostolid-like anemone							O		Yes	2	Unk.	Kojima & Watanabe (2015)		See # 70
72	***Epizoanthus* cf. nov. sp.**	X	V	V						No	2	Vent			

73	Platyhelminthes Unk. sp.					O				No	1	Vent	Fujikura et al. (1997)		
74	*Abyssocladia* sp.							O		No	1	Vent	Kojima & Watanabe (2015)		
75	Nematoda Unk. sp.	X	X	X			C			No	1	Both		Dr. Stace Beaulieu	
76	cf. *Folliculinopsis* sp.			X			C			No	1	Vent		Dr. Stace Beaulieu	

Appendix 6: The R script for the statistical analyses and figure generation used for this thesis.

Final Thesis Script
Thomas Giguère
13/02/2020

Packages Used:

```
library("vegan")
## Warning: package 'vegan' was built under R version 3.6.2
## Loading required package: permute
## Loading required package: lattice
## This is vegan 2.5-6
library("ggplot2")
## Warning: package 'ggplot2' was built under R version 3.6.2
library("ape")
## Warning: package 'ape' was built under R version 3.6.2
library("lmtest")
## Warning: package 'lmtest' was built under R version 3.6.2
## Loading required package: zoo
##
## Attaching package: 'zoo'
## The following objects are masked from 'package:base':
##
##     as.Date, as.Date.numeric
library("qpcR")
## Warning: package 'qpcR' was built under R version 3.6.2
## Loading required package: MASS
## Loading required package: minpack.lm
## Warning: package 'minpack.lm' was built under R version 3.6.2
## Loading required package: rgl
## Warning: package 'rgl' was built under R version 3.6.2
```

```
## Loading required package: robustbase
## Warning: package 'robustbase' was built under R version 3.6.2
## Loading required package: Matrix
```

Table 4. Percent differences in COI nucleotide sequences between Alvinocarididae shrimp species.

Using this matrix, I took the averages between the species to create Table 4.

```
setwd("C:/Users/Thomas/Desktop/Stats Files")
Rimi.DNA <- read.dna("Alvinocarididae 08.fas", format = "fasta")
Gene_dist <- dist.gene(Rimi.DNA, method = "percentage", pairwise.deletion = FALSE, variance = FALSE)
#Gene_dist #Not displayed because it creates an enormous table.
```

Figure 9. Ratios between the number of specimens and taxa present in the samples collected from the central Mariana BASC vent sites during the FK161129 cruise. Red circle = Burke vent site. Green triangle = Hafa Adai vent site. Blue square = Illium-Alice Springs vent site, Purple cross = Perseverance vent site. Numbers in each shape represent the number of samples collected from each vent site; the numbers ascend with the number of taxa identified in each sample (y-axis)

```
SampVsTax <- read.csv("C:/Users/Thomas/Documents/School Work/Grad/Most Important Files/Thes Stat/Sample v Specimen2.csv"
, check.names=TRUE)
head(SampVsTax)
##   Dive Sample Taxa Specimens
## 1   IA      1    1         1
## 2   IA      2    1        37
## 3   IA      3    2        18
## 4   IA      4    4        16
## 5   IA      5    5        86
## 6   IA      6    7       251

SvT <- ggplot(SampVsTax, aes(x = Specimens, y = Taxa, label = Sample))+
  geom_point(aes(size = 4, shape = Dive, color = Dive, legend.position = "none"))+
```

```
  geom_text(aes(size=4))+
  theme(axis.line.x = element_line(colour = "black"),
        axis.line.y = element_line(colour = "black"),
        legend.position = "none",
        panel.background = element_blank())

## Warning: Ignoring unknown aesthetics: legend.position

print(SvT)
```

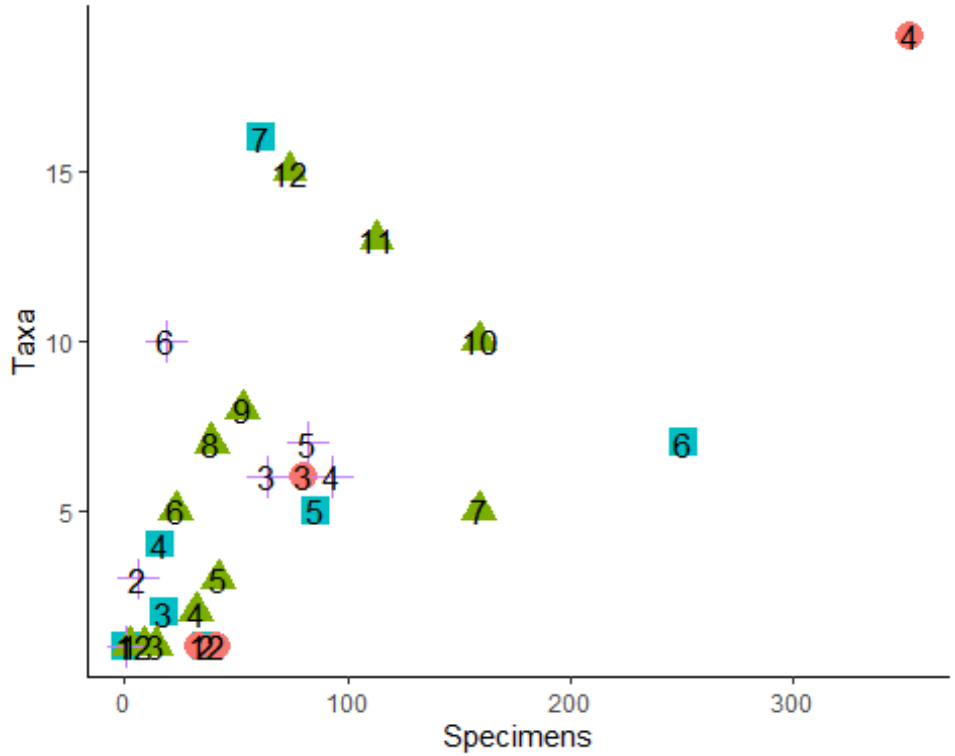

Figure 10. Rarefaction curves for each vent site sampled during the 2016 Hydrothermal Hunt cruise. The rarefaction curve labeled "Total" represents the combined results from all four vent sites.

```
RarMar <- read.csv("C:/Users/Thomas/Documents/School Work/Grad/Most Important Files/Thes Stat/Rarefaction 04.csv", row.names=1, check.names=FALSE)
raremax <- min(rowSums(RarMar))
col <- c("red", "green", "blue", "violet", "black")
lty <- c("solid")
lwd <- c(1, 2)
pars <- expand.grid(col = col, lty = lty, stringsAsFactors = FALSE)
head(pars)
##      col   lty
## 1    red solid
## 2  green solid
## 3   blue solid
## 4 violet solid
## 5  black solid

out<- with(pars[1:26, ],
         rarecurve(RarMar, step = 20, sample = raremax, col = col,
                   lty = lty, label = FALSE))
```

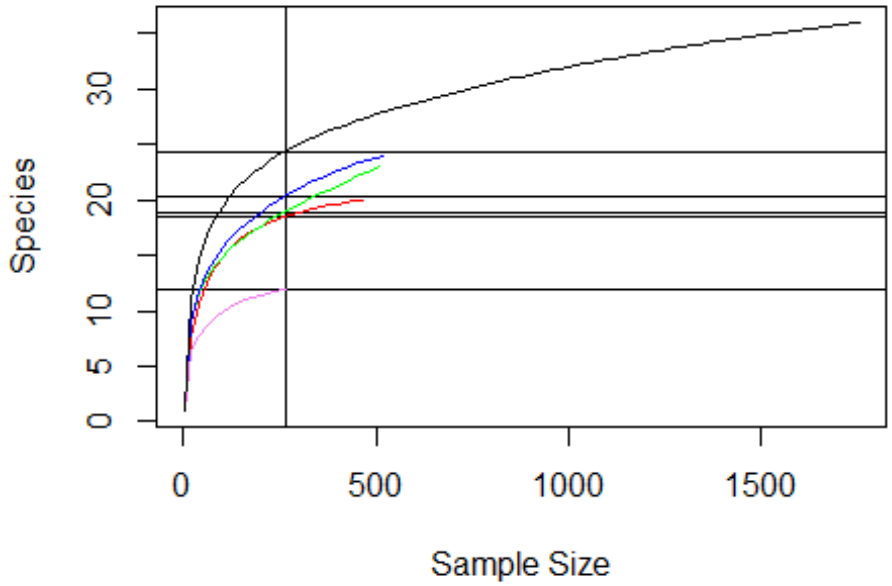


```
Nmax <- sapply(out, function(x) max(attr(x, "Subsample")))
Smax <- sapply(out, max)
plot(c(1, max(Nmax)), c(1, max(Smax)), xlab = "Number of Specimens", ylab = "Number of Taxa", type = "n") + for (i in seq_along
(out)) {
  N <- attr(out[[i]], "Subsample")
  with(pars, lines(N, out[[i]], col = col[i], lty = lty[i], lwd = lwd[i]))
}
```

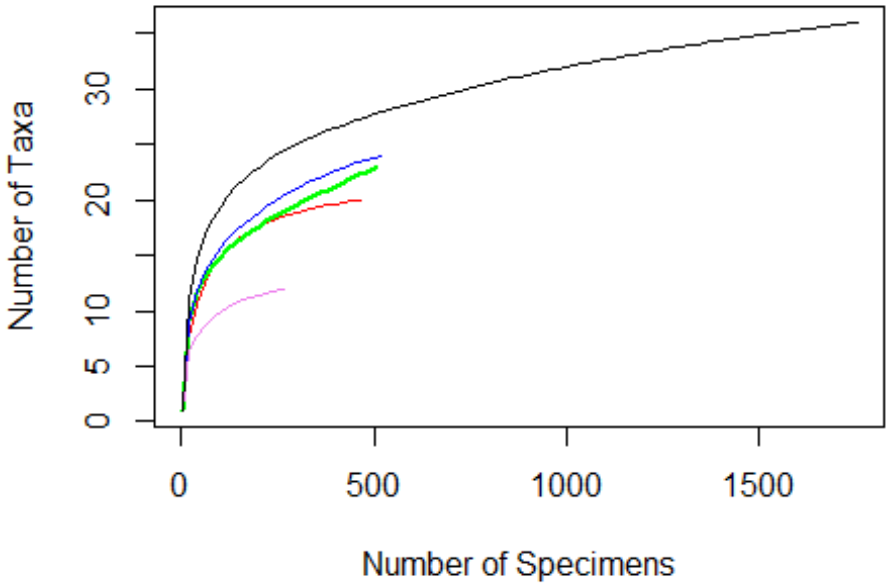


```
## integer(0)
```

Figure 11. Derived from the data on Table 5. The x-axis represents the number of vent sites where a species is present. The y-axis represents the number of taxa that occur in each group on the x-axis.

```
taxa <- read.csv("C:/Users/Thomas/Documents/School Work/Grad/Most Important Files/Thes Stat/2019-05-01 Quick Histo.csv", row.names=1, check.names=FALSE)
hist(taxa$Taxa, col = "black", border = "white", main = NA, ylab = "Number of Species", xlab = "Number of Vent Field Occurrences", xlim = c(-1,9), include.lowest = TRUE)
```

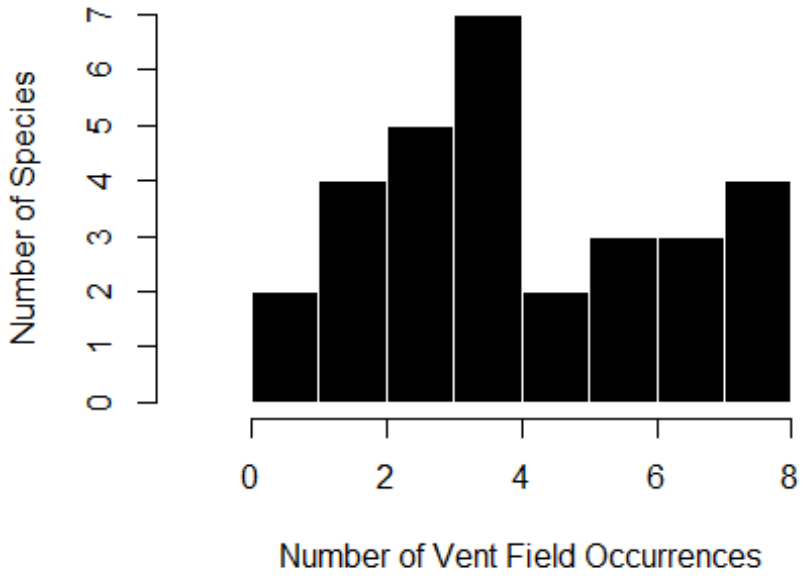

Table 8. The pairwise β-diversity values of the Mariana BASC vent sites. The β_J-diversity values are above the diagonal line. The β_{RC}-diversity values are below the diagonal line and they are presented on a scale between 1 and -1. The average β_J = 0.5161 and the median β_J = 0.5443. The average β_{RC} = -0.1078 and the median β_{RC} = -0.0539. β_{RC}-diversity values that fall outside the 95% confidence intervals are presented in bold. The vent sites are presented as follows: IA = Illium-Alice Springs, B = Burke, HA = Hafa Adai, P = Perseverance, F = Forecast, S = Snail, A = Archaean, UP = Urashima-Pika.

```
MBASC <- read.csv("C:/Users/Thomas/Documents/School Work/Grad/Most Important Files/Thes Stat/PA MBB 15.csv", row.names =1, check.names=FALSE)

jaMBASC <- vegdist(MBASC, method = "jaccard")
rcMBASC <- raupcrick(MBASC, null="r1", nsimul = 9999, chase = FALSE)
```

```
jaMBASC
##           AI         B        HA        Pe         F         S         A
## B  0.25000000
## HA 0.03846154 0.22222222
## Pe 0.51851852 0.45833333 0.50000000
## F  0.39285714 0.44444444 0.42857143 0.62500000
## S  0.70370370 0.66666667 0.69230769 0.64705882 0.60000000
## A  0.66666667 0.62500000 0.65384615 0.50000000 0.55000000 0.53846154
## UP 0.66666667 0.62500000 0.65384615 0.50000000 0.55000000 0.27272727 0.46153846

rcMBASC
##        AI      B     HA     Pe      F      S      A
## B  0.5821
## HA 0.0054 0.2956
## Pe 0.6453 0.2032 0.4795
## F  0.7907 0.8180 0.8810 0.8396
## S  0.8555 0.5333 0.7586 0.2991 0.1683
## A  0.8206 0.4604 0.7181 0.0447 0.1161 0.0461
## UP 0.8227 0.4602 0.7080 0.0429 0.1135 0.0005 0.0167
```

Table 10. The pairwise β-diversity values of the Mariana Arc vent sites. The β_J-diversity values are above the diagonal line. The β_{RC}-diversity values are below the diagonal line and they are presented on a scale between 1 and -1. The average β_J = 0.8322 and the median β_J = 0.8667. The average β_{RC} = 0.4156 and the median β_{RC} = 0.6701. β_{RC}-diversity values that fall outside the 95% confidence intervals are presented in bold. The vent sites are presented as follows: N = Nikko, K2 = Kasuga-2, NW-E = Northwest Eifuku, D = Daikoku, C = Chamorro, ED = East Diamante, R = Ruby, NW-R = Northwest Rota, SX = Seamount X.

```
MVA <- read.csv("C:/Users/Thomas/Documents/School Work/Grad/Most Important Files/Thes Stat/PA MArc 04.csv", row.names=1
, check.names=FALSE)

jaMVA <- vegdist(MVA, method = "jaccard")
```

```
rcMVA<- raupcrick(MVA, null="r1", nsimul = 9999, chase = FALSE)

jaMVA
##            N       K2      NW-E        D        C       ED        R         NW-R
## K2    0.5333333
## NW-E 0.8400000 0.8750000
## D     0.4666667 0.5000000 0.8800000
## C     0.8666667 0.9285714 0.9000000 0.9333333
## ED    0.8260870 0.7500000 0.8148148 0.7000000 0.8235294
## R     0.9285714 0.9166667 1.0000000 0.9230769 1.0000000 0.9411765
## NW-R 0.8125000 0.8666667 0.7368421 0.8750000 0.8000000 0.9000000 1.0000000
## SX    0.8888889 0.8000000 0.7500000 0.8823529 0.7000000 0.8500000 1.0000000 0.7500000

rcMVA
##          N     K2   NW-E      D      C      ED      R   NW-R
## K2    0.0295
## NW-E 0.9907 0.9900
## D     0.0079 0.0147 0.9965
## C     0.7058 0.9024 0.9015 0.9263
## ED    0.9587 0.6394 0.9945 0.4835 0.5192
## R     0.8232 0.7476 1.0000 0.7848 1.0000 0.8952
## NW-R 0.6249 0.7886 0.3248 0.8479 0.3693 0.9604 1.0000
## SX    0.9322 0.5876 0.5098 0.9046 0.1220 0.8902 1.0000 0.2973
```

Table 11. The pairwise β-diversity values of the Juan de Fuca Ridge vent sites. The β_J-diversity values are above the diagonal line. The β_{RC}-diversity values are below the diagonal line and they are presented on a scale between 1 and -1. The average β_J = 0.5114. The average β_{RC} = -0.5147. β_{RC}-diversity values that fall outside the 95% confidence intervals are presented in bold. The vent sites are presented as follows: Ex = Explorer, MV = Middle Valley, En = Endeavor, CA = Co-Axial, A = Axial, NC = North Cleft, SC = South Cleft

```
JdF <- read.csv("C:/Users/Thomas/Documents/School Work/Grad/Most Important Files/Thes Stat/PA JdF 07.csv", row.names=1, check.names=FALSE)
```

```
jaJdF <- vegdist(JdF, method = "jaccard")
rcJdF<- raupcrick(JdF, null="r1", nsimul = 9999, chase = FALSE)

jaJdF
##          Ex        MV        En        CA         A        NC
## MV 0.5306122
## En 0.4888889 0.5423729
## CA 0.4571429 0.6153846 0.5531915
## A  0.4523810 0.4909091 0.5094340 0.4523810
## NC 0.4285714 0.5961538 0.4666667 0.2258065 0.3902439
## Sc 0.5666667 0.7021277 0.6428571 0.5666667 0.5789474 0.4827586

rcJdF
##       Ex     MV     En     CA      A     NC
## MV 0.2117
## En 0.0659 0.9792
## CA 0.0075 0.8126 0.3292
## A  0.0167 0.7309 0.7197 0.0161
## NC 0.0033 0.7543 0.0430 0.0001 0.0025
## Sc 0.0090 0.3112 0.0406 0.0081 0.0023 0.0003
```

Figure 12. Dendrograms illustrating the β_J-diversity of the Mariana BASC (A), Mariana Arc (B) and Juan de Fuca Ridge (C) systems; the names of each vent site are given on the right of each dendrogram. The dendrograms are generated from the β_J values on Tables 8, 10 & 11 and are constructed using the unweighted pair group method with arithmetic mean (UPGMA).

Mariana BASC:

```
hcJAmbasc <- hclust(jaMBASC, method = "average")
hcdJAmbasc <- as.dendrogram(hcJAmbasc)
plot(hcdJAmbasc, type = "rectangle", ylab = "Mariana BASC", xlab = "Beta-Diversity (Jaccard)", xlim = c(1,-0.3), horiz = TRUE)
```

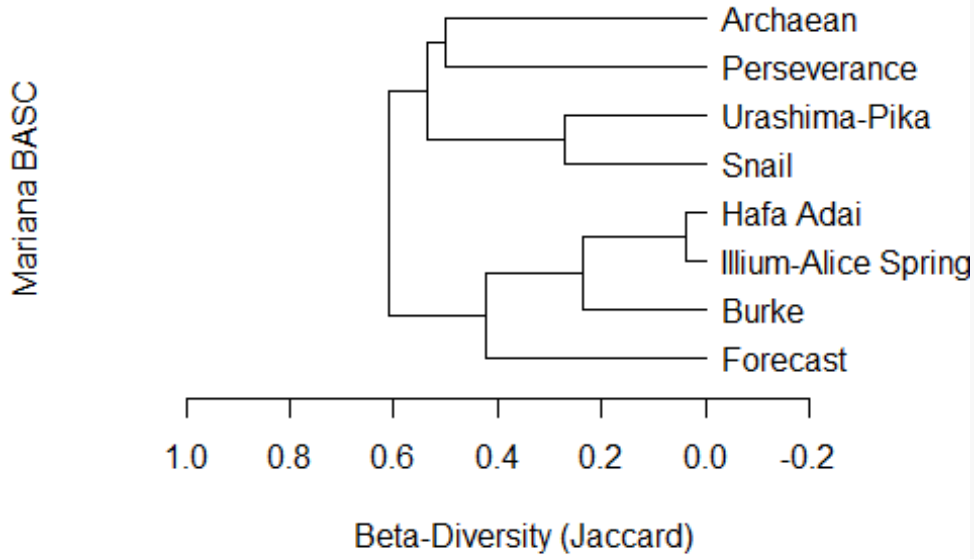

Mariana Arc:

```
hcJAmva <- hclust(jaMVA, method = "average")
hcdJAmva <- as.dendrogram(hcJAmva)
plot(hcdJAmva, type = "rectangle", ylab = "Mariana Arc", xlab = "Beta-Diversity (Jaccard)", xlim = c(1,-0.3), horiz = TRUE)
```

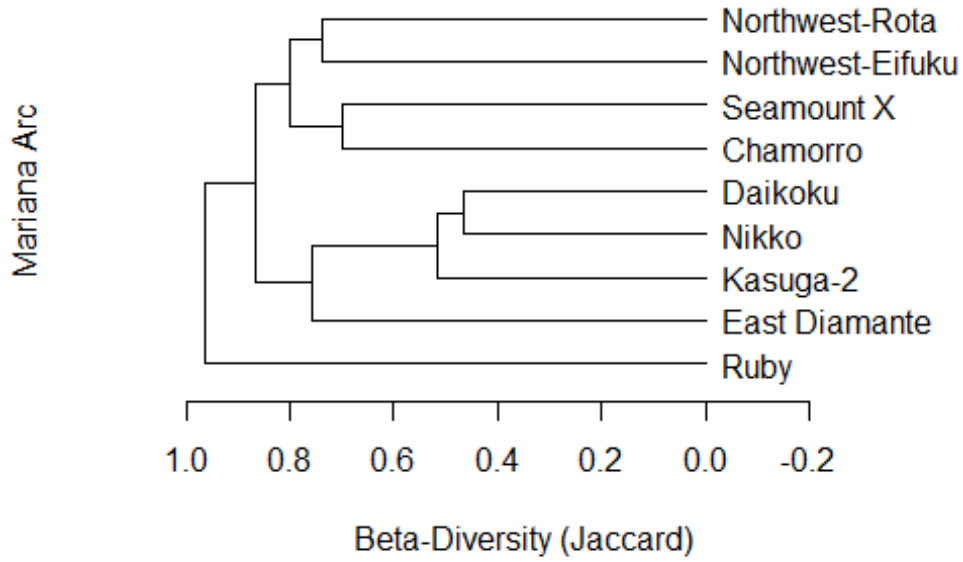

Juan de Fuca Ridge:

```
hcJAjdf <- hclust(jaJdF, method = "average")
hcdJAjdf <- as.dendrogram(hcJAjdf)
plot(hcdJAjdf, type = "rectangle", ylab = "Juan de Fuca Ridge", xlab = "Beta-Diversity (Jaccard)", xlim = c(1,-0.3), horiz = TRUE)
```

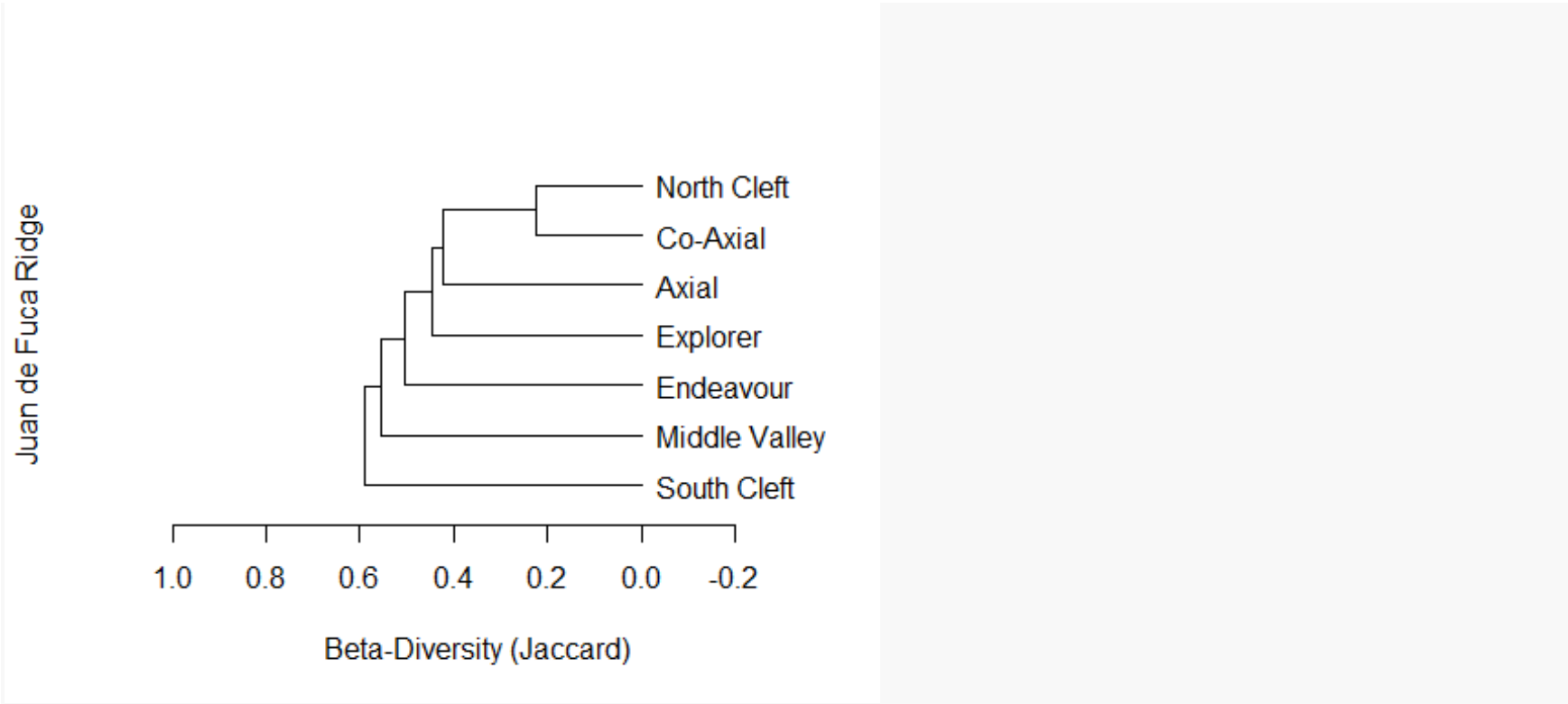

Figure 13. Boxplots representing the regional β_J-diversity for the Juan de Fuca Ridge (JdF), the Mariana Arc (MArc) and the Mariana BASC (MBASC) vent sites. The β-diversity axis represents dissimilarity values; lower values indicate that the vent assemblages are more similar than higher values.

```
Compare <- read.csv("C:/Users/Thomas/Documents/School Work/Grad/Most Important Files/Thes Stat/regional comparison of beta.csv", check.names=FALSE)
boxplot(BetaJ~Region, data=Compare, xlab="Regions", ylab="Beta-Diversity (Jaccard)")
```

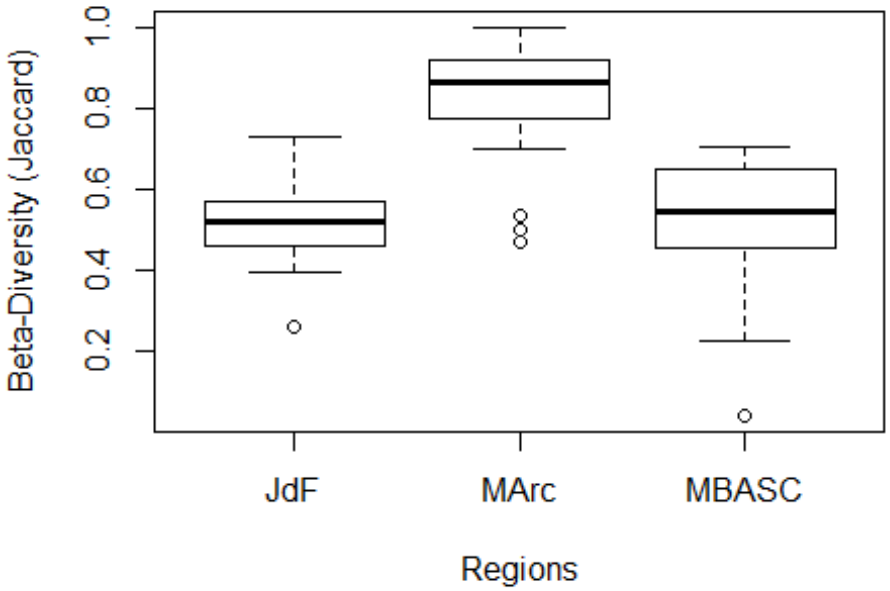

Figure 14. Boxplots representing the regional β_{RC}-diversity for the Juan de Fuca Ridge (JdF), the Mariana Arc (MArc) and the Mariana BASC (MBASC) vent sites, calculated using the Raup-Crick Index. On the β-diversity axis, values below zero indicate that the vent assemblages are more similar to each other than expected by random chance and values above zero indicate that assemblages are more dissimilar than expected by random chance. The horizontal lines on the 0.9 and -0.9 β-diversity values indicate significant deviation from the null expectation of random assembly used in the Raup-Crick index.

```
boxplot(BetaRC~Region, data=Compare, xlab="Regions", ylab="Beta-Diversity (Jaccard)")
```

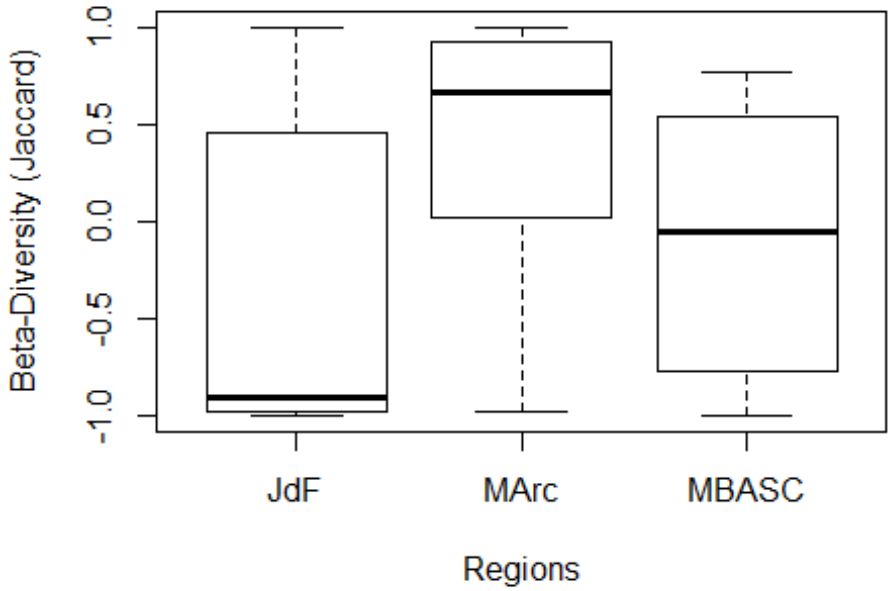

Figure 15. A non-metric multidimensional scaling (nMDS) plot illustrating the (dis)similarity in species composition between the animal assemblages present among the vent sites of the Mariana BASC and Arc using the β_J values (image A) and the β_{RC} values (image B). F = Forecast, HA = Hafa Adai, AI = Illium-Alice Springs, B = Burke, S = Snail, UP = Urashima-Pika, Pe = Perseverance, A = Archaean, R = Ruby, C = Chamorro, SX = Seamount X, NW-E = Northwest Eifuku, NR-R = Northwest Rota, ED = East Diamante, K2 = Kasuga-2, N = Nikko, D = Daikoku.

```
M <- read.csv("C:/Users/Thomas/Documents/School Work/Grad/Most Important Files/Thes Stat/PA Mariana 05.csv", row.names=1, check.names=FALSE)
MbetaJ <- vegdist (M, method = "jaccard")
MbetaRC <-raupcrick(M, null="r1", nsimul = 9999, chase = FALSE)
```

```
MbetaJ
##             AI         B        HA        Pe         F         S
## B    0.25000000
## HA   0.03846154 0.22222222
## Pe   0.48148148 0.41666667 0.46153846
## F    0.46428571 0.51851852 0.50000000 0.60869565
## S    0.70370370 0.66666667 0.69230769 0.58823529 0.63157895
## A    0.66666667 0.62500000 0.65384615 0.43750000 0.57894737 0.53846154
## UP   0.66666667 0.62500000 0.65384615 0.43750000 0.57894737 0.27272727
## N    0.94444444 0.97058824 0.94285714 1.00000000 0.92592593 1.00000000
## K2   0.94117647 0.93548387 0.93939394 0.95833333 0.92000000 1.00000000
## NW-E 0.86842105 0.91891892 0.86486486 0.89655172 0.86666667 1.00000000
## D    1.00000000 1.00000000 1.00000000 1.00000000 1.00000000 1.00000000
## C    1.00000000 1.00000000 1.00000000 1.00000000 1.00000000 1.00000000
## ED   0.97500000 0.97297297 0.97435897 0.96551724 0.96774194 1.00000000
## R    1.00000000 1.00000000 1.00000000 1.00000000 1.00000000 1.00000000
## NW-R 0.93548387 0.96551724 0.93333333 0.90000000 0.95652174 1.00000000
## SX   0.96969697 0.96666667 0.96875000 0.95454545 0.95833333 1.00000000

##             A        UP         N        K2       NW-E         D
## B
## HA
## Pe
## F
## S
## A
## UP   0.46153846
## N    1.00000000 1.00000000
## K2   0.94736842 0.94736842 0.53333333
## NW-E 0.92000000 0.96153846 0.84000000 0.87500000
## D    1.00000000 1.00000000 0.46666667 0.50000000 0.88000000
## C    1.00000000 1.00000000 0.86666667 0.92857143 0.90000000 0.93333333
```

```
## ED   0.95833333 0.95833333 0.82608696 0.75000000 0.81481481 0.70000000
## R    1.00000000 1.00000000 0.92857143 0.91666667 1.00000000 0.92307692
## NW-R 0.93750000 1.00000000 0.81250000 0.86666667 0.73684211 0.87500000
## SX   0.94117647 0.94117647 0.88888889 0.80000000 0.75000000 0.88235294

##             C        ED         R       NW-R
## B
## HA
## Pe
## F
## S
## A
## UP
## N
## K2
## NW-E
## D
## C
## ED   0.82352941
## R    1.00000000 0.94117647
## NW-R 0.80000000 0.90000000 1.00000000
## SX   0.70000000 0.85000000 1.00000000 0.75000000

MbetaRC
##          AI      B     HA     Pe      F      S      A     UP      N     K2
## B    0.0001
## HA   0.0001 0.0001
## Pe   0.0004 0.0001 0.0002
## F    0.0006 0.0049 0.0022 0.0278
## S    0.0292 0.0107 0.0228 0.0030 0.0080
## A    0.0137 0.0050 0.0094 0.0001 0.0035 0.0019
## UP   0.0131 0.0061 0.0085 0.0002 0.0033 0.0001 0.0002
## N    0.9999 1.0000 0.9991 1.0000 0.9800 1.0000 1.0000 1.0000
```

```
## K2   0.9975 0.9938 0.9964 0.9895 0.9517 1.0000 0.9445 0.9404 0.0013
## NW-E 0.9965 0.9999 0.9945 0.9736 0.9551 1.0000 0.9503 0.9956 0.7257 0.8093
## D    1.0000 1.0000 1.0000 1.0000 1.0000 1.0000 1.0000 1.0000 0.0004 0.0011
## C    1.0000 1.0000 1.0000 1.0000 1.0000 1.0000 1.0000 1.0000 0.4160 0.7425
## ED   1.0000 1.0000 1.0000 0.9992 0.9999 1.0000 0.9892 0.9906 0.6145 0.1808
## R    1.0000 1.0000 1.0000 1.0000 1.0000 1.0000 1.0000 1.0000 0.6231 0.5437
## NW-R 0.9742 0.9938 0.9625 0.7557 0.9707 1.0000 0.8568 1.0000 0.2690 0.4963
## SX   0.9988 0.9974 0.9993 0.9712 0.9845 1.0000 0.8931 0.8902 0.6945 0.2443

##       NW-E      D      C     ED      R   NW-R
## B
## HA
## Pe
## F
## S
## A
## UP
## N
## K2
## NW-E
## D    0.8642
## C    0.6228 0.7672
## ED   0.7377 0.0875 0.1984
## R    1.0000 0.5843 1.0000 0.7199
## NW-R 0.0568 0.5632 0.1761 0.7586 1.0000
## SX   0.1152 0.6458 0.0345 0.5294 1.0000 0.0939

nmdsMbJ <- metaMDS(MbetaJ, k=2)
## Run 0 stress 0.05571174
## Run 1 stress 0.0557188
## ... Procrustes: rmse 0.002039378  max resid 0.006823518
## ... Similar to previous best
## Run 2 stress 0.05572689
```

```
## ... Procrustes: rmse 0.003286171  max resid 0.01101576
## Run 3 stress 0.06134623
## Run 4 stress 0.05663241
## Run 5 stress 0.05572032
## ... Procrustes: rmse 0.00534447  max resid 0.01789447
## Run 6 stress 0.05571951
## ... Procrustes: rmse 0.005184194  max resid 0.01735906
## Run 7 stress 0.05662136
## Run 8 stress 0.06099269
## Run 9 stress 0.06099489
## Run 10 stress 0.05571929
## ... Procrustes: rmse 0.002146573  max resid 0.007183289
## ... Similar to previous best
## Run 11 stress 0.05572498
## ... Procrustes: rmse 0.006021578  max resid 0.02015104
## Run 12 stress 0.0557162
## ... Procrustes: rmse 0.001477233  max resid 0.00493009
## ... Similar to previous best
## Run 13 stress 0.08788443
## Run 14 stress 0.05572128
## ... Procrustes: rmse 0.005507714  max resid 0.01843951
## Run 15 stress 0.06098818
## Run 16 stress 0.05664616
## Run 17 stress 0.0566317
## Run 18 stress 0.05572335
## ... Procrustes: rmse 0.00588679  max resid 0.01970582
## Run 19 stress 0.06134431
## Run 20 stress 0.05572087
## ... Procrustes: rmse 0.002430163  max resid 0.008136627
## ... Similar to previous best
## *** Solution reached

nmdsMbRC <- metaMDS(MbetaRC, k=2)
```

```
## Run 0 stress 0.05682916
## Run 1 stress 0.05507588
## ... New best solution
## ... Procrustes: rmse 0.0437575  max resid 0.1489405
## Run 2 stress 0.0554444
## ... Procrustes: rmse 0.01005428  max resid 0.02625448
## Run 3 stress 0.05682896
## Run 4 stress 0.05476716
## ... New best solution
## ... Procrustes: rmse 0.01263642  max resid 0.04482617
## Run 5 stress 0.05682803
## Run 6 stress 0.05544565
## Run 7 stress 0.08613118
## Run 8 stress 0.08520048
## Run 9 stress 0.0852009
## Run 10 stress 0.05688375
## Run 11 stress 0.05682834
## Run 12 stress 0.05695672
## Run 13 stress 0.05682944
## Run 14 stress 0.05695635
## Run 15 stress 0.05688351
## Run 16 stress 0.05507595
## ... Procrustes: rmse 0.01325038  max resid 0.04496873
## Run 17 stress 0.05683009
## Run 18 stress 0.0873115
## Run 19 stress 0.05688509
## Run 20 stress 0.05507268
## ... Procrustes: rmse 0.01299875  max resid 0.04488631
## *** No convergence -- monoMDS stopping criteria:
##     20: stress ratio > sratmax

nmdsMbJ
```

```
##
## Call:
## metaMDS(comm = MbetaJ, k = 2)
##
## global Multidimensional Scaling using monoMDS
##
## Data:     MbetaJ
## Distance: jaccard
##
## Dimensions: 2
## Stress:     0.05571174
## Stress type 1, weak ties
## Two convergent solutions found after 20 tries
## Scaling: centring, PC rotation
## Species: scores missing
```

```
nmdsMbRC
```

```
##
## Call:
## metaMDS(comm = MbetaRC, k = 2)
##
## global Multidimensional Scaling using monoMDS
##
## Data:     MbetaRC
## Distance: raupcrick
##
## Dimensions: 2
## Stress:     0.05399206
## Stress type 1, weak ties
## Two convergent solutions found after 20 tries
## Scaling: centring, PC rotation
## Species: scores missing
```

```
stressplot(nmdsMbJ)
```

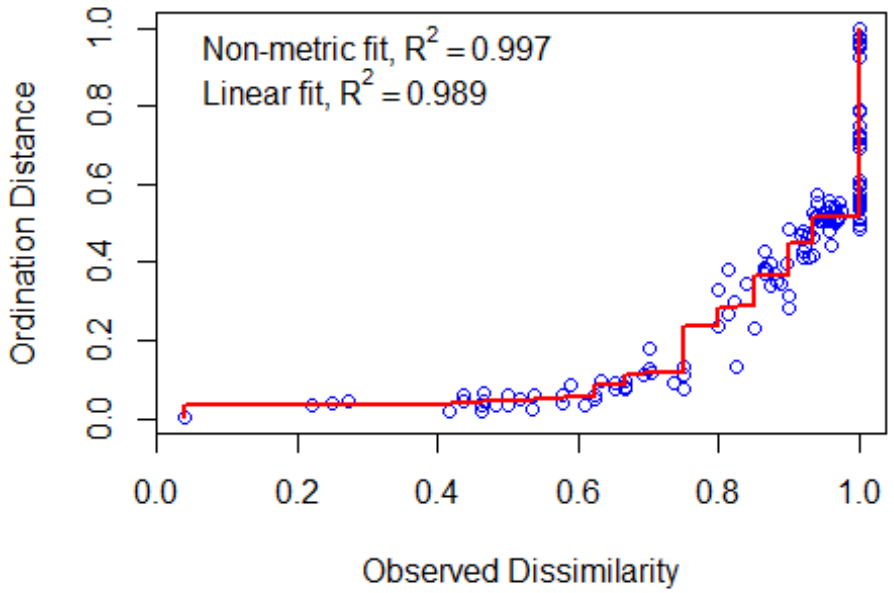


```
stressplot(nmdsMbRC)
```

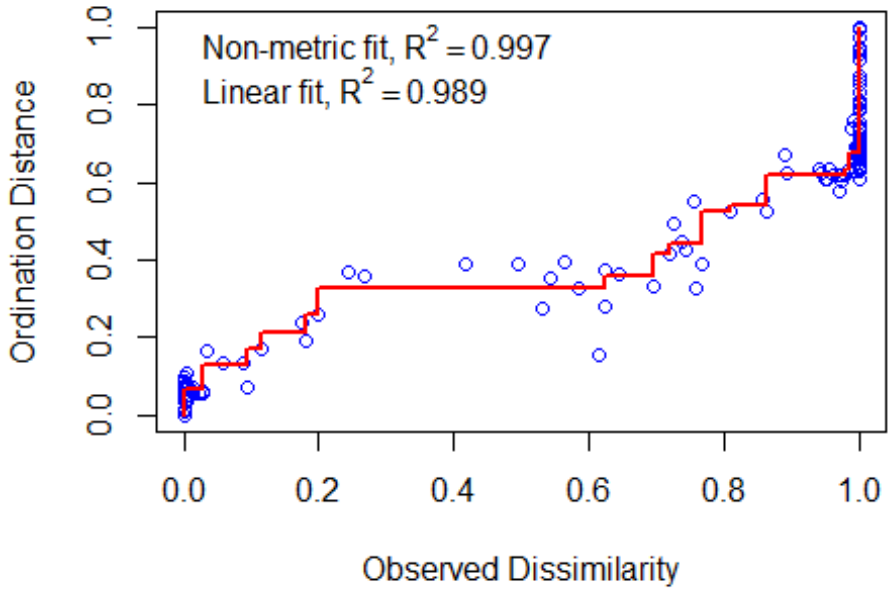

Image A

```
treat = c(rep("MBASC",8), rep("MVA",9))
colors = c(rep("red",8), rep("blue", 9))

ordiplot(nmdsMbJ, type = "n") + for(i in unique(treat)) {
  ordihull(nmdsMbJ$point[grep(i,treat),], draw = "polygon",
        groups=treat[treat==i],col=colors[grep(i,treat)],label=F)} +
orditorp(nmdsMbJ, display="sites", col = c(rep("black",8), rep("black",9)),air=0.01,cex=1.25)
```

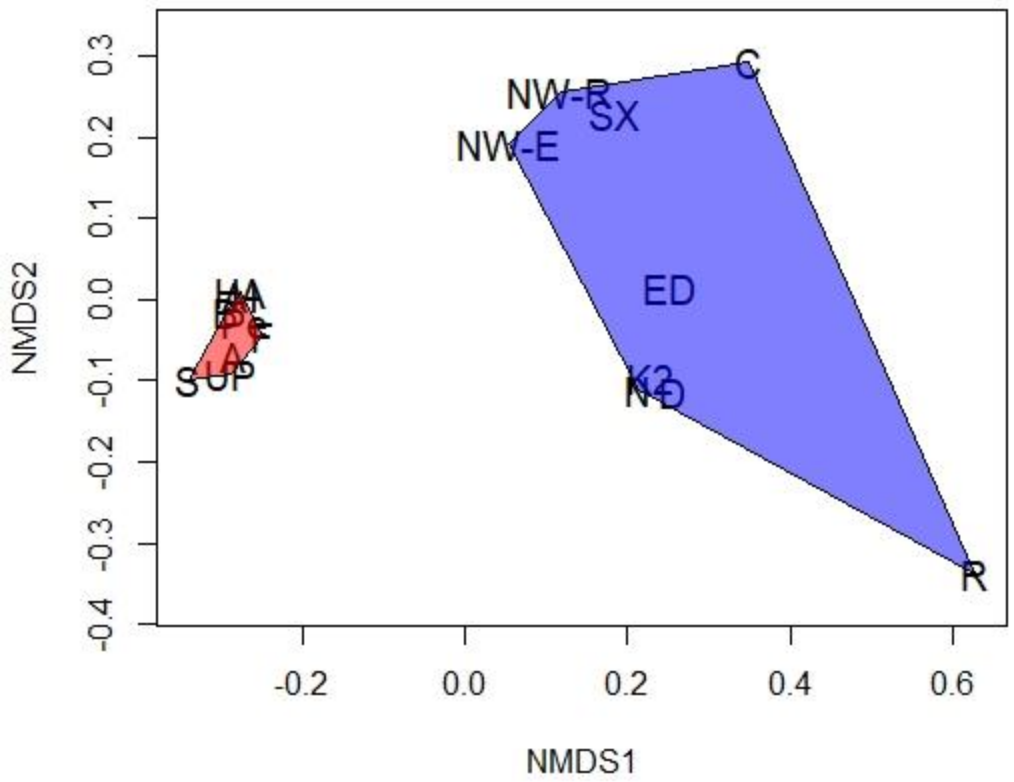

Image B

```
ordiplot(nmdsMbRC, type = "n") + for(i in unique(treat)) {
  ordihull(nmdsMbRC$point[grep(i,treat),], draw = "polygon",
          groups=treat[treat==i],col=colors[grep(i,treat)],label=F)} +
orditorp(nmdsMbRC, display="sites", col = c(rep("black",8), rep("black",9)),air=0.01,cex=1.25)
```

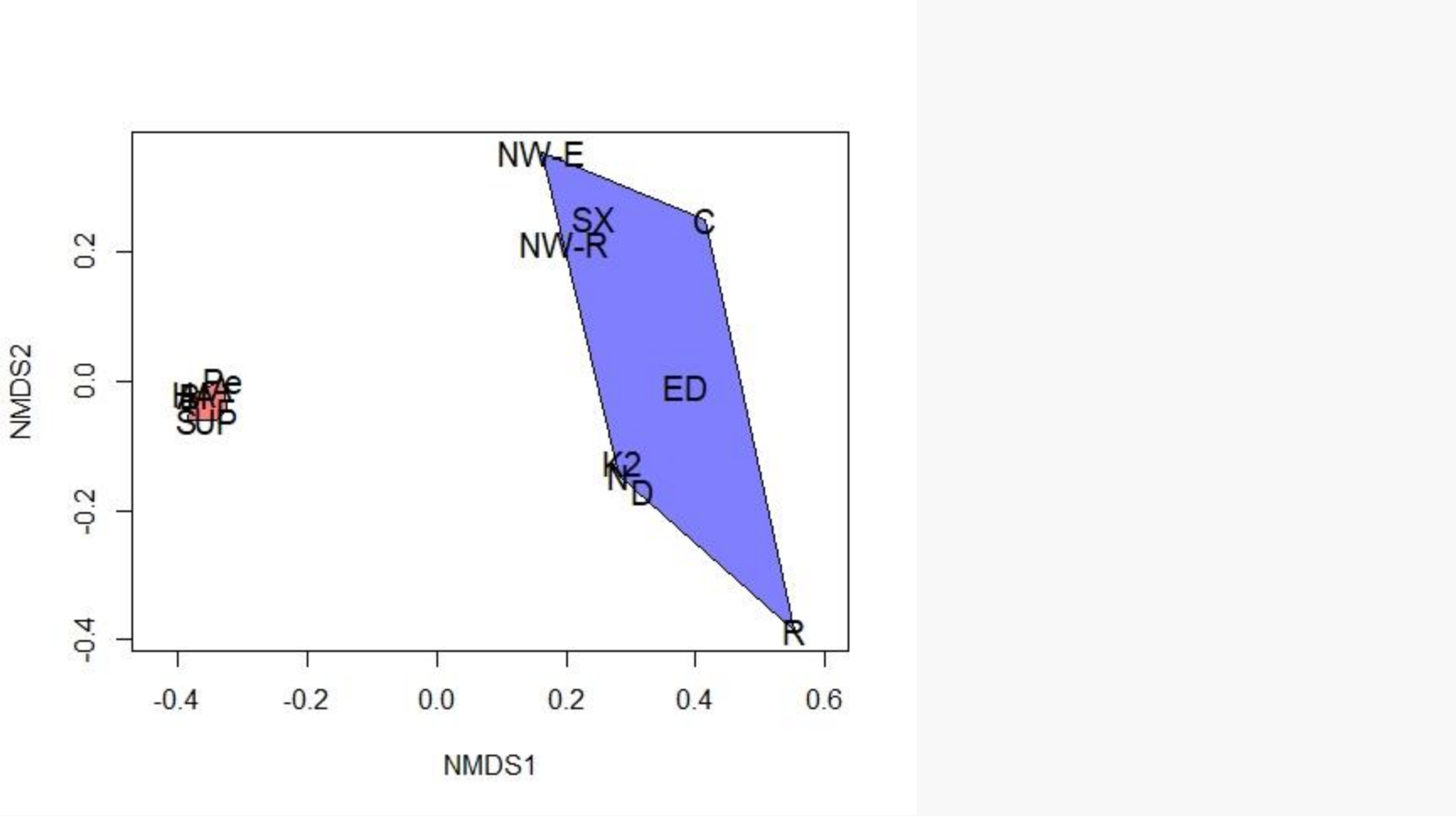

Distance to Centroid Tests (Jaccard)

```
regions <- factor(c(rep(1,8), rep(2,9)), labels = c("Backarc","Arc"))
mod <- betadisper(MbetaJ, regions)
mod
```

```
##
##  Homogeneity of multivariate dispersions
##
## Call: betadisper(d = MbetaJ, group = regions)
##
## No. of Positive Eigenvalues: 15
## No. of Negative Eigenvalues: 1
##
## Average distance to median:
## Backarc     Arc
##  0.3523  0.5561
##
## Eigenvalues for PCoA axes:
## (Showing 8 of 16 eigenvalues)
##  PCoA1  PCoA2  PCoA3  PCoA4  PCoA5  PCoA6  PCoA7  PCoA8
## 2.1534 0.7844 0.6204 0.5296 0.3938 0.3785 0.2882 0.2502
plot(mod)
```

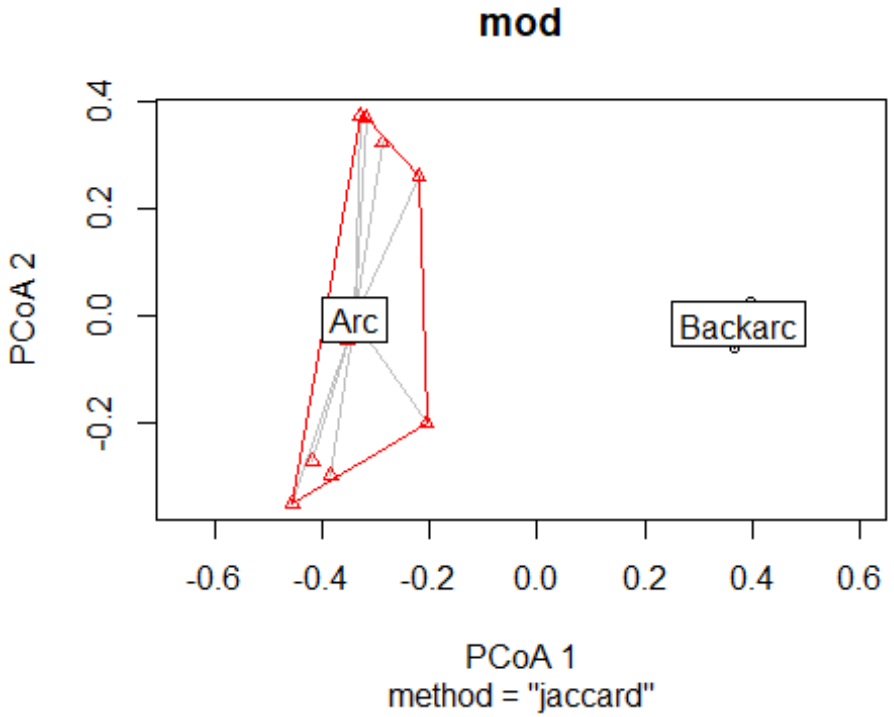


```
anova(mod)
## Analysis of Variance Table
##
## Response: Distances
##           Df  Sum Sq  Mean Sq F value    Pr(>F)
## Groups     1 0.17589 0.175894  22.984 0.0002366 ***
## Residuals 15 0.11479 0.007653
## ---
## Signif. codes:  0 '***' 0.001 '**' 0.01 '*' 0.05 '.' 0.1 ' ' 1
permutest(mod, pairwise = TRUE)
##
## Permutation test for homogeneity of multivariate dispersions
```

```
## Permutation: free
## Number of permutations: 999
##
## Response: Distances
##           Df  Sum Sq  Mean Sq      F N.Perm Pr(>F)
## Groups     1 0.17589 0.175894 22.984    999  0.001 ***
## Residuals 15 0.11479 0.007653
## ---
## Signif. codes:  0 '***' 0.001 '**' 0.01 '*' 0.05 '.' 0.1 ' ' 1
##
## Pairwise comparisons:
## (Observed p-value below diagonal, permuted p-value above diagonal)
##            Backarc   Arc
## Backarc           0.002
## Arc     0.00023658
(mod.HSD <- TukeyHSD(mod))
##   Tukey multiple comparisons of means
##     95% family-wise confidence level
##
## Fit: aov(formula = distances ~ group, data = df)
##
## $group
##                 diff       lwr       upr     p adj
## Arc-Backarc 0.2037901 0.1131863 0.2943939 0.0002366
```

Distance to Centroid Tests (Raup-Crick)

```
regions2 <- factor(c(rep(1,8), rep(2,9)), labels = c("Backarc","Arc"))
mod2 <- betadisper(MbetaRC, regions2)
## Warning in betadisper(MbetaRC, regions2): some squared distances are negative
## and changed to zero
mod2
##
##  Homogeneity of multivariate dispersions
```

```
##
## Call: betadisper(d = MbetaRC, group = regions2)
##
## No. of Positive Eigenvalues: 9
## No. of Negative Eigenvalues: 7
##
## Average distance to median:
##  Backarc      Arc
## 0.004701 0.367687
##
## Eigenvalues for PCoA axes:
## (Showing 8 of 16 eigenvalues)
##   PCoA1   PCoA2   PCoA3   PCoA4   PCoA5   PCoA6   PCoA7   PCoA8
## 3.49079 1.05123 0.36601 0.27554 0.22265 0.08831 0.06326 0.00437
plot(mod2)
```

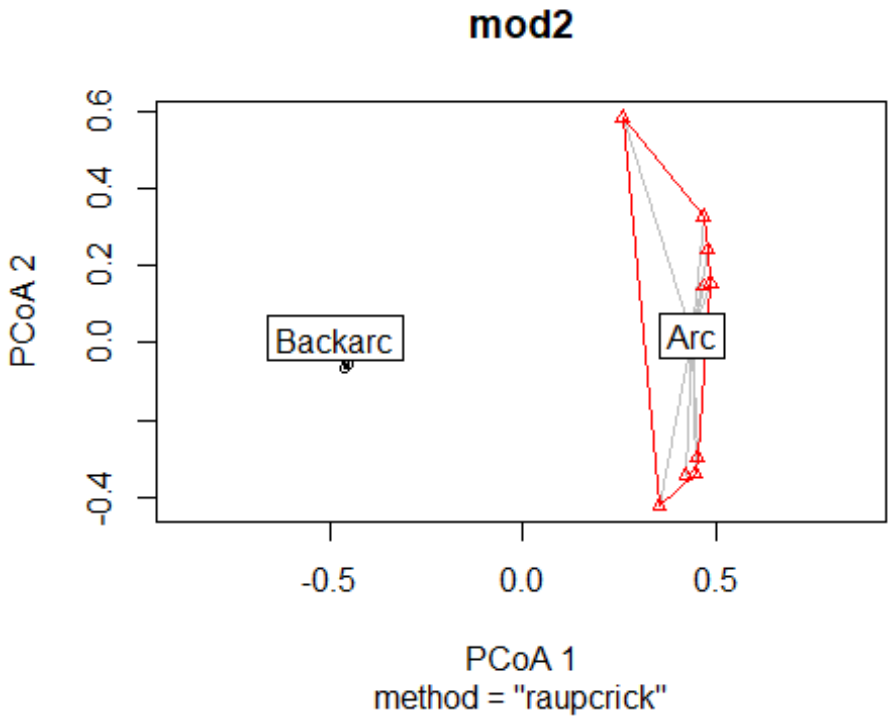


```
anova(mod2)
## Analysis of Variance Table
##
## Response: Distances
##           Df  Sum Sq Mean Sq F value    Pr(>F)
## Groups     1 0.55804 0.55804   41.44 1.119e-05 ***
## Residuals 15 0.20199 0.01347
## ---
## Signif. codes:  0 '***' 0.001 '**' 0.01 '*' 0.05 '.' 0.1 ' ' 1
permutest(mod, pairwise = TRUE)
##
## Permutation test for homogeneity of multivariate dispersions
```

```
## Permutation: free
## Number of permutations: 999
##
## Response: Distances
##           Df  Sum Sq  Mean Sq      F N.Perm Pr(>F)
## Groups     1 0.17589 0.175894 22.984    999  0.001 ***
## Residuals 15 0.11479 0.007653
## ---
## Signif. codes:  0 '***' 0.001 '**' 0.01 '*' 0.05 '.' 0.1 ' ' 1
##
## Pairwise comparisons:
## (Observed p-value below diagonal, permuted p-value above diagonal)
##           Backarc   Arc
## Backarc           0.001
## Arc     0.00023658
(mod.HSD2 <- TukeyHSD(mod))
##   Tukey multiple comparisons of means
##     95% family-wise confidence level
##
## Fit: aov(formula = distances ~ group, data = df)
##
## $group
##                 diff       lwr       upr     p adj
## Arc-Backarc 0.2037901 0.1131863 0.2943939 0.0002366
```

Additional Statistical Tests:

Multiple Regression - Alpha Diversity

All environmental variable combinations tried for regression models:
-Isolation ***(Alpha & Beta-Diversity)***
-Depth ***(Alpha & Beta-Diversity)***
-DistanceFromArc ***(Alpha & Beta-Diversity)***

-Isolation + Depth ***(Alpha-Diversity)***
-Isolation + DistanceFromArc ***(Alpha-Diversity)***
-Depth + DistanceFromArc ***(Alpha-Diversity)***
-Isolation + Depth + DistanceFromArc ***(Alpha-Diversity)***
-Log(Isolation) ***(Alpha & Beta-Diversity)***
-Log(Depth) ***(Alpha & Beta-Diversity)***
-Log(DistanceFromArc) ***(Alpha & Beta-Diversity)***
-Log(Isolation) + Log(Depth) ***(Alpha-Diversity)***
-Log(Isolation) + Log(DistanceFromArc) ***(Alpha-Diversity)***
-Log(Depth) + Log(DistanceFromArc) ***(Alpha-Diversity)***
-Log(Isolation) + Log(Depth) + Log(DistanceFromArc) ***(Alpha-Diversity)***

The 3 best models

```
Nvo3A <- read.csv("C:/Users/Thomas/Documents/School Work/Grad/Most Important Files/Thes Stat/Enviro MBASC 3A.csv", check.names=TRUE)

BLM1 <- lm(SpeciesRichness ~ DistanceFromArc, data=Nvo3A)
BLM2 <- lm(SpeciesRichness ~ LogDFA, data = Nvo3A)
BLM3 <- lm(SpeciesRichness ~ Depth + DistanceFromArc, data=Nvo3A)

summary(BLM1) #R-adjusted = 0.7126
##
## Call:
## lm(formula = SpeciesRichness ~ DistanceFromArc, data = Nvo3A)
##
## Residuals:
##     Min      1Q  Median      3Q     Max
## -6.7113 -1.0525 -0.2668  2.7970  4.4360
##
## Coefficients:
##                Estimate Std. Error t value Pr(>|t|)
## (Intercept)     9.72091    2.13737   4.548  0.00390 **
```

```
## DistanceFromArc  0.12361    0.02885   4.284  0.00518 **
## ---
## Signif. codes:  0 '***' 0.001 '**' 0.01 '*' 0.05 '.' 0.1 ' ' 1
##
## Residual standard error: 3.774 on 6 degrees of freedom
## Multiple R-squared:  0.7537, Adjusted R-squared:  0.7126
## F-statistic: 18.36 on 1 and 6 DF,  p-value: 0.00518

summary(BLM2) #R-adjusted = 0.7279
##
## Call:
## lm(formula = SpeciesRichness ~ LogDFA, data = Nvo3A)
##
## Residuals:
##     Min      1Q  Median      3Q     Max
## -7.0629 -0.6953  0.8708  2.0797  3.3761
##
## Coefficients:
##             Estimate Std. Error t value Pr(>|t|)
## (Intercept)  -11.012      6.412  -1.717  0.13673
## LogDFA        11.074      2.494   4.441  0.00437 **
## ---
## Signif. codes:  0 '***' 0.001 '**' 0.01 '*' 0.05 '.' 0.1 ' ' 1
##
## Residual standard error: 3.672 on 6 degrees of freedom
## Multiple R-squared:  0.7667, Adjusted R-squared:  0.7279
## F-statistic: 19.72 on 1 and 6 DF,  p-value: 0.004372

summary(BLM3) #R-adjusted = 0.8472
##
## Call:
## lm(formula = SpeciesRichness ~ Depth + DistanceFromArc, data = Nvo3A)
##
```

```
## Residuals:
##       1       2       3       4       5       6       7       8
##  2.77001  0.09837  1.64379 -4.68559 -1.39698 -0.81770  1.36069  1.02742
##
## Coefficients:
##                 Estimate Std. Error t value Pr(>|t|)
## (Intercept)     21.352732   4.895275   4.362  0.00728 **
## Depth           -0.004714   0.001881  -2.507  0.05405 .
## DistanceFromArc  0.172795   0.028769   6.006  0.00184 **
## ---
## Signif. codes:  0 '***' 0.001 '**' 0.01 '*' 0.05 '.' 0.1 ' ' 1
##
## Residual standard error: 2.752 on 5 degrees of freedom
## Multiple R-squared:  0.8908, Adjusted R-squared:  0.8472
## F-statistic:  20.4 on 2 and 5 DF,  p-value: 0.003937
```

Testing assumptions - Based on http://r-statistics.co/Assumptions-of-Linear-Regression.html

1. "The regression model is linear in parameters

```
plot(BLM1,1)
```

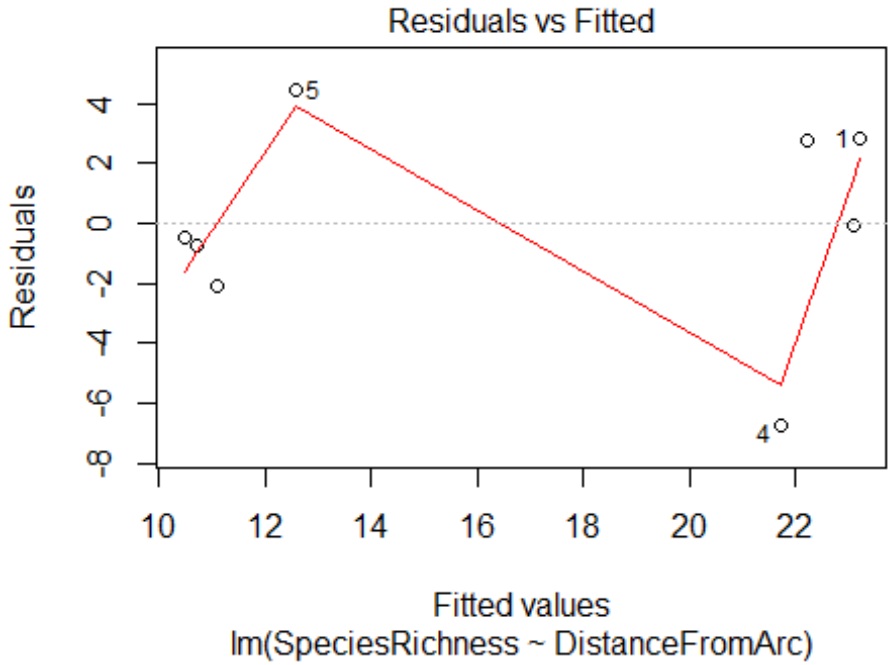
Residuals vs Fitted
Residuals
Fitted values
lm(SpeciesRichness ~ DistanceFromArc)
5
1
4
-8
-6
-4
-2
0
2
4
10
12
14
16
18
20
22

```
plot(BLM2,1)
```

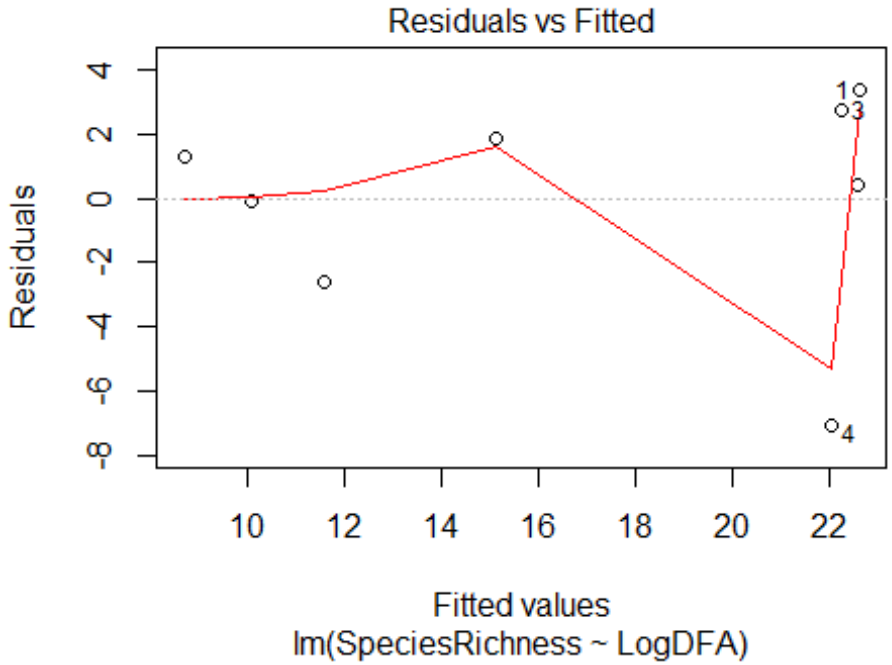
Residuals vs Fitted
Residuals
4
2
0
-2
-4
-6
-8
10
12
14
16
18
20
22
Fitted values
lm(SpeciesRichness ~ LogDFA)
1
3
4

```
plot(BLM3,1)
```

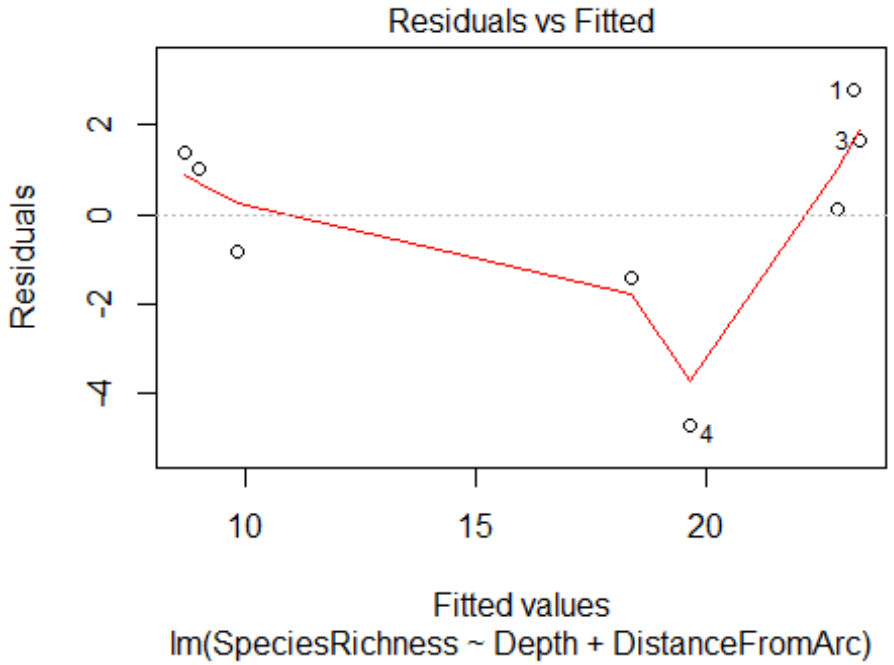

Model 1 (with Distance From Arc as the explanatory variable) may not be linear, though it is diffiult to assess with such a small dataset.

Model 2 (log-transformed Disance From Arc values) may also not be linear, though it seems better than model 1.

Model 3 (Distance From Arc + Depth as explanatory variables) appear to be the most linear.

2. "The mean of residuals is zero"

```
mean(BLM1$residuals)
## [1] -2.498002e-16
mean(BLM2$residuals)
## [1] -4.440892e-16
mean(BLM1$residuals)
```

```
## [1] -2.498002e-16
```

All three models satisfy this assumption

3. Homoscedasticity

```
bptest(BLM1)
##
##  studentized Breusch-Pagan test
##
## data:  BLM1
## BP = 0.70603, df = 1, p-value = 0.4008
bptest(BLM2)
##
##  studentized Breusch-Pagan test
##
## data:  BLM2
## BP = 1.5077, df = 1, p-value = 0.2195
bptest(BLM3)
##
##  studentized Breusch-Pagan test
##
## data:  BLM3
## BP = 2.1333, df = 2, p-value = 0.3442
```

All three models satisfy this assumption.

4. “No autocorrelation of residuals”

```
acf(BLM1$residuals)
```

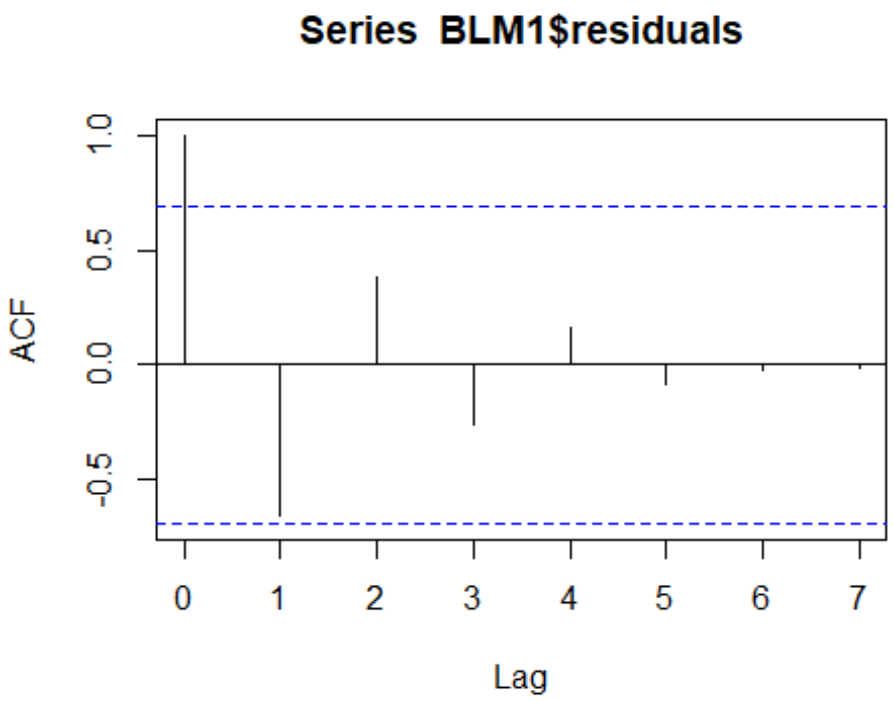


```
acf(BLM2$residuals)
```

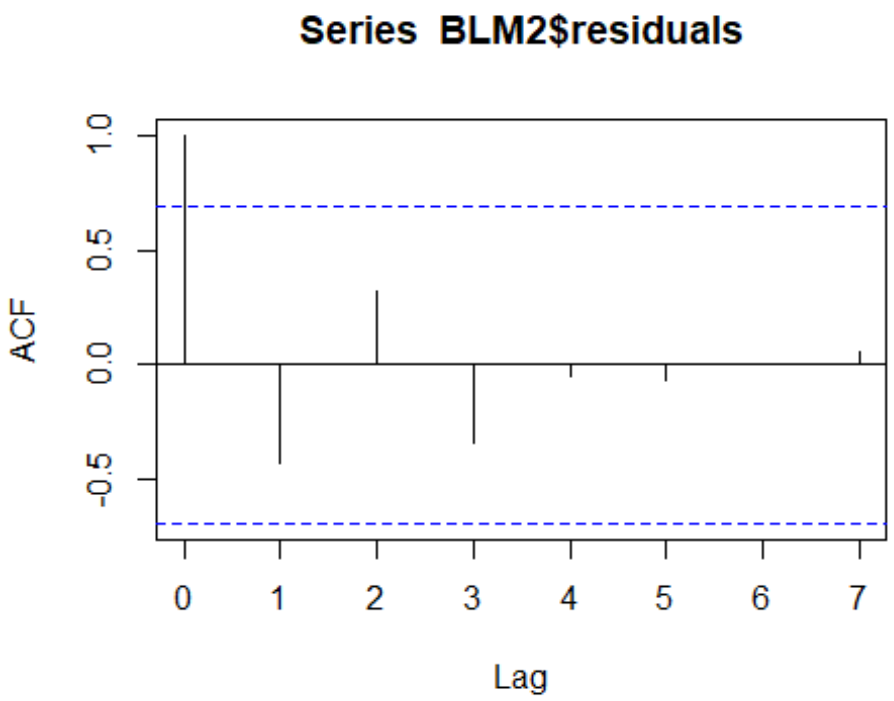


```
acf(BLM3$residuals)
```

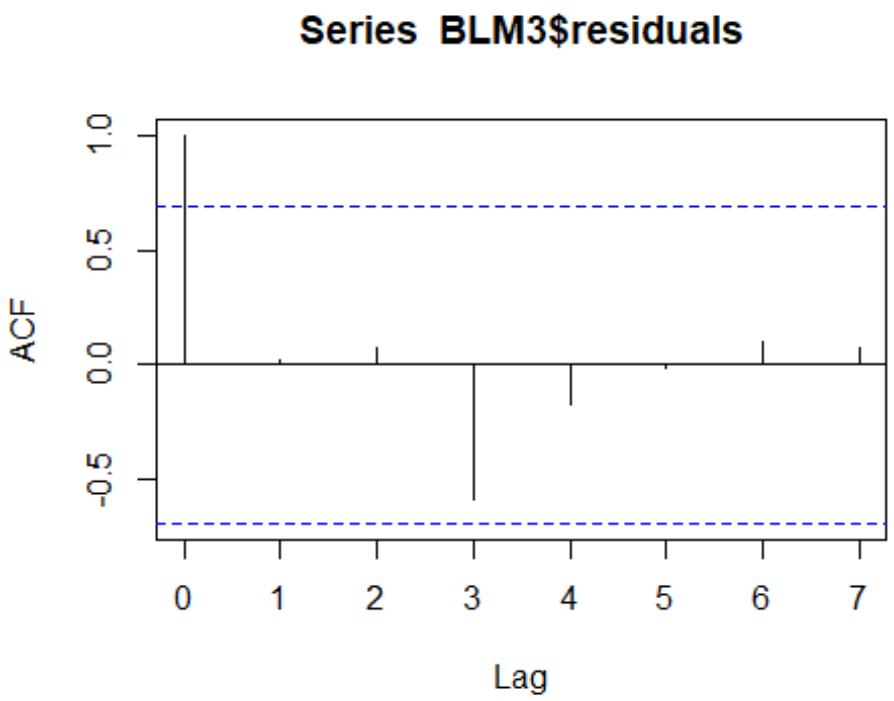

This assumption is satisfied in all three models

5.“The X variables and residuals are uncorrelated”

```
cor.test(Nvo3A$DistanceFromArc, BLM1$residuals)
##
##  Pearson's product-moment correlation
##
## data:  Nvo3A$DistanceFromArc and BLM1$residuals
## t = 3.004e-17, df = 6, p-value = 1
```

```
## alternative hypothesis: true correlation is not equal to 0
## 95 percent confidence interval:
##  -0.7046729  0.7046729
## sample estimates:
##          cor
## 1.226392e-17

cor.test(Nvo3A$LogDFA, BLM2$residuals)
##
##  Pearson's product-moment correlation
##
## data:  Nvo3A$LogDFA and BLM2$residuals
## t = 2.3241e-16, df = 6, p-value = 1
## alternative hypothesis: true correlation is not equal to 0
## 95 percent confidence interval:
##  -0.7046729  0.7046729
## sample estimates:
##          cor
## 9.488172e-17

cor.test(Nvo3A$DistanceFromArc, BLM3$residuals)
##
##  Pearson's product-moment correlation
##
## data:  Nvo3A$DistanceFromArc and BLM3$residuals
## t = 5.8367e-17, df = 6, p-value = 1
## alternative hypothesis: true correlation is not equal to 0
## 95 percent confidence interval:
##  -0.7046729  0.7046729
## sample estimates:
##          cor
## 2.382808e-17
```

```
cor.test(Nvo3A$Depth, BLM3$residuals)
##
##  Pearson's product-moment correlation
##
## data:  Nvo3A$Depth and BLM3$residuals
## t = 7.4516e-16, df = 6, p-value = 1
## alternative hypothesis: true correlation is not equal to 0
## 95 percent confidence interval:
##  -0.7046729  0.7046729
## sample estimates:
##          cor
## 3.042116e-16
```

All three models satisfy this assumption.

6. "The number of observations must be greater than number of Xs"

Given that sample size is n=8 and only one or two independent variables are used in the models, this assumption is satisfied for all three.

7. "The variability in X values is positive."

```
var(Nvo3A$DistanceFromArc)
## [1] 2444.125
var(Nvo3A$LogDFA)
## [1] 0.3098266
var(Nvo3A$Depth)
## [1] 571866.4
```

Models 1 and 3 satisfy this assumption, but model 2 may violate it. The Log values are very close, which is driving the small number. The variability in x-values is still positive, but this small value is questionable

8. The regression model is correctly specified

All satisified

9. “No perfect multicollinearity”

```
cor.test(Nvo3A$DistanceFromArc, Nvo3A$Depth, method="pearson")
##
##  Pearson's product-moment correlation
##
## data:  Nvo3A$DistanceFromArc and Nvo3A$Depth
## t = 2.2844, df = 6, p-value = 0.06242
## alternative hypothesis: true correlation is not equal to 0
## 95 percent confidence interval:
##  -0.04359856  0.93657620
## sample estimates:
##       cor
## 0.6820281
```

Depth and Distance from the Arc are almost significantly correlated (p = 0.06).

10. “Normality of residuals”

```
plot(BLM1,2)
```

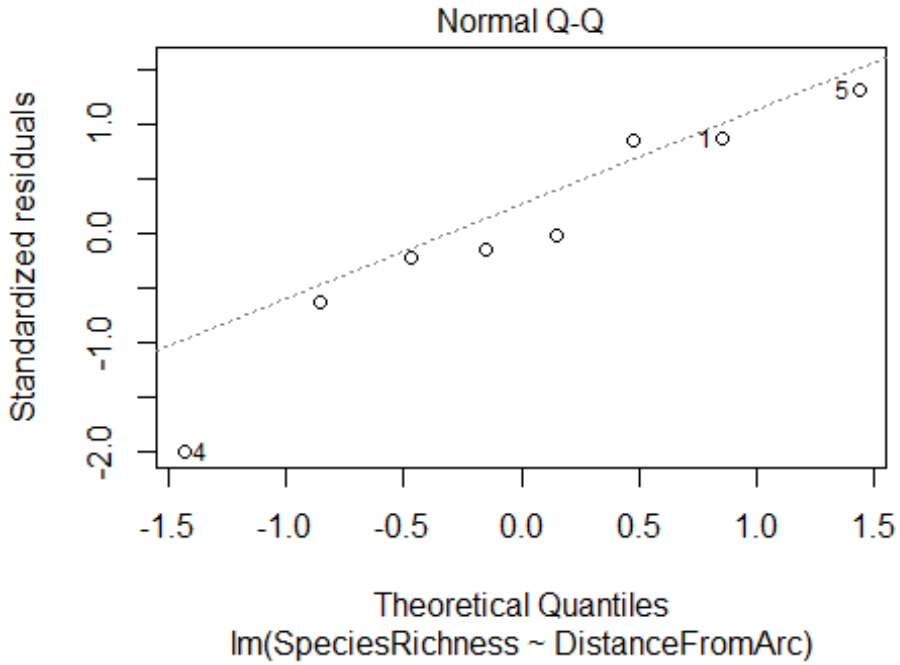
Normal Q-Q
Standardized residuals
1.0
0.0
-1.0
-2.0
5
1
4
-1.5
-1.0
-0.5
0.0
0.5
1.0
1.5
Theoretical Quantiles
lm(SpeciesRichness ~ DistanceFromArc)

```
plot(BLM2,2)
```

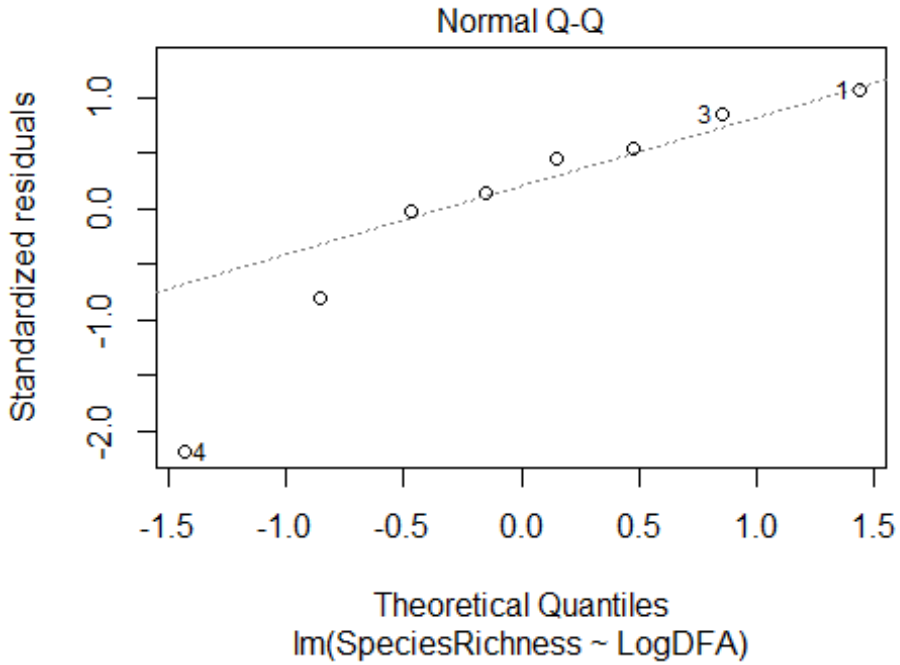
Normal Q-Q
Standardized residuals
1.0
0.0
-1.0
-2.0
1
3
4
-1.5
-1.0
-0.5
0.0
0.5
1.0
1.5
Theoretical Quantiles
lm(SpeciesRichness ~ LogDFA)

```
plot(BLM3,2)
```

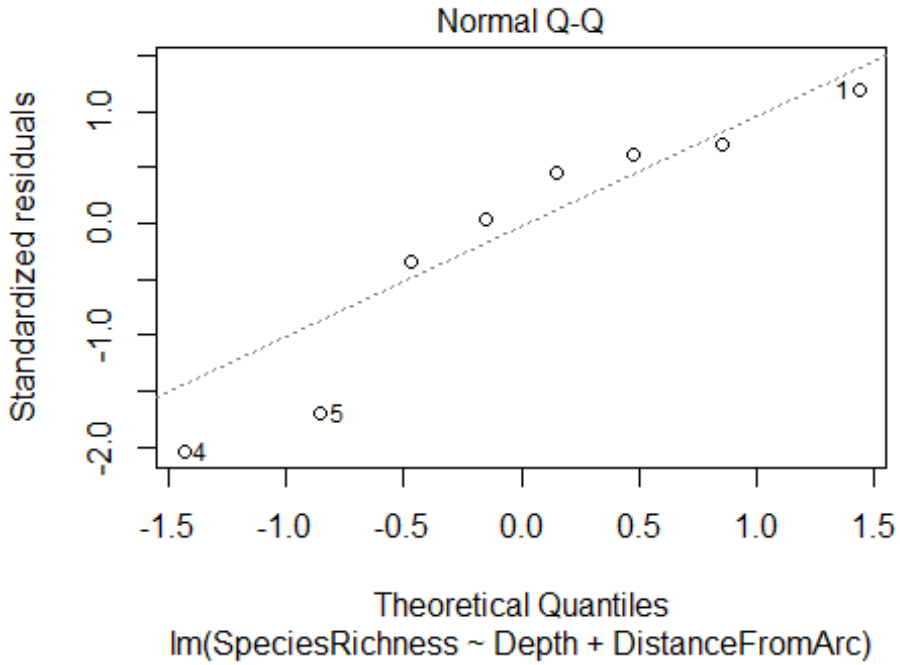

All three models do not seem to violate this assumption.

Additional Test: Major Outliers

```
plot(BLM1,5)
```

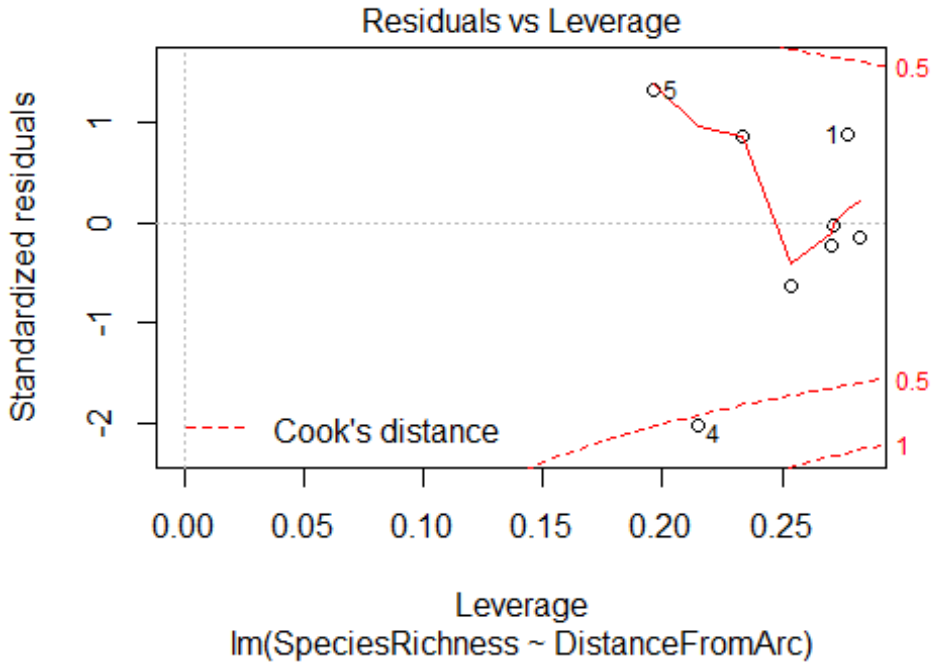
Residuals vs Leverage
Standardized residuals
Leverage
lm(SpeciesRichness ~ DistanceFromArc)
Cook's distance
0.5
0.5
1
5
1
4
0.00
0.05
0.10
0.15
0.20
0.25
-2
-1
0
1

```
plot(BLM2,5)
```

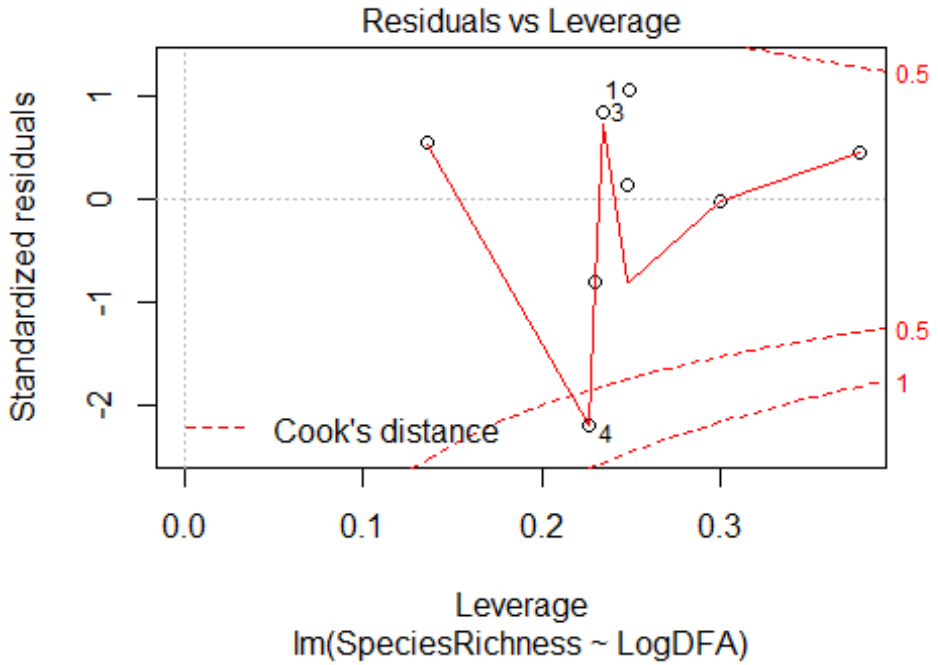
Residuals vs Leverage
Standardized residuals
1
0
-1
-2
0.0
0.1
0.2
0.3
Leverage
lm(SpeciesRichness ~ LogDFA)
Cook's distance
0.5
0.5
1
1
3
4

```
plot(BLM3,5)
```

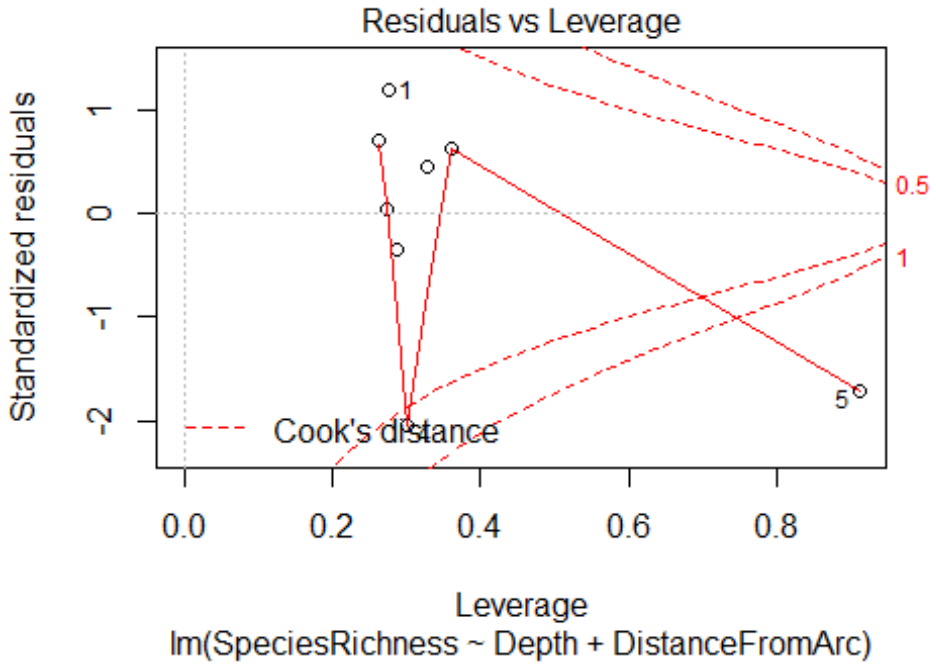

Model 3 is the only model of these three with a significant outlier, which happens to be the Forecast vent field. This is because Forecast is located at a notably shallower depth than all other vent sites in the Mariana Backarc Spreading Center.

Akaike's Test to determine best model (for small data sets)

```
AICc(BLM1)
## [1] 50.05089
AICc(BLM2)
## [1] 49.6147
AICc(BLM3)
## [1] 49.14005
```

All three models are very similar.

Partial Correlations

```
t.values3 <- BLM3$coeff / sqrt(diag(vcov(BLM3)))
partcorr3 <- sqrt((t.values3^2)/((t.values3^2) + BLM3$df.residual))
partcorr3
##     (Intercept)           Depth DistanceFromArc
##       0.8898843       0.7462260       0.9371628
```

Simple Linear Regression - Beta Diversity (Jaccard)

Best model

```
Beta <- read.csv("C:/Users/Thomas/Documents/School Work/Grad/Most Important Files/Thes Stat/Beta MBASC1.csv", check.names
=TRUE)
BLM4 <- lm(BetaJ ~ LogDFA, data=Beta)

summary(BLM4) #R-Adjusted = 0.3413

##
## Call:
## lm(formula = BetaJ ~ LogDFA, data = Beta)
##
## Residuals:
##      Min       1Q   Median       3Q      Max
## -0.39254 -0.09209  0.05770  0.07119  0.17288
##
## Coefficients:
##             Estimate Std. Error t value Pr(>|t|)
## (Intercept)  0.29234    0.06296   4.643 8.62e-05 ***
## LogDFA       0.15357    0.03966   3.872 0.000652 ***
## ---
```

```
## Signif. codes:  0 '***' 0.001 '**' 0.01 '*' 0.05 '.' 0.1 ' ' 1
##
## Residual standard error: 0.132 on 26 degrees of freedom
## Multiple R-squared:  0.3657, Adjusted R-squared:  0.3413
## F-statistic: 14.99 on 1 and 26 DF,  p-value: 0.0006523
```

Testing assumptions - Based on http://r-statistics.co/Assumptions-of-Linear-Regression.html

1. "The regression model is linear in parameters

```
plot(BLM4,1)
```

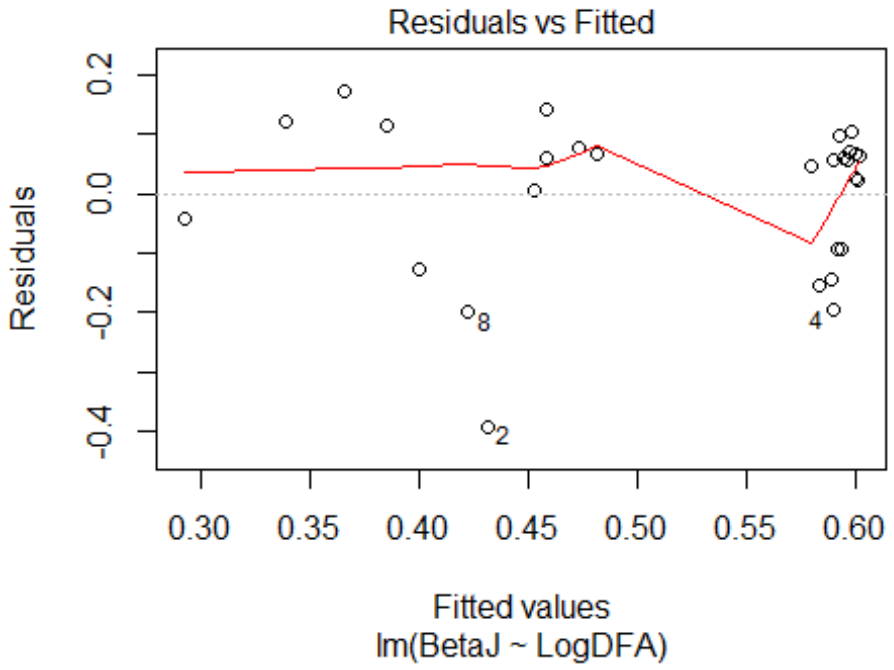

Model 4 appears to be linear. Therefore, this assumption appears to not be violated.

2 “The mean of residuals is zero”

```
mean(BLM4$residuals)
## [1] 3.557054e-18
```

This model satisfies this assumption.

3. Homoscedasticity

```
bptest(BLM4)
##
##  studentized Breusch-Pagan test
##
## data:  BLM4
## BP = 1.6499, df = 1, p-value = 0.199
```

This model satisfies this assumption.

4. “No autocorrelation of residuals”

```
acf(BLM4$residuals)
```

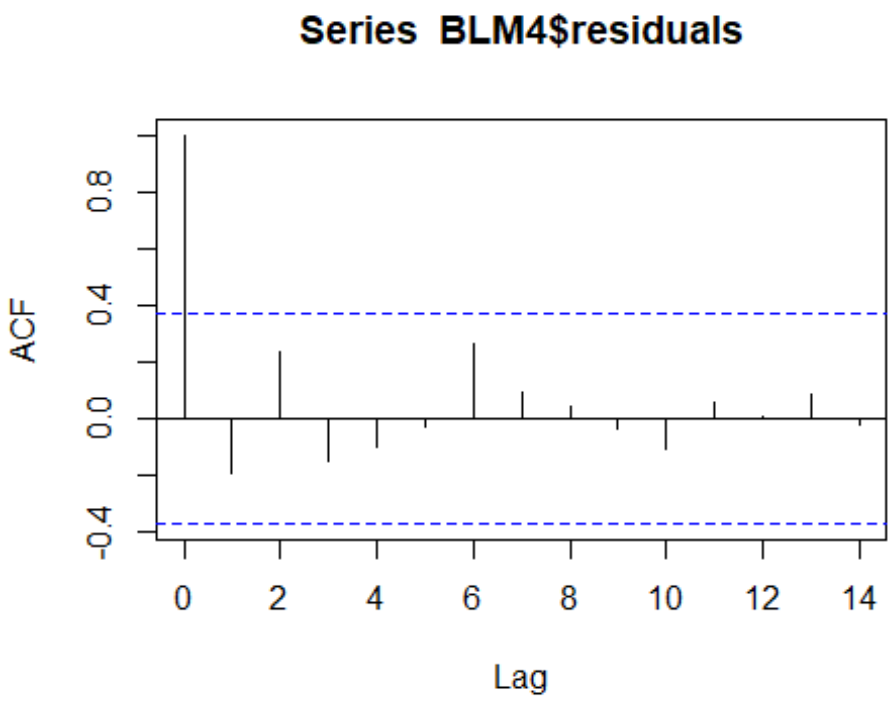

This model does not violate this assumption.

5.“The X variables and residuals are uncorrelated”

```
cor.test(Beta$LogDFA, BLM4$residuals)
##
##  Pearson's product-moment correlation
##
## data:  Beta$LogDFA and BLM4$residuals
## t = 7.9206e-16, df = 26, p-value = 1
```

```
## alternative hypothesis: true correlation is not equal to 0
## 95 percent confidence interval:
##  -0.3730769  0.3730769
## sample estimates:
##          cor
## 1.553362e-16
```

This model satisfies this assumption.

6. "The number of observations must be greater than number of Xs"

Given that sample size is n=8 and only two independent variables are used in the model, this assumption is satisfied.

7. "The variability in X values is positive."

```
var(Beta$LogDFA)
## [1] 0.4104123
```

Positive, so it satisfies the assumption.

9. "No perfect multicollinearity"

This model satisfies this assumption.

10. "Normality of residuals"

```
plot(BLM4,2)
```

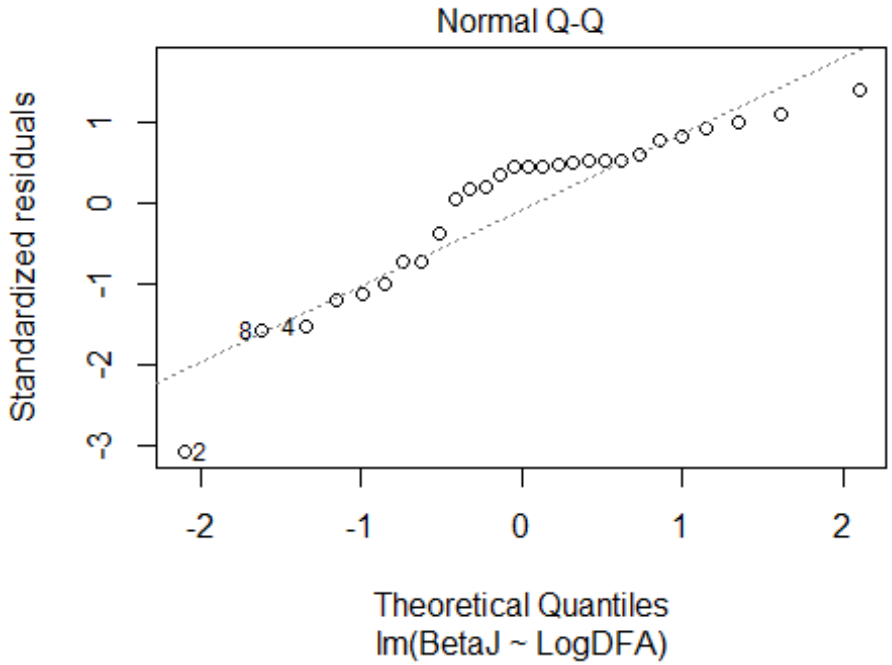

This model does not violate this assumption.

Additional Test: Major Outliers

```
plot(BLM4,5)
```

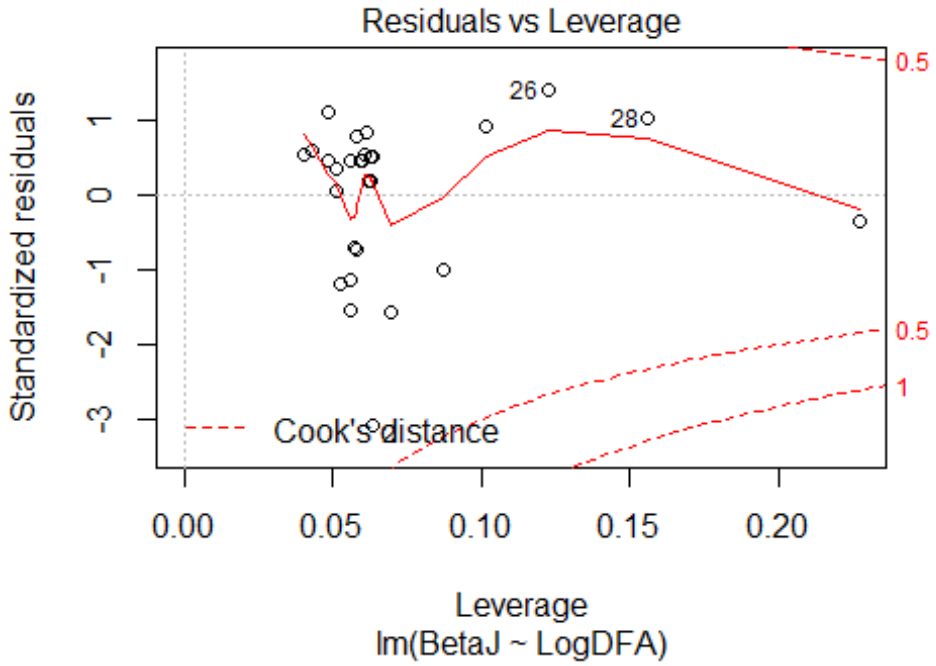

No significant outliers in these models.

Simple Linear Regression - Beta Diversity (Raup-Crick)

Best model

```
Beta <- read.csv("C:/Users/Thomas/Documents/School Work/Grad/Most Important Files/Thes Stat/Beta MBASC1.csv", check.names =TRUE)
BLM5 <- lm(BetaRC ~ Distance, data=Beta)
```

```
summary(BLM5) #R-Adjusted = 0.4595

##
## Call:
## lm(formula = BetaRC ~ Distance, data = Beta)
##
## Residuals:
##     Min      1Q  Median      3Q     Max
## -0.8377 -0.4208  0.1066  0.2761  0.8923
##
## Coefficients:
##              Estimate Std. Error t value Pr(>|t|)
## (Intercept) -0.7535709  0.1608862  -4.684 7.74e-05 ***
## Distance     0.0020525  0.0004194   4.894 4.44e-05 ***
## ---
## Signif. codes:  0 '***' 0.001 '**' 0.01 '*' 0.05 '.' 0.1 ' ' 1
##
## Residual standard error: 0.4832 on 26 degrees of freedom
## Multiple R-squared:  0.4795, Adjusted R-squared:  0.4595
## F-statistic: 23.95 on 1 and 26 DF,  p-value: 4.441e-05
```

Testing assumptions - Based on http://r-statistics.co/Assumptions-of-Linear-Regression.html

1. "The regression model is linear in parameters

```
plot(BLM5,1)
```

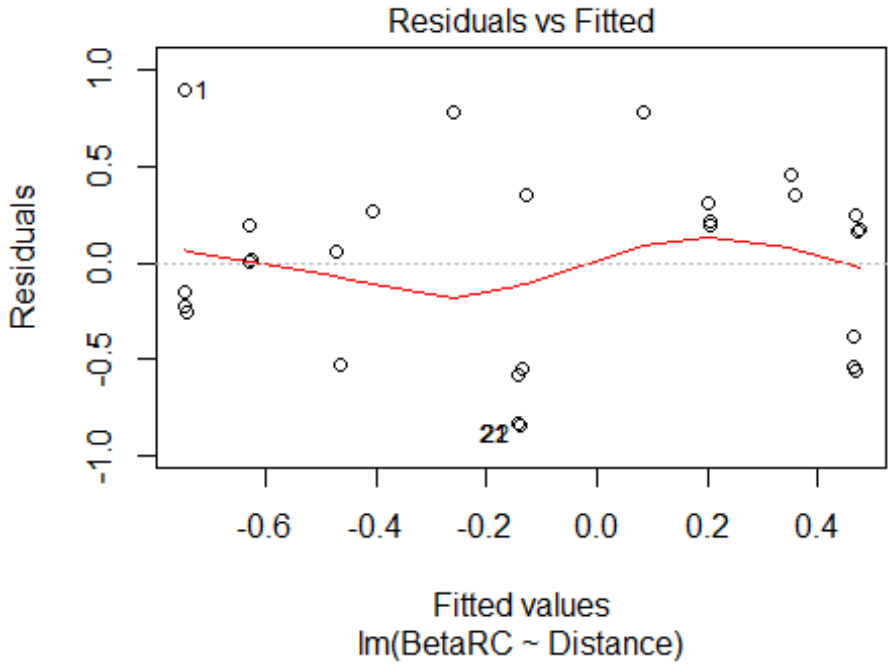

Model 5 appears to be linear. Therefore, this assumption appears to not be violated.

2 “The mean of residuals is zero”

```
mean(BLM5$residuals)
## [1] -6.591949e-17
```

This model satisfies this assumption.

3. Homoscedasticity

```
bptest(BLM5)
##
##  studentized Breusch-Pagan test
##
## data:  BLM5
## BP = 0.024076, df = 1, p-value = 0.8767
```

This model satisfies this assumption.

4. "No autocorrelation of residuals"

```
acf(BLM5$residuals)
```

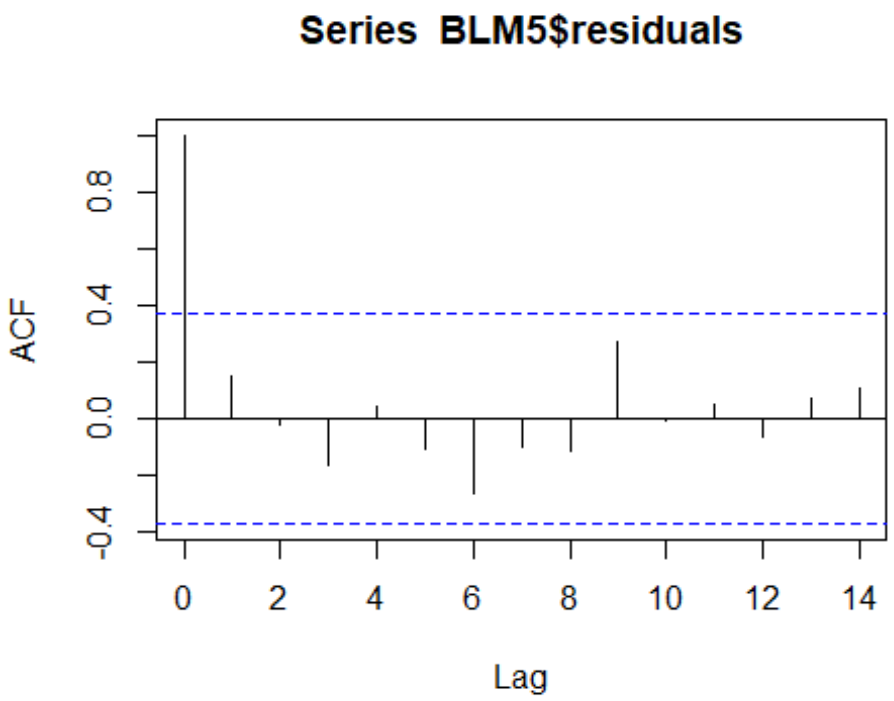

This model does not violate this assumption.

5.“The X variables and residuals are uncorrelated”

```
cor.test(Beta$Distance, BLM5$residuals)
##
##  Pearson's product-moment correlation
##
## data:  Beta$Distance and BLM5$residuals
## t = -2.6137e-16, df = 26, p-value = 1
## alternative hypothesis: true correlation is not equal to 0
## 95 percent confidence interval:
```

```
##  -0.3730769  0.3730769
## sample estimates:
##          cor
## -5.125985e-17
```

This model satisfies this assumption.

6. "The number of observations must be greater than number of Xs"

Given that sample size is n=8 and only two independent variables are used in the model, this assumption is satisfied.

7. "The variability in X values is positive."

```
var(Beta$Distance)
## [1] 49174.15
```

Positive, so it satisfies the assumption.

9. "No perfect multicollinearity"

This model satisfies this assumption.

10. "Normality of residuals"

```
plot(BLM5,2)
```

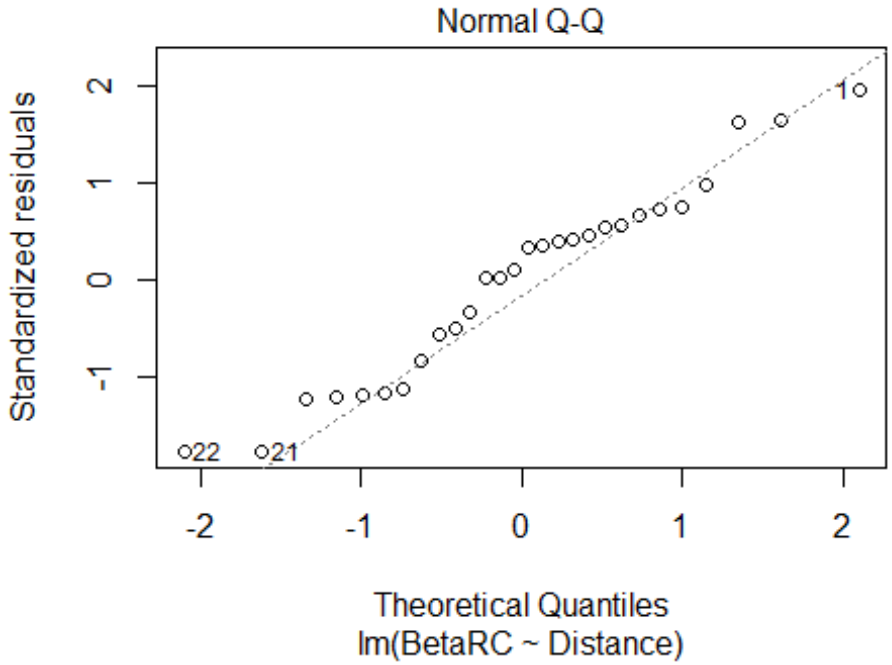

This model does not violate this assumption.

Additional Test: Major Outliers

```
plot(BLM5,5)
```

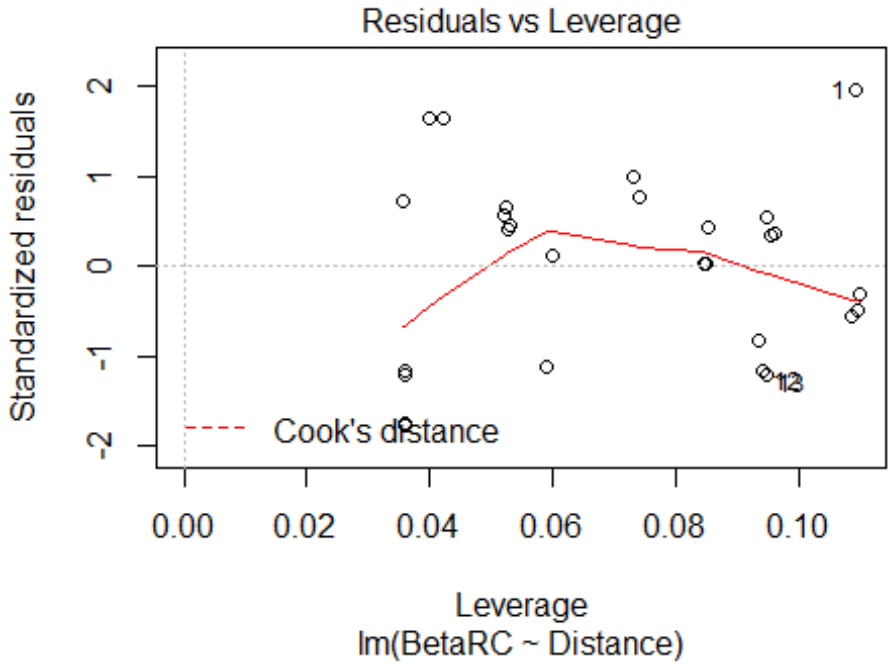

No significant outliers in these models.